

New Decentralized Algorithms for Spacecraft Formation Control Based on a Cyclic Approach

by

Jaime Luís Ramírez Riberos

B.S., Universidad de los Andes (2001 & 2002)

M.S., Texas A&M University (2006)

Submitted to the Department of Aeronautics and Astronautics
in partial fulfillment of the requirements for the degree of

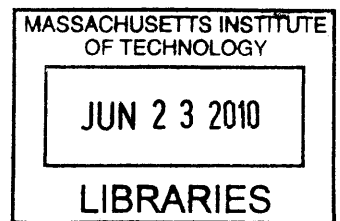
Doctor of Philosophy

at the

MASSACHUSETTS INSTITUTE OF TECHNOLOGY

June 2010

ARCHIVES



© Massachusetts Institute of Technology 2010. All rights reserved.

Author
Department of Aeronautics and Astronautics
May 20, 2010

Certified by
Emilio Frazzoli
Associate Professor of Aeronautics and Astronautics
Thesis Committee Chair

Certified by
David W. Miller
Professor of Aeronautics and Astronautics

Certified by
Jean-Jacques Slotine
Professor of Mechanical Engineering and Information Sciences

Certified by
Raymond Sedwick
Assistant Professor of Aerospace Engineering, University of Maryland

Accepted by
Eytan Modiano
Chair, Committee on Graduate Students

New Decentralized Algorithms for Spacecraft Formation Control Based on a Cyclic Approach

by

Jaime Luís Ramírez Riberos

Submitted to the Department of Aeronautics and Astronautics
on May 21, 2010, in partial fulfillment of the
requirements for the degree of
Doctor of Philosophy

Abstract

When considering the formation control problem for large number of spacecraft, the advantages of implementing control approaches with a centralized coordination mechanism can be outpaced by the risks associated with having a primary vital control unit. Additionally, in formations with a large number of spacecraft, a centralized approach implies an inherent difficulty in gathering and broadcasting information from/to the overall system. Therefore, there is a need to explore efficient decentralized control approaches. In this thesis a new approach to spacecraft formation control is formulated by exploring and enhancing the recent results on the theory of convergence to geometric patterns and exploring the analysis of this approach using the tools of contracting theory.

First, an extensive analysis of the cyclic pursuit dynamics leads to developing control laws useful for spacecraft formation flight which, as opposed to the most common approaches in the literature, do not track fixed relative trajectories and therefore, reduce the global coordination requirements. The proposed approach leads to local control laws that verify global emergent behaviors specified as convergence to a particular manifold. A generalized analysis of such control approach by using tools of partial contraction theory is performed, producing important convergence results. By applying and extending results from the theory of partially contracting systems, an approach to deriving sufficient conditions for convergence is formulated. Its use is demonstrated by analyzing several examples and obtaining global convergence results for nonlinear, time varying and more complex interconnected distributed controllers.

Experimental results of the implementation of these algorithms were obtained using the SPHERES testbed on board the International Space Station, validating many of the important properties of this decentralized control approach. They are believed to be the first implementation of decentralized formation flight in space. To complement the results we also consider a short analysis of the advantages of decentralized versus centralized approach by comparing the optimal performance and the effects of complexity and robustness for different architectures and address the issues of implementing decentralized algorithms in a inherently coupled system like the Electromagnetic Formation Flight.

Thesis Committee Chair: Emilio Frazzoli

Title: Associate Professor of Aeronautics and Astronautics

Thesis Committee Member: David W. Miller
Title: Professor of Aeronautics and Astronautics

Thesis Committee Member: Jean-Jacques Slotine
Title: Professor of Mechanical Engineering and Information Sciences

Thesis Committee Member: Raymond Sedwick
Title: Assistant Professor of Aerospace Engineering, University of Maryland

Acknowledgments

This work was enabled by the Department of Defense, the National Science Foundation and the National Aeronautics and Space Administration. I am grateful to these institutions for their commitment to programs that supported my graduate studies. There are also many notable individuals who contributed to my research, thesis development and overall experience at MIT. I would like to thank a few of them in particular.

To Marco Pavone whose input was invaluable in developing an important part of the theory of cyclic pursuit controllers, an initial spark of this work. To Professor Jean-Jacques Slotine whose bright ideas and encouragement were fundamental to my thesis completion. I did not foresee how valuable he would be as a member of my committee.

To a great advisor, Professor Emilio Frazzoli for taking me on as his student. His encouragement, patience and dedication in sharing his consistently wise point of view made the completion of my doctoral studies possible while widening my interests to new research topics. To Professor David W. Miller for his support, positioning me to learn and share with him as one of his own students though I was not officially one of them. The opportunities that he gave me to work on exciting projects have been fundamental not only for my PhD work but for my future career as a space engineer-scientist. To Professor Ray Sedwick, a respected member of my committee who trusted my capabilities when he selected me as his student and later left me in good hands at MIT.

To many on the SPHERES team with whom I worked alongside long days and early weekend mornings and expect to continue collaborating with in the future. To Dr. Alvar Saenz-Otero, dedicated manager and scientist whose work has sustained such a magnificent testing platform. To others at the SSL, including Dr. Daniel Kwon who continues supporting the lab from a distance. To my colleagues Jake Katz and Amer Fejzic who listened to my improvable ideas and frustrations and made my days at MIT more enjoyable.

Finally, I have to thank the most important part of this whole effort, my family. To Jaime and Gilma to whom I owe everything. Their love and support has given me strength amid the melancholy of being far away from them. To John and Barbara for so candidly believing in me. Most importantly, to Christina, for not letting me get off track and for her unconditional caring love and support. This PhD belongs to her too.

Contents

1	Introduction	17
1.1	Spacecraft Formation Flight	17
1.2	Problem Statement	23
1.3	Thesis Objective	24
1.4	Approach	25
1.4.1	Approach overview	25
1.4.2	A new approach to formation flight: generalized pursuit	26
2	Literature Review	35
2.1	Background	35
2.1.1	Notation	36
2.1.2	Kronecker product	36
2.1.3	Determinant of block matrices	37
2.1.4	Rotation matrices	37
2.1.5	Circulant matrices	37
2.1.6	Block rotational-circulant matrices	38
2.1.7	Graph representation of multi-agent systems	39
2.1.8	Contraction theory	40
2.1.9	Decentralized systems theory	41
2.2	Decentralized Approach to Multivehicle Cooperative Control	43
2.2.1	Potential functions and behavioral approaches	43
2.2.2	Multiple instantiations of the state	44

2.2.3	Consensus problem and approach to formation control	45
2.2.4	Contraction analysis and synchronization	48
2.2.5	Cyclic pursuit	48
2.2.6	Spacecraft formation control	50
2.2.7	Electromagnetic formation flight	53
2.3	Summary and Gap Analysis	55
3	Cyclic Pursuit Controllers for Spacecraft Formation Applications	57
3.1	Introduction	57
3.2	Cyclic-Pursuit Control Laws for Single-Integrator Models	59
3.2.1	Cyclic pursuit in three dimensions with control on the center of the formation	60
3.2.2	Case $k_c = 0$, i.e., no control on the center of the formation.	62
3.2.3	Case $k_c > 0$, i.e., control on the center of the formation.	63
3.2.4	Convergence to circular formations with a prescribed radius	64
3.3	Cyclic-Pursuit Control Laws for Double-Integrator Models	69
3.3.1	Dynamic cyclic pursuit with reference coordinate frame	70
3.3.2	Control law with relative information only	73
3.4	General Trajectories: Conformal Mapping	79
3.5	Applications of Cyclic-Pursuit Algorithms	82
3.5.1	Interferometric imaging in deep space	83
3.5.2	On reaching natural trajectories	85
3.5.3	Including Earth's oblateness effect	87
3.6	Summary and Conclusions of the Chapter	90
4	Contraction Theory Approach to Formation Control	93
4.1	Introduction	95
4.1.1	Time varying and nonlinear manifolds	100
4.2	Cyclic Controllers for Convergence to Formation	102
4.2.1	Generalized cyclic approach to formation control	103

4.2.2	Distributed global convergence to a desired formation size	108
4.2.3	Extension to second order systems	113
4.3	Convergence Primitives Approach	115
4.4	Applications	119
4.5	Summary and Conclusions of the Chapter	130
5	Comparison of the Generalized Cyclic Approach to Relevant Architectures	131
5.1	Introduction	131
5.2	Benchmark Problem	132
5.3	Synthesis of Decentralized Controllers	133
5.4	Cost Metrics	139
5.5	Results	141
6	Experimental Results: Decentralized Formation Flight in Microgravity Environment	143
6.1	Introduction	143
6.1.1	The SPHERES testbed	144
6.2	Algorithm Implementation	146
6.3	Description and Results of the Tests	148
6.3.1	Test 1: Joining maneuver 2-sat to 3-sat formation	149
6.3.2	Test 2: Convergence to 3-sat formation from arbitrary initial conditions	150
6.3.3	Test 3: Pure relative formation maintenance	153
6.3.4	Test 4: Implementation with a fault detection and recovery algorithm	157
6.3.5	Test 5: Implementation with a collision avoidance mechanism	160
6.3.6	Test 6: Implementation as a random initialization algorithm	161
6.4	Performance Analysis	164
6.5	Summary and Conclusions of the Chapter	169
7	Decentralized Control in Electromagnetic Formation Flight	171
7.1	Introduction	171
7.1.1	Electromagnetic Formation Flight	172

7.2	Token Based Decoupled Maneuvering	175
7.2.1	Lower level problem solution	177
7.2.2	Higher level problem solution	179
7.3	Decoupled Regulation by Resource Allocation	183
7.3.1	Schedule based regulator	183
7.3.2	Frequency division	186
7.3.3	Resource allocation: Simulation results	190
7.4	Distributed Computation of the Solution to the Dipole Equation	195
7.4.1	Theoretical description	195
7.4.2	Convergence analysis	197
7.4.3	Closed loop convergence	200
7.5	Summary and Conclusion of the Chapter	202
8	Conclusions and Final Remarks	205
8.1	Thesis Summary and Conclusions	205
8.2	Contributions	206
8.2.1	Secondary contributions	208
8.3	Future Work	208
A	Mathematical derivation of proofs	211
A.1	\mathcal{CR} Matrices	211
A.2	System (3.10) in Polar Coordinates	213
A.3	Proof of Lemma 3.2.8	214
A.4	Proof that $v_i \notin T_{(\varrho^*, \varphi^*)} \tilde{\mathcal{M}}$	219
A.5	Eigenvalues of the projected Laplacian	220

List of Figures

1-1	As research on multi-vehicle missions evolve, several concepts with increasing number of vehicles have been proposed, left: TPF-I, center: System F6, right: SI. (source: NASA, DoD)	19
1-2	Thesis approach diagram	29
3-1	Convergence to circular trajectories centered at the origin. Left Figure: First coordinate as a function of time for each agent. Right Figure: Trajectories in 3D.	64
3-2	A formation achieves a formation with some arbitrary trajectories by selecting specific linear and nonlinear transformations	83
3-3	u-v plane coverage by a system of multiple spacecraft. (Source [16])	84
3-4	Convergence from random initial conditions to symmetric formations. Left Figure: Circular trajectories. Right Figure: Archimedes' spiral trajectories.	85
3-5	Convergence to elliptical trajectories with dynamics including J_2 terms.	90
4-1	Constraint description of \mathcal{M}_5	99
4-2	Different cyclic topologies	104
4-3	Agents converge to a cube in 3D. (Snapshots every 30 seconds).	122
4-4	Agents converge to a packed grid by imposing some convergence constraints shown by the arrows, two different cases can be designed following the same argument.	127
5-1	Optimal Cost as the number of vehicle increases	136
5-2	Optimal Cost as the number of vehicle increases	139

5-3	Trade space Performance vs Complexity of Implementation as a function of the number of vehicles in the formation	142
5-4	Trade space Performance vs Cost of Robustness as a function of the number of vehicles in the formation	142
6-1	Picture of three SPHERES satellites performing a test on board the ISS. (Fotocredit: NASA - SPHERES)	145
6-2	Experimental results from Test 1: Position and velocity vs. time. From left to right: satellites 1, 2 and 3. Maneuvers indicated by numbers.	151
6-3	Experimental results from Test 1: x-z plane. Sequence of maneuvers a) Maneuver 1 , b) Maneuver 2, c) Maneuver 3 and d) Maneuver 4.	151
6-4	Experimental results from Test 2: Position and velocity vs. time. From left to right: satellites 1, 2 and 3.	152
6-5	Experimental results from Test 2: x-z plane. Sequence of maneuvers a) and b).	153
6-6	Experimental results from Test 3: Sequence of maneuvers indicated by colors.	155
6-7	Experimental results from Test 3: Position, velocity and control commands vs. time.	156
6-8	Experimental results from Test 4. Top: perception of the formation by each satellite.	159
6-9	Experimental results from Test 5: Trajectories.	162
6-10	Experimental results from Test 5: States vs. time.	163
6-11	Experimental results from Test 5: Relative states SPH1 to SPH3 vs. time.	164
6-12	Experimental results from Test 6: Trajectories.	165
6-13	Experimental results from Test 6: SPH1 States vs. time.	166
6-14	Experimental results from Test 6: SPH2 States vs. time.	166
6-15	Experimental results from Test 6: SPH3 States vs. time.	167
6-16	Error in symmetry for three cases in table 6.1. from left to right P162.T2, P273.T4, P273.T6. Cyclic Pursuit cases are the two on the right.	168

7-1	Optimal minimum current two-vehicle maneuvers in Clohessy-Wiltshire dynamics	180
7-2	Optimal reconfiguration maneuver - Clohessy-Wiltshire dynamics only two vehicles actuate at the same time.	182
7-3	Optimal reconfiguration maneuver - Clohessy-Wiltshire dynamics only two vehicles actuate at the same time.	183
7-4	. Basic results showing the principle of operation of the implementation of decentralization by resource division	189
7-5	Time Division allocation - Disturbance rejection transient	191
7-6	Currents in coils Time Division for different number of vehicles actuating at a time - Bottom: Steady State Cyclic Pursuit (2 active vehicles)	192
7-7	Frequency Division allocation - Disturbance rejection transient. The x -input is zoomed into the first 25 seconds	193
7-8	Frequency Division allocation - Steady State Cyclic Pursuit. The x -input is zoomed into the first 25 seconds	194
7-9	Figure showing a group of vehicles following a circular trajectory setting up the dipoles in a distributed manner.	201

List of Tables

- 5.1 Different topologies considered for comparison of decentralized controller . . . 138
- 6.1 Comparative fuel use for several control architectures 168
- 7.1 Variable descriptions for the higher level DP optimization problem 181
- 7.2 Increase in RMS current in coils as the number of vehicles that can be moved
at a time changes 181
- 7.3 Minimum maneuver time as the number of vehicles that can be moved at a
time changes 182
- 7.4 Sequential Distributed Dipole Solution 198

Chapter 1

Introduction

1.1 Spacecraft Formation Flight

Conceptual architectures using multiple satellites to achieve a cooperative objective have been extensively researched in recent years. The main motivation behind these concepts is the general opinion that a multi-vehicle system could surpass the performance and have enhanced characteristics compared to those of a single unit.

Among the characteristics of multi-vehicle systems, the intrinsic parallelism of a multi-agent system provides robustness to failures of single agents, and in many cases can guarantee better time efficiency. Moreover, it is possible to reduce the total implementation and operation cost, increase reactivity and system reliability, and add flexibility and modularity as compared to monolithic approaches.

Numerous applications of multi-agent cooperative systems have been foreseen in surveillance missions, demining, planetary exploration, coordinated attack, and some of them have been successfully implemented in ground robots [49], unmanned air vehicles [8], autonomous underwater vehicles [98] and satellites [105]. In particular several applications have been foreseen for multi-agent technology in space (see Fig. 1-1).

In interferometric missions, the idea that multiple formation flying spacecraft can obtain

better performance than a structurally connected spacecraft by achieving larger baselines and improved flexibility is exploited. Several missions using multi-spacecraft systems with the science objective of detecting life components in extra-solar planets have been proposed. Formations of up to 30 spacecraft have been studied for the Stellar Imager concept [9, 27].

Multi-aperture telescopes are another possible application. In this approach, a set of vehicles achieve improved optical performance and better coverage of multiple targets by providing a flexible reconfigurable system. Additionally, enhanced upgradeability is considered as a projected advantage as modules could be changed or added and an assembly mission could be performed in space achieving total apertures otherwise impossible to launch as a monolithic unit [81].

Another example is synthetic aperture radar (SAR) missions for earth imaging and remote sensing. SAR is an implementation of radar technology that uses many small antennas distributed among two or several spacecraft instead of using a single rotating antenna, are used to sense the reflection of electromagnetic wavefronts off the earth. An improvement of the overall performance achieved by implementing large and variable baselines between antennas [13, 89].

Scientific missions for improved measurements of the earth's magnetosphere have also been proposed which would take advantage of acquiring simultaneous measurements of the magnetic field at locations separated by a few kilometers [57].

More recent multi-satellite missions consider clusters of satellites performing as a fractionated spacecraft architecture. In that case, the spacecraft would interchange information while maintaining neighboring positions in a way such that different components that are traditionally located in a single satellite could be physically situated on different satellites distributing functions among the different vehicles. This fractionated architecture has improved reliability and upgradeability, since replacement of individual components would be reduced to deorbiting the module to be replaced and launching a new component into the configuration [12, 46].



Figure 1-1: As research on multi-vehicle missions evolve, several concepts with increasing number of vehicles have been proposed, left: TPF-I, center: System F6, right: SI. (source: NASA, DoD)

Scharf and Hadaegh defined spacecraft formation flying in [83] as “a set of more than one spacecraft whose dynamic states are coupled through a common control law. In particular, at least one member of the set must 1) track a desired state relative to another member, and 2) the tracking control law must at the minimum depend upon the state of this other member.”

This definition could be relaxed in the sense that tracking a desired relative state is a restrictive condition. For example, in the case where the mission objective can be achieved by maintaining the vehicles confined to a given region or holding some structural behavior without tracking specific trajectories.

Multi-agent systems are not linked just through their control. Systems with multiple actuation that have some level of coordination can be considered multi-agent systems. The level of interconnection or coupling of the elements in a multi-agent system may vary between different architectures. One can think for example of the case of multiple actuators and sensors in an actively controlled structure [50]. The dynamic coupling in this case is structural, that is, without applying control, the state evolution of one node depends on the state of some other. A tethered system [18], is a structurally coupled system with a more relaxed interconnection. In this type of system the formation is linked through tethers which imply kinematic constraints. This makes the state evolution of one vehicle dependent on the state of some others. On the other hand, the coupling can be caused by the actuation. Elec-

tromagnetic formation flight technology uses electromagnetic forces to control the relative motion between spacecraft. The spacecraft are not actually structurally connected, and thus, if no electromagnetic actuation is performed, the evolution of the state of one vehicle does not depend on any other. However, when the electromagnets are activated in more than one vehicle the evolution of the state of one of the vehicles depends on the state of some of the others. Additionally, the system could be coupled through measurements. If the information that an agent requires to be able to perform its task is obtained through different agents, any control law based on that information couples the system. Finally, the interconnection between vehicles can be given by the mission objective pursued by the control system. If the objective is determined with respect to relative states, like the case of formation flight, even if the system is decoupled in every other manner, the system is coupled through its performance.

Control strategies have been classically categorized into centralized approaches, and decentralized approaches. A centralized approach is an implementation where a “central” computation unit (not necessarily on one of the spacecraft) has access to all the states of the system and has the capability to communicate the optimal control commands to each actuator in the overall system [10]. This can be considered in terms of design, the simplest architecture to achieve optimal performance.

In a decentralized scheme, each vehicle has available only partial information of the formation and decides its own actuation command at each period. The information available to each vehicle can be implemented in the form of measurements or communication. The problem of synthesizing decentralized controllers for an arbitrary interconnection topology is an open problem, and several approaches to deriving control laws have been studied in the last 30 or 40 years. The sub optimality arises given the knowledge of only partial information. Different instantiations of a coordination state can coexist in different vehicles and thus, what is optimal for one instantiation is not necessarily optimal for a different vehicle.

However, decentralization has several important features that could largely impact the

realization of a mission. Some of the most important features of decentralized control and estimation which are especially applicable to space systems are:

- Launch and deployment independence,
- Robustness to failures and delays of a central unit,
- Module repeatability,
- Simplified addition and rejection of modules.

Moreover, for decentralized implementations that only require local information, decentralization has additional advantages in the sense of:

- Linear dependence of the communication complexity with the number of vehicles,
- Simplicity of implementation, especially, a reduced order of the controller states

As examples, consider a centralized mission for which the payload of the central controller fails, then the whole mission fails, or even before launch, if its development process is delayed, the whole system is delayed. Additionally, there is an important inverse relationship between simplicity and reliability. Decentralized systems can be simpler to implement and validate because in principle, the operation of each satellite does not depend on the others.

Considering the interest in decentralized approaches, the proposed thesis looks also at the decentralization problem from a control perspective exploring a special type of decentralized controller.

Scharf et al. [83] identified the three main areas that have not been thoroughly addressed in the spacecraft formation flight control literature: 1) rigorous stability conditions for cyclic and behavioral architectures, 2) reduced algorithmic information requirements, and 3) increased robustness/autonomy. A control method that exploits cyclic topologies is studied in this thesis. The general approach considers a generalization of the cyclic pursuit approaches and extends its analysis as a manifold convergence problem, which uses local information to

converge to global equilibrium states that are in a manifold. This approach can efficiently address some of these mentioned areas.

This thesis explores the cyclic-pursuit based algorithms recently presented in the literature because of its fitness for space applications and extend for application in space. Additionally, the problem is studied under a different theoretical approach which leads to defining other, more general control algorithms and describe the problem as convergence to manifolds with desired properties instead of convergence to (time varying) fixed-point trajectories. Common approaches to formation control have focused on the convergence to fixed points of the relative states. The research in this thesis presents control algorithms that achieve convergence to manifolds and have valuable characteristics including not requiring coordination on specific relative positions, simplicity of implementation, reduced number of communication links (n links for n agents), reduced number of computations to achieve a formation, global convergence, synchronization, a better fuel performance than other decentralized algorithms and improved robustness.

Another aspect considered in this thesis, strongly motivated by the decentralization objective, considers the extension and drawbacks of applying decentralized control techniques to an inherently coupled system such as Electromagnetic Formation Flight.

Electromagnetic Formation Flight technology (EMFF) is a concept developed by the Space Systems Lab at MIT, also independently envisioned by Boeing (Formerly Hughes Aerospace) and a Japanese research group at the university of Tokyo [34]. Its principle of operation is the force created by the interaction of magnetic fields generated by current running through High Temperature Superconducting (HTS) coils. These electromagnetic coils generate fields equivalent at long distance to magnetic dipoles, which can be steered in any three dimensional direction by the combination of currents running through three orthogonal coils.

Theoretical studies have demonstrated the superiority of electromagnetic formation flight versus other propulsion methods for several applications, and a testbed has been built and

used to demonstrate the operational principles for control. Open loop control, position hold and trajectory tracking have been successfully demonstrated in a two-vehicle configuration. EMFF is a maturing technology and due to the complexity of the challenge, the control approaches have considered only centralized techniques. An EMFF system will benefit from decentralization and this work presents techniques to address the issue.

The main portion of this work addresses the development and validation of new control techniques based on the cyclic pursuit approaches and its extensions based on contraction theory and concluding sections perform a preliminary study the implications of the proposed decentralized control approach and the mechanisms to implement it in EMFF systems.

1.2 Problem Statement

Satellite formation flight is an enabling technology in the early stages of its realization and as new applications are envisioned, some of them consider increasingly larger number of spacecraft achieving geometric patterns.

As the number of spacecraft increases in a cooperative multiagent system, the implementation of centralized control approaches becomes less viable, and it is important to identify effective methods for decentralized spacecraft formation control. Most common decentralized approaches require global coordination mechanisms, by tracking relative states they constrain unnecessary degrees of freedom and/or imply information transfer requirements that scale poorly with the number of agents in the formation.

Mission objectives in several kinds of space applications, may not require tracking specific fixed point trajectories of the relative states but can be achieved by maintaining the overall state of the system within a given manifold. Among several approaches to cooperative control, the cyclic-pursuit algorithm, presents promising features; specifically, it has properties of reduced information flow and global convergence to manifolds. The analysis of this type of controller can efficiently address areas in the formation flight control field that have not

been thoroughly explored. This approach could bring benefits to spacecraft formation control missions in terms of reduced information requirements, reduced fuel consumption and increased robustness and autonomy. However, the theoretical results for this algorithm are restricted so far to the single integrator case, with convergence only to circles or logarithmic spirals and precarious robustness properties.

Additionally, promising technologies like EMFF systems are highly coupled through their actuation. Such coupling does not allow for a direct extrapolation of decentralized techniques that do not account for this coupling. Specifically, the actuation in one vehicle requires at least one other vehicle to be actuated, and the fact that the input command of one vehicle affects all the other active vehicles.

1.3 Thesis Objective

The main objective of this thesis can be summarized as:

To contribute to the field of multi-satellite systems formation control enhancing the current state of research in the area of distributed controllers. The work in this thesis will address the development of formation control algorithms where a global geometric behavior emerges from local control rules, not based on trajectory tracking, leading to improved properties in terms of complexity scaling, global convergence and control effort.

Under the overall objective of studying a new approach to decentralized spacecraft formation control, the specific objective is to develop control laws based on the idea of manifold convergence, especially cyclic algorithms for satellite formation flight.

The following subobjectives are considered:

1. Analysis of the dynamics of cyclic pursuit algorithms for three dimensional cases and second order dynamics.
2. Development of controllers for the application of the cyclic pursuit approach in spacecraft applications, namely:

- (a) Approaches considering low earth orbit dynamics that converge to near natural relative orbital trajectories.
 - (b) Control approaches for deep space missions that achieve the formation objective merely based on relative information.
3. Extension to more complex interconnection topologies and nonlinear controllers to improve the properties of the cyclic pursuit algorithms and achieve more complex objectives, specifically by developing a theoretical approach to analyze the convergence properties of more general dynamical systems.
 4. Experimental validation of the control approaches in the SPHERES testbed and analysis of their properties.

Additionally, secondary objectives also addressed in this work include

1. A framework to compare between the interconnection topology of low-level control architectures, considering the system performance. Specifically, focusing on comparing the manifold convergence methods to other architectures.
2. Developing techniques to decentralize electromagnetic formation flight considering methods for implementation of EMFF that do not require the use of centralized computation,

1.4 Approach

1.4.1 Approach overview

The general approach to address the objectives of this thesis consists of exploring formation controllers inspired by the cyclic pursuit algorithm, extending and analyzing the applicability of this approach for spacecraft formation flight problem, and presenting a framework that achieves a deeper approach to more general dynamic systems.

At first, the analysis of the control laws is based on a linear eigendecomposition analysis. For the basic cases, analytical expressions for the eigenvectors can be derived given the special structure of the circulant matrices describing the underlying topology. Then, a framework considering results from contraction theory is presented. By introducing the analysis of this control algorithms using the framework of partial contraction theory, the control laws can be extended to more general cases and obtain results for more complex situations.

The basic elements of the control approach developed in the thesis is framed by considering the performance on a benchmark problem as compared to other architectures. Different topologies are analyzed by defining a performance quadratic metric and cost metrics that convey the cost of the complexity of the implementation and the robustness to failures.

Additionally, the analysis of some proposed techniques for the decentralized implementation of Electromagnetic Formation Flight are studied. The approach to understanding the performance of the techniques is through simulation, comparing them to a centralized implementation and preliminary analytical results describing their characteristics.

1.4.2 A new approach to formation flight: generalized pursuit

Following the results in the literature by Pavone and Frazzoli [67] and by Ren [76] this thesis starts by considering the cyclic pursuit approaches for achieving convergence to formation while not tracking a specific trajectory.

In the most common approach to formation flight, the distributed control methods are based on tracking relative states with respect to other vehicles. For a set of n agents with state described by the variable x_i , $i \in \{1, \dots, n\}$. The most basic description of such approach considers the system [60]:

$$\dot{\mathbf{x}}_i = \mathbf{u}_i \tag{1.1}$$

$$\mathbf{u}_i = \sum_{j \in \mathcal{N}_i} k_{ij} (\mathbf{x}_j - \mathbf{x}_i - h_{ij}(t)) \tag{1.2}$$

The underlying idea in this case is the fact that each vehicle tracks a position with respect to a set of neighbors. This problem is actually an instantiation of the more general consensus problem [62], which has been widely studied in many other context, leading to a wide array of theoretical results extensible to the formation control problem. This approach has been later generalized to more complex dynamic cases [24], double integrators [72].

On a different approach to formation control, Pavone and Frazzoli [67] studied the cyclic pursuit control algorithm, by analyzing the dynamic behavior of the system:

$$\dot{\mathbf{x}}_i = kR(\alpha)(\mathbf{x}_{i+1} - \mathbf{x}_i), \quad R(\alpha) = \begin{pmatrix} \cos \alpha & \sin \alpha \\ -\sin \alpha & \cos \alpha \end{pmatrix}. \quad (1.3)$$

where $\alpha \in [-\pi, \pi)$ is constant and the overall dynamics of the n agents are described as:

$$\dot{\mathbf{x}} = k\hat{A}\mathbf{x}, \quad (1.4)$$

\hat{A} being a block circulant matrix.

The eigenvalues and eigenvectors of the dynamic matrix \hat{A} can be analytically determined based on the special characteristic of the circulant matrix which defines the underlying topology.

The specific case when $\alpha = \pi/n$, leads to two eigenvalues on the imaginary axis, which determine the circular steady state behavior. If $\alpha < \pi/n$, all the eigenvalues are in the left hand plane which determines the global convergence to a point. On the other hand, if the angle $\alpha > \pi/n$, two eigenvalues will be in the right hand plane determining a unstable expanding spiral behavior.

In a more recent work, Ren [74] extended these results for more general topologies, by considering the case:

$$\dot{\mathbf{x}} = \sum_{j \in \mathcal{N}(i)} a_{ij} C(\mathbf{x}_j - \mathbf{x}_i) \quad (1.5)$$

under the same general idea, selecting C to be a rotation matrix of angle θ , the author determines that for a critical angle θ_c , two eigenvalues can be located on the imaginary axis, leading to rotating circular formations and correspondingly if the angle $\theta > \theta_c$, the right hand eigenvalues will imply an spiraling behavior and presents a first approach to double integrators.

Building upon such ideas, the work on this thesis explores theoretical approaches that verify convergence characteristics of the more general case:

$$\dot{\mathbf{x}}_i = \mathbf{f}(\mathbf{x}) + \mathbf{u}_i \quad (1.6)$$

$$\mathbf{u}_i = \sum_{j \in \mathcal{N}(i)} k(\mathbf{x}, t) A_{ij}(\mathbf{x}, t) (\mathbf{x}_j - \mathbf{x}_i) \quad (1.7)$$

by defining invariant manifolds to which convergence is shown using the results from partial contraction theory.

The approach using contraction theory is used for several reasons: First, an analytic derivation of eigenvalues and eigenvectors for more complex topologies might not be straightforward, second, it allows extensions to the case of time varying and nonlinear controllers. This way, the analysis of the controllers for more useful applications using more complex formations, and showing global convergence properties for nonlinear controllers can be achieved.

The general focus of the theoretical part of this thesis is the derivation of sufficient conditions for global convergence using the control approaches to achieve different type of geometric patterns and behaviors without tracking relative trajectories. Global convergence properties are an important feature since they guarantee that a stable formation is achieved from any initial state. The possibly large dimensionality of the state, in the case of multi-agent systems, makes global convergence an important feature of the control approach. The main focus of the thesis is to consider cyclic topology and controllers derived from it, having in mind that this topology minimizes the number of links. However, the idea of convergence to manifolds is general enough and could be extended to more general interconnections.

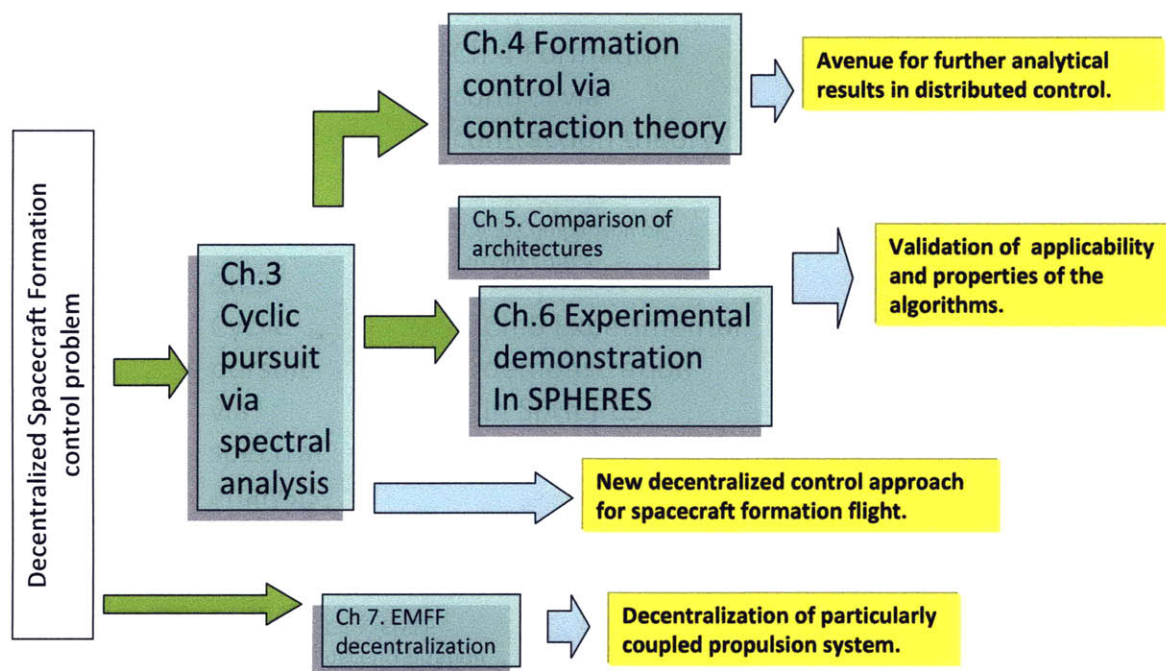


Figure 1-2: Thesis approach diagram

Figure 1-2 illustrate the general flow of the thesis. The theoretical analysis of the proposed control approach is achieved by considering two directions. In a first approach, an eigendecomposition of the cyclic pursuit dynamics is developed and the required extensions and results for application in the spacecraft formation flight problem are derived. In a second part the analysis to more complex dynamical systems is extended by considering the results of contraction theory. These results define a new path to the analysis of the formation control problem and open new avenues of research which is not specific to the spacecraft formation flight problem. The validation of the approach in a testbed on the ISS and an analysis of the advantages of such approach in a specific benchmark problem validate the applicability and the characteristics of the results of the theoretical work. Finally, further extensions consider

the implementation of decentralized techniques in EMFF systems.

1.4.2.1 Cyclic pursuit for spacecraft formation applications

In the first part of the thesis, the cyclic pursuit algorithm is analyzed and exploited for applications in spacecraft formation flight. The same general idea of identifying the eigenvectors and eigenvalues by considering the properties of circulant matrices is used to determine the convergence properties of controllers for double integrators. Second order dynamics are more relevant to the spacecraft formation flight problem.

For the most basic case, the eigendecomposition of the dynamics for a second order system with a control law is presented, which similarly to the approach presented by Ren [74], require an agreement on an inertial frame. In this thesis, the generalization to achieve control of the center of the formation is also addressed. Additionally, this controller includes a feedforward term that makes the dynamics a straightforward extrapolation of the first order system and allows for a simpler description of the overall time evolution.

Another control algorithm for the case of double integrator dynamics which uses only relative measurements to its neighbors is proposed and analyzed under the same idea of dynamic eigendecomposition. In this case it is also shown that by varying a set of parameters the system can be setup to converge to Archimedean spirals, logarithmic spirals and circles.

The idea is extended to achieve more interesting configurations by considering a similarity transformation. The control law on each vehicle uses a transformation of the cyclic pursuit that in the transformed space achieves circular formations, but in the actual physical space the trajectories are not necessarily so. A simple application of this approach is shown to be a similarity transformation of the trajectories which converges to elliptical trajectories. The importance of converging to elliptical trajectories is the fact that for near circular low earth orbits, ellipses are near-natural relative trajectories. This situation is exploited to consider controllers that can be used to achieve global formation acquisition and maintenance in the same lines of the cyclic pursuit algorithm which do not track relative trajectories but

converge to the manifold of trajectories that are near-natural and require a reduced control effort to be maintained.

A last improvement in exploring the cyclic pursuit algorithm via a linear analysis, aimed to enhance the implementation of cyclic pursuit approaches for spacecraft formation flight is related to its robustness. In the cyclic-pursuit approach, cyclic trajectories occur only when two non-zero eigenvalues are on the imaginary axis and all other non-zero eigenvalues have negative real parts. This makes the behavior not robust from a practical point of view. An approach to address the problem is using a nonlinear version of the controller.

Intuitively, for a controller in which if the agents are “close to each other” they will spiral out by setting $\alpha_i > \pi/n$; and conversely, if they are “far from each other”, the spacecraft will spiral in by setting $\alpha_i < \pi/n$. The approach to the proof of the local stability of the systems uses a sequence of coordinate transformations such that a formation is an equilibrium point of the coordinate system.

1.4.2.2 Contraction theory approach to generalized pursuit

The eigendecomposition approach to analyze the properties of a system is limited in its nature to linear or linearized systems with a very specific structure. With the purpose of expanding the results to nonlinear, more complex interconnections and time varying cases the tools of contraction theory are explored. In doing this, the underlying idea of the cyclic pursuit algorithm is generalized as a method to achieve convergence of the formation to a specified manifold and not necessarily to tracking a trajectory.

Contraction theory is presented as a powerful method to approach the convergence analysis of distributed control problems for which methods like Lyapunov functions might not be suitable. In the contraction theory approach, the general idea consists of showing the negative definiteness of a projected Jacobian matrix which encompasses the dynamics of an agreement subspace. Showing the negative definiteness of a matrix in the case of a distributed system can turn more attainable than demonstrating the negativity of a Lyapunov

rate, function of multiple states that depend on each other.

The results from partial contraction theory developed by Pham and Slotine [68] describe the problem of convergence to an invariant manifold of the dynamics system as the problem of showing convergence of an auxiliary system that describes the dynamics of a component perpendicular to the desired manifold.

In a first result, applying the contraction approach to a generalized version of the cyclic pursuit approach leads to a generalization to time varying and state dependent cyclic controllers, namely with the structure:

$$\dot{x}_i = \sum_{j \in \mathcal{N}} k(\mathbf{x}, t) R(\mathbf{x}, t) (x_i - x_j)$$

Convergence results extend straightforward to achieving polygons, circular and spiral rotating formations, address time varying and state dependent gains and coupling matrices.

Then, a series of results and corollaries of extending the contraction theory approach to time varying subspaces and linear combinations of basic primitives are derived. Specifically, a result on the linear combination of basic control functions shown to converge to basic manifolds \mathcal{M}_i , which are dubbed 'primitives', of the form:

$$\dot{\mathbf{x}} = \sum_i \mathbf{f}_i(\mathbf{x})$$

such that:

$$V_i : \mathbb{R}^n \rightarrow \mathbb{R}^{p_i}, \quad V_i \mathbf{f}_i(\bar{\mathbf{x}}) = 0, \quad V_i \bar{\mathbf{x}} = 0, \quad \forall \bar{\mathbf{x}} \in \mathcal{M}_i$$

showing conditions for the overall system to achieve convergence to the intersection of the individual manifolds, namely $\mathbf{x} \rightarrow \bar{\mathbf{x}} \in \mathcal{M} = \bigcap \mathcal{M}_i$. Several applications of using these results are shown to illustrate the proposed idea.

1.4.2.3 Applications and experiments

Another important component of developing the algorithms presented in this thesis considers the implementation of the controllers in actual hardware. The SPHERES testbed is used as a platform to obtain experimental results for different control laws derived from the algorithms presented in this part of the thesis.

First, the basic algorithms were tested to verify their performance and a comparison to simulations is presented. In this part the implementation of decentralized methods for spacecraft formation flight subject to the constraints of real flight hardware in microgravity environment was validated.

Additionally, several hardware tests demonstrated the use of these decentralized control algorithms for diverse space scenarios foreseeable in an actual spacecraft formation flight mission.

1.4.2.4 A benchmark problem framing the results

As a concluding remark of the approach, in a small section a comparison of different control architectures for formation flight is performed, highlighting the improved performance of control algorithms derived from the generalized pursuit approach in a trade analysis based on a benchmark control problem. Some metrics were defined that can be applied for analyzing the different cases of interest. The metrics considers the performance and competing dimensions that take s into account the complexity of implementation and the cost of making it robust to failures. Architectures that can address the problem and for which an optimal performance can be calculated are studied and a trade analysis based on the defined metrics is done.

1.4.2.5 Decentralization of EMFF

As a complement to the decentralization results in this thesis, the idea of decentralization applied to a unique actuation system intended for formation flight applications is considered.

Most of the decentralization techniques fail in their implementation for electromagnetic formation flight due to the fact that a different type of coupling is present in this type of system. With the purpose of achieving the benefit of decentralization in these systems, an analysis of some ideas for decentralization of electromagnetic formation is proposed. The general approach in this section is rather heuristic given the difficulty of the problem, and some different proposed ideas are presented.

A natural approach for the application of forces in a decentralized way in a EMFF system consists of decoupling the dynamics of the system. Some possibilities are inspired on the resource allocation schemes used in communication systems. In a time divided resource allocation, the system is decoupled by allocating time slots of operation for subsets of vehicles. During a time slot the active subset of vehicles can actuate, and the rest of vehicles remain 'inactive'. By alternating the set of vehicles that are active, the desired forces can be achieved under the advantage that applying the closed loop control to achieve desired trajectories, the vehicles would need to solve a set of dipole equations of reduced dimensionality.

In a frequency divided resource allocation strategy, subsets of vehicles can act simultaneously applying orthogonal currents for each different subset decoupling the actuation. The time average interaction with vehicles with an orthogonal frequency will be nulled, allowing for decoupling the interaction with vehicles other than the ones in its own subset. Different type of orthogonal functions can be more effective in different situations. Sine functions and square sine functions are studied.

Another approach to addressing the problem investigates options of a protocol for setting up the dipoles in a distributed manner and eliminating the dependence in a central unit. An approach using a distributed protocol for the solution to the dipole equation is proposed which consists of defining a synchronized protocol that by calculating the local solution to a local optimization problem and sharing this solution value through a communication network achieve convergence to the global solution.

Chapter 2

Literature Review

In this section, a short review of some mathematical background and an assessment of the literature covering the topics concerning this thesis is presented. First, we present some specific mathematical concepts that are of major importance in this thesis and the notation that we use throughout the document.

The literature review starts with a section that presents the results regarding the theory and developments of decentralized control. In a second section, a short description of different approaches that have been presented in the context of cooperative control and especially those approaches that have been specifically presented for the case of satellite cooperative flight will be shortly described. A third section highlights papers that have considered in some extent the selection of different interconnection architectures. A fourth section presents the literature describing the special case of decentralized controllers describing coordination by cyclic pursuit algorithms and as a last section the developments and state of the art of research on electromagnetic formation flight technology will be discussed.

2.1 Background

In this section, we provide some definitions and results from matrix and graph theory.

2.1.1 Notation

This is the notation that will be used throughout the document. Let $\mathbb{R}_{>0}$ and $\mathbb{R}_{\geq 0}$ denote the positive and nonnegative real numbers, respectively, and denote as $\mathbb{R}(x)$ the real part(s) of the complex element x . Let I_n denote the identity matrix of size n ; we let A^\top and A^* denote, respectively, the transpose and the conjugate transpose of a matrix A . A block diagonal matrix with block diagonal entries A_i is denoted $\text{diag}[A_i]$. For an $n \times n$ matrix A , we let $\text{eig}(A)$ denote the set of eigenvalues of A , and we refer to its k th eigenvalue as $\lambda_{A,k}$, $k \in \{1, \dots, n\}$ (or simply as λ_k when there is no possibility of confusion). Also denote as λ_{max} the largest eigenvalue such that $\mathbb{R}(\lambda_{max}) \geq \mathbb{R}(\lambda_k)$ for all k .

The state of a single agent i is denoted by x_i which in general $x_i \in R^2$ and the overall state of the system will be denoted as $\mathbf{x} = [x_1^T, x_2^T, \dots, x_n^T]^T$. Additionally, let $j \doteq \sqrt{-1}$.

In general we consider a matrix A to be positive definite if $\lambda_{(A+A^\top),k} > 0$ for all k and denote it as $A > 0$. Similarly, a matrix A is said to be positive semi-definite if $\lambda_{(A+A^\top),k} \geq 0$ and is denoted as $A \geq 0$.

Definition 2.1.1 Flow-invariant manifolds

A flow invariant manifold \mathcal{M} of a system $\dot{\mathbf{x}} = f(\mathbf{x})$ is a manifold such that if $x(t_o) \in \mathcal{M}$ then $\mathbf{x}(t > t_o) \in \mathcal{M}$. In this work flow invariant manifolds that can be described as the nullspace of a smooth operator $\bar{\mathbf{x}} \in \mathcal{M} \Rightarrow V(\bar{\mathbf{x}}, t) = 0, \frac{d}{dt}(V(\bar{\mathbf{x}}, t)) = 0$ are considered.

2.1.2 Kronecker product

Let A and B be $m \times n$ and $p \times q$ matrices, respectively. Then, the Kronecker product $A \otimes B$ of A and B is the $mp \times nq$ matrix

$$A \otimes B = \begin{bmatrix} a_{11}B & \dots & a_{1n}B \\ \vdots & & \vdots \\ a_{m1}B & \dots & a_{mn}B \end{bmatrix}.$$

If λ_A is an eigenvalue of A with associated eigenvector ν_A and λ_B is an eigenvalue of B with associated eigenvector ν_B , then $\lambda_A\lambda_B$ is an eigenvalue of $A \otimes B$ with associated eigenvector $\nu_A \otimes \nu_B$. Moreover: $(A \otimes B)(C \otimes D) = AC \otimes BD$, where A, B, C and D are matrices with appropriate dimensions.

2.1.3 Determinant of block matrices

If A, B, C and D are matrices of size $n \times n$ and $AC = CA$, then:

$$\det \left(\begin{bmatrix} A & B \\ C & D \end{bmatrix} \right) = \det(AD - CB). \quad (2.1)$$

2.1.4 Rotation matrices

A rotation matrix is a real square matrix whose transpose is equal to its inverse and whose determinant is $+1$. The eigenvalues of a rotation matrix in two dimensions are $e^{\pm j\alpha}$, where α is the magnitude of the rotation. The eigenvalues of a rotation matrix in three dimensions are 1 and $e^{\pm j\alpha}$, where α is the magnitude of the rotation about the rotation axis; for a rotation about the axis $(0, 0, 1)^T$, the corresponding eigenvectors are $(0, 0, 1)^T, (1, +j, 0)^T, (1, -j, 0)^T$. Denote $R(\alpha)$ or R_α a rotation matrix of angle α .

2.1.5 Circulant matrices

A circulant matrix C is an $n \times n$ matrix having the form

$$C = \begin{bmatrix} c_0 & c_1 & c_2 & \dots & c_{n-1} \\ c_{n-1} & c_0 & c_1 & \dots & \vdots \\ \vdots & & & & c_1 \\ c_1 & c_2 & \dots & \dots & c_0 \end{bmatrix} \quad (2.2)$$

The elements of each row of C are identical to those of the previous row, but are shifted one position to the right and wrapped around. The following theorem summarizes some of the properties of circulant matrices.

Theorem 2.1.2 (Adapted from Theorem 7 in [28]) *Every $n \times n$ circulant matrix C has eigenvectors*

$$\psi_k = \frac{1}{\sqrt{n}} (1, e^{2\pi jk/n}, \dots, e^{2\pi jk(n-1)/n})^T, \quad k \in \{0, 1, \dots, n-1\}, \quad (2.3)$$

and corresponding eigenvalues

$$\lambda_k = \sum_{p=0}^{n-1} c_p e^{2\pi jkp/n}, \quad (2.4)$$

and can be expressed in the form $C = U\Lambda U^*$, where U is a unitary matrix whose k -th column is the eigenvector ψ_k , and Λ is the diagonal matrix whose diagonal elements are the corresponding eigenvalues. Moreover, let C and B be $n \times n$ circulant matrices with eigenvalues $\{\lambda_{B,k}\}_{k=1}^n$ and $\{\lambda_{C,k}\}_{k=1}^n$, respectively; then,

1. C and B commute, that is, $CB = BC$, and CB is also a circulant matrix with eigenvalues $\text{eig}(CB) = \{\lambda_{C,k} \lambda_{B,k}\}_{k=1}^n$;
2. $C + B$ is a circulant matrix with eigenvalues $\text{eig}(C + B) = \{\lambda_{C,k} + \lambda_{B,k}\}_{k=1}^n$.

From Theorem 2.1.2 all circulant matrices share the same eigenvectors, and the same matrix U diagonalizes all circulant matrices.

2.1.6 Block rotational-circulant matrices

The set of matrices that can be written as $L \otimes R$ where $L \in \mathbb{R}^N$ is a circulant matrix and $R \in \mathbb{R}^3$ is a rotation matrix about a fixed axis all belong to a group of matrices denoted in this thesis as \mathcal{CR} .

Lemma 2.1.3 *The set \mathcal{CR} forms a commutative matrix algebra. That is, for any two matrices $A, B \in \mathcal{CR}$*

1. *A and B commute, that is, $AB = BA$, and $AB \in \mathcal{CR}$ with eigenvalues $\text{eig}(AB) = \{\lambda_{A,k} \lambda_{B,k}\}_{k=1}^n$;*
2. *$(A + B) \in \mathcal{CR}$ with eigenvalues $\text{eig}(A + B) = \{\lambda_{A,k} + \lambda_{B,k}\}_{k=1}^n$.*

The proof is based on the fact that all \mathcal{CR} matrices are diagonalizable by the same matrix T of linearly independent eigenvectors and is shown in appendix A.1.

2.1.7 Graph representation of multi-agent systems

This section presents a short review of the approach to the description of the interaction topology using graphs commonly used in the literature of cooperative control (adapted from [77]).

A weighted graph can be mathematically described of a node set $\mathcal{V} = \{1, 2, \dots, n\}$, an edge set $\mathcal{E} \subseteq \mathcal{V} \times \mathcal{V}$ and an adjacency matrix $A = [a_{ij}] \in \mathbb{R}^{n \times n}$.

The interaction topology of a network of agents is commonly considered to be represented by a graph $\mathcal{G} = (\mathcal{V}, \mathcal{E})$, where the set of nodes are the vehicles and the edges denote the interconnection between vehicles. An edge (i, j) denotes the fact that vehicle j can obtain information regarding the state of vehicle i . For the case of an undirected graph $(i, j) \in \mathcal{E}$ implies $(j, i) \in \mathcal{E}$. The weighted adjacency matrix A is defined such that a_{ij} is a positive quantity if $(j, i) \in \mathcal{E}$ and 0 otherwise.

A tree is a graph such that every node has exactly one incoming edge except for one node. A spanning tree is a tree that reaches every node of the graph. The neighbors of agent i are denoted by $\mathcal{N}_i = \{j \in \mathcal{V} : (i, j) \in \mathcal{E}\}$. Several similar definitions are presented in the literature for the Laplacian matrix. Commonly the Laplacian is defined as the normalized

matrix $L = [l_{ij}]$ such that:

$$L = \begin{cases} l_{ii} = 1 \\ l_{ij} = \frac{-a_{ij}}{\sum_{j \neq i} a_{ij}} \quad i \neq j \end{cases} \quad (2.5)$$

L has always a 0 eigenvalue with eigenvector $\mathbf{1}_n$, where $\mathbf{1}_n = \{1, 1, \dots, 1\} \in \mathbb{R}^n$ and it has multiplicity 1 if and only if the graph contains a spanning tree.

2.1.8 Contraction theory

The work of Lohmiller & Slotine [47], Pham & Slotine [68] and Chung & Slotine [19] have laid the groundwork for the development of control approaches based on contraction theory. The main result of contraction theory can be summarized in the following theorem:

Theorem 2.1.4 *Contraction [68]* Consider in \mathbb{R}^n , the deterministic system

$$\dot{x} = \mathbf{f}(\mathbf{x}, t) \quad (2.6)$$

where \mathbf{f} is a smooth nonlinear function. Denote the Jacobian matrix of \mathbf{f} with respect to \mathbf{x} as $\frac{\partial \mathbf{f}}{\partial \mathbf{x}}$. If there exists a square invertible matrix $\Theta(\mathbf{x}, t)$ such that $\Theta(\mathbf{x}, t)^T \Theta(\mathbf{x}, t)$ is uniformly positive definite and the matrix:

$$\mathbf{F} = \left(\dot{\Theta} + \Theta \frac{\partial \mathbf{f}}{\partial \mathbf{x}} \right) \Theta(\mathbf{x}, t)^{-1} \quad (2.7)$$

is uniformly negative definite, then all the system trajectories converge exponentially to a single trajectory. The system is said to be contracting.

Based on the contraction results, Pham and Slotine extended the theory to convergence to flow invariant subspaces. A main result that defines the partial contraction theory is presented [68] in the following:

Theorem 2.1.5 *Partial contraction [68]* Consider a flow-invariant subspace \mathcal{M} and associated orthonormal projection matrix V . A particular solution $\mathbf{x}_p(t)$ of the system 2.6 converges exponentially to \mathcal{M} if the system

$$\dot{\mathbf{y}} = V\mathbf{f}(V^\top \mathbf{y}, t) \quad (2.8)$$

is contracting with respect to \mathbf{y} . If the above condition is fulfilled for all \mathbf{x}_p then starting from initial conditions, all trajectories of the system will exponentially converge to \mathcal{M} .

This last theorem is shown to have important implications in defining a framework for convergence to manifolds, where the positive definiteness of a projected Laplacian is a sufficient condition to show convergence to specific manifold, with results that can be extended to nonlinear systems.

2.1.9 Decentralized systems theory

Fueled by research in economics, the decentralized control problem was initially formulated by the end of the 1950's and later reexamined in the 1970's in the context of linear systems. The work by Aoki [5] is one of the first references to discuss the stabilization of decentralized linear time invariant dynamical systems. He defines decentralized systems as “dynamical systems with several controllers, each operating on the system with partial information on the states of the system”.

Additionally its work mentions a key characteristic of this type of systems: “In decentralized systems, a realistic assumption must therefore be made that no control agent possesses the complete descriptions of the systems to be controlled and of the environments in which the systems are to operate. Since each agent possesses a different set of information on the true system state, it is possible for the system to become unstable in the absence of communication among control agents”.

The decentralized control theory deals essentially with the problem of defining controllers

K_i that stabilize the system

$$\dot{x} = Ax + \sum B_i u_i \quad (2.9)$$

$$y_i = C_i x \quad (2.10)$$

where the information available to u_i is assumed to be:

$$I_i(t) = \{y_i(\eta), u_i(\zeta) : \eta \in [0, t], \zeta \in [0, t]\} \quad (2.11)$$

Given the classic motivation of the problem as the interaction of a coupled system through individual control stations, the general problem considers coupling through the A , B or C matrices and is generally described as the problem of multiple control stations.

In general the theory of decentralized control has focused on the problem where the system is interconnected through their non-actuated dynamics instead of through the control.

It has been long known that the synthesis of controller for a linear system under a decentralized scheme is in general a non-convex problem. Constraining the structure of the controller results in nonlinear constraints that make the problem non-convex. Recent development studying the optimality of decentralized controllers have derived conditions on the structure of the problem that hold optimality. Work by Rotkowitz and Lall [80] has proposed a property dubbed “Quadratic Invariance”, namely that $KGK \in S$ for all $K \in S$, where K and G are the controller and plant transfer functions respectively. This property is shown to be a sufficient condition for convexity of the problem. A more recent work by Motee et al. [56] describes structures for which the problem holds convexity properties.

2.2 Decentralized Approach to Multivehicle Cooperative Control

Several approaches have been described in the literature to design control laws for achieving decentralized cooperative control of multivehicle systems, among them navigation or potential functions, leader follower strategies, behavior based, flocking, graph description and consensus mechanisms.

2.2.1 Potential functions and behavioral approaches

The research on potential functions approach is based on the basic idea of setting up a control law that is the gradient of some potential (or navigation) function that has minimum(a) at the desired target(s), then, the equilibrium is found when a specific configuration is achieved and the gradients of the navigation functions are zero.

One of the seminal papers on navigation functions was presented by Koditschek in the early 1990's [37] and one of the first publications considering this methods in the case of a formation of satellites was presented by McInnes [53]. He presents a cooperative control strategy for stationkeeping a constellation of satellites in a circular orbit around earth. By using a scalar artificial potential function he shows the convergence to the desired configuration.

In the context of cooperative control, Ogren et al. [59] presented artificial potential functions as a method for coordination of multiple vehicles. Olfati-Saber and Murray [64] introduced a more complete mechanism to define a potential function approach that guarantees collision-free stabilization of a system of multiple vehicles to an unambiguous formation based on only distance measurements. More recent research by Dimarogonas et al. [21–23] presents a similar approach by defining navigation functions with sufficient properties to guarantee convergence of multiple agents while capturing multi-agent proximity situations. Other recent work [111], approaches the problem of maintaining formation while avoiding obstacles,

including cases when the environment is time varying [48], by using potential functions. Izzo and Petazzi [30] also presented a related work to achieve several types of formations based on a behavioral approach.

An approach similar in objective to the initial part of this thesis has been recently presented by Sepulchre *et al.* and Paley *et al.* [66,88] using a potential function methodology to stabilize parallel formations or circular formations. Their work considers general interconnection topologies, however, the analysis is restricted to dynamics of unicycle agents with constant speed and the convergence results for their work are only local.

2.2.2 Multiple instantiations of the state

Another relevant topic presented in the literature refers to addressing the cooperative control problem by implementing individual controllers on each vehicle based on estimation of the full state of the formation, thus the control is reduced to defining a MIMO controller for the full state knowledge on each agent. In this case the decentralization effects are not present in the controller but in the state estimation.

Several authors have addressed this problem under different assumptions. Carpenter [14] implements Speyer's work for the case of formation flight. In Speyer's work [97] the problem of defining optimal LQG decentralized controllers is presented where the agents share measurement and control information with each other and each one produces its own control based on its local Kalman best estimate. An elaborate communication network where a link is drawn to every other node forming a total of $n(n - 1)/2$ links is considered with the objective that the controllers can be computed using the best estimate of the state of the system given the information from all the sensors.

The work by Smith and Hadaegh [93,95], addresses the issue of having on each vehicle, parallel estimators that calculate a best estimate of the full state of the system, but also the option of implementing equivalent copies of a centralized controller on each spacecraft which has enough measurements to reconstruct the state of the formation [94].

2.2.3 Consensus problem and approach to formation control

A more recent approach to the cooperative control problem has arisen from the perspective of consensus. The consensus problem in networks of agents describes the problem of achieving agreement with respect to a quantity of interest by exchanging information within other agents.

Olfati-Saber et al. [62, 63] present a very comprehensive review of the literature in the topic. Here, we briefly discuss contributions that build up the consensus approach and the connection to the cooperative control problem.

In the most common approach to formation flight, the distributed control methods are based on tracking relative states with respect to other vehicles. For a set of n agents with state described by the variable $x_i, i \in \{1, \dots, n\}$. The most basic description of such approach considers the system [60]:

$$\dot{\mathbf{x}}_i = \mathbf{u}_i \quad (2.12)$$

$$\mathbf{u}_i = \sum_{j \in \mathcal{N}_i} k_{ij}(\mathbf{x}_j - \mathbf{x}_i - h_{ij}(t)) \quad (2.13)$$

The underlying idea in this case is the fact that each vehicle tracks a position with respect to a set of neighbors. This is actually an instantiation of the consensus problem [62].

The consensus problem appears initially in the context of distributed computing but has become increasingly popular and has been translated to many other areas of research. This framework is used to address multiple related problems like collective behavior of flocks and swarms, sensor fusion, random networks, synchronization of coupled oscillators, algebraic connectivity of complex networks, asynchronous distributed algorithms, formation control for multi-robot systems, optimization-based cooperative control, dynamic graphs, complexity of coordinated tasks, and consensus-based belief propagation in Bayesian networks (for references of publications on those topics refer to [62]).

Among the most commonly studied consensus protocols is the linear protocol for the

network of n first order systems $\dot{x}_i = u_i$:

$$u_i = \sum_{j \in \mathcal{N}_i} k_{ij} (x_j(t) - x_i(t)) \quad (2.14)$$

then, the dynamics of the overall system can be written as:

$$\dot{x} = -kLx \quad (2.15)$$

where L is the graph Laplacian in eq. 2.5. Since, $\mathbf{1}_n$ is an eigenvector of the system, if all eigenvalues except the zero eigenvalue are in the Right Hand Plane (RHP) and the graph is connected, it is straightforward to show that $x = (\alpha, \alpha, \dots, \alpha)$ is a solution to the system, moreover it can be shown that for balanced graphs $\alpha = 1/N \sum_i x_i(0)$. An offset b_i can be added to the coordinates such that the equilibrium reaches some desired relative states $x_i - x_j = b_i - b_j = h_{ij}$.

This control approach generalizes to any type of interconnection topologies and has been widely studied. However, the coordination to formation is done through the vector differences $h_{ij} = b_j - b_i$ which need to be coordinated via some mechanism throughout the whole formation, and constrains the formation to an specific instantiation of its structure.

Consensus protocols for double integrators have also been presented in the literature, (modified from [77]):

$$\ddot{x}_i = u_i \quad (2.16)$$

$$u_i = - \sum_{j \in \mathcal{N}_i} k_{ij} [(x_j(t) - x_i(t)) + \gamma (\dot{x}_j(t) - \dot{x}_i(t))] \quad (2.17)$$

The work of Fax and Murray [24] was one of the first introductions of the problem of consensus in the context of cooperative control. The problem of consensus as an alignment problem was studied by Jadbabaie [31] in a paper presenting a formal analysis to the flocking model used by Vicsek et al. [106] where simulations of a simplified model were used to study the

self-ordered motion in systems of particles with biologically motivated interaction. Extending Jadbabaie's work, Olfati-Saber [60] presented results that connect results of flocking behavior to the consensus problem.

Moreau [55] presented an analysis for the specific case of consensus for convex mappings. His idea generalizes consensus results to the most general types of protocols that satisfy convexity assumptions. These protocols are shown to embrace a great variety of cases including consensus over stochastic matrix protocols, nonlinear synchronization protocols, time varying graphs, swarming and flocking models. An extension to Moreau's work was recently presented by Angeli and Blimman [4] which includes the possibility of arbitrary bounded time-delays and relaxes the convexity assumption to simply mappings that strictly decrease the diameter of a set-valued Lyapunov function.

Ren and Beard [71, 78] considered the problem of information consensus in the presence of limited and unreliable information exchange with dynamically changing topologies with an important result, showing that, consensus can be asymptotically achieved under time switching graphs if the union of the directed interaction graphs have a spanning tree frequently enough as the time topology changes in time. This result defines in a more direct way similar ones presented in the results by Moreau [55] and Olfati-Saber [61].

In the extension of consensus to the case of second order systems is presented by Ren and Atkins [74, 77], the authors introduced consensus protocols when knowledge of derivatives of the disagreement are available and assume double integrator dynamics. They show that in that case, unlike the first-order dynamics case, having a spanning tree is a necessary rather than a sufficient condition for consensus and the cases of bounded control input, lack of knowledge of relative velocities and partial knowledge of the reference state is known are considered. An important result concerning this last case is that consensus is reached asymptotically if and only if the reference state flows to all of the vehicles in the team.

Lafarriere's [40] approach to stabilization of vehicle formations using the consensus approach for second order systems presents some parallel results considering a more general

structure, showing a direct relationship between the rate of convergence to the desired formation and the eigenvalues of the Laplacian matrix.

2.2.4 Contraction analysis and synchronization

In an interesting more recent approach Chung and Slotine [17, 19] present tools of contraction analysis to synthesize control laws that achieve synchronized motion by introducing a unified synchronization framework for cooperative control problems. This work considers an approach similar to consensus while following a desired trajectory but generalizes the results from [74] to a much more extensive type of dynamical systems. In their approach, a matrix dubbed the influence matrix is related to a Laplacian, but it does not have zero eigenvalues. The convergence properties are presented in terms of necessary conditions for contracting mappings. These results are shown to be useful for satellite attitude coordination as well.

2.2.5 Cyclic pursuit

An approach that has received recent attention in the context geometric pattern formation is the cyclic pursuit algorithm. Such an approach is attractive since it is distributed and requires the minimum number of communication links (n links for n agents) to achieve a formation.

Justh et al. [33] presented two strategies to achieve, respectively, rectilinear and circle formation; their approach, however, requires all-to-all communication among agents.

Lin et al. [45] exploited cyclic pursuit (where each agent i pursues the next $i+1$, modulo n) to achieve alignment among agents, while Marshall et al. in [51, 52] extended the classic cyclic pursuit to a system of wheeled vehicles, each subject to a single non-holonomic constraint, and studied the possible equilibrium formations and their stability.

Pavone and Frazzoli [67] developed distributed control policies for convergence to symmetric formations for ground non-holonomic robots. The key characteristics of that approach

are the proof of global stability and exponential convergence formations, namely rendez-vous to a single point, circles, and logarithmic spirals.

Their work consider n ordered mobile agents in the plane, with positions at time $t \geq 0$ denoted $\mathbf{x}_i(t) = [x_{i,1}(t), x_{i,2}(t)]^T \in \mathbb{R}^2$, $i \in \{1, 2, \dots, n\}$, where agent i pursues the next $i + 1$ modulo n .

The dynamics of each agent are considered a simple integrator:

$$\begin{aligned}\dot{\mathbf{x}}_i &= \mathbf{u}_i, \\ \mathbf{u}_i &= R(\alpha)(\mathbf{x}_{i+1} - \mathbf{x}_i),\end{aligned}\tag{2.18}$$

where $R(\alpha)$, $\alpha \in [-\pi, \pi)$, is a rotation matrix. They describe as $\mathbf{x} = [\mathbf{x}_1^T, \mathbf{x}_2^T, \dots, \mathbf{x}_n^T]^T$; the dynamics of the overall system which can be written in compact form as $\dot{\mathbf{x}} = \hat{A} \mathbf{x}$, and prove that:

Theorem 2.2.1 $\hat{A}(\alpha)$ has exactly two zero eigenvalues, and

1. if $0 \leq |\alpha| < \pi/n$, all non-zero eigenvalues lie in the open left-half complex plane;
2. if $|\alpha| = \pi/n$, two non-zero eigenvalues lie on the imaginary axis, while all other non-zero eigenvalues lie in the open left-half complex plane;
3. if $\pi/n < |\alpha| < 2\pi/n$, two non-zero eigenvalues lie in the open right-half complex plane, while all other non-zero eigenvalues lie in the open left-half complex plane;

After proving that the matrix \hat{A} is diagonalizable it is straightforward to show that agents starting at any initial condition (except for a set of measure zero) in \mathbb{R}^{2n} and evolving under (2.18) exponentially converge:

1. if $0 \leq |\alpha| < \pi/n$, to a single limit point, namely their initial center of mass;
2. if $|\alpha| = \pi/n$, to an evenly spaced circle formation;

3. if $\pi/n < |\alpha| < 2\pi/n$, to an evenly spaced logarithmic spiral formation.

These results are derived for agents operating in \mathbb{R}^2 and with a single-integrator dynamics, (ii) the center of mass is determined by the initial positions of the agents, and (iii) the radius of a circular formation is also determined by the initial positions of the agents.

Ren [73, 75] has recently presented an approach that generalizes this work by considering the problem as *coordinate coupling*, and representing the dynamics by using kronecker product properties. In particular, the fact mentioned in 2.1.2 is used and the case of general type of interconnections is studied by analyzing the location of the eigenvalues of the system $L \otimes R$, where L is the interconnection Laplacian and R is the rotation matrix.

2.2.6 Spacecraft formation control

A review of the literature for the different proposed implementations of cooperative control presented in the context of spacecraft cooperative flight includes the work detailed in this section.

Wang and Hadaegh's [108] work present one of the first approaches to the application of cooperative control in the context of the satellite formations. In this seminal work they studied different schemes to generate a desired formation and derived control laws based on nearest neighbor tracking, borrowing concepts of cooperative control that had been maturing on other fields, especially from ground robotics.

The work of Kapila et al. [36] studies leader-follower configurations in the context of Clohessy-Wiltshire dynamics. The authors define control strategies based on linear pulsed control where LQ or pole placement strategies are setup based on the discrete state transformation matrix of the dynamics. Their results are mainly illustrative simulations showing the control performance.

Kang et al. [35], proposed a different approach to formation control derived from previous approaches in the context of ground robots. In their work, an error function is defined as a

function of a parameter s . This parameter itself depends on some function of the state, for example the state of a leader or more general cases where the dependence is on relationships of the state of the formation. The stability analysis is based on Lyapunov methods.

The work by Folta and Quinn [26] addresses the formation problem in a more straightforward implementation for a leader/follower architecture defining intermediate transition states and using state transition matrices to solve for open loop δV impulses to reach the next step until eventually reduce the error to the desired state. In [104], Ulybishev considers an LQR design based on the description of a formation of satellites using two planar parameters ΔV and ΔT that describe the state on a circular orbit.

In the work by Carpenter [14, 15], one of the first approaches to decentralized formation control is presented. In his paper, Speyer's framework [97] is applied to the specific case of formation of satellites. It is however a very complete study and presents a framework for decentralized spacecraft formation control to be further studied.

The work by Beard et al. [6, 7] presents an important framework that generalizes other architectures by considering 3 levels of control in formation flight coordination. Their consideration is that at the highest level of abstraction, the agents must coordinate the subtask. At the next level there should be a mechanism to coordinate the motion of the vehicles to achieve the desired objective of the task, and at the lower level, a controller that makes each spacecraft be consistent with the desired coordination mechanism is to be implemented. In particular, Lyapunov analysis is performed to define a controller that would converge to achieve the objective.

An interesting point is presented in the work of Beard et al. [7] on differences between three approaches in the literature: "In leader-following, coordination is achieved through shared knowledge of the leaders states. In the behavioral approach, coordination is achieved through shared knowledge of the relative configuration states. In the virtual structure approach, coordination is achieved through shared knowledge of the states of the virtual structure"

In the work by Lawton, [42, 43], proportional derivative controller approaches are derived to achieve convergence are based on Lyapunov analysis. The target locations are specified by linear transformations which allow for a clear presentation of their convergence properties.

In the work by Queiroz [69], an adaptive control scheme is proposed for coordination of multiple satellites in a Leader/Follower(s) architecture.

The work by Fax [24, 25] presents a valuable analysis of necessary conditions for stability. This work is one of the first publications where a direct connection between the information topology and the stability conditions of the system are presented. It presents results which define stability conditions in terms of the eigenvalues of the Laplacian matrix when assuming an identical copy of the control used on each vehicle. At the same time, Fax's work discusses the importance of coordination as flow of information in the improvement of performance.

The work by Mebashi and Hadaegh [54] established important guidelines for Leader/Follower assignments by expressing the information structure as a directed graph. Their work restricts to a type of "proper leader/follower configurations" where each follower has at most one leader. The design of a decentralized controller design is expressed as a *LMI* where the particular structure of the matrix K is considered and the gains are obtained by solving a Lyapunov inequality.

The work by Schaub and Alfriend [84] considered impulsive maneuvers to control orbital parameters in order to maintain the formation. Related to this approach, the work by Tillerson [102, 103] considers the control of a formation by solving a linear programming problem to calculate the set of impulses that minimizes a linear cost function while achieving the final boundary conditions.

In the work by Smith and Hadaegh [91], control using relative positions as states was studied and a family of equivalent controllers is defined such that a topology switch strategy can be presented. This approach assumes that each vehicle can have enough knowledge of the other vehicles to reconstruct the full state of the formation.

Tanner et al. [99, 100] studied the problem from the perspective of input-output stability

from a leader input to internal state of the formation and characterizes the way this input affects stability performance. In a more generalized version based on this approach Açikmeşe et al. [1] formulate the problem of I/O stability via control interactions between the spacecraft. This formulation is shown to be useful in characterizing disturbance propagation as a function of the partition interconnection topology. In their work, the authors present a very inclusive analysis of stability of formation with important conclusions regarding the performance of different architectures. Necessary conditions for stability are presented, extending some of the concepts of Input-Output stability initially studied by Sontag and Wang [96] and applying stability analysis by defining conditions for bounded performance in terms of bounded strictly increasing gain functions of the state and the disturbances. Additionally, they present a frequency domain criteria for stability in terms of Linear Matrix Inequalities that is proven helpful to identify stability and disturbance attenuation in terms of the interconnection.

Ren [71, 78] presented the idea of using a decentralized version of the virtual structure originally presented by [6] but proposed an implementation that would not require a centralized unit, instead, the reference frame of the formation would be defined by agreement through consensus protocols using inter-vehicle communication.

In the work of Chung [17] contraction theory and synchronization approach is proposed for achieving regularly spaced spacecraft formations in the context of a multi-satellite formation with arbitrary number of spacecraft converging into a common time-varying trajectory.

2.2.7 Electromagnetic formation flight

The research on electromagnetic formation flight is relatively new and is in an early stage of its development. It has been proposed as a propellantless technology able to control the relative motion in a formation of spacecraft [38]. Kaneda et al. [34] also proposed and tested the use of electromagnets to generate forces between vehicles.

The main equations that describe Electromagnetic Formation Flight (EMFF)'s principle

of operation is:

$$\mathbf{F}_i^{EM} = \sum_{j \neq i}^n f_{i,j}^{EM} \quad (2.19)$$

where:

$$f_{i,j}^{EM}(\boldsymbol{\mu}_i, \boldsymbol{\mu}_j) = \frac{3\mu_o}{4\pi} \left(-\frac{\boldsymbol{\mu}_i \cdot \boldsymbol{\mu}_j}{|\mathbf{d}_{ij}|^5} \mathbf{d}_{ij} - \frac{\boldsymbol{\mu}_i \cdot \mathbf{d}_{ij}}{|\mathbf{d}_{ij}|^5} \boldsymbol{\mu}_j - \frac{\boldsymbol{\mu}_j \cdot \mathbf{d}_{ij}}{|\mathbf{d}_{ij}|^5} \boldsymbol{\mu}_i + 5 \frac{(\boldsymbol{\mu}_i \cdot \mathbf{d}_{ij})(\boldsymbol{\mu}_j \cdot \mathbf{d}_{ij})}{|\mathbf{d}_{ij}|^7} \mathbf{d}_{ij} \right) \quad (2.20)$$

represents the electromagnetic force caused by dipole j to dipole i , where $\boldsymbol{\mu}_i$ is the dipole vector generated by currents running in the coils of vehicle i , μ_o is the permeability constant, \mathbf{d}_{ij} is the relative position vector between vehicles and \mathbf{F}_i^{EM} is the electromagnetic force acting vehicle i . The force on each vehicle is coupled to the force on each one of the others by its dependence on the dipoles of the other vehicles in the formation.

Kwon presented an analysis of its feasibility [39], which demonstrated favorable capabilities in several mission scenarios as compared to propulsion systems that require expendables for their operation.

The Space Systems Laboratory at MIT has built a 2D testbed for this technology and tested control algorithms that have demonstrated controllability to achieve different maneuvers [44].

An analysis of the dynamics of EMFF and the initial approaches to control strategies were presented by Schweighart and Ahsun & Miller [2,87]. Ahsun and Miller [3] presented an adaptive control method to deal with uncertainties in the model and proposed a dipole switching strategy to deal with the effects of Earth magnetic field causing angular momentum-build up in low Earth orbiting systems.

The control strategies so far proposed require a centralized unit to solve for the dipole setup that achieves the desired forces by simultaneously solving the set of n nonlinear equa-

tions. [3]. In such a control scheme, these equations are to be solved at every control period and the results are to be communicated to each other vehicle in real time.

2.3 Summary and Gap Analysis

The decentralized control problem has been widely studied for several decades. There is not however, a straightforward answer to the synthesis of decentralized controllers. Research in the last decade has considered the correlation between the decentralized control problem and the consensus problem, a widely studied problem in the literature in different fields. One of the most commonly accepted approaches to decentralized formation flight control is the control of relative state with respect to some neighbors. The basics of such approach can be analyzed with tools of consensus theory.

However, a control approach where there is not a need in coordination of the relative offsets for each neighbor can be desired and useful in many situations. Control approaches that are not based on tracking relative trajectories while still achieving the desired geometry have been studied. Some authors have considered potential functions, and more recently a cyclic pursuit approach in the context of ground robots. Such approaches can be useful for the specific case of formation flying space missions.

The most essential gap identified in the literature, for which this thesis presents a contribution, is the approach to design spacecraft formation flight controllers not based on relative trajectory tracking but on convergence to a manifold.

It is also identified that as a first step in such direction, an extension of the cyclic pursuit to the dynamics of spacecraft formation flight can be used. All previous work on cyclic pursuit consider planar and the analysis has been restricted to single integrator dynamics. As part of extending the approach to more useful applications, the extension to generalized trajectories and types of formations are also identified as missing elements.

Another identified gap is the lack of results for global convergence approached to 'splay-

state' formations, e.g. regular formations with equally spaced separations of a given size and the development of a theoretical approach that can use those results as building block to generalize the cyclic pursuit approaches.

And finally, the lack of approaches that can be used to decentralize Electromagnetic Formation Flight or reduce its dependence on a central computing unit.

Chapter 3

Cyclic Pursuit Controllers for Spacecraft Formation Applications

3.1 Introduction

In the context of formation flight, the problem of formation of *geometric patterns* is of particular interest. Engineering applications of this problem include distributed sensing using mobile sensor networks, and space missions with multiple spacecraft flying in formation, the major focus of this thesis. Within the robotics community, many distributed control strategies have been recently proposed for convergence to geometric patterns as was mentioned in the literature review in chapter 2. Several authors have addressed the idea of using distributed controllers to converge to patterns, exploiting cyclic pursuit approaches (where each agent i pursues the next $i + 1$, modulo n) with extension to non-holonomic planar vehicles, and studied the possible equilibrium formations and convergence to patterns as equilibrium of artificial potential functions.

The problem of formation of geometric patterns has been the subject of intensive research efforts also within the aerospace community. In an authoritative survey paper on formation flying [83], Scharf *et al.* propose a division of formation flying architectures into

three main classes, namely: (i) Multiple-Input Multiple-Output (MIMO), in which the formation is treated as a single multiple-input, multiple-output plant, (ii) Leader/Follower, in which individual spacecraft controllers are connected hierarchically, and (iii) cyclic, in which individual spacecraft controllers are connected non-hierarchically. According to Scharf *et al.*, by allowing non-hierarchical connections between individual spacecraft controllers, cyclic algorithms can perform better than Leader/Follower algorithms, and can distribute control effort more evenly. Moreover, cyclic algorithms are generally more robust than MIMO algorithms, for which a local failure can have a global effect [83]. Finally, cyclic algorithms can also be completely decentralized in the sense that there is neither a coordinating agent nor instability resulting from single point failures [83]. The two primary drawbacks of cyclic algorithms are that the stability of these algorithms and their information requirements are poorly understood [83]; in particular, the stability analysis of cyclic algorithms is difficult since the cyclic structure introduces feedback paths.

Motivated by the previous discussion, the objective of the work presented on this chapter is to consider a class of cyclic algorithms for formation flight, for which a rigorous stability analysis is possible and for which the information requirements are minimal. The starting point is the previous work by Pavone and Frazzoli [67], where distributed control policies for ground mobile agents that draw inspiration from the simple idea of cyclic pursuit were developed which guarantee convergence to symmetric formations. The key features of such control laws [67] include global stability and the capability to achieve a variety of formations, namely rendez-vous to a single point, circles, and logarithmic spirals; moreover, those control laws are distributed and require the minimum number of communication links (n links for n agents) that a cyclic structure can have.

The organization of this chapter is as follows. In Section 3.2.1 we introduce basic concepts of the cyclic-pursuit control laws for single-integrator models in two dimensions. In Section 3.2 we extend our previous results along two directions: (i) in Section 3.2.1 we address the case in which agents move in \mathbb{R}^3 and it is desired to control the center of the formation, and

(ii) in Section 3.2.4 we study “robust” convergence to evenly-spaced circular formations with a prescribed radius. Then, in Section 3.3, we extend our control laws to double-integrator models in three dimensions. In particular, we develop control laws that only require *relative* measurements of position and velocity with respect to the two leading neighbors in the ring topology of cyclic pursuit, and allow the agents to converge from *any* initial condition (except for a set of measure zero) to a single point, an evenly-spaced circular formation, an evenly-spaced logarithmic spiral formation, or an evenly-spaced Archimedes’ spiral formation (an Archimedes’ spiral is a spiral with the property that successive turnings have a constant separation distance), depending on some tunable control parameters. Control laws that only rely on relative measurements are indeed of critical importance in deep-space missions, where global measurements may not be available. In Section 3.5 we discuss potential applications, including spacecraft formation for interferometric imaging and convergence to zero-effort orbits, and we argue that Archimedes’ spiral formations are very useful symmetric formations for applications. Finally, in Section 3.6 a summary of the chapter and conclusions are drawn.

3.2 Cyclic-Pursuit Control Laws for Single-Integrator Models

In this section, we extend the results in [67] in three directions: (i) we address the case in which agents move in \mathbb{R}^3 , (ii) we consider control of the center of the formation, and (iii) we study convergence to evenly-spaced circular formations with a prescribed radius. First issues (i) and (ii) are addressed.

3.2.1 Cyclic pursuit in three dimensions with control on the center of the formation

Let there be n ordered mobile agents in the space, their positions at time $t \geq 0$ denoted by

$$\mathbf{x}_i(t) = [x_{i,1}(t), x_{i,2}(t), x_{i,3}(t)]^T \in \mathbb{R}^3, \quad i \in \{1, 2, \dots, n\},$$

and let $\mathbf{x} = [\mathbf{x}_1^T, \mathbf{x}_2^T, \dots, \mathbf{x}_n^T]^T$. The dynamics of each agent are described by a simple vector integrator

$$\dot{\mathbf{x}}_i = k_g \mathbf{u}_i, \quad k_g \in \mathbb{R}_{>0}; \quad (3.1)$$

henceforth, without loss of generality, k_g can be assumed to be 1, since it is just a time scaling factor. Consider the following three-dimensional generalization of the cyclic-pursuit control law in equation (2.18):

$$\mathbf{u}_i = R(\alpha)(\mathbf{x}_{i+1} - \mathbf{x}_i) - k_c \mathbf{x}_i, \quad k_c \in \mathbb{R}_{\geq 0}, \quad (3.2)$$

where $R(\alpha)$, $\alpha \in [-\pi, \pi)$, is the rotation matrix (with rotation axis $(0, 0, 1)^T$ without loss of generality):

$$R(\alpha) = \begin{bmatrix} \cos \alpha & \sin \alpha & 0 \\ -\sin \alpha & \cos \alpha & 0 \\ 0 & 0 & 1 \end{bmatrix}. \quad (3.3)$$

The overall system can be written in compact form as

$$\dot{\mathbf{x}} = -(\mathcal{L} + k_c I_{3n}) \mathbf{x}, \quad (3.4)$$

where $\mathcal{L} = L_1 \otimes R(\alpha)$ and L_1 is a laplacian for 1-circulant topology:

$$L_1 = \begin{bmatrix} 1 & -1 & 0 & \dots & \dots \\ 0 & 1 & -1 & 0 & \dots \\ \vdots & \vdots & \vdots & \vdots & \vdots \\ -1 & 0 & \dots & 0 & 1 \end{bmatrix} \quad (3.5)$$

The analysis starts with the following theorem, that characterizes the spectrum of $-\mathcal{L}$.

Theorem 3.2.1 *$-\mathcal{L}$ has exactly three zero eigenvalues, and*

1. *if $0 \leq |\alpha| < \pi/n$, all non-zero eigenvalues lie in the open left-half complex plane;*
2. *if $|\alpha| = \pi/n$, two non-zero eigenvalues lie on the imaginary axis, while all other non-zero eigenvalues lie in the open left-half complex plane;*
3. *if $\pi/n < |\alpha| < 2\pi/n$, two non-zero eigenvalues lie in the open right-half complex plane, while all other non-zero eigenvalues lie in the open left-half complex plane.*

Moreover, $L \otimes R(\alpha)$ is diagonalizable for all $\alpha \in [-\pi, \pi)$ as described in appendix A.1.

Proof: By the properties of the Kronecker product, the $3n$ eigenvalues of $-\mathcal{L}$ are:

$$\begin{aligned} \lambda_k &= e^{2\pi jk/n} - 1, \\ \lambda_k^+ &= (e^{2\pi jk/n} - 1) e^{j\alpha}, \\ \lambda_k^- &= (e^{2\pi jk/n} - 1) e^{-j\alpha}, \end{aligned} \quad (3.6)$$

where $k \in \{1, \dots, n\}$. Note that for $k \in \{1, \dots, n-1\}$ the eigenvalues λ_k lie in the open left-half complex plane, while for $k = n$ we have $\lambda_n = 0$; moreover, the $2n$ eigenvalues $\{\lambda_k^\pm\}_{k=1}^n$ are the same as those in Theorem 2.2.1. Then, the claim follows from Theorem 2.2.1. \blacksquare

Corollary 3.2.2 *When $\alpha = \pi/n$, the two eigenvalues that lie on the imaginary axis are $\lambda_{n-1}^+ = -j 2 \sin(\pi/n)$ and $\lambda_1^- = j 2 \sin(\pi/n)$, with corresponding eigenvectors μ_{n-1}^+ and μ_1^- .*

When $\pi/n < \alpha < 2\pi/n$, the two eigenvalues with positive real part are λ_{n-1}^+ and λ_1^- , with corresponding eigenvectors μ_{n-1}^+ and μ_1^- ; moreover, the real parts of λ_{n-1}^+ and λ_1^- are both equal to $2 \sin(\pi/n) \sin(\alpha - \pi/n)$.

Proof: The proof reduces to a straightforward verification in equation (3.6). ■

Now the formations that can be achieved with control law (3.2) can be studied. The case with $k_c = 0$ and the case with $k_c > 0$ are separately studied.

3.2.2 Case $k_c = 0$, i.e., no control on the center of the formation.

Combining Theorem 3.2.1 and Corollary 3.2.2 (where, in particular, the eigenvectors corresponding to the dominant eigenvalues are explicitly given), it is easy to show (the arguments are virtually identical to those in Section 3.5 of [67] and are omitted in the interest of brevity) that agents starting at any initial condition (except for a set of measure zero) in \mathbb{R}^{3n} and evolving under (3.4) exponentially converge:

1. if $0 \leq |\alpha| < \pi/n$, to a single limit point, namely their initial center of mass;
2. if $|\alpha| = \pi/n$, to an evenly spaced circle formation, whose radius is determined by the initial positions of the agents;
3. if $\pi/n < |\alpha| < 2\pi/n$, to an evenly spaced logarithmic spiral formation.

The center of the formation is determined by the initial positions of the agents. Similar results have recently appeared in [76].

Remark 3.2.3 *When $k_c = 0$, the control law in equation (3.2) only requires the measurement of the relative position $(\mathbf{x}_{i+1} - \mathbf{x}_i)$; however, it uses a rotation matrix that is common to all agents. Hence, control law (3.2) requires that all agents agree upon a common orientation, but it does not require a consensus on a common origin.*

3.2.3 Case $k_c > 0$, i.e., control on the center of the formation.

The case $k_c > 0$ is studied now; in this case the center of the formation is no longer determined by the initial positions of the spacecraft, instead it always converges, exponentially fast, to the origin. In fact, when $k_c > 0$ the eigenvalues of $-L \otimes R(\alpha)$ are shifted toward the left-hand complex plane by an amount precisely equal to k_c , while the eigenvectors are left unchanged. Then, the following corollary is a simple consequence of Corollary 3.2.2.

Corollary 3.2.4 *Assume $k_c > 0$; then, if $0 \leq |\alpha| \leq \pi/n$, all of the eigenvalues are in the left-hand complex plane. If, instead, $\pi/n < |\alpha| < 2\pi/n$ we have*

1. *if $k_c > 2 \sin(\pi/n) \sin(\alpha - \pi/n)$, all of the eigenvalues are in the open left-hand complex plane;*
2. *if $k_c = 2 \sin(\pi/n) \sin(\alpha - \pi/n)$, two non-zero eigenvalues lie on the imaginary axis, while all other eigenvalues lie in the open left-hand complex plane;*
3. *if $k_c < 2 \sin(\pi/n) \sin(\alpha - \pi/n)$, two non-zero eigenvalues lie in the open right-hand complex plane, while all other eigenvalues lie in the open left-hand complex plane;*

Accordingly, by appropriately selecting α and k_c , the agents, starting at any initial condition (except for a set of measure zero) in \mathbb{R}^{3n} and evolving under (3.4), exponentially converge to the origin, or to an evenly spaced circle formation centered at the origin, or to an evenly spaced logarithmic spiral formation centered at the origin. Simulation results are presented in Figure 3-1, where 7 agents reach a circular formation centered at the origin.

Remark 3.2.5 *When $k_c > 0$, the control law in equation (3.2) requires that the agents agree on a common reference frame (i.e., both a common origin and a common orientation); in particular, each agent needs to measure its relative position ($\mathbf{x}_{i+1} - \mathbf{x}_i$) and know its absolute position \mathbf{x}_i .*

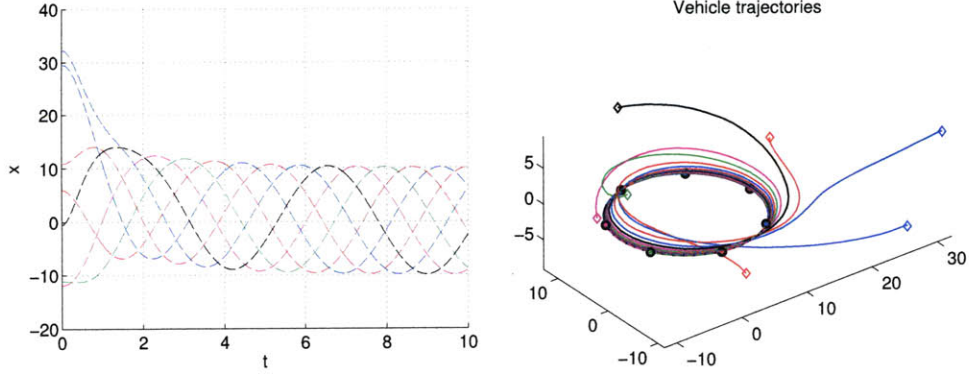


Figure 3-1: Convergence to circular trajectories centered at the origin. Left Figure: First coordinate as a function of time for each agent. Right Figure: Trajectories in 3D.

Remark 3.2.6 Note that the center of the formation can be chosen to be any point in \mathbb{R}^3 . Assume, in fact, that we desire a formation centered at $c \in \mathbb{R}^3$. Then, if we modify the control law (3.2) according to

$$\mathbf{u}_i = R(\alpha)(\mathbf{x}_{i+1} - \mathbf{x}_i) - k_c(\mathbf{x}_i - \mathbf{x}_c), \quad k_c \in \mathbb{R}_{>0}, \quad (3.7)$$

it is immediate to see that the center of the formation will converge exponentially to \mathbf{x}_c .

3.2.4 Convergence to circular formations with a prescribed radius

Circular trajectories occur only when two non-zero eigenvalues are on the imaginary axis and all other non-zero eigenvalues have negative real part, which makes this behavior not robust from a practical point of view. In this section we address the problem of *robust* convergence to a circular motion on a circle of *prescribed* radius around the (fixed) center of mass of the group, with all agents being evenly spaced on the circle. Here, by robust we mean that the circular formation is now a locally stable equilibrium of a non-linear system. The key idea is to make the rotation angle a function of the state of the system.

Specifically, let there be n ordered mobile agents in the plane, their positions at time $t \geq 0$ denoted by $\mathbf{x}_i(t) = [x_{i,1}(t), x_{i,2}(t)]^T \in \mathbb{R}^2$, $i \in \{1, 2, \dots, n\}$, where agent i pursues the

next $i + 1$ modulo n . The kinematics of each agent is described by

$$\begin{aligned}\dot{\mathbf{x}}_i &= k_g \mathbf{u}_i, \\ \mathbf{u}_i &= R(\alpha_i)(\mathbf{x}_{i+1} - \mathbf{x}_i),\end{aligned}\tag{3.8}$$

where the rotation angle α_i is now a function of the state of the system:

$$\alpha_i = \frac{\pi}{n} + k_\alpha (r - \|\mathbf{x}_{i+1} - \mathbf{x}_i\|), \quad k_\alpha, r \in \mathbb{R}_{>0}.\tag{3.9}$$

Without loss of generality, we assume $k_g = 1$. In equation (3.9) the constant k_α is a gain, while r is the desired inter-agent distance. Intuitively, if the agents are “close to each other” with respect to r , they will spiral out since $\alpha_i > \pi/n$; conversely, if they are “far from each other” with respect to r , they will spiral in since $\alpha_i < \pi/n$. It is easy to see that a *splay state formation* whereby all agents move on a circle of radius $r/(2 \sin(\pi/n))$ around the (fixed) center of mass of the group, with all agents being evenly spaced on the circle, is a *relative equilibrium* for the system. The next theorem shows that such equilibrium is locally stable.

Theorem 3.2.7 *A splay-state formation is a locally stable relative equilibrium for system (3.8) - (3.9).*

Proof: A sequence of coordinate transformations is first considered such that a splay-state formation is indeed an equilibrium point (and not a *relative equilibrium*). Consider the change of coordinates $\mathbf{p}_i \doteq \mathbf{x}_{i+1} - \mathbf{x}_i$, $i \in \{1, 2, \dots, n\}$. In the new coordinates, the system becomes (the index i is, as usual, modulo n)

$$\dot{\mathbf{p}}_i = R(\alpha_{i+1}) \mathbf{p}_{i+1} - R(\alpha_i) \mathbf{p}_i, \quad \text{where } \alpha_i = \frac{\pi}{n} + k_\alpha (r - \|\mathbf{p}_i\|).\tag{3.10}$$

By introducing polar coordinates, i.e., by letting the first coordinate $p_{i,1} = \varrho_i \cos \vartheta_i$ and the second coordinate $p_{i,2} = \varrho_i \sin \vartheta_i$, with $\varrho_i \in \mathbb{R}_{\geq 0}$ and $\alpha_i \in \mathbb{R}$, the system becomes, after some

algebraic manipulations (see Appendix A.2 for the details),

$$\dot{\varrho}_i = \varrho_{i+1} \cos((\vartheta_{i+1} - \vartheta_i) - \alpha_{i+1}(\varrho_{i+1})) - \varrho_i \cos(\alpha_i(\varrho_i)), \quad (3.11)$$

$$\dot{\vartheta}_i = \frac{\varrho_{i+1}}{\varrho_i} \sin((\vartheta_{i+1} - \vartheta_i) - \alpha_{i+1}(\varrho_{i+1})) + \sin(\alpha_i(\varrho_i)), \quad (3.12)$$

$$\alpha_i(\varrho_i) = \frac{\pi}{n} + k_\alpha (r - \varrho_i), \quad (3.13)$$

where we have made explicit the dependence of α_i on ϱ_i . Finally, by letting $\varphi_i = \vartheta_{i+1} - \vartheta_i$, we obtain

$$\dot{\varrho}_i = \varrho_{i+1} \cos(\varphi_i - \alpha_{i+1}(\varrho_{i+1})) - \varrho_i \cos(\alpha_i(\varrho_i)), \quad (3.14)$$

$$\dot{\varphi}_i = \frac{\varrho_{i+2}}{\varrho_{i+1}} \sin(\varphi_{i+1} - \alpha_{i+2}(\varrho_{i+2})) + \sin(\alpha_{i+1}(\varrho_{i+1})) - \frac{\varrho_{i+1}}{\varrho_i} \sin(\varphi_i - \alpha_{i+1}(\varrho_{i+1})) - \sin(\alpha_i(\varrho_i)), \quad (3.15)$$

$$\alpha_i(\varrho_i) = \frac{\pi}{n} + k_\alpha (r - \varrho_i). \quad (3.16)$$

Define $\varrho \doteq (\varrho_1, \dots, \varrho_n)^T$ and $\varphi \doteq (\varphi_1, \dots, \varphi_n)^T$; in the new system of coordinates ϱ - φ , a splay state formation corresponds to an equilibrium *point* $\varrho^* = (r, \dots, r)^T$ and $\varphi^* = (\frac{2\pi}{n}, \dots, \frac{2\pi}{n}, -\frac{2\pi(n-1)}{n})^T$. In compact form we write

$$\begin{bmatrix} \dot{\varrho} \\ \dot{\varphi} \end{bmatrix} = f(\varrho, \varphi). \quad (3.17)$$

The linearization of system (3.17) around the equilibrium point (ϱ^*, φ^*) is

$$\dot{\varrho}_i = \cos(\pi/n)(\varrho_{i+1} - \varrho_i) - k_\alpha r \sin(\pi/n)(\varrho_{i+1} + \varrho_i) - r \sin(\pi/n) \varphi_i, \quad (3.18)$$

$$\dot{\varphi}_i = (k_\alpha \cos(\pi/n) + \frac{1}{r} \sin(\pi/n))(\varrho_{i+2} - 2\varrho_{i+1} + \varrho_i) + \cos(\pi/n)(\varphi_{i+1} - \varphi_i). \quad (3.19)$$

Without loss of generality we set $r = 1$; the linearized system can be written in compact

form as

$$\begin{bmatrix} \dot{\varrho} \\ \dot{\varphi} \end{bmatrix} = \begin{bmatrix} a_n L_1 - 2k_\alpha s_n I_n & -s_n I_n \\ b_n L_1^2 & c_n L_1 \end{bmatrix} \begin{bmatrix} \varrho \\ \varphi \end{bmatrix} \doteq P \begin{bmatrix} \varrho \\ \varphi \end{bmatrix}, \quad (3.20)$$

where $s_n \doteq \sin(\pi/n)$, $c_n \doteq \cos(\pi/n)$, $a_n \doteq (k_\alpha s_n - c_n)$, $b_n \doteq k_\alpha c_n + s_n$, and L_1 is a 1-circulant laplacian described in eq. 3.5. The spectrum of P is characterized by the following Lemma.

Lemma 3.2.8 *The matrix P has $2n-3$ eigenvalues with negative real part, and 3 eigenvalues with zero real part. The eigenvalues with zero real part are $\lambda_1 = 0$, and $\lambda_{2,3} = \pm 2js_n$; the corresponding eigenvectors v_1 , v_2 and v_3 are:*

$$v_1 = (\mathbf{1}_n, -2k_\alpha \mathbf{1}_n)^T, \quad (3.21)$$

$$v_2 = (\psi_1, -2b_n e^{\pi j/n} \psi_1)^T, \quad (3.22)$$

$$v_3 = \bar{v}_2, \quad (3.23)$$

where $\mathbf{1}_n = (1, 1, \dots, 1)^T \in \mathbb{R}^n$, ψ_1 is the eigenvector for $k = 1$ in equation (2.3) and \bar{v} indicates the complex conjugate of v .

Proof: The proof of this lemma is presented in Appendix A.3. ■

System (3.17) is constrained to evolve on a subset of \mathbb{R}^{2n} . To see why this is the case, recall that from the definition of \mathbf{p}_i we have $\sum_{i=1}^n \mathbf{p}_i = 0$, or equivalently $\sum_{i=1}^n R(\vartheta_1) \mathbf{p}_i = 0$. In polar coordinates these constraints become $\sum_{i=1}^n \varrho_i \cos(\vartheta_i - \vartheta_1) = 0$ and $\sum_{i=1}^n \varrho_i \sin(\vartheta_i - \vartheta_1) = 0$. Thus, in the system of coordinates ϱ - φ , the following two constraints must hold at all time

$$g_1(\varrho, \varphi) = \sum_{i=1}^n \varrho_i \cos\left(\sum_{k=1}^{i-1} \varphi_k\right) = 0, \quad (3.24)$$

$$g_2(\varrho, \varphi) = \sum_{i=1}^n \varrho_i \sin\left(\sum_{k=1}^{i-1} \varphi_k\right) = 0. \quad (3.25)$$

Moreover, by definition of φ , the following constraint must hold at all time

$$g_3(\varrho, \varphi) = \sum_{i=1}^n \varphi_i = 0. \quad (3.26)$$

Let $g(\varrho, \varphi) = (g_1(\varrho, \varphi), g_2(\varrho, \varphi), g_3(\varrho, \varphi))^T$ and define

$$\mathcal{M} \doteq \{(\varrho, \varphi) \in \mathbb{R}^{2n} : g(\varrho, \varphi) = 0\} \subset \mathbb{R}^{2n}. \quad (3.27)$$

Note that $(\varrho^*, \varphi^*) \in \mathcal{M}$. The Jacobian of $g(\varrho, \varphi)$ evaluated at the equilibrium point is

$$G = \begin{bmatrix} 1 & \cos(2\pi/n) & \dots & \cos(2\pi(n-1)/n) & -\sum_{i=2}^n r \sin(2\pi(i-1)/n) & \dots & -r \sin(2\pi(n-1)/n) & 0 \\ 0 & \sin(2\pi/n) & \dots & \sin(2\pi(n-1)/n) & \sum_{i=2}^n r \cos(2\pi(i-1)/n) & \dots & r \cos(2\pi(n-1)/n) & 0 \\ 0 & 0 & \dots & 0 & 1 & \dots & 1 & 1 \end{bmatrix} \quad (3.28)$$

Let $B_\delta(\varrho^*, \varphi^*)$ be the open ball of radius $\delta > 0$ centered at point (ϱ^*, φ^*) in \mathbb{R}^{2n} . The rank of G is clearly 3; then, there exists $\delta > 0$ such that $\tilde{\mathcal{M}} \doteq \mathcal{M} \cap B_\delta(\varrho^*, \varphi^*) \subset \mathbb{R}^{2n}$ is a submanifold of \mathbb{R}^{2n} . The tangent space of $\tilde{\mathcal{M}}$ at (ϱ^*, φ^*) , that we call $T_{(\varrho^*, \varphi^*)}\tilde{\mathcal{M}}$, is an invariant subspace of P (since $\tilde{\mathcal{M}}$, by construction, is invariant under (3.17), i.e., $f(\varrho, \varphi) \in T_{(\varrho, \varphi)}\tilde{\mathcal{M}}$ for all $(\varrho, \varphi) \in \tilde{\mathcal{M}}$) and has dimension $2n - 3$. Pick a basis $\{w_1, \dots, w_{2n-3}\}$ of $T_{(\varrho^*, \varphi^*)}\tilde{\mathcal{M}}$ and complete it to a basis W of \mathbb{R}^{2n} . Then, with respect to this basis, P takes the upper-triangular form

$$\begin{bmatrix} P_{1,1} & P_{1,2} \\ 0_{3 \times (2n-3)} & P_{2,2} \end{bmatrix}, \quad (3.29)$$

where $0_{3 \times (2n-3)}$ is the zero matrix with 3 rows and $2n - 3$ columns. Since our system is constrained to evolve, at (ϱ^*, φ^*) , along the tangent space $T_{(\varrho^*, \varphi^*)}\tilde{\mathcal{M}}$, the local stability of the equilibrium point is *solely* determined by the eigenvalues of $P_{1,1}$.

Now it is shown that the three eigenvalues of $P_{2,2}$ are exactly the three eigenvalues of P

that have real part equal to zero. It is possible to show (see Appendix A.4) that

$$G \cdot v_i \neq 0, \quad \text{for each } i \in \{1, 2, 3\},$$

where v_i , $i \in \{1, 2, 3\}$, are the three eigenvectors associated to the three eigenvalues with zero real part. Therefore, we have $v_i \notin T_{(\varrho^*, \varphi^*)} \tilde{\mathcal{M}}$, $i \in \{1, 2, 3\}$. Let y_i be the components of v_i with respect to the basis W ; define $y_{i,1}$ as the vector of components with respect to $\{w_1, \dots, w_{2n-3}\}$, and $y_{i,2}$ as the vector of components with respect to the remaining basis vectors in W . Since $v_i \notin T_{(\varrho^*, \varphi^*)} \tilde{\mathcal{M}}$, vector $y_{i,2}$ is non-zero. Since v_i is an eigenvector of P with eigenvalue λ_i , we can write

$$\begin{bmatrix} P_{1,1} & P_{1,2} \\ 0_{3 \times (2n-3)} & P_{2,2} \end{bmatrix} \begin{bmatrix} y_{i,1} \\ y_{i,2} \end{bmatrix} = \lambda_i \begin{bmatrix} y_{i,1} \\ y_{i,2} \end{bmatrix}, \quad (3.30)$$

and therefore $P_{2,2} y_{i,2} = \lambda_i y_{i,2}$, i.e., λ_i is an eigenvalue of $P_{2,2}$, $i \in \{1, 2, 3\}$. Since, we have $\text{eig}(P_{1,1}) = \text{eig}(P) \setminus \text{eig}(P_{2,2})$, we conclude, by using Lemma 3.2.8, that all eigenvalues of $P_{1,1}$ have negative real part. Therefore, the equilibrium point (ϱ^*, φ^*) is locally stable. ■

3.3 Cyclic-Pursuit Control Laws for Double-Integrator Models

In this section, we extend the previous cyclic-pursuit control laws to double integrators. A control law is presented first, which requires each agent to be able to measure its absolute position and velocity; then, the of design a control law that only requires *relative* measurements of position and velocity is detailed. The approach to the problem is done through spectral analysis to completely characterize the dynamics of the second order system. Particularly, this approach shows how the position behavior is characterized by exactly the same eigenvectors and eigenvalues as in the first order system.

As before, let $\mathbf{x}_i(t) = [x_{i,1}(t), x_{i,2}(t), x_{i,3}(t)]^T \in \mathbb{R}^3$ be the position at time $t \geq 0$ of the i^{th} agent, $i \in \{1, 2, \dots, n\}$, and let $\mathbf{x} = [\mathbf{x}_1^T, \mathbf{x}_2^T, \dots, \mathbf{x}_n^T]^T$. Moreover, let $R(\alpha)$ be the rotation matrix in three dimensions with rotation angle $\alpha \in [-\pi, \pi)$ and rotation axis $(0, 0, 1)^T$ (see equation (3.3)).

Now the case where the the dynamics of each agent are described by a double-integrator model is analyzed:

$$\ddot{\mathbf{x}}_i = \mathbf{u}_i. \quad (3.31)$$

3.3.1 Dynamic cyclic pursuit with reference coordinate frame

Consider the following feedback control law

$$\begin{aligned} \mathbf{u}_i = & k_d R(\alpha)(\mathbf{x}_{i+1} - \mathbf{x}_i) + R(\alpha)(\dot{\mathbf{x}}_{i+1} - \dot{\mathbf{x}}_i) \\ & - k_c k_d \mathbf{x}_i - (k_c + k_d) \dot{\mathbf{x}}_i, \quad k_d \in \mathbb{R}_{>0}, k_c \in \mathbb{R}. \end{aligned} \quad (3.32)$$

Note that each agent needs to measure both its absolute position (if $k_c \neq 0$) and its absolute velocity (if $k_c \neq -k_d$). The overall dynamics of the n agents are described by:

$$\begin{bmatrix} \dot{\mathbf{x}} \\ \ddot{\mathbf{x}} \end{bmatrix} = \begin{bmatrix} 0 & I_{3n} \\ k_d A(\alpha) & A(\alpha) - k_d I_{3n} \end{bmatrix} \mathbf{x} \doteq C(\alpha) \mathbf{x}, \quad (3.33)$$

where $A(\alpha) \doteq -L_1 \otimes R(\alpha) - k_c I_{3n}$ and L_1 is the matrix defined in equation (3.5). The following theorem characterizes eigenvalues and eigenvectors of $C(\alpha)$.

Theorem 3.3.1 *Assume that $-k_d$ is not an eigenvalue of $A(\alpha)$. The eigenvalues of the state matrix $C(\alpha)$ in equation (3.33) are the union of:*

- the $3n$ eigenvalues of $A(\alpha)$,
- $-k_d$, with multiplicity $3n$.

In other words, $\text{eig}(C(\alpha)) = \text{eig}(A(\alpha)) \cup \{-k_d\}$. Moreover, the eigenvector of $C(\alpha)$ corresponding to the k th eigenvalue $\lambda_k \in \text{eig}(A(\alpha))$, $k \in \{1, \dots, 3n\}$, is:

$$\nu_k \doteq \begin{bmatrix} \nu_{k,1} \\ \nu_{k,2} \end{bmatrix} = \begin{bmatrix} \mu_k \\ \lambda_k \mu_k \end{bmatrix}, \quad k \in \{1, \dots, 3n\}, \quad (3.34)$$

where μ_k is the eigenvector of $A(\alpha)$ corresponding to λ_k . The $3n$ (independent) eigenvectors corresponding to the eigenvalue $-k_d$ (that has multiplicity $3n$) are

$$\nu_k \doteq \begin{bmatrix} \nu_{k,1} \\ \nu_{k,2} \end{bmatrix} = \begin{bmatrix} -k_d^{-1} e_{k-3n} \\ e_{k-3n} \end{bmatrix}, \quad k \in \{3n+1, \dots, 6n\}, \quad (3.35)$$

where e_j is the j th vector of the canonical basis in \mathbb{R}^{3n} .

Proof: First, we compute the eigenvalues of $C(\alpha)$. The eigenvalues of $C(\alpha)$ are, by definition, solutions to the characteristic equation:

$$0 = \det \begin{bmatrix} \lambda I_{3n} & -I_{3n} \\ -k_d A(\alpha) & \lambda I_{3n} - (A(\alpha) - k_d I_{3n}) \end{bmatrix}. \quad (3.36)$$

By using the result in equation (2.1), we obtain

$$\begin{aligned} 0 &= \det(\lambda^2 I_{3n} - \lambda(A(\alpha) - k_d I_{3n}) - k_d A(\alpha)) \\ &= \det((\lambda + k_d) I_{3n}) \det(\lambda I_{3n} - A(\alpha)). \end{aligned}$$

Thus, the eigenvalues of $C(\alpha)$ must satisfy $0 = \det((\lambda + k_d) I_{3n})$ and $0 = \det(\lambda I_{3n} - A(\alpha))$; hence, the first part of the claim is proved.

By definition, the eigenvector $[\nu_{k,1}^T \ \nu_{k,2}^T]^T$ corresponding to the eigenvalue λ_k , $k = 1, \dots, 6n$, satisfies the eigenvalue equation:

$$\lambda_k \begin{bmatrix} \nu_{k,1} \\ \nu_{k,2} \end{bmatrix} = \begin{bmatrix} 0 & I_{3n} \\ k_d A(\alpha) & A(\alpha) - k_d I_{3n} \end{bmatrix} \begin{bmatrix} \nu_{k,1} \\ \nu_{k,2} \end{bmatrix} \quad (3.37)$$

$$= \begin{bmatrix} \nu_{k,2} \\ k_d A(\alpha)\nu_{k,1} + A(\alpha)\nu_{k,2} - k_d \nu_{k,2} \end{bmatrix}. \quad (3.38)$$

Thus, we obtain

$$\lambda_k \nu_{k,1} = \nu_{k,2}, \quad (3.39)$$

$$\lambda_k \nu_{k,2} = k_d A(\alpha)\nu_{k,1} + A(\alpha)\nu_{k,2} - k_d \nu_{k,2}, \quad (3.40)$$

and therefore

$$\lambda_k(k_d + \lambda_k)\nu_{k,1} = (k_d + \lambda_k)A(\alpha)\nu_{k,1}. \quad (3.41)$$

If $\lambda_k = -k_d$, then we have $3n$ eigenvectors given by $[-k_d^{-1}e_j, e_j]^T$, $j = \{1, \dots, 3n\}$. If, instead, $\lambda_k \in \text{eig}(A(\alpha))$ (note that by assumption $-k_d \notin \text{eig}(A(\alpha))$), we obtain from equation (3.41)

$$\lambda_k \nu_{k,1} = A(\alpha)\nu_{k,1},$$

and we obtain the claim. ■

The study of the formations that can be achieved with control law (3.32) can be addressed now.

Theorem 3.3.2 *Assume that $-k_d$ is not an eigenvalue of $A(\alpha)$. Then, agents' positions starting at any initial condition (except for a set of measure zero) in \mathbb{R}^{3n} and evolving under (3.33) exponentially converge:*

1. if $k_c = 0$, to formations centered at the initial center of mass, in particular:

(a) if $0 \leq |\alpha| < \pi/n$, to a single limit point;

(b) if $|\alpha| = \pi/n$, to an evenly spaced circle formation;

(c) if $\pi/n < |\alpha| < 2\pi/n$, to an evenly spaced logarithmic spiral formation;

2. if $k_c > 0$, to formations centered at the origin, in particular:

(a) if $0 \leq |\alpha| \leq \pi/n$, to a single limit point;

(b) if $\pi/n < |\alpha| < 2\pi/n$

i. if $k_c > 2 \sin(\pi/n) \sin(\alpha - \pi/n)$, to a single limit point;

ii. if $k_c = 2 \sin(\pi/n) \sin(\alpha - \pi/n)$, to an evenly spaced circle formation;

iii. if $k_c < 2 \sin(\pi/n) \sin(\alpha - \pi/n)$, to an evenly spaced logarithmic spiral formation.

Proof: As a consequence of Theorem 3.3.1, the eigenvectors of $C(\alpha)$ are linearly independent. Indeed, the eigenvectors ν_k for $k \in \{1, \dots, 3n\}$ are linearly independent since the vectors μ_k are (see Theorem 3.2.1); moreover, the eigenvectors ν_k for $k \in \{3n + 1, \dots, 6n\}$ are clearly linearly independent. Since, by assumption, $-k_d \notin \text{eig}(A(\alpha))$, the independence of the eigenvectors of $C(\alpha)$ follows.

Then, the proof is a simple consequence of Theorem 3.2.1, Corollary 3.2.2, Theorem 3.3.1, and the arguments in Section 3.5 of [67].

■

3.3.2 Control law with relative information only

Consider the following feedback control law:

$$\mathbf{u}_i = k_1 R^2(\alpha) \left((\mathbf{x}_{i+2} - \mathbf{x}_{i+1}) - (\mathbf{x}_{i+1} - \mathbf{x}_i) \right) + k_2 R(\alpha) (\dot{\mathbf{x}}_{i+1} - \dot{\mathbf{x}}_i), \quad (3.42)$$

where k_1 and k_2 are two real constants (not necessarily positive). In this case, each agent only needs to measure its *relative* position with respect to the positions of agents $i + 1$ and $i + 2$ (note that $(\mathbf{x}_{i+2} - \mathbf{x}_{i+1}) = ((\mathbf{x}_{i+2} - \mathbf{x}_i) - (\mathbf{x}_{i+1} - \mathbf{x}_i))$), and its *relative* velocity with respect to the velocity of agent $i + 1$. Note that control law (3.42) uses a rotation matrix that is common to all agents; hence, it requires that all agents agree upon a common orientation, but it does *not* require a consensus on a common origin. Indeed, in the case of spacecraft, agreement on the orientation can be easily achieved by using star trackers.

It is possible to verify that

$$L_1^2 = \begin{bmatrix} 1 & -2 & 1 & 0 & \dots & 0 \\ 0 & 1 & -2 & 1 & \dots & 0 \\ \vdots & & & & & \vdots \\ -2 & 1 & 0 & \dots & \dots & 1 \end{bmatrix}. \quad (3.43)$$

Then, the overall dynamics of the n agents can be written in compact form as

$$\begin{bmatrix} \dot{\mathbf{x}} \\ \ddot{\mathbf{x}} \end{bmatrix} = \begin{bmatrix} 0 & I_{3n} \\ k_1 L_1^2 \otimes R^2(\alpha) & -k_2 (L_1 \otimes R(\alpha)) \end{bmatrix} \mathbf{x} \doteq F(\alpha) \mathbf{x}. \quad (3.44)$$

Let $A(\alpha) \doteq -L_1 \otimes R(\alpha)$, and define

$$\beta_{\pm} \doteq \frac{k_2}{2} \pm \sqrt{\left(\frac{k_2}{2}\right)^2 + k_1}. \quad (3.45)$$

The following theorem characterizes eigenvalues and eigenvectors of $F(\alpha)$.

Theorem 3.3.3 *Assume that $\beta_{\pm} \neq 0$. The eigenvalues of the state matrix $F(\alpha)$ in equation (3.44) are the union of:*

- *the $3n$ eigenvalues of $A(\alpha)$, each one multiplied by β_+ ,*
- *the $3n$ eigenvalues of $A(\alpha)$, each one multiplied by β_- .*

In other words, $\text{eig}(F(\alpha)) = \beta_+ \text{eig}(A(\alpha)) \cup \beta_- \text{eig}(A(\alpha))$. Moreover, the eigenvector of $F(\alpha)$ corresponding to the k th eigenvalue $\lambda_k \in \beta_+ \text{eig}(A(\alpha))$, $k \in \{1, \dots, 3n\}$, is:

$$\nu_k \doteq \begin{bmatrix} \nu_{k,1} \\ \nu_{k,2} \end{bmatrix} = \begin{bmatrix} \mu_k \\ \lambda_k \mu_k \end{bmatrix}, \quad k \in \{1, \dots, 3n\}, \quad (3.46)$$

where μ_k is the eigenvector of $A(\alpha)$ corresponding to the eigenvalue λ_k/β_+ . Similarly, the eigenvector corresponding to the k th eigenvalue $\lambda_{3n+k} \in \beta_- \text{eig}(A(\alpha))$, $k \in \{1, \dots, 3n\}$, is:

$$\nu_{3n+k} \doteq \begin{bmatrix} \nu_{3n+k,1} \\ \nu_{3n+k,2} \end{bmatrix} = \begin{bmatrix} \mu_k \\ \lambda_k \mu_k \end{bmatrix}, \quad k \in \{1, \dots, 3n\}, \quad (3.47)$$

where μ_k is the eigenvector of $A(\alpha)$ corresponding to the eigenvalue λ_k/β_- .

Proof: First, we compute the eigenvalues of $F(\alpha)$. Note that, by the properties of the Kronecker product, $L^2 \otimes R^2(\alpha) = (L \otimes R(\alpha))^2 = A^2(\alpha)$. The eigenvalues of $F(\alpha)$ are, by definition, solutions to the characteristic equation:

$$0 = \det \left(\begin{bmatrix} \lambda I_{3n} & -I_{3n} \\ -k_1 A^2(\alpha) & \lambda I_{3n} - k_2 A(\alpha) \end{bmatrix} \right). \quad (3.48)$$

Using the result in equation (2.1) we have that

$$\begin{aligned} 0 &= \det (\lambda^2 I_{3n} - k_2 \lambda A(\alpha) - k_1 A^2(\alpha)) \\ &= \det \left((\lambda I_{3n} - \beta_+ A(\alpha)) (\lambda I_{3n} - \beta_- A(\alpha)) \right). \end{aligned} \quad (3.49)$$

Then, the first part of the claim is proven.

By definition, the eigenvector $[\nu_{k,1} \ \nu_{k,2}]^T$ corresponding to the eigenvalue λ_k , $k \in \{1, \dots, 6n\}$, satisfies the eigenvalue equation:

$$\lambda_k \begin{bmatrix} \nu_{k,1} \\ \nu_{k,2} \end{bmatrix} = \begin{bmatrix} 0 & I_{3n} \\ k_1 A^2(\alpha) & k_2 A(\alpha) \end{bmatrix} \begin{bmatrix} \nu_{k,1} \\ \nu_{k,2} \end{bmatrix} \quad (3.50)$$

$$= \begin{bmatrix} \nu_{k,2} \\ k_1 A^2(\alpha) \nu_{k,1} + k_2 A(\alpha) \nu_{k,2} \end{bmatrix}. \quad (3.51)$$

Thus, we obtain

$$\lambda_k \nu_{k,1} = \nu_{k,2}, \quad (3.52)$$

$$\lambda_k \nu_{k,2} = k_1 A^2(\alpha) \nu_{k,1} + k_2 A(\alpha) \nu_{k,2},$$

and therefore,

$$\lambda_k^2 \nu_{k,1} = k_1 A^2(\alpha) \nu_{k,1} + k_2 A(\alpha) \lambda_k \nu_{k,1}, \quad (3.53)$$

which can be rewritten as

$$(\lambda_k I_{3n} - \beta_+ A(\alpha))(\lambda_k I_{3n} - \beta_- A(\alpha)) \nu_{k,1} = 0. \quad (3.54)$$

Therefore, if $\lambda_k \in \beta_+ \text{eig}A(\alpha)$ (analogous arguments hold if $\lambda_k \in \beta_- \text{eig}A(\alpha)$), the above equation is satisfied by letting $\nu_{k,1}$ be equal to μ_k , in fact in this case (notice that μ_k is the eigenvector of $A(\alpha)$ corresponding to the eigenvalue λ_k/β_+ and that $\beta_+ \neq 0$):

$$\lambda_k \nu_{k,1} = \frac{\lambda_k}{\beta_+} \beta_+ \mu_k = \beta_+ A(\alpha) \mu_k = \beta_+ A(\alpha) \nu_{k,1}, \quad (3.55)$$

and the claim easily follows. ■

By appropriately choosing k_1 , k_2 and α , it is possible to obtain a variety of formations. Here we focus only on circular formations and Archimedes' spiral formations (an Archimedes'

spiral is a spiral with the property that successive turnings have a constant separation distance), which are arguably among the most important symmetric formations for applications. In particular, Archimedes' spiral formations are useful for the solution of the coverage path-planning problem, where the objective is to ensure that at least one agent eventually moves to within a given distance from any point in the target environment. More applications will be discussed in Section 3.5. Circular formations are initially considered.

3.3.2.1 Circular formations with only relative information

To start, consider the following lemma.

Lemma 3.3.4 *The vector $w_k = \begin{bmatrix} 0_{3n \times 1} \\ \mu_k \end{bmatrix}$, where $0_{3n \times 1}$ is the zero matrix with $3n$ rows and 1 column, is a generalized eigenvector for the zero eigenvalues λ_k , where $k = n, 2n, 3n$.*

Proof: The claim can be easily obtained by direct verification into the equation $(F(\alpha) - \lambda_k I_{6n})w_k = \nu_k$. ■

Theorem 3.3.5 *Let $k_2 = 2 \cos(\pi/2n)$ and $k_1 = -(k_2/2)^2 - \sin^2(\pi/2n)$. Moreover, assume that $\alpha = \pi/2n$; then, the system converges to an evenly spaced circular formation whose geometric center has constant velocity.*

Proof: With the above choices for k_1 and k_2 , it is straightforward to verify that $\beta_{\pm} = e^{j\pi/(2n)}$. From Theorem 3.3.3, $F(\alpha)$ has exactly two eigenvalues on the imaginary axis, a zero eigenvalue with algebraic multiplicity 6 and geometric multiplicity 3, and all other eigenvalues $\beta_{\pm}\lambda_k$ in the open left-half complex plane with linearly independent eigenvectors. Then, by using Theorem 3.3.3 and Lemma 3.3.4, it is possible to show that, as $t \rightarrow +\infty$, the time evolution of the system satisfies

$$\begin{bmatrix} \mathbf{x}(t) \\ \dot{\mathbf{x}}(t) \end{bmatrix} = \begin{bmatrix} \mathbf{x}_G \\ \dot{\mathbf{x}}_G \end{bmatrix} + t \begin{bmatrix} \dot{\mathbf{x}}_G \\ 0_{3n \times 1} \end{bmatrix} + c_1 \begin{bmatrix} \mathbf{w}_{dom}^1 \\ -\omega \mathbf{w}_{dom}^2 \end{bmatrix} + c_2 \begin{bmatrix} \mathbf{w}_{dom}^2 \\ \omega \mathbf{w}_{dom}^1 \end{bmatrix}, \quad (3.56)$$

where \mathbf{x}_G and $\dot{\mathbf{x}}_G$ are the initial position and velocity of the center of the formation, c_1 and c_2 are constants that depend on the initial conditions, ω is a constant equal to $2 \sin(\frac{\pi}{n})$, and, finally, the eigenfunctions \mathbf{w}_{dom}^p , $p \in \{1, 2\}$, are given by:

$$\begin{aligned}\mathbf{w}_{dom}^1 &= [\cos(\omega t + \delta_1), \sin(\omega t + \delta_1), 0, \dots, \cos(\omega t + \delta_n), \sin(\omega t + \delta_n), 0], \\ \mathbf{w}_{dom}^2 &= [\sin(\omega t + \delta_1), -\cos(\omega t + \delta_1), 0, \dots, \sin(\omega t + \delta_n), -\cos(\omega t + \delta_n), 0],\end{aligned}\quad (3.57)$$

where $\delta_i = 2\pi(i-1)/n$, $i \in \{1, \dots, n\}$. (Note that $\dot{\mathbf{w}}_{dom}^1 = -\omega \mathbf{w}_{dom}^2$, $\dot{\mathbf{w}}_{dom}^2 = \omega \mathbf{w}_{dom}^1$.) ■

Next we show how to choose k_1 , k_2 and α to achieve Archimedes' spiral formations; note that an Archimedes' spiral is described in polar coordinates by the equation $\varrho(\varphi) = a\varphi$, with $a \in \mathbb{R}_{>0}$.

3.3.2.2 Archimedes' spiral formations with only relative information

Consider first the following lemma.

Lemma 3.3.6 *Let $k_1 = -(k_2/2)^2$ and assume $\alpha = \pi/n$. Then, $w_k = \begin{bmatrix} 0_{3n \times 1} \\ \mu_k \end{bmatrix}$ is a generalized eigenvector for the eigenvalue λ_k/β .*

Proof: The claim can be easily obtained by direct verification into the equation $(F(\alpha) - \lambda_k I_{6n})w_k = \nu_k$. ■

Theorem 3.3.7 *Let $k_1 = -(k_2/2)^2$, and assume $k_2 > 0$ and $\alpha = \pi/n$. Then, the system converges to an Archimedes' spiral formation whose geometric center has constant velocity.*

Proof: In this case we have $\beta_+ = \beta_- \in \mathbb{R}_{>0}$, and thus $\lambda_k = \lambda_{k+3n}$ for all $k \in \{1, \dots, 3n\}$; as a consequence, the eigenvalues of $F(\alpha)$ are $\beta \text{eig}(A(\alpha))$. Hence, $F(\alpha)$ has exactly two eigenvalues on the imaginary axis, each one with algebraic multiplicity 2 and geometric multiplicity 1, a zero eigenvalue with algebraic multiplicity 6 and geometric multiplicity 3, and all other eigenvalues $\beta_{\pm}\lambda_k$ in the open left-half complex plane. Then, by using Theorem

3.3.3 and Lemma 3.3.6, it is possible to show that, as $t \rightarrow +\infty$, the time evolution of the system satisfies

$$\begin{aligned} \begin{bmatrix} \mathbf{x}(t) \\ \dot{\mathbf{x}}(t) \end{bmatrix} &= \begin{bmatrix} \mathbf{x}_G \\ \dot{\mathbf{x}}_G \end{bmatrix} + t \begin{bmatrix} \dot{\mathbf{x}}_G \\ 0_{3n \times 1} \end{bmatrix} + d_1 \begin{bmatrix} 0_{3n \times 1} \\ \mathbf{w}_{dom}^1 \end{bmatrix} + d_2 \begin{bmatrix} 0_{3n \times 1} \\ \mathbf{w}_{dom}^2 \end{bmatrix} \\ &+ (c_1 + d_1 t) \begin{bmatrix} \mathbf{w}_{dom}^1 \\ -\omega \mathbf{w}_{dom}^2 \end{bmatrix} + (c_2 + d_2 t) \begin{bmatrix} \mathbf{w}_{dom}^2 \\ \omega \mathbf{w}_{dom}^1 \end{bmatrix}, \end{aligned} \quad (3.58)$$

where \mathbf{x}_G and $\dot{\mathbf{x}}_G$ are the initial position and velocity of the center of the formation, c_1 , c_2 , d_1 and d_2 are constants that depend on the initial conditions, ω is a constant equal to $2 \sin(\frac{\pi}{n})$, and, finally, the eigenfunctions \mathbf{w}_{dom}^p , $p \in \{1, 2\}$, are defined in equation (3.57). Then, agents will perform spiraling trajectories; the radial growth rate is a constant equal to $\sqrt{d_1 + d_2}$, and the center of the formation moves with constant velocity $\dot{\mathbf{x}}_G$ defined by the initial conditions. ■

3.4 General Trajectories: Conformal Mapping

In this section, the extension to achieving more general and useful behaviors is presented based on the idea of similarity transformation of the control space. In this approach, invertible transformations are applied to the controller to achieve more general trajectories while maintaining the desirable properties of global convergence and synchronization of the cyclic pursuit algorithms.

The approach is described for the case of the basic cyclic pursuit controllers in single integrators which can be extended to second order following the results in the previous sections.

Proposition 3.4.1 *Consider the system $\dot{\mathbf{x}} = f(\mathbf{x})$, $\mathbf{x} \in \mathbb{R}^N$ that converges to the invariant*

set $\mathcal{M}_x \subset \mathbb{R}^N$.

And consider an arbitrary differentiable homeomorphic mapping $\mathbf{x}' = h(\mathbf{x})$, $h : \mathbb{R}^N \rightarrow \mathbb{R}^N$.

Then, a control strategy for which the dynamics of the system are such that $\dot{\mathbf{x}}' = \nabla_x h f(h^{-1}(\mathbf{x}'))$ converges to an invariant set in $\mathcal{M}_{x'}$, where: $\bar{\mathbf{x}}' \in \mathcal{M}_{x'} = h(\bar{\mathbf{x}})$, $\bar{\mathbf{x}} \in \mathcal{M}_x$.

Proof: Consider the variable $\mathbf{x} = h^{-1}(\mathbf{x}')$. Its dynamics are given by

$$\dot{\mathbf{x}} = \frac{d(h^{-1}(\mathbf{x}'))}{dt} = \nabla_{x'} h^{-1} \dot{\mathbf{x}}' = \nabla_{x'} h^{-1} \nabla_x h f(h^{-1}(\mathbf{x}')) \quad (3.59)$$

Since h is homeomorphic then $\mathbf{x} = h^{-1}(\mathbf{x}')$, $h^{-1} : \mathbb{R}^N \rightarrow \mathbb{R}^N$, $\dot{\mathbf{x}}' = (\nabla_x h) \dot{\mathbf{x}}$ and locally $\nabla_{x'} h^{-1} \nabla_x h = I$. Then the dynamics of x are:

$$\dot{\mathbf{x}} = f(\mathbf{x}) \quad (3.60)$$

which converge to $\mathcal{M}_x = h^{-1}(\mathcal{M}_{x'})$, then $\mathbf{x}' = h(\mathbf{x}) \rightarrow h(\mathcal{M}_x)$. ■

A similarity transformation is a particular case of the above approach. Consider for example a simple case, a linear invertible transformation $\mathbf{x} = (I_n \otimes T) \mathbf{x}' \doteq \hat{T} \mathbf{x}$, where $T \in \mathbb{R}^{3 \times 3}$ is an invertible matrix. Consider the system in 3.4 with:

$$\dot{\mathbf{x}} = -\mathcal{L} \mathbf{x} - k_c \mathbf{x} \quad (3.61)$$

which was shown to converge to a circular formation. By applying the above proposition $\nabla_x h = \hat{T}$ the control law becomes:

$$u_i = TRT^{-1}(x_{i+1} - x_i) - k_c x_i \quad (3.62)$$

the dynamics of the transformed system become:

$$\mathbf{x} = \hat{T}(-\mathcal{L} - k_c)\hat{T}^{-1}\mathbf{x} \quad (3.63)$$

which is of course a similarity transformation of the system in eq. 3.4. For this new system the eigenvalues are the same as those of the non-transformed system, but the eigenvectors are $\mu' = \hat{T}\mu$.

Of course, each vehicle could have different invertible mappings, $y_i = \nabla_x h_i f(h_k^{-1}y_k)$, then $\mathbf{x} = \text{diag}[h_i^{-1}(y_i)]$, $\nabla_x h = \text{diag}[\nabla_x h_i]$.

Fig. 3-2 illustrate an example where for a set of 4 single-integrator agents the control function:

$$u_i = \nabla_x h_i R(h_{i+1}^{-1}(\mathbf{x}_{i+1}) - h_i^{-1}(\mathbf{x}_i)) - k_c \nabla_x h_i h_i^{-1}(\mathbf{x}_i) \quad (3.64)$$

where the functions h are:

$$\begin{bmatrix} r' \\ \theta' \\ z' \end{bmatrix} = h_1(r, \theta, z) = \begin{pmatrix} (0.1 + \cos(\theta)) \\ \theta \\ z \end{pmatrix} \quad (3.65)$$

$$\begin{bmatrix} r' \\ \theta' \\ z' \end{bmatrix} = h_2(r, \theta, z) = \begin{pmatrix} (0.4 + \cos(\theta)) \\ \theta \\ z \end{pmatrix} \quad (3.66)$$

$$\begin{bmatrix} x \\ y \\ z \end{bmatrix} = h_3(x, y, z) = \begin{bmatrix} 1.5 & 0.45 & 0.45 \\ 0.45 & 3 & 0.45 \\ 0 & 0.45 & 1.5 \end{bmatrix} \begin{bmatrix} x \\ y \\ z \end{bmatrix} \quad (3.67)$$

and

$$\begin{bmatrix} x \\ y \\ z \end{bmatrix} = h_3(x, y, z) = I_3 \begin{bmatrix} x \\ y \\ z \end{bmatrix} \quad (3.68)$$

where r, θ, z are cylindrical coordinates in the respective coordinate set.

This section presented an approach that substantially extends the results in the literature by defining *transformations* of the basic cyclic pursuit control laws such that the formation converges to more general types of trajectories and can be useful in many contexts. In the next section we describe a situation where this similarity transformation approach is used to converge to natural trajectories of a system with more specific dynamics.

3.5 Applications of Cyclic-Pursuit Algorithms

In the past few years, cyclic pursuit has received considerable attention in the control community (see Section 3.1); however to date, to the best of the authors' knowledge, no application has been proposed for which cyclic pursuit is a particularly effective control strategy. In this section, we discuss application domains in which cyclic pursuit is indeed an ideal candidate control law.

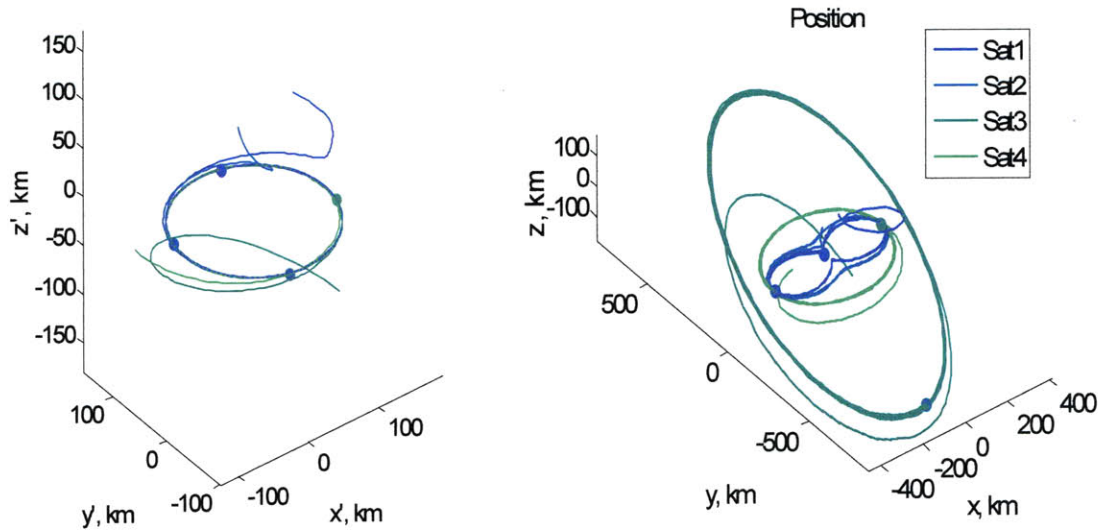


Figure 3-2: A formation achieves a formation with some arbitrary trajectories by selecting specific linear and nonlinear transformations

3.5.1 Interferometric imaging in deep space

Interferometric imaging, i.e., image reconstruction from interferometric patterns, is an application of formation flight that has been devised and studied for space missions such as NASA's Terrestrial Planet Finder - Interferometer (TPF-I) and Stellar Imager (SI) and ESA's Darwin.

The general problem of interferometric imaging consists of performing measurements in a way that enough information about the frequency content of the image is obtained. Such coverage problem is independent of the global positions of the spacecraft [16]; additionally, missions like TPF-i and Darwin consider locations far out of the reach of GPS signals and are expected to only rely on relative measurements to perform reconfigurations and observation maneuvers.

The general problem of interferometric imaging consists of performing measurements in a region of the observation plane in such a way that enough information about the spatial frequency content of the image is obtained. A heuristic solution to this coverage problem has been proposed to be the set of *Archimedes' spiral* trajectories [16], where the baselines for

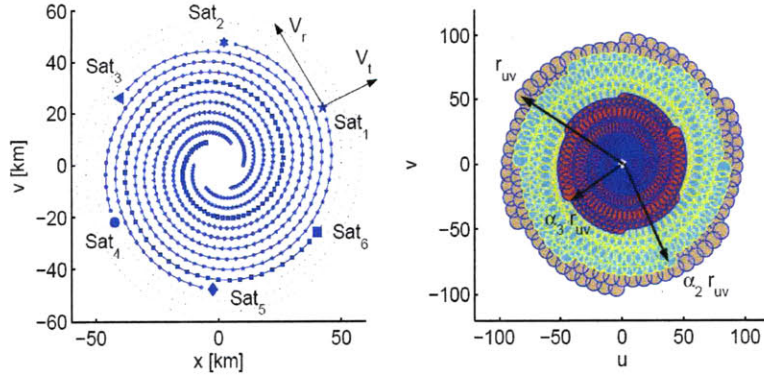


Figure 3-3: u-v plane coverage by a system of multiple spacecraft. (Source [16])

each pair of sensors describe “coverage discs” as shown in Fig.3-3. The coverage requirement is a nonlinear function that conveys the fact that the trajectories of the “coverage discs” should allow for a minimum amount of time to be spent at each region of the u-v plane to be covered. Such coverage constraint can be written as [16]:

$$\sum_k^{N_R} \frac{ba_k}{v_r(a_k|x_{i+1}(t) - x_i(t)|)} \geq \bar{C} \quad (3.69)$$

Where $v_r(\rho)$ is the radial component of the velocity as a function of the intersatellite distance, N_R is the number of rings formed by an specific configuration, and \bar{C} is a parameter of the image that defines the total amount of light collection time for each spatial frequency. b has the value 1 for odd total number of vehicles and 2 for even and a_i is a geometric parameter that defines the ratio between the radius of the formation and the distant between neighbors i and $i + k$.

Figure 3-4 shows simulated trajectories resulting from the application of control law (3.42); the initial positions are random inside a volume of $(10km)^3$. In the first case spacecraft converge to circular trajectories, while in the second case spacecraft converge to Archimedes’ spirals. The inertial frame for the plots is the geometric center of the configuration.

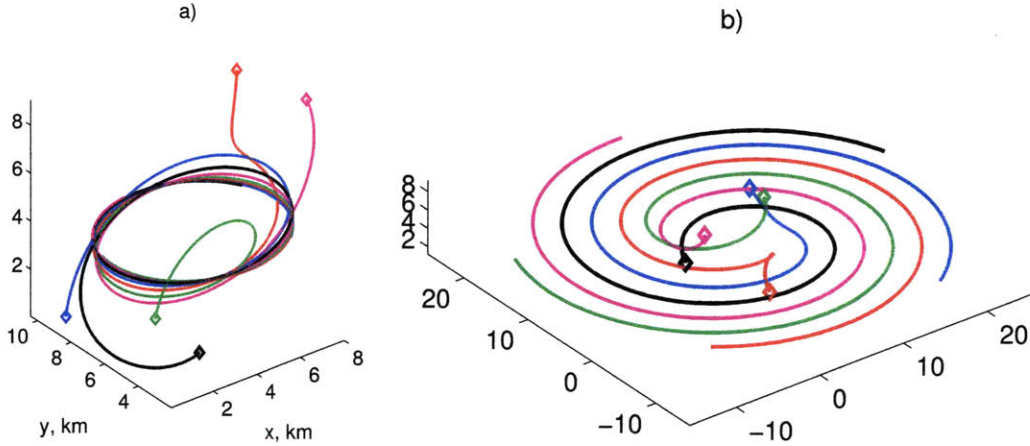


Figure 3-4: Convergence from random initial conditions to symmetric formations. Left Figure: Circular trajectories. Right Figure: Archimedes' spiral trajectories.

3.5.2 On reaching natural trajectories

In this section we modify the previous control laws to achieve convergence to elliptical trajectories. Consider the application of a similarity transformation to the rotation matrix $R(\alpha)$, as shown in Section 3.4

It is straightforward to see that the trajectories arising with the previous control laws are then transformed according to

$$\tilde{\mathbf{x}}_i(t) = T\mathbf{x}_i(t), \quad i \in \{1, \dots, n\}; \quad (3.70)$$

in particular, circular trajectories can be transformed into *elliptical* trajectories.

Indeed, the above approach is useful to allow the system to globally converge to low-effort trajectories. Consider the dynamic system

$$\begin{aligned} \ddot{\mathbf{x}}_i &= f(\mathbf{x}_i, \dot{\mathbf{x}}_i) + \mathbf{u}_i \\ &= f(\mathbf{x}_i, \dot{\mathbf{x}}_i) - (f(\mathbf{x}_i, \dot{\mathbf{x}}_i) - \mathbf{u}_{nom_i}), \end{aligned} \quad (3.71)$$

which has a zero-effort ($\mathbf{u}_i=0$) invariant set \mathbf{x}_i^* , for which $f(\mathbf{x}_i^*, \dot{\mathbf{x}}_i^*) = \mathbf{u}_{nom_i}$. If we use a

controller for which the state reaches $\mathbf{x}_i^*(t)$ as $t \rightarrow \infty$, then the control effort will tend to $\mathbf{u}_i = 0$ as $t \rightarrow \infty$.

In the case of the dynamics of relative orbits slightly perturbed from a circular orbit, elliptical relative trajectories are closed near-natural trajectories (i.e. theoretically they require no control effort); in the following section, cyclic-pursuit controllers are proposed as promising algorithms for formation acquisition, maintenance and reconfiguration.

3.5.2.1 Clohessy-Wiltshire model

The Clohessy-Wiltshire model approximates the motion of a spacecraft with respect to a frame that follows a circular orbit with angular velocity ω_R and radius $R_{ref} = (\mu_{\oplus}/\omega_R^2)^{1/3}$, where μ_{\oplus} is the gravitational constant of Earth. The equations of motion $\ddot{\mathbf{x}}_i = f(\mathbf{x}_i, \mathbf{u}_i)$ are:

$$\begin{aligned}\ddot{x}_i &= 2\omega_R\dot{y}_i + 3\omega_R^2x_i + u_{ix}, \\ \ddot{y}_i &= -2\omega_R\dot{x}_i + u_{iy}, \\ \ddot{z}_i &= -\omega_R^2z_i + u_{iz},\end{aligned}\tag{3.72}$$

where the x , y and z coordinates are expressed in a right-handed orthogonal reference frame such that the x -axis is aligned with the radial vector of the reference orbit, the z -axis is aligned with the angular momentum vector of the reference orbit, and the y -axis completes the right-handed orthogonal frame.

Consider a formation of spacecraft that use the cyclic-pursuit controller

$$\begin{aligned}\mathbf{u}_i &= -f(\mathbf{x}_i) + k_g(k_dTR(\alpha)T^{-1}(\mathbf{x}_{i+1} - \mathbf{x}_i) + TR(\alpha)T^{-1}(\dot{\mathbf{x}}_{i+1} - \dot{\mathbf{x}}_i) \\ &\quad - k_c k_d \mathbf{x}_i - (k_c + k_d/k_g)\dot{\mathbf{x}}_i),\end{aligned}\tag{3.73}$$

with $k_g = \omega_R/(2 \sin(\pi/n))$, and

$$T = \begin{bmatrix} \frac{1}{2} & 0 & 0 \\ 0 & 1 & 0 \\ z_0 \cos(\phi_z) & z_0 \sin(\phi_z) & 1 \end{bmatrix}, \quad (3.74)$$

where z_0 and ϕ_z are tunable parameters (their roles will become clear later). Then, from the results in Section 3.3, we obtain, as $t \rightarrow \infty$,

$$\mathbf{x}_i(t) = \mathbf{x}_i^*(t) = T \begin{bmatrix} r \sin(\omega_R t + \delta_i) \\ r \cos(\omega_R t + \delta_i) \\ 0 \end{bmatrix}, \quad i \in \{1, \dots, n\}, \quad (3.75)$$

where $\delta_i = 2\pi(i-1)/n$, and r is a constant that depends on the initial conditions. Thus, we obtain

$$\begin{aligned} x_i^*(t) &= \frac{1}{2}r \sin(\omega_R t + \delta_i), \\ y_i^*(t) &= r \cos(\omega_R t + \delta_i), \\ z_i^*(t) &= z_0 r \sin(\omega_R t + \delta_i + \phi_z); \end{aligned} \quad (3.76)$$

hence, the formation will converge to an evenly-spaced elliptical formation with an $x : y$ ratio equal to $1 : 2$, a $y : z$ ratio equal to $1 : z_0$, and a phasing between the x and z motion equal to ϕ_z . By replacing these equations into equation (3.72), it is easily shown that as $\mathbf{x}(t) \rightarrow \mathbf{x}^*(t)$, we have $\mathbf{u} \rightarrow 0$.

3.5.3 Including Earth's oblateness effect

A more accurate model for the motion of a spacecraft formation considers the effects of the oblateness of the Earth, specifically the higher order spherical harmonics of the gravitational

force model, denoted as J_k . In [86], Schweighart and Sedwick show that the equations of motion relative to a circular non-Keplerian reference orbit and including the J_2 term are well approximated by the linear system:

$$\ddot{x}_i = 2\omega_R c \dot{y}_i + (5c^2 - 2)\omega_R^2 x_i + u_{xi} + \frac{3}{4}K_{J_2} \cos(2\bar{k}t), \quad (3.77)$$

$$\ddot{y}_i = -2\omega_R c \dot{x}_i + u_{yi} + \frac{1}{2}K_{J_2} \sin(2\bar{k}t), \quad (3.78)$$

$$\ddot{z}_i = -q^2 z_i + 2lq \cos(qt + \Phi) + u_{zi}, \quad (3.79)$$

where, again, the x , y and z coordinates are expressed in a right-handed orthogonal reference frame such that the x -axis is aligned with the radial vector of the reference orbit, the z -axis is aligned with the angular momentum vector of the reference orbit, and the y -axis completes the right-handed orthogonal frame; moreover, $c = \sqrt{1+s}$, $s = \frac{3J_2 R_e^2}{8r_{ref}^2} (1 + 3\cos(2i_{ref}))$, $K_{J_2} = \frac{3\omega_R^2 J_2 R_e^2}{r_{ref}} \sin^2(i_{ref})$, R_e is the nominal radius of the earth, $\bar{k} = c + \frac{3J_2 R_e^2}{2r_{ref}^2} \cos^2 i_{ref}$, r_{ref} and i_{ref} are parameters of the reference orbit, q is approximately equal to $c\omega_R$, and Φ , l are time varying functions of the difference in orbit inclination (see ref. [86] for the details). Zero-effort trajectories (i.e, trajectories with $\mathbf{u}_i = 0$) for the above dynamic model are shown to be:

$$\begin{aligned} x^*(t) &= x_0 \cos(\omega_R t \sqrt{1-s}) + \frac{\sqrt{1-s}}{2\sqrt{1+s}} y_0 \sin(\omega_R t \sqrt{1-s}) + x_{cc}(t), \\ y^*(t) &= x_0 \frac{-2\sqrt{1+s}}{\sqrt{1-s}} \sin(\omega_R t \sqrt{1-s}) + y_0 \cos(\omega_R t \sqrt{1-s}) + y_{cc}(t), \\ z^*(t) &= (lt + m) \sin(qt + \Phi), \end{aligned} \quad (3.80)$$

with

$$\mathbf{x}_{cc}(t) = [\alpha(\cos(2\bar{k}t) - \cos(\omega_R t \sqrt{1-s})), \beta \sin(2\bar{k}t) - \frac{2\sqrt{1+s}}{\sqrt{1-s}} \alpha(\cos(\omega_R t \sqrt{1-s})), 0]^T, \quad (3.81)$$

where α , β , and m are constants that depend on the reference orbit parameters and for brevity are not discussed here. (For details we refer the reader to the work of Schweighart and Sedwick [86].) As in the previous section, by defining the control coordinates in a reference frame centered in $\mathbf{x}_{cc}(t)$, and using the decentralized cyclic-pursuit controller in equation (3.73) with a transformation matrix

$$T = \begin{bmatrix} \frac{\sqrt{1-s}}{2\sqrt{1+s}} & 0 & 0 \\ 0 & 1 & 0 \\ z_0 \cos(\phi_z) & z_0 \sin(\phi_z) & 1 \end{bmatrix}, \quad (3.82)$$

and $k_g = \omega_R \sqrt{1-s} / (2 \sin(\pi/n))$, it is straightforward to show that the formation will converge to elliptical trajectories centered at the point $\mathbf{x}_{cc}(t)$. Then, as $t \rightarrow \infty$, $\mathbf{x}(t) \rightarrow$

$$T \begin{bmatrix} r \sin(\omega_R t + \delta_i) \\ r \cos(\omega_R t + \delta_i) \\ 0 \end{bmatrix} + \mathbf{x}_{cc}, \text{ and thus, as } t \rightarrow \infty, \text{ the trajectories for } x(t), y(t) \text{ are those}$$

described in equation (3.80), and we have that:

$$\begin{aligned} u_x &\rightarrow 0, \\ u_y &\rightarrow 0, \\ u_z &\rightarrow (\omega_R^2 - q^2) + 2lq \cos(qt + \Phi) \approx 2lq \cos(qt + \Phi). \end{aligned} \quad (3.83)$$

The last term corresponds to the cohesive force required to maintain the formation when the orbits are not coplanar (i.e. the spacecraft have different inclination and thus different J_2 secular drift rates). For $z_o \rightarrow 0$, then $q = \omega_R$, $l \rightarrow 0$ and the theoretical required thrust converges to zero.

Figure 3-5 shows simulation results for the control laws described in this section. The system is simulated using dynamics including the J_2 terms. The results show convergence from random initial positions to the desired orbits, i.e., an evenly-spaced elliptical formation

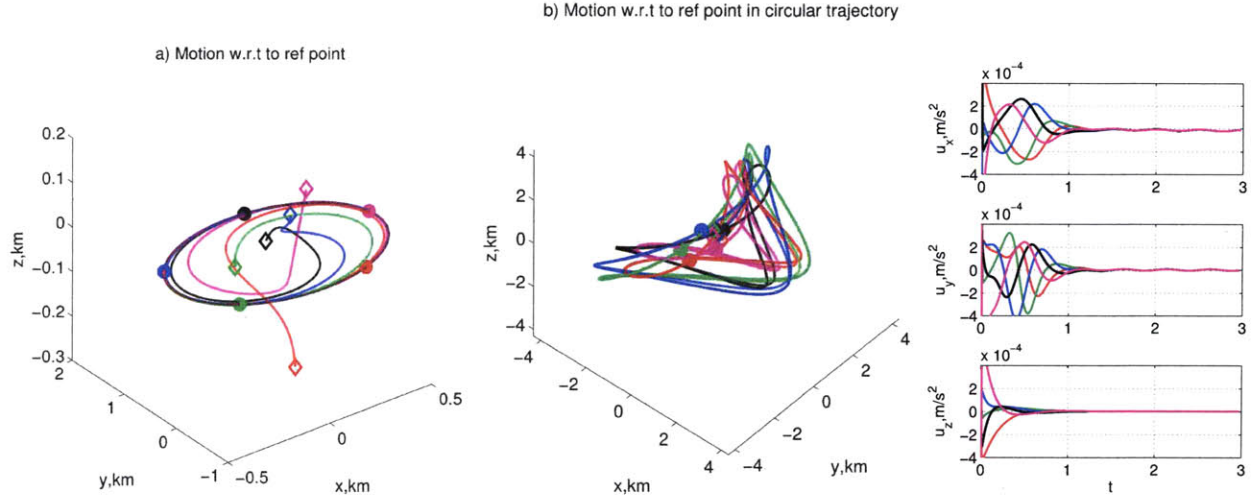


Figure 3-5: Convergence to elliptical trajectories with dynamics including J_2 terms.

in the desired plane. It is also shown (Fig. 3-5b) how the control effort reduces as the spacecraft reach the desired low-effort trajectories. In this case the orbits are coplanar and the differential J_2 effects in the z direction converge to 0. The dots indicate the positions after 3 orbits. 3-5a) is a 3D view of the trajectories with respect to reference point \mathbf{x}_{cc} . Fig. 3-5b) is a 3D view of the trajectories with respect to non-keplerian circular orbit. 3-5c) is a plot of the control effort versus time, showing that as $t \rightarrow \infty$, $\mathbf{u} \rightarrow 0$.

Although the achieved trajectories are not natural trajectories for a free orbiting body, the proposed decentralized control law allows convergence to elliptical formations that are near-natural and would require low fuel consumption for their maintenance.

3.6 Summary and Conclusions of the Chapter

Linear cyclic pursuit dynamics were analyzed using an eigendecomposition approach. The special structure of the underlying structure, specifically block rotational-circulant matrices allows for the derivation of analytical expressions of the decomposition. This analytical description of the dynamics allowed for developing controllers suited for spacecraft control problems of interest.

The main contributions of this chapter are threefold. First, building upon previous work on cyclic-pursuit algorithms, we rigorously study cyclic, distributed control laws for formation flying, for both single-integrator and double-integrator models in three dimensions. Second, we described a method to achieve decentralized controllers based on the cyclic pursuit structure that achieve convergence to linear and nonlinear transformations of circular trajectories.

And lastly, we discuss potential applications and describe the application of the control approach including spacecraft formation for interferometric imaging and LEO formation acquisition and maintenance. The control laws are based on those theoretical results and are shown to be fit to deal with the (linearized) relative dynamics of spacecraft, e.g., in the Earth's gravitational field. A key feature of the control approach is that, unlike other approaches, they do not require any agreement on a set of predetermined trajectories.

Chapter 4

Contraction Theory Approach to Formation Control

In this chapter, an alternative direction in the analysis of control laws inspired as a generalization of the cyclic pursuit control laws from Chapter 3 is presented. This alternative approach is introduced as a tool to embrace more general dynamical systems, placing the previous results in the more general context of convergence to manifolds. Understanding the problem as such could be more intuitive, opens an alternative road to verifying global convergence for more complex distributed controllers and can be applied in the case of non-autonomous and nonlinear dynamics.

The proposed approach is based in the theory of partial contraction, shortly mentioned in Section 2.1. It yields global convergence results and direct extensions for nonlinear systems and more general dynamic cases. It also allows the introduction of *convergence primitives*, where control laws consist of combinations of simpler control laws, converge to a subspace defined where the constraints in the desired configuration are convergence subspaces of the primitives and the combination of them achieves more complex formations. Particularly, the contraction theory results lead to identifying sufficient conditions for the convergence to a given manifold. Then, distributed control laws that satisfy these conditions can be proposed

and their convergence properties verified.

Contraction theory proves itself as a valuable method to analyze the convergence of distributed systems for which methods like Lyapunov functions might not be suitable. In the contraction theory approach, the general idea consists of showing the negative definiteness of a projected Jacobian matrix which characterizes the dynamics of an agreement subspace. Showing the negative definiteness of a matrix in the case of a distributed system can turn more attainable than demonstrating the negativeness of a Lyapunov rate which is a function of multiple states that depend on each other.

In a first result, applying the contraction approach to a generalized version of the cyclic pursuit approach leads to a generalization to time varying and state dependent cyclic controllers. Convergence results extend in a straightforward way to achieving polygons, circular and spiral rotating formations, addressing time varying and state dependent gains and coupling matrices. Then, a series of results and corollaries of extending the contraction theory approach to time varying subspaces and linear combinations of basic primitives are derived. Specifically, a result on the linear combination of basic control functions shown to converge to basic manifolds \mathcal{M}_i , which are dubbed 'primitives'. Several applications of applying these results are shown to illustrate the proposed idea.

Since our main objective is the introduction of the dynamic analysis approach, we focus on examples using simple integrator dynamics but illustrate in a later section the proposed approach to implementing the control algorithms in more general contexts.

The distribution of this chapter is as follows: Section 4.1 introduces the approach to convergence analysis based on contraction theory, it is extended by studying a comparison to the approaches in the previous literature and specifically describing the contraction theory approach to the control laws as related to an example previously presented in the literature. Then, Section 4.2 derives control laws for global convergence to regular polygonal formations and presents a result for global convergence to a regular formation of specific size. Section 4.3 describes the convergence results of the approach based on control primitives which are

illustrated through applications in a later Section 4.4. Brief concluding remarks are presented in Section 4.5.

4.1 Introduction

In this section we introduce the basic idea of contraction theory, and describe the relationship to an example in a recent work by Pham and Slotine [68]. Then, we extend the results by addressing the case of convergence to time varying manifolds.

Consider the system with closed loop dynamics:

$$\dot{\mathbf{x}} = \mathbf{f}(\mathbf{x}, t) \tag{4.1}$$

where $\mathbf{x} \in \mathbb{R}^n$, and consider a flow invariant manifold of $\mathbf{f}(\mathbf{x}, t)$, defined as the subset $\mathcal{M} \subset \mathbb{R}^n$ such that $\mathbf{f}(\bar{\mathbf{x}}) \in \mathcal{M}$ for all $\bar{\mathbf{x}} \in \mathcal{M}$.

Consider a smooth, continuous transformation $V(\mathbf{x}) : \mathbb{R}^n \rightarrow \mathbb{R}^p$, such that the invariant manifold \mathcal{M} can be described as the null space of $V(\mathbf{x})$, i.e. $\mathcal{M} : \{\bar{\mathbf{x}} \mid V(\bar{\mathbf{x}}) = 0\}$.

The dynamics of the perpendicular projection $\mathbf{y} = \bar{V}\mathbf{x}$ can be written as:

$$\begin{aligned} \dot{\mathbf{y}} &= \nabla_x \mathbf{f}(\mathbf{x}, t) \\ &= \nabla_x \mathbf{f}(\mathbf{y}, \bar{\mathbf{x}}, t) \end{aligned} \tag{4.2}$$

The general idea of the partial contraction theory consists of showing the contractive behavior of the above system. If this perpendicular system is shown to be contracting, all trajectories of this system will converge to the same one, $\mathbf{y} = 0$ is a specific trajectory of the system, therefore all trajectories of 4.1 will converge to trajectories in $\mathbf{y} = V(\mathbf{x}) = 0$.

As mentioned in the introduction to the contraction theory in Section 2.1, the system 4.1 is said to be contracting if there exists a square invertible transformation $\Theta(\mathbf{x}, t)$ such that

$\Theta(\mathbf{x}, t)^T \Theta(\mathbf{x}, t)$ is uniformly positive definite and the matrix:

$$\mathbf{F} = \left(\dot{\Theta} + \Theta \frac{\partial \mathbf{f}}{\partial \mathbf{x}} \right) \Theta^{-1} \quad (4.3)$$

is uniformly negative definite, where $\frac{\partial \mathbf{f}}{\partial \mathbf{x}}$ is the Jacobian matrix of \mathbf{f} with respect to \mathbf{x} .

Θ can be an identity transformation, and in many cases it is a sufficient definition to show convergence. In other cases, as will be shown in an example, the problem consists of finding a transformation Θ .

Now, consider a linear case where $V(\mathbf{x})$ is a linear transformation, $V \in \mathbb{R}^{p \times n}$.

Consider an orthogonal partition of the state space $\bar{V}\bar{V}^\top = I_p$ and $\bar{V}^\top \bar{V} + \bar{U}^\top \bar{U} = I_n$ such that $V = T\bar{V}$. Then, the Jacobian of the perpendicular projection, also referred in this thesis as the projected Jacobian is:

$$J_y = \frac{d(\bar{V}\mathbf{f}(\mathbf{x}, t))}{dy} \quad (4.4)$$

$$= \bar{V} \left(\frac{d\mathbf{f}(\bar{V}^\top \mathbf{y} + \bar{U}^\top \bar{U}\mathbf{x}, t)}{dy} \right) \quad (4.5)$$

$$= \bar{V} \left(\frac{d\mathbf{f}(\mathbf{x})}{d\mathbf{x}} \right) \bar{V}^\top \quad (4.6)$$

If V is row independent, T is an invertible transformation. It is clear that for an invertible T , $\bar{V} \frac{d\mathbf{f}(\mathbf{x})}{d\mathbf{x}} \bar{V}^\top = TV \frac{d\mathbf{f}(\mathbf{x})}{d\mathbf{x}} V^\top T^\top < 0 \Leftrightarrow V \frac{d\mathbf{f}(\mathbf{x})}{d\mathbf{x}} V^\top < 0$. Therefore, we can define a sufficient condition for global convergence to the manifold $V(x) = 0$ to be:

$$V \left(\frac{d\mathbf{f}(\mathbf{x}, t)}{d\mathbf{x}} \right) V^\top < 0 \quad (4.7)$$

4.1.0.1 Example

As an introductory example of the application of the approach, we present results for a three-vehicle cyclic pursuit control algorithm as related to an example presented by Pham and Slotine [68].

In their example, Pham and Slotine consider the set of Androno-Hopf oscillators related to locomotive behavior of salamanders:

$$\dot{\mathbf{x}}_i = \mathbf{f}(\mathbf{x}_i) + \mathbf{u}_i \quad (4.8)$$

$$\mathbf{f} \begin{bmatrix} x \\ y \end{bmatrix} = k_1 \begin{bmatrix} x - y - x^3 - xy^2 \\ x + y - y^3 - yx^2 \end{bmatrix} \quad (4.9)$$

while adding a cyclic coupling:

$$\dot{\mathbf{x}}_1 = \mathbf{f}(\mathbf{x}_1) + k(R_{2\pi/3}\mathbf{x}_2 - \mathbf{x}_1) \quad (4.10)$$

$$\dot{\mathbf{x}}_2 = \mathbf{f}(\mathbf{x}_2) + k(R_{2\pi/3}\mathbf{x}_3 - \mathbf{x}_2) \quad (4.11)$$

$$\dot{\mathbf{x}}_3 = \mathbf{f}(\mathbf{x}_3) + k(R_{2\pi/3}\mathbf{x}_1 - \mathbf{x}_3) \quad (4.12)$$

where $R(\alpha)$ is a rotation matrix for an angle α , and the overall system can then defined as:

$$\dot{\mathbf{x}} = \mathbf{f}(\mathbf{x}) - k\mathbf{L}\mathbf{x} \quad (4.13)$$

The manifold \mathcal{M}_a , which defines circular formations about the origin:

$$\mathcal{M}_a = \{R(2\pi/3)(\mathbf{x}), R(\pi/3)(\mathbf{x}), \mathbf{x}\} \quad (4.14)$$

can be shown to be an invariant manifold of $\mathbf{f}(x)$ and also an invariant manifold of $\mathbf{L}_s = \mathbf{L} + \mathbf{L}^\top$.

For $k > 2/3$, the eigenvalues of the projected Laplacian VLV^\top are guaranteed to be less than the eigenvalues of the projected Jacobian of \mathbf{f} , $V \left(\frac{\mathbf{f}(\mathbf{x})}{d\mathbf{x}} \right) V^\top$, and thus the negative definiteness of the projected Jacobian of $\mathbf{f}(\mathbf{x}) - k\mathbf{L}$ is verified. If $\mathbf{f}(\mathbf{x}) = 0$, the convergence to \mathcal{M}_a is also verified.

Now if instead a cyclic pursuit approach is applied, such that

$$\begin{aligned}
\dot{\mathbf{x}}_1 &= \mathbf{f}(\mathbf{x}_1) + kR_{\pi/3}(\mathbf{x}_2 - \mathbf{x}_1) \\
\dot{\mathbf{x}}_2 &= \mathbf{f}(\mathbf{x}_2) + kR_{\pi/3}(\mathbf{x}_3 - \mathbf{x}_2) \\
\dot{\mathbf{x}}_3 &= \mathbf{f}(\mathbf{x}_3) + kR_{\pi/3}(\mathbf{x}_1 - \mathbf{x}_3)
\end{aligned} \tag{4.15}$$

in this case the overall dynamics can be described as:

$$\dot{\mathbf{x}} = \mathbf{f}(\mathbf{x}) - \mathcal{L}\mathbf{x} \tag{4.16}$$

where $\mathcal{L} = L \otimes R(\pi/3)$, with L being the laplacian of the ring topology described in eq. 3.5. Then, when considering the same invariant manifold, \mathcal{M}_a , it is found that $V\mathcal{L}V^\top \leq 0$, $V\mathbf{f}(\mathbf{x})V^\top < 0$ and the convergence to the manifold is verified for this dynamical system too. However, in the case when $\mathbf{f} = 0$, the convergence to V is not verified because the projected Laplacian is only positive semidefinite.

On the other hand, consider looking at the convergence to the larger subset:

$$\mathcal{M}_n = \{\bar{\mathbf{x}} : (\mathbf{x}_{i+1} - \mathbf{x}_i) = R_{\frac{2\pi}{n}}(\mathbf{x}_{i+2} - \mathbf{x}_{i+1})\}, \quad \forall i < n - 1 \tag{4.17}$$

that describes states where the vehicles are in a regular polygon formation as shown in figure 4-1. Notice that $\mathcal{M}_a \subset \mathcal{M}_n$. \mathcal{M}_n can be shown to be a flow-invariant manifold for the cyclic pursuit law:

$$\begin{aligned}
\dot{\mathbf{x}}_{i+1} - \dot{\mathbf{x}}_i &= R(\alpha)(\mathbf{x}_{i+2} - \mathbf{x}_{i+1}) - R_{\frac{2\pi}{n}}(\mathbf{x}_{i+1} - \mathbf{x}_i) \\
&= R_{\frac{2\pi}{n}}R(\alpha)(\mathbf{x}_{i+3} - \mathbf{x}_{i+2}) - R_{\frac{2\pi}{n}}R(\alpha)(\mathbf{x}_{i+2} - \mathbf{x}_{i+1}) \\
&= R_{\frac{2\pi}{n}}(\dot{\mathbf{x}}_{i+2}) - R_{\frac{2\pi}{n}}(\dot{\mathbf{x}}_{i+1}) \\
\dot{\mathbf{x}}_{i+1} - \dot{\mathbf{x}}_i &= R_{\frac{2\pi}{n}}(\dot{\mathbf{x}}_{i+2} - \dot{\mathbf{x}}_{i+1})
\end{aligned} \tag{4.18}$$

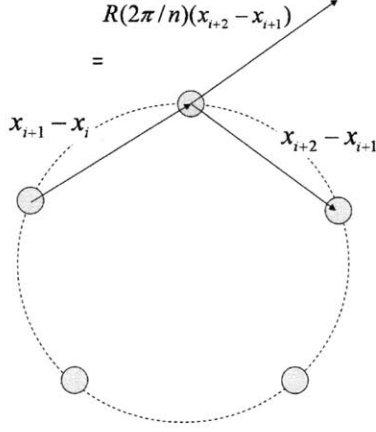


Figure 4-1: Constraint description of \mathcal{M}_5

Then, the matrix V_{rn} , such that $V_{rn}\bar{\mathbf{x}} = 0 \Leftrightarrow \mathbf{x} \in \mathcal{M}_n$ is:

$$V_{rn} = \begin{bmatrix} -I & I + R_{\frac{2\pi}{n}} & -R_{\frac{2\pi}{n}} & 0 & \dots & 0 \\ 0 & -I & I + R_{\frac{2\pi}{n}} & -R_{\frac{2\pi}{n}} & 0 & \dots \\ \vdots & \vdots & \vdots & \vdots & \vdots & \vdots \end{bmatrix} \quad (4.19)$$

In the case of 3 vehicles, with $\alpha = \pi/3$, V_r corresponds to:

$$V_{r3} = \begin{bmatrix} -1 & 0 & 3/2 & \sqrt{3}/2 & -1/2 & -\sqrt{3}/2 \\ 0 & -1 & -\sqrt{3}/2 & 3/2 & \sqrt{3}/2 & -1/2 \end{bmatrix} \quad (4.20)$$

And the transformed Jacobian is:

$$V_{r3}\mathcal{L}_sV_{r3}^\top = \begin{bmatrix} -6 & -3\sqrt{3} \\ 3\sqrt{3} & -6 \end{bmatrix} \quad (4.21)$$

which is negative definite, with $\lambda(V_{r3}\mathcal{L}_sV_{r3}^\top) = \{-6, -6\}$, which verifies the global convergence to manifold \mathcal{M}_n if $\text{eig}(V_{r3}\text{diag}[\frac{d\mathbf{f}(\mathbf{x})+\mathbf{f}^\top(\mathbf{x})}{d\mathbf{x}}]V_{r3}^\top) < 6$. In Section 4.2, a generalized result that addresses analytical results for any number of vehicles and under combinations of different cyclic topologies is shown.

4.1.1 Time varying and nonlinear manifolds

After having introduced the general concept, the case of a more complex type of systems, namely nonlinear systems with possibly time varying convergence manifolds are introduced in this section. The framework presented by Pham and Slotine in their previous work [68] discusses the convergence for linear time invariant manifolds. It is possible however, to extend their results to a more general version considering nonlinear, time varying manifolds by proceeding in a similar manner. Such results are shown useful in the developments and applications presented in the later sections.

A very helpful extension of the contraction theory approach consists of showing the contracting properties of an auxiliary system that has solutions of the actual system as particular solutions. Consider a nonlinear system that can be written in the form:

$$\dot{\mathbf{x}} = F(\mathbf{x}, t)\mathbf{x} \quad (4.22)$$

with an invariant manifold $\bar{\mathbf{x}} \in \mathcal{M} : \{\bar{\mathbf{x}} : V\bar{\mathbf{x}} = 0\}$, such that $VF(\bar{\mathbf{x}})\bar{\mathbf{x}} = 0$.

Consider the auxiliary system:

$$\dot{\mathbf{z}} = F(\mathbf{z}, t)\mathbf{z} \quad (4.23)$$

which has specific solutions $\mathbf{z}(t) = \mathbf{x}(t)$ and $\mathbf{z} = 0$.

The dynamics of the perpendicular projection are given by:

$$\dot{\mathbf{y}} = \bar{V}F(\mathbf{z}, t)(\bar{V}^\top \mathbf{y} + \bar{U}^\top \bar{U}\mathbf{x}) \quad (4.24)$$

then, the projected Jacobian is:

$$J_y = \bar{V}F(\mathbf{z}, t)\bar{V}^\top \quad (4.25)$$

Therefore, the auxiliary system is contracting if:

$$(\dot{\Theta} + \Theta(\bar{V}F(\mathbf{z}, t)\bar{V}^\top))\Theta^{-1} < 0 \quad \text{uniformly} \quad (4.26)$$

in which case all trajectories converge to the same one, and $\mathbf{x}(t) = 0$ is one of them. Again, since $V = T\bar{V}$, then:

$$VF(\mathbf{x}, t)V^\top < 0 \quad \text{uniformly} \quad (4.27)$$

is a sufficient condition for convergence to \mathcal{M} .

The following theorem, extends the partial contraction theory for convergence to nonlinear and time varying manifolds:

Theorem 4.1.1 *Consider a nonlinear system that can be written in the form:*

$$\dot{\mathbf{x}} = F(\mathbf{x}, t)\mathbf{x} \quad (4.28)$$

with a (possibly time varying) invariant manifold $\bar{\mathbf{x}} \in \mathcal{M}(t) : \{\bar{\mathbf{x}} : V(t)\bar{\mathbf{x}} = 0\}$, such that $\frac{d}{dt}(V(t)\bar{\mathbf{x}}) = 0$. Then, the system converges to $\mathbf{x} \in \mathcal{M}(t)$ if $\exists \Theta$:

$$(\dot{\Theta} + \Theta(\dot{V}V^\top + VF(\mathbf{x}, t)V^\top))\Theta^{-1} < 0 \quad \text{uniformly} \quad (4.29)$$

or,

$$(\dot{V}V^\top + VF(\mathbf{x}, t)V^\top) < 0 \quad \text{uniformly} \quad (4.30)$$

Proof:

The dynamics of the perpendicular projection are given by:

$$\dot{\mathbf{y}} = \dot{\bar{V}}(\bar{V}^\top \mathbf{y} + \bar{U}^\top \bar{U}\mathbf{x}) + \bar{V}F(\mathbf{z}, t)(\bar{V}^\top \mathbf{y} + \bar{U}^\top \bar{U}\mathbf{x}) \quad (4.31)$$

then, the projected Jacobian is:

$$J_y = \dot{\bar{V}}\bar{V}^\top + \bar{V}F(\mathbf{z}, t)\bar{V}^\top \quad (4.32)$$

Therefore, the auxiliary system is contracting if:

$$(\dot{\Theta} + \Theta(\dot{\bar{V}}\bar{V} + \bar{V}F(\mathbf{z}, t)\bar{V}^\top))\Theta^{-1} < 0 \quad \textit{uniformly} \quad (4.33)$$

in which case all trajectories converge to the same one, and $\mathbf{x}(t) = 0$ is one of them. Again, since $V = T\bar{V}$, $\dot{V} = T\dot{\bar{V}}$ then:

$$\dot{V}V^\top + VF(\mathbf{x}, t)V^\top < 0 \quad \textit{uniformly} \quad (4.34)$$

is a sufficient condition for convergence to \mathcal{M} . ■

4.2 Cyclic Controllers for Convergence to Formation

The most common approach to formation control studied in the literature defines laws based on tracking relative positions to a set of neighbors. This approach is not always the most desirable, and the control effort can often be significantly reduced by eliminating the 'unnecessary' constraints in the formation degrees of freedom. Then the convergence is given as converging to desired manifolds defined by linear or nonlinear constraints. Additionally, if the emergent behavior is an overall formation state with some unconstrained degrees of freedom, a leader or a pair of leaders can control those states for the whole formation without the need of a global coordination mechanism reassigning relative position targets.

Some authors have studied the convergence to relevant symmetric formations by using potential functions, e.g. [64, 88]. A main pitfall is convergence to local equilibria, leading to a lack of global convergence guarantees and unpredictability of the behavior under

disturbances. These difficulties exacerbate in the time-varying case. Guaranteed global convergence to formation, in itself a highly desirable property, also has important implications in the robustness of the formation architecture.

The results of applying the above described contraction theory approach to the problem are presented by consider the generalization of the cyclic pursuit to time varying, state varying control functions. This also leads to addressing the proof of global convergence for a type of distributed controllers based on cyclic topologies.

4.2.1 Generalized cyclic approach to formation control

Based on the presented approach and the time varying extension on the previous section, we present theoretical results for the convergence to symmetric formations based on control laws that generalize the cyclic pursuit algorithm to more general interconnections and nonlinear cases. First we show the global convergence of a basic control law to regular polygons under a generalized nonlinear cyclic topology with any number of vehicles and then we show how this result directly verifies the global convergence to rotating circular formations in the case of the basic cyclic pursuit algorithm.

These control law generalizes the results and allow the design of distributed algorithms that converge to formations with geometric characteristics that depend on a common coordination state, and can be time varying. One can think for example a satellite formation that expands, contracts (by varying α) or speeds up (by varying k) as a function of its location in orbit.

Consider the first order system $\dot{\mathbf{x}} = f(\mathbf{x}) + \mathbf{u}$ and the generalized symmetric cyclic control law:

$$\mathbf{u}_i(\mathbf{x}, t) = \sum_{m \in \mathcal{N}_r} k_m(\mathbf{x}, t) \left(R_m(\mathbf{x}, t)(\mathbf{x}_{[i+m]} - \mathbf{x}_i) + R_m^\top(\mathbf{x}, t)(\mathbf{x}_{[i-m]} - \mathbf{x}_i) \right) \quad (4.35)$$

where \mathcal{N}_r is a set of relative neighbors in the ordered set $\{1, \dots, N\}$, and $[p] \in \{1, \dots, N\}$

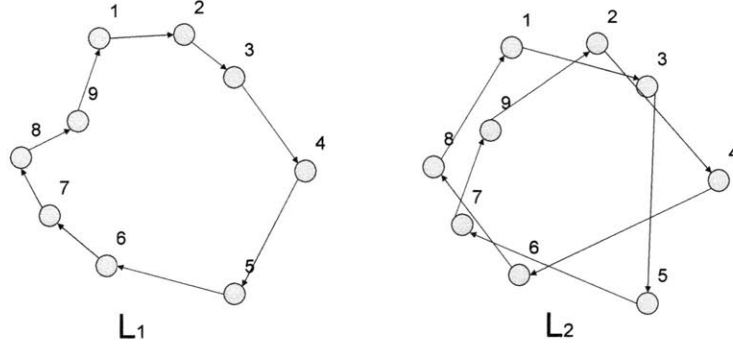


Figure 4-2: Different cyclic topologies

indicates p modulo N . The expression in eq. (4.35) indicated that for each link $\{i, [i + m]\}$ there is a symmetric link $\{i, [i - m]\}$. $k_m(\mathbf{x}, t) \in \mathbb{R}_{\geq 0}$ is a gain and $R(\mathbf{x}, t)$ is a coupling matrix that can be selected to achieve different behaviors. A general description of the overall dynamics of a system can then be written as:

$$\begin{aligned}
 \dot{\mathbf{x}} &= \mathbf{f}(\mathbf{x}) - \sum_m k_m(\mathbf{x}, t) ((L_m \otimes R_m(\mathbf{x}, t) + L_m^\top \otimes R_m^\top(\mathbf{x}, t))) \mathbf{x} \\
 &\doteq \mathbf{f}(\mathbf{x}) - \sum_m k_m(\mathbf{x}, t) (\mathcal{L}_m(\mathbf{x}, t) + \mathcal{L}_m^\top(\mathbf{x}, t)) \mathbf{x}
 \end{aligned} \tag{4.36}$$

and

$$\mathcal{L}_{sm}(\mathbf{x}, t) \doteq (\mathcal{L}_m(\mathbf{x}, t) + \mathcal{L}_m^\top(\mathbf{x}, t)) \tag{4.37}$$

where \mathbf{x} is the vector describing the overall state of the system and L_m are m -circulant Laplacian matrices describing cyclic underlying topologies with interconnections to each m -other agent as show in fig. 4-2.

Now, consider the manifold \mathcal{M}_n , presented in section 4.1:

$$\mathcal{M}_n = \{\bar{\mathbf{x}} : (\mathbf{x}_{i+1} - \mathbf{x}_i) = R_{\frac{2\pi}{n}}(\mathbf{x}_{i+2} - \mathbf{x}_{i+1})\} = \{\bar{\mathbf{x}} : V_{rn}\bar{\mathbf{x}} = 0\}, \quad (4.38)$$

which can be shown (straightforward from eq. (4.18)) to be a flow-invariant manifold of the dynamic system $\dot{\mathbf{x}} = k(\mathbf{x}, t)(\mathcal{L}_{sm}(\mathbf{x}, t))\mathbf{x}$.

Note that V_{rn} can be written for the general case of n vehicles in $3D$ as:

$$V_{rn} = (K \otimes I_3)(I_n \otimes R_\eta)((L_1 \otimes R_{\pi/N}) + (L_1^\top \otimes R_{\pi/N}^\top)) \doteq K_n \mathcal{R}_\eta \mathcal{L}^{(N)} \quad (4.39)$$

with $K = [I_{n-3} | 0_{3n-3}]$, L_1 is a cyclic Laplacian for a 1-circulant topology and R_η is a rotation matrix for any value η .

Since V_{rn} is full row rank, there exists an invertible transformation $V_{rn} = T\bar{V}_{rn}$ such that if $\bar{V}_{rn}A(\bar{V}_{rn})^\top > 0$ then $V_{rn}AV_{rn}^\top > 0$, where the columns of \bar{V}_{rn} are a set of orthonormal basis such that $\bar{V}_{rn}(\bar{V}_{rn})^\top = I$. Then, following the results of partial contraction theory described in sec 4.1, we have that if:

$$K_n \mathcal{R}_\eta \mathcal{L}^{(N)} \left(\frac{d\mathbf{f}(\mathbf{x})}{dx} - \sum_m k_m(\mathbf{x}, t) \mathcal{L}_{sm}(\mathbf{x}, t) \right) (\mathcal{L}^{(N)})^\top \mathcal{R}_\eta^\top K_n^\top < 0 \quad \text{uniformly} \quad (4.40)$$

then, the system converges to \mathcal{M}_n .

Since \mathcal{R}_η , $\mathcal{L}^{(N)}$, $\mathcal{L}_{sm}(\mathbf{x}, t) \in \mathcal{CR}$, the calculation of the eigenvalues of their product and correspondingly verifying that $K_n \mathcal{R}_\eta \mathcal{L}^{(N)} (\sum_m k_m(\mathbf{x}, t) \mathcal{L}_{sm}(\mathbf{x})) (\mathcal{L}^{(N)})^\top \mathcal{R}_\eta^\top K_n^\top < 0$ *uniformly* is straightforward and is shown in appendix A.5. The results are applied in the following theorem:

Theorem 4.2.1 Distributed nonlinear approach for global convergence to symmetric formations

Consider the distributed system with a generalized cyclic topology, using control law in eq.

(4.35):

$$\dot{\mathbf{x}}_i = \mathbf{f}(\mathbf{x}) + \mathbf{u}_i(\mathbf{x}, t) \quad (4.41)$$

$$\mathbf{u}_i(\mathbf{x}, t) = \sum_{m \in \mathcal{N}_r} k_m(\mathbf{x}, t) (R_m(\mathbf{x}, t)(\mathbf{x}_{[i+m]} - \mathbf{x}_i) + R(-\alpha_m(\mathbf{x}, t))(\mathbf{x}_{[i-m]} - \mathbf{x}_i)) \quad (4.42)$$

for which a description of the overall dynamics is written as:

$$\dot{\mathbf{x}} = \mathbf{f}(\mathbf{x}) - \sum_m k_m(\mathbf{x}, t) \mathcal{L}_{sm}(\mathbf{x}, t) \mathbf{x} \quad (4.43)$$

\mathbf{x} is the vector describing the overall state, $\bar{\mathbf{x}}$ is a particular regular polygonal state, and $V_{rn} \mathbf{f}(\bar{\mathbf{x}}) = 0$. Then, if:

$$\sup_{\mathbf{p}, t} \left\{ \lambda_{max} \left(\mathcal{R}_\eta \mathcal{L}^{(N)} \frac{\partial \mathbf{f}(\mathbf{p})}{\partial \mathbf{x}} (\mathcal{L}^{(N)})^\top \mathcal{R}_\eta^\top \right) - \min_{\substack{1 < i < N \\ q \in \{-1, 0, 1\}}} 4 \left(1 - \cos \left(\frac{2i\pi}{N} \right) \right) \sum_m k_m(\mathbf{p}, t) \left(\cos(q\alpha_m(\mathbf{p}, t)) - \cos \left(q\alpha_m(\mathbf{p}, t) - \frac{2im\pi}{N} \right) \right) \right\} < 0 \quad (4.44)$$

for some η , the system globally converges to a regular polygon.

Specifically, if $\mathbf{f}(\mathbf{x}) = 0$ the system globally converges to a regular polygon formation if:

$$\sup_{\mathbf{p}, t} \sum_m k_m(\mathbf{p}, t) (\cos(q\alpha_m(\mathbf{p}, t)) - \cos(q\alpha_m(\mathbf{p}, t) - 2im\pi/N)) > 0 \quad (4.45)$$

$\forall q \in \{-1, 0, 1\}, i \in \{2, N-1\}$.

Proof: For a regular formation $V_{rn} \bar{\mathbf{x}} = 0$, $V_{rn} \mathcal{L}_{sm}(\bar{\mathbf{x}}, t) \bar{\mathbf{x}} = 0$, then $V_{rn}(\mathbf{f}(\bar{\mathbf{x}}) - \sum k_m \mathcal{L}_{sm}(\bar{\mathbf{x}}, t) \bar{\mathbf{x}}) = 0$, therefore \mathcal{M}_n is an invariant manifold of the system.

From the results in Section A.5.1 it is also true that $\lambda \{ \mathcal{R} \mathcal{L} \sum_m k_m(\mathbf{x}, t) \mathcal{L}_{sm}(\mathbf{x}, t) \mathcal{L}^\top \mathcal{R}^\top \} \geq \min_{\substack{1 < i < N \\ q \in \{-1, 0, 1\}}} \lambda_{ik}$ defined in eq. A.5.1, and that if $\mathcal{R} \mathcal{L} X \mathcal{L} \mathcal{R} < 0$, then $K_n \mathcal{R}_\eta \mathcal{L} X \mathcal{L} \mathcal{R}_\eta K_n^\top < 0$ for a particular matrix X .

Thus, if condition in eq. (4.44) is satisfied, then $V_{rn}(\frac{\partial \mathbf{f}(x)}{\partial x} - \sum_m k_m(\mathbf{x}, t)\mathcal{L}_{sm}(\mathbf{x}, t)_m)V_{rn}^\top < 0$ and therefore \mathbf{x} exponentially converges to $\bar{\mathbf{x}} \in \mathcal{M}_n$. \blacksquare

If $\mathbf{f}(\mathbf{x}) = 0$, the above conditions in $\mathbf{f}(\bar{\mathbf{x}})$ are satisfied and the global convergence to $V_{rn}\mathbf{x} = 0$ is verified for specific combinations of $k_m(\mathbf{x}, t)$, $\alpha_m(\mathbf{x}, t)$. For the case of a 1-circulant topology L_1 , if $k(\mathbf{x}, t) > 0$ and $|\alpha(\mathbf{x}, t)| < 2\pi/N$, convergence to a symmetric formation is guaranteed.

Remark 4.2.2 *The Laplacian $\mathcal{L}_{sm}(\mathbf{x}, t)$ is the symmetric part of the Laplacian $\mathcal{L}_m(\mathbf{x}, t) = L_m \otimes R$. From the properties of positive negative matrices $VAV^\top < 0$ iff $V(A + A^\top)V^\top < 0$.*

It was shown that the manifold \mathcal{M}_n is an invariant manifold of the cyclic pursuit control law $R(\alpha)(\mathbf{x}_{[i+m]} - \mathbf{x}_i)$, then, verifying the conditions for convergence for the symmetric control law $\mathbf{u} = \sum k_m(\mathbf{x}, t)(\mathcal{L}_m(\mathbf{x}, t) + \mathcal{L}_m(\mathbf{x}, t)^\top)\mathbf{x}$ is a direct proof of convergence to circular rotating formations for the directed topology $\mathbf{u} = \sum k_m(\mathbf{x}, t)\mathcal{L}_m(\mathbf{x}, t)\mathbf{x}$, with asymmetric control law $u_i = k_m(\mathbf{x}, t)R(\alpha)(\mathbf{x}_{[i+m]} - \mathbf{x}_i)$ generalizing the results for cyclic pursuit.

This last result verifies the convergence to rotating regular formations resulting for k, α constants, agreeing with the results obtained through linear analysis presented in [67, 70, 73].

Proposition 4.2.3 *For a ring topology (L_1), if $|\alpha| = \pi/N$, the formation converges to a regular polygon with a constant size*

Proof: When a symmetric configuration is achieved:

$$\mathbf{x}_{i+m} - \mathbf{x}_i = R(-2\pi m/N)(\mathbf{x}_i - \mathbf{x}_{i-m}) \quad (4.46)$$

Then

$$\begin{aligned} \mathbf{u}_i &= R(\pi/N)(\mathbf{x}_{i+1} - \mathbf{x}_i) + R(-\pi/N)(\mathbf{x}_{i-1} - \mathbf{x}_i) \\ &= R(\pi/N)(R(-2\pi/N)(\mathbf{x}_i - \mathbf{x}_{i-1})) + R(-\pi/N)(\mathbf{x}_{i-1} - \mathbf{x}_i) \\ &= R(-\pi/N)(\mathbf{x}_i - \mathbf{x}_{i-1}) + R(-\pi/N)(\mathbf{x}_{i-1} - \mathbf{x}_i) = 0 \end{aligned} \quad (4.47)$$

■

similarly, for a more general cyclic topology, the condition for $k_m(\bar{\mathbf{x}}, t)$, $\alpha_m(\bar{\mathbf{x}}, t)$ to achieve a regular polygon with fixed size is given by:

$$\begin{aligned}
 \mathbf{u}_i &= \sum_m k_m(\bar{\mathbf{x}}, t) (R(\alpha_m(\bar{\mathbf{x}}, t))(R(-2\pi m/N)(\bar{\mathbf{x}}, t_i - \bar{\mathbf{x}}, t_{[i-m]})) \\
 &\quad + R(-\alpha_m(\bar{\mathbf{x}}, t))(\bar{\mathbf{x}}, t_{[i-m]} - \bar{\mathbf{x}}, t_i)) = 0 \\
 &= \sum_m k_m(\bar{\mathbf{x}}, t) (R(\alpha_m(\bar{\mathbf{x}}, t) - 2\pi m/N) - R(-\alpha_m(\bar{\mathbf{x}}, t))) = 0 \tag{4.48}
 \end{aligned}$$

4.2.2 Distributed global convergence to a desired formation size

The previous section addresses the problem of converging to a formation under a general cyclic interconnection. However, the subspace to which convergence is defined allows for the size of the formation to be an uncontrolled state of the system. In general the problem of global convergence to a splay-state formation using only neighbor information has been sought after in the literature. As mentioned in the introduction we consider the approach to a formation without constraining the relative states to be an specified vector.

One approach that converges to formations without specifying fixed relative vectors in a global frame consists of using structural potential functions of the magnitude of the distance to the neighbors [64]. When using only relative magnitude information, if the interconnection is not a rigid graph, the global convergence to the desired formation is impossible due to the ambiguity of the possible equilibrium configurations. An extra piece of information, allows our approach to achieve global convergence results, namely, the agreement on an orientation which in the case of spacecraft flight can be achieved by individual star trackers. In the case of the cyclic pursuit, an approach similar to the one presented in previous work [70], where the angle of the formation is defined as a dynamic variable that depends on the relative distance to the neighbor seems a reasonable approach however, the stability results are only local.

In this section, using an extension to the approach in the previous section we present a distributed control law for which *global* convergence to the desired size can be guaranteed. Specifically, we determine a sufficient condition in the magnitude of an arbitrary function that guarantees convergence to the desired formation from any initial conditions.

The overall structure of the proof consists of first showing that a sufficient condition on the bounds of an arbitrary odd function $f(x)$ guarantees convergence to a symmetric formation, i.e. convergence to the invariant manifold \mathcal{M}_n . And then, to show that the trajectories within that manifold lead to a formation of the desired size.

Theorem 4.2.4 Global convergence to a regular formation of a desired size

Consider a set of agents with first order dynamics $\dot{\mathbf{x}}_i = \mathbf{u}_i$, interconnected under an undirected cyclic topology with control law:

$$u_i = R_{\pi/N}(\mathbf{x}_{i+1} - \mathbf{x}_i) + R_{\pi/N}^\top(\mathbf{x}_{i-1} - \mathbf{x}_i) + f(|\mathbf{x}_{i+1} - \mathbf{x}_i| - \rho)(\mathbf{x}_{i+1} - \mathbf{x}_i) \quad (4.49)$$

where $f(z)$ is an arbitrary bounded odd function of z , such that $zf(z) > 0$ for $z \neq 0$ and $f(0) = 0$. The overall dynamics can be written as:

$$\dot{\mathbf{x}} = (-\mathcal{L}_s + G(\mathbf{x}))\mathbf{x} \quad (4.50)$$

Global convergence to $\mathcal{M}_{n\rho}$, the manifold of regular formations with intervehicle distance ρ , $\bar{\mathbf{x}} \in \mathcal{M}_{n\rho} = \{\bar{\mathbf{x}} : V_{rn}\mathbf{x} = 0, |\mathbf{x}_i - \mathbf{x}_j| = \rho \forall i, j\}$ is guaranteed if:

$$\lambda_{\min}(\bar{V}_{rn}\mathcal{L}_s(\bar{V}_{rn})^\top) > Nf_{\max}\lambda_{\max}(\bar{V}_{rn}A_1(\bar{V}_{rn})^\top) \quad (4.51)$$

where \bar{V}_{rn} is the matrix of orthonormal bases for V_{rn} , \mathcal{L}_s is the symmetric circulant rotational

Laplacian defined in Section 4.1, A_1 is the matrix $A_1 = \begin{bmatrix} -I & I & 0 & \dots \\ 0 & 0 & 0 & \dots \\ \vdots & \vdots & \vdots & \vdots \end{bmatrix}$ and $f(x) < f_{\max}$.

Proof: To start, consider the following two lemmas:

Lemma 4.2.5 *The manifold \mathcal{M}_n is a flow-invariant manifold of the dynamics in eq. (4.50)*

Proof: It has been shown above that \mathcal{M}_n is an invariant manifold of \mathcal{L}_s , namely $V_{rn}\mathcal{L}_s\bar{\mathbf{x}} = 0$ for $\bar{\mathbf{x}}$ such that $V_{rn}\bar{\mathbf{x}} = 0$. For a regular formation $|\mathbf{x}_{k+1} - \mathbf{x}_k| = |\mathbf{x}_{i+1} - \mathbf{x}_i|$ then $f(|\mathbf{x}_{k+1} - \mathbf{x}_k| - \rho) = f(|\mathbf{x}_{i+1} - \mathbf{x}_i| - \rho)$, and thus without any loss of generality $F(\mathbf{x}) = (f(|\mathbf{x}_2 - \mathbf{x}_1|)L_1 \otimes I_3)\mathbf{x}$.

Then, $V_{rn}(-\mathcal{L}_s + G(\mathbf{x}))\bar{\mathbf{x}} = f(|\mathbf{x}_2 - \mathbf{x}_1|)V_{rn}(L_1 \otimes I_3)\bar{\mathbf{x}} = 0$. ■

Lemma 4.2.6 *$\text{eig}(V_{rn}A_{is}\bar{V}_{rn}^\top) = \text{eig}(\bar{V}_{rn}A_{ks}\bar{V}_{rn}^\top)$ for all $i, k \in \{1, \dots, N\}$, where $A_{is} = (A_i + A_i^\top)$. $A_i = a^{(i)} \otimes I_3$, $a^{(i)} = \{a_{i,j}^{(i)}\} \in \mathbb{R}^{N \times N}$ is a matrix of zeros except the elements $a_{i,i}^{(i)} = -1$, $a_{i,i+1}^{(i)} = 1$. A_1 was explicitly described above.*

Proof: $\text{eig}(\bar{V}_{rn}A_{is}\bar{V}_{rn}^\top) = \text{eig}(\bar{V}_{rn}A_{ks}\bar{V}_{rn}^\top)$ if and only if there exists a similarity transformation such that:

$$T\bar{V}_{rn}A_{is}\bar{V}_{rn}^\top = \bar{V}_{rn}A_{ks}\bar{V}_{rn}^\top T \quad (4.52)$$

Notice that $T_{ik}A_i = A_kT_{ki}$ where $T_{ik} = T_{ki}^\top = (I_n - L_{k-i}) \otimes I_2$, for example, in the case of $i = 1, k = 2$:

$$T_{12}A_1 = A_2T_{12}^\top \quad (4.53)$$

$$\begin{bmatrix} 0 & I & 0 & \dots \\ 0 & 0 & I & \dots \\ \vdots & \vdots & \vdots & \vdots \\ I & 0 & \dots & 0 \end{bmatrix} \begin{bmatrix} -I & I & 0 & \dots \\ 0 & 0 & 0 & \dots \\ 0 & 0 & 0 & \dots \\ \vdots & \vdots & \vdots & \vdots \end{bmatrix} = \begin{bmatrix} 0 & 0 & 0 & \dots \\ 0 & -I & I & \dots \\ 0 & 0 & 0 & \dots \\ \vdots & \vdots & \vdots & \vdots \end{bmatrix} \begin{bmatrix} 0 & 0 & 0 & \dots & I \\ I & 0 & 0 & \dots \\ 0 & I & 0 & \dots \\ \vdots & \vdots & \vdots & \vdots \end{bmatrix} \quad (4.54)$$

and correspondingly $T_{ik}A_{is} = A_{ks}T_{ki}$. Then we have that $\bar{V}_{rn}\bar{V}_{rn}^\top = I$, therefore by defining $T = \bar{V}_{rn}T\bar{V}_{rn}^\top$:

$$T\bar{V}_{rn}A_{is}\bar{V}_{rn}^\top = \bar{V}_{rn}T\bar{V}_{rn}^\top\bar{V}_{rn}A_{is}\bar{V}_{rn}^\top = \bar{V}_{rn}TA_{is}\bar{V}_{rn}^\top \quad (4.55)$$

and

$$\bar{V}_{rn}A_{ks}\bar{V}_{rn}^T T = \bar{V}_{rn}A_{ks}\bar{V}_{rn}^T \bar{V}_{rn} T \bar{V}_{rn}^T = \bar{V}_{rn}A_{ks}T\bar{V}_{rn}^T \quad (4.56)$$

shows the desired equivalence. ■

Based on the above lemmas, we can then show that condition (4.51) guarantees convergence to the invariant manifold \mathcal{M}_n . Specifically, invoking the results in [110] and [68] introduced in Section 4.1 the convergence to the manifold $\mathcal{M}_n : \{\bar{\mathbf{x}} : \bar{V}_{rn}\bar{\mathbf{x}}\}$ is guaranteed if the projected Laplacian of the auxiliary system $\dot{\mathbf{y}} = (-\mathcal{L}_s + G(\mathbf{x}))\mathbf{y}$ is negative definite, i.e.

$$\bar{V}_{rn}(-\mathcal{L}_s + G(\mathbf{x}))\bar{V}_{rn}^T < 0 \quad (4.57)$$

This can be guaranteed if

$$\lambda_{\min}(\bar{V}_{rn}\mathcal{L}_s\bar{V}_{rn}^T) > \lambda_{\max}(\bar{V}_{rn}G(\mathbf{x})\bar{V}_{rn}^T) \quad (4.58)$$

Since

$$\lambda_{\max}(\bar{V}_{rn}G(\mathbf{x})\bar{V}_{rn}^T) = \lambda_{\max}(\bar{V}_{rn} \sum_{i=1}^N f(\mathbf{x}_{i+1} - \mathbf{x}_i)A_i(\mathbf{x})(\bar{V}_{rn})^T) \quad (4.59)$$

$$< Nf_{\max}\lambda_{\max}(\bar{V}_{rn}A_i(\mathbf{x})(\bar{V}_{rn})^T) \quad (4.60)$$

eq. (4.51) guarantees eq. (4.57) and thus, convergence to \mathcal{M}_n .

Now, it is shown that convergence to \mathcal{M}_n implies convergence to $\mathcal{M}_{n\rho}$. Having that

$\mathcal{L}\bar{\mathbf{x}} = 0$ then, the dynamics of the distance between any two vehicles in \mathcal{M}_n are given by:

$$\begin{aligned}
\frac{d}{dt}|\mathbf{x}_{i+1} - \mathbf{x}_i| &= \frac{(\mathbf{x}_{i+1} - \mathbf{x}_i)^\top}{|\mathbf{x}_{i+1} - \mathbf{x}_i|}(\dot{\mathbf{x}}_{i+1} - \dot{\mathbf{x}}_i) \\
&= \frac{(\mathbf{x}_{i+1} - \mathbf{x}_i)^\top}{|\mathbf{x}_{i+1} - \mathbf{x}_i|} f(|\mathbf{x}_{i+2} - \mathbf{x}_{i+1}| - \rho)(\mathbf{x}_{i+2} - \mathbf{x}_{i+1}) - f(|\mathbf{x}_{i+1} - \mathbf{x}_i| - \rho)(\mathbf{x}_{i+1} - \mathbf{x}_i) \\
&= \frac{(\mathbf{x}_{i+1} - \mathbf{x}_i)^\top}{|\mathbf{x}_{i+1} - \mathbf{x}_i|} (f(|\mathbf{x}_{i+1} - \mathbf{x}_i| - \rho)R_{2\pi/N}(\mathbf{x}_{i+1} - \mathbf{x}_i) - f(|\mathbf{x}_{i+1} - \mathbf{x}_i| - \rho)(\mathbf{x}_{i+1} - \mathbf{x}_i)) \\
&= \frac{(\mathbf{x}_{i+1} - \mathbf{x}_i)^\top}{|\mathbf{x}_{i+1} - \mathbf{x}_i|} (f(|\mathbf{x}_{i+1} - \mathbf{x}_i| - \rho)(R_{2\pi/N} - I_3)(\mathbf{x}_{i+1} - \mathbf{x}_i)) \\
&= -\cos(\pi/N)f(|\mathbf{x}_{i+1} - \mathbf{x}_i| - \rho)|\mathbf{x}_{i+1} - \mathbf{x}_i|
\end{aligned} \tag{4.61}$$

defining $z = |\mathbf{x}_{i+1} - \mathbf{x}_i| - \rho$:

$$\dot{z} = -\cos(\pi/N)f(z)(z + \rho). \tag{4.62}$$

A Lyapunov function candidate for this system is $V = \frac{1}{2}z^2$, yielding

$$\dot{V} = -\cos(\pi/N)zf(z)(z + \rho) \tag{4.63}$$

Since $f(z)$ is an odd function, $zf(z) > 0$ for $z \neq 0$. Furthermore, $z + \rho = |\mathbf{x}_{i+1} - \mathbf{x}_i| > 0$, so that $\dot{V} \leq 0$. Using Lasalle's Invariant Set Theorem [90], the system (4.50) globally converges to the largest invariant set where $\dot{V} = 0$, namely $\mathcal{M}_{n\rho}$. ■

Note that the global guarantee in this control approach is defined by an upper bound on the arbitrary function $f(z)$. This bound is easily implementable by a saturation function or an arctangent function.

The two results presented in this section generalize results of cyclic control approach to nonlinear systems. Specifically, we introduce an analysis approach that achieves *global* guarantees for a generalized version of cyclic pursuit, which includes time-varying and state-dependent gains and coupling matrices as well as more general cyclic interconnections. Additionally, we introduce a decentralized control approach with *global* convergence guarantees

to a regular formation by defining upper bounds on a function that controls the separation between vehicles.

4.2.3 Extension to second order systems

In the derivation of the results we define the systems as first order systems. In general, for space applications we consider control approaches for second order systems. This section presents an approach based on a sliding mode control that shows a straightforward extension of the first order integrators to more complex dynamics when there is knowledge of a reference velocity for the whole formation.

Let again, $\mathbf{x}_i(t) = [x_{i,1}(t), x_{i,2}(t), x_{i,3}(t)]^\top \in \mathbb{R}^3$ be the position at time $t \geq 0$ of the i^{th} agent, $i \in \{1, 2, \dots, n\}$, and let $\mathbf{x} = [\mathbf{x}_1^\top, \mathbf{x}_2^\top, \dots, \mathbf{x}_n^\top]^\top$.

Consider a linear first order system:

$$\dot{\mathbf{x}}_i = \sum A_{ij}(\mathbf{x}_j - \mathbf{x}_i) \quad (4.64)$$

shown to converge to manifold \mathcal{M}_1 .

If the dynamics of each agent are now described by a second order model:

$$\begin{aligned} \dot{\mathbf{x}}_i &= \mathbf{v}_i \\ \dot{\mathbf{v}}_i &= f(\mathbf{x}_i, \mathbf{v}_i) + \mathbf{u}_i \end{aligned} \quad (4.65)$$

consider the feedback control law:

$$\mathbf{u}_i = -f(\mathbf{x}_i, \mathbf{v}_i) + k_d \sum A_{ij}(\mathbf{x}_j - \mathbf{x}_i) + \sum A_{ij}(\mathbf{v}_j - \mathbf{v}_i) - k_d \mathbf{v}_i, \quad k_d \in \mathbb{R}_{>0}. \quad (4.66)$$

A useful form to describe the second order system is by using the sliding variables defined

as:

$$\mathbf{s}_i = k_d \mathbf{x}_i + \mathbf{v}_i \quad (4.67)$$

Then, the dynamics of the overall system (4.65) with control law (4.66) can be written as:

$$\ddot{\mathbf{x}}_i = \sum A_{ij} (k_d (\mathbf{x}_j - \mathbf{x}_i) + (\mathbf{v}_j - \mathbf{v}_i)) - k_d \mathbf{v}_i \quad (4.68)$$

$$= \sum A_{ij} ((k_d \mathbf{x}_j + \mathbf{v}_j) - (k_d \mathbf{x}_i + \mathbf{v}_i)) - k_d \mathbf{v}_i \quad (4.69)$$

Then, the system dynamics are described by the equations:

$$\dot{\mathbf{s}}_i = \sum A_{ij} (\mathbf{s}_j - \mathbf{s}_i) \quad (4.70)$$

$$\dot{\mathbf{x}}_i = -k_d \mathbf{x}_i + \mathbf{s}_i \quad (4.71)$$

The first equation describes a first order system for which global convergence to a manifold $\mathcal{M} \subset R^3$ can be analyzed following the approach in the previous sections, the second equation is an stable first order filter with input \mathbf{s}_i and output \mathbf{x}_i . Then, the trajectories of the agents under control law (4.66) are the filtered response of trajectories of the first order system. Under the control law in eq. (4.66), the physical trajectories converge to trajectories which are just the response of the filter $G_{k_d}(j\omega) = \frac{1}{1+jk_d\omega}$ to the trajectories of the first order system with initial conditions $\mathbf{s}(0) = k_d \mathbf{x}(0) + \dot{\mathbf{x}}(0)$. This last subsection provides an approach for the implementation of the control laws described in this chapter for the case of spacecraft formations, where $f(\mathbf{x}, \mathbf{v})$ can be a local description of the gravitational dynamics with respect to some reference frame.

4.3 Convergence Primitives Approach

In this section we present an approach to formation control based on the combination of primitives. This approach is an extension of theorem 4.1. Using the idea of primitives, controllers that converge to more complex subspaces can be designed and their global convergence properties verified.

Theorem 4.3.1 *Consider the system:*

$$\dot{\mathbf{x}} = \sum_i \mathbf{f}_i(\mathbf{x}) \quad (4.72)$$

where each dynamic primitive $\mathbf{f}_i(\mathbf{x})$ has an invariant manifold \mathcal{M}_i :

$$V_i : \mathbb{R}^n \rightarrow \mathbb{R}^{p_i}, \quad V_i \mathbf{f}_i(\bar{\mathbf{x}}) = 0, \quad V_i \bar{\mathbf{x}} = 0, \quad \forall \bar{\mathbf{x}} \in \mathcal{M}_i \quad (4.73)$$

with $\text{rank}(V_i) = p_i$.

Then, if either:

$$i.) \quad \sum_i V \frac{\partial}{\partial \mathbf{x}} \mathbf{f}_i(\mathbf{x}) V^\top < 0 \quad (4.74)$$

or,

$$ii.) \quad \begin{bmatrix} V_1 \frac{df_1}{dx} V_1^\top & V_1 \frac{df_2}{dx} V_2^\top & \dots & V_1 \frac{df_n}{dx} V_n^\top \\ V_2 \frac{df_1}{dx} V_1^\top & V_2 \frac{df_2}{dx} V_2^\top & \dots & V_2 \frac{df_n}{dx} V_n^\top \\ \vdots & \vdots & \vdots & \vdots \\ V_n \frac{df_1}{dx} V_1^\top & V_n \frac{df_2}{dx} V_2^\top & \dots & V_n \frac{df_n}{dx} V_n^\top \end{bmatrix} < 0 \quad (4.75)$$

where $\text{span}\{V^\top\} = \text{span}\{[V_1^\top V_2^\top \dots V_n^\top]\}$. Then:

$$\mathbf{x} \rightarrow \bigcap_i \mathcal{M}_i \quad \text{as } t \rightarrow \infty \quad (4.76)$$

Proof: For the first condition consider $\bar{\mathbf{x}}$, a particular solution such that $0 = V_i \mathbf{x} = V_j \mathbf{x} = \dots = V_n \mathbf{x}$. Since V is full row rank, there exists a linear transformation $V = T\bar{V}$ where \bar{V} is an orthonormal partition of \mathbb{R}^n and $TVAV^T T^T < 0 \Leftrightarrow VAV^T < 0$. Then, if condition (A.29) holds, the system $\dot{\mathbf{y}} = V\dot{\mathbf{x}}$ is contracting with respect to \mathbf{y} and any trajectory of the system \mathbf{y} converges to the same solution, namely $\mathbf{x} \rightarrow \bar{\mathbf{x}} \in \bigcap_i \mathcal{N}(V_i) = \bigcap_i \mathcal{M}_i$.

For the second sufficient condition, consider the auxiliary system:

$$\mathbf{y} = \begin{bmatrix} \mathbf{y}_1 \\ \mathbf{y}_2 \\ \vdots \\ \mathbf{y}_n \end{bmatrix} = \begin{bmatrix} V_1 \\ V_2 \\ \vdots \\ V_n \end{bmatrix} \mathbf{x}, \quad (4.77)$$

then:

$$\dot{\mathbf{y}}_i = \sum_k \bar{V}_i \mathbf{f}_k (\bar{V}_k^T \mathbf{y}_k + U_k^T U_k \mathbf{x}) \quad (4.78)$$

$V_i = T\bar{V}_i$, where \bar{V}_i are orthonormal projections of the state such that $\bar{V}_i \bar{V}_i^T = I_{p_i}$, and $\bar{V}_i^T \bar{V}_i + U_i^T U_i = I_n$. Since $\text{rank}(V_i) = p_i$, T is an invertible matrix. The Jacobian of the system $\dot{\mathbf{y}}$ with respect to \mathbf{y} is:

$$\begin{bmatrix} \bar{V}_1 \frac{df_1}{dx} \bar{V}_1^T & \bar{V}_1 \frac{df_2}{dx} \bar{V}_2^T & \dots & \bar{V}_1 \frac{df_n}{dx} \bar{V}_n^T \\ \bar{V}_2 \frac{df_1}{dx} \bar{V}_1^T & \bar{V}_2 \frac{df_2}{dx} \bar{V}_2^T & \dots & \bar{V}_2 \frac{df_n}{dx} \bar{V}_n^T \\ \vdots & \vdots & \vdots & \vdots \\ \bar{V}_n \frac{df_1}{dx} \bar{V}_1^T & \bar{V}_n \frac{df_2}{dx} \bar{V}_2^T & \dots & \bar{V}_n \frac{df_n}{dx} \bar{V}_n^T \end{bmatrix} \quad (4.79)$$

which can be written as:

$$\text{diag}[T_i] \begin{bmatrix} V_1 \frac{df_1}{dx} V_1^\top & V_1 \frac{df_2}{dx} V_2^\top & \cdots & V_1 \frac{df_n}{dx} V_n^\top \\ V_2 \frac{df_1}{dx} V_1^\top & V_2 \frac{df_2}{dx} V_2^\top & \cdots & V_2 \frac{df_n}{dx} V_n^\top \\ \vdots & \vdots & \vdots & \vdots \\ V_n \frac{df_1}{dx} V_1^\top & V_n \frac{df_2}{dx} V_2^\top & \cdots & V_n \frac{df_n}{dx} V_n^\top \end{bmatrix} \text{diag}[T_i^\top] \quad (4.80)$$

and $\text{diag}[T_i]$ is an invertible transformation, such that $TVAV^\top T^\top < 0$ if and only if $V^\top AV^\top < 0$. Then, the negative definiteness in eq. (4.75), proves the global convergence to $y = 0$, i.e $\mathbf{x} \rightarrow \bar{\mathbf{x}} \in \bigcap_i \mathcal{N}(V_i) = \bigcap_i \mathcal{M}_i$. ■

Notice that additionally, if $V \frac{\partial}{\partial \mathbf{x}} \mathbf{f}_i(\mathbf{x}) V^\top \leq 0$ then $V \sum_i \frac{\partial}{\partial \mathbf{x}} \mathbf{f}_i(\mathbf{x}) V^\top$ is at least semidefinite negative. If one of the summation terms is positive definite or if the summation is full rank, it is positive definite.

Corollary 4.3.2 Consider a set of N agents with dynamics $\dot{\mathbf{x}}_i = u_i$ grouped in sets \mathcal{S}_s $s \in \{m, n, nm\}$, and a set of control laws $u_m = f_m(\mathbf{x}), u_n = f_n(\mathbf{x}), u_{nm} = f_{nm}(\mathbf{x})$ corresponding to each group where $f_s(\mathbf{x})$ depends only on elements of set \mathcal{S}_s and has corresponding invariant manifolds \mathcal{M}_s with respective set of transformations V_s , for which $V_s f_s = 0$.

Control law f_m interconnects agents in set $S_m \subset S$, control law f_n interconnect agents in the set $S_n \subset S$, $S_m \cap S_n = \emptyset$, and control law f_{nm} interconnect agents in set S_n and S_m .

If f_s , individually converge to their invariant subspaces \mathcal{M}_s , i.e. $V_s \frac{df_s}{dx} V_s^\top < 0$ for all i , then, a sufficient condition for the global convergence of the system $\dot{\mathbf{x}} = \sum_s f_s(\mathbf{x})$ to the subspace $\mathcal{M} = \bigcap_i \mathcal{M}_i$ is:

$$\begin{bmatrix} V_k \frac{df_k}{dx} V_k^\top & V_l \left(\frac{df_{kl}}{dx} + \frac{df_l}{dx}^\top \right) V_{kl}^\top \\ V_{kl} \left(\frac{df_l}{dx} + \frac{df_{kl}}{dx}^\top \right) V_l^\top & V_l \frac{df_l}{dx} V_l^\top \end{bmatrix} < 0 \quad (4.81)$$

for all $k, l \in s$. This result can be extended to more than two sets of disjoint groups n, m with interconnecting links nm .

Proof: Since $g_m \cap g_n = \emptyset$, $V_n f_m = 0$, the Jacobian has a block tridiagonal structure:

$$J = \begin{bmatrix} V_m \frac{df_m}{dx} V_m^\top & V_m \frac{df_{ml}}{dx} V_{ml}^\top & 0 & 0 & \dots & 0 \\ V_{ml} \frac{df_m}{dx} V_m^\top & V_{ml} \frac{df_{ml}}{dx} V_{ml}^\top & V_{ml} \frac{df_l}{dx} V_l^\top & 0 & \dots & 0 \\ 0 & V_l \frac{df_{ml}}{dx} V_{ml}^\top & \ddots & \vdots & \vdots & \\ 0 & 0 & \dots & V_{np} \frac{df_{np}}{dx} V_n^\top & V_n \frac{df_n}{dx} V_n^\top & \end{bmatrix} \quad (4.82)$$

given the block tridiagonal structure the positive definiteness result can be verified by verifying the positive definiteness of the lower dimensional matrices following the next proposition. ■

Proposition 4.3.3 *A block tridiagonal matrix with positive block entries A_{ii} :*

$$A = \begin{bmatrix} A_{11} & A_{12} & 0 & 0 & \dots & 0 \\ A_{21} & A_{22} & A_{23} & 0 & \dots & 0 \\ 0 & A_{32} & A_{33} & A_{34} & \dots & 0 \\ \vdots & \vdots & \vdots & \vdots & \vdots & \vdots \\ 0 & \dots & 0 & 0 & A_{n,n-1} & A_{n,n} \end{bmatrix} \quad (4.83)$$

and $A_{11} > 0$, $A_{nn} > 0$, is positive definite if the submatrices

$$A = \begin{bmatrix} A_{ii} & 2A_{i,i+1} \\ 2A_{i+1,i} & A_{i+1,i+1} \end{bmatrix} \quad (4.84)$$

are positive definite.

Proof: By partitioning the space as $\mathbf{x} = [x_1 \ x_2 \ \dots \ x_n]$, the quadratic form is:

$$\begin{aligned}
\mathbf{x}^\top \mathbf{A} \mathbf{x} &= x_1^\top A_{11} x_1 + x_1^\top (A_{12} + A_{21}^\top) x_2 + x_2^\top A_{22} x_2 + x_1^\top (A_{23} + A_{32}^\top) x_3 + x_3^\top A_{33} x_3 + \dots \\
&= \frac{1}{2} x_1^\top A_{11} x_1 + \frac{1}{2} x_1^\top A x_1 + x_1^\top (A_{12} + A_{21}^\top) x_2 + \frac{1}{2} x_2^\top A_{22} x_2 + \frac{1}{2} x_2^\top A_{22} x_2 + \dots + \frac{1}{2} x_n^\top A x_n \\
&= \frac{1}{2} x_1^\top A x_1 + \frac{1}{2} \begin{bmatrix} x_1 \\ x_2 \end{bmatrix}^\top \begin{bmatrix} A_{11} & 2A_{12} \\ 2A_{21} & A_{22} \end{bmatrix} \begin{bmatrix} x_1 & x_2 \end{bmatrix} + \frac{1}{2} \begin{bmatrix} x_2 \\ x_3 \end{bmatrix}^\top \begin{bmatrix} A_{22} & 2A_{23} \\ 2A_{32} & A_{33} \end{bmatrix} \begin{bmatrix} x_2 & x_3 \end{bmatrix} + \dots + \frac{1}{2} x_n^\top A x_n
\end{aligned} \tag{4.85}$$

which is positive if the condition in eq. (4.84) is met. ■

In the next section, we illustrate the application of the results in this section with a series of examples where application of the theorem and the discussed corollaries give insight into the construction of different convergence mechanisms.

4.4 Applications

In a first example we present a useful application of the analysis approach to define a decentralized control algorithm based on a set of primitives whose global convergence properties can be verified from the results of theorems 4.3.1 and 4.1.1.

Example 4.4.1 Global convergence to time varying formation with only relative information

Consider a formation flight mission where we are interested in achieving a cubic formation with each one of the vehicles in a vertex of the cube and allow the cube to rotate perpendicular to one of the faces with time varying angular velocity $\omega(t)$. This is the case for example of a formation continuously tracking a point on the ground while following an orbit around the planet.

The following control approach is proposed: Consider the group of 8 agents \mathbf{x}_i , $i \in \{1, \dots, 8\}$, with agent groups defined as $\mathcal{S}_l = \{s_1, s_2, \dots, s_m\}$, $\mathcal{S}_1 = \{1, 2, 3, 4\}$, $\mathcal{S}_{12} = \{3, 4, 6, 5\}$, $\mathcal{S}_2 = \{5, 6, 7, 8\}$, and a control law based on sets of vehicles \mathcal{S}_1 and \mathcal{S}_3 , following the cyclic pursuit

dynamics:

$$u_{s_i} = k_\omega(t)R_l(t)(\mathbf{x}_{s_{i+1}} - \mathbf{x}_{s_i}) \quad \text{for } s_i \in \mathcal{S}_1, \mathcal{S}_2 \quad (4.86)$$

with $k_\omega = \omega(t)/(2 \sin(\pi/4))$, and for \mathcal{S}_{12} a time varying coupling control law that converges to a planar square formation:

$$u_{s_i} = k_1 (R_l(t)(\mathbf{x}_{s_{i+1}} - \mathbf{x}_{s_i}) + R_l^\top(t)(\mathbf{x}_{s_{i-1}} - \mathbf{x}_{s_i})) \quad \text{for } s_i \in \mathcal{S}_{12} \quad (4.87)$$

where $R_l(t) \in \mathbb{R}^{3 \times 3}$ is a rotation that can vary its principal axis with time. Namely, the rotation matrices can be defined as $R_l = T_l(t)R_{\pi/4}T_l^\top(t)$, where T_1 is a constant arbitrary direction matrix (we can assume $T_1 = I$ without loss of generality), $T_2 = T_1$, and

$$T_{12}(t) = \begin{bmatrix} 0 & -\sin(\phi(t)) & \cos(\phi(t)) \\ 0 & \cos(\phi(t)) & -\sin(\phi(t)) \\ 1 & 0 & 0 \end{bmatrix} T_1 \quad (4.88)$$

where we assume $\dot{\phi}(t) = \omega(t) \geq 0$.

The dynamics of the overall system are defined as $\dot{\mathbf{x}} = A(t)\mathbf{x}$, and the constraints defining the convergence subspace $\mathcal{M} = \{\bar{\mathbf{x}} : V(t)\mathbf{x} = 0\}$, $V(t)^\top = \begin{bmatrix} V_1^\top & V_2^\top & V_3(t)^\top \end{bmatrix}$ where, in a similar manner to eq. 4.19:

$$V_1 = \begin{bmatrix} K_\eta \hat{\mathcal{L}}^{(4)} & \mathbf{0}_{6 \times 6} \end{bmatrix} \quad (4.89)$$

$$V_2 = \begin{bmatrix} \mathbf{0}_{6 \times 6} & K_\eta \hat{\mathcal{L}}^{(4)} \end{bmatrix} \quad (4.90)$$

$$V_{12}(t) = \begin{bmatrix} \mathbf{0}_{6 \times 3} & K_\eta \mathcal{L}^{(4)} \hat{T}_{12}(t) & \mathbf{0}_{6 \times 3} \end{bmatrix} \quad (4.91)$$

where we use the notation $\hat{T} = I_n \times T$ and \mathcal{M} can be shown to be a flow invariant manifold since $(\dot{V}(t) + VA(t))\bar{\mathbf{x}} = 0$.

From theorem 4.3.1 and theorem 4.1.1 we have a way to numerically verify sufficient conditions for the global convergence and stability to the desired subspace, namely it defines constraints in the minimum value of k_1 as a function of the upper bound in the magnitude of $\omega(t)$, namely $\omega_{max} \geq |\omega(t)|$ such that:

$$\sup_t \left(\dot{V}(t)V(t)^\top + V(t)A(t)V(t)^\top \right) < 0 \quad (4.92)$$

To see how this is true, notice that $\dot{V}_1 = 0$, $\dot{V}_2 = 0$, and

$$\dot{V}_{12}(t) = \begin{bmatrix} \mathbf{0}_{6 \times 3} & K_\eta \mathcal{L}^{(4)}[\omega(t)^\times] \hat{T}_{12}(t) & \mathbf{0}_{6 \times 3} \end{bmatrix} \quad (4.93)$$

$$= \omega(t) \begin{bmatrix} \mathbf{0}_{6 \times 3} & K_\eta \mathcal{L}^{(4)}[\hat{z}^\times] \hat{T}_{12}(\phi) & \mathbf{0}_{6 \times 3} \end{bmatrix} := \omega(t)D(\phi) \quad (4.94)$$

where $[\hat{z}^\times]$ is the skew-symmetric matrix $I_n \otimes \begin{bmatrix} 0 & 0 & -1 \\ 0 & 0 & 0 \\ 1 & 0 & 0 \end{bmatrix}$.

Since $V(t) = V(\phi(t))$ then $V(\phi)A(\phi)V(\phi)^\top = VAV^\top$ is obviously a constant because the reference frame is arbitrary.

$D(\phi)V(\phi)^\top$ can be verified to be positive semidefinite, the above condition can be guaranteed if:

$$\omega_{max} \left[\max_{0 < \phi < 2\pi} (D(\phi)V(\phi)^\top) \right] < VAV^\top \quad (4.95)$$

The term in brackets can be numerically calculated for a given gain k_1 , thus defining an upper bound in ω_{max} for which global convergence is guaranteed. Figure 4-3 shows the time history of the control approach converging to formation and achieving the desired rotating configuration.

As a second example that illustrates the application to derive convergence properties for general control a formation of vehicles surrounding a target is studied:

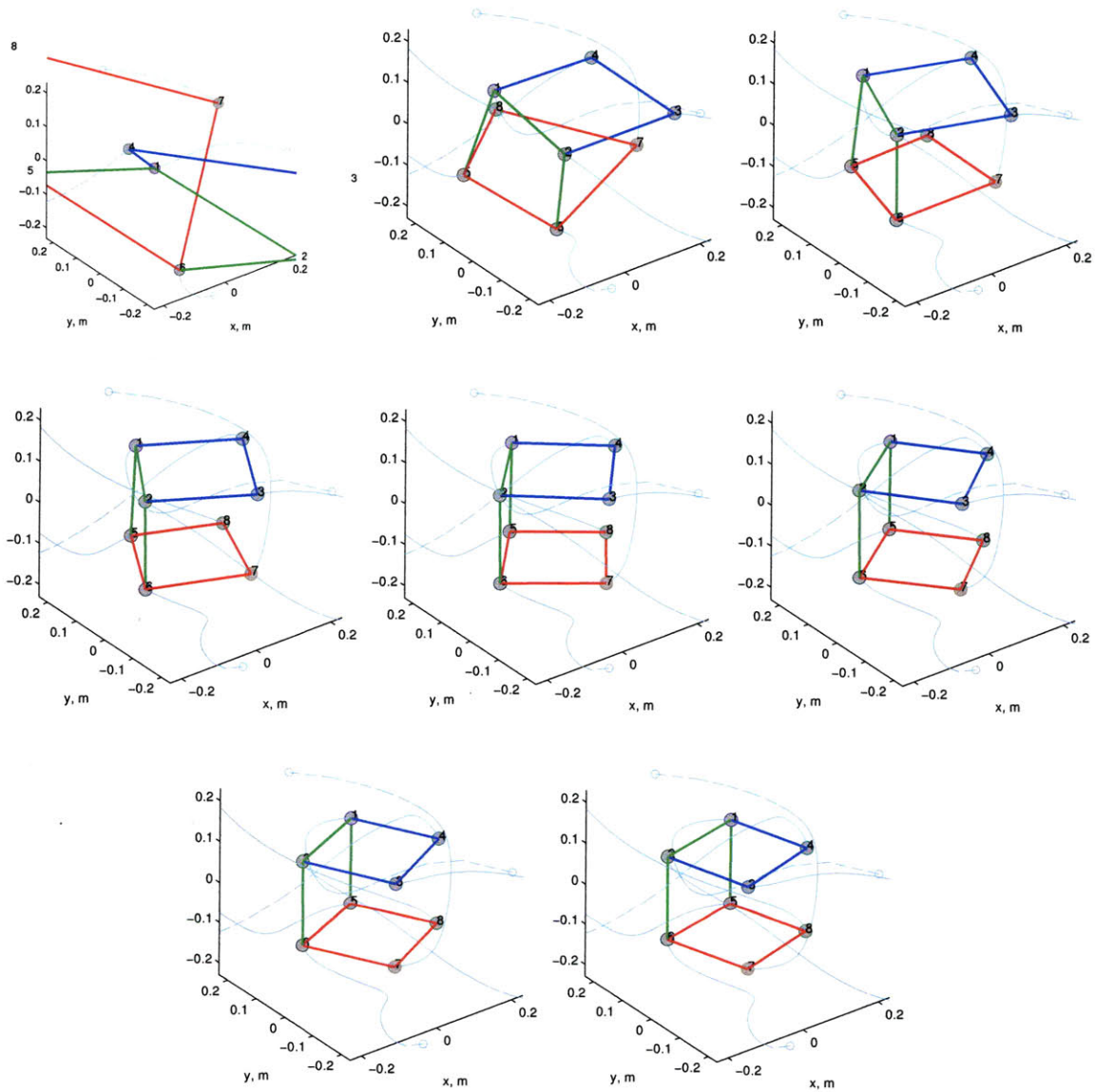


Figure 4-3: Agents converge to a cube in 3D. (Snapshots every 30 seconds).

Example 4.4.2 A regular formation surrounding an (un)cooperative target Consider a system of $n + 1$ agents, n of them with dynamics as in eq. 4.35, and a leader agent with state \mathbf{x}_1 that uses information from all others and/or all other agents use information from it:

$$\dot{\mathbf{x}}_1 = f_p(\mathbf{x}_1, \mathbf{x}) \quad (4.96)$$

$$\dot{\mathbf{x}}_i = R(\mathbf{x}_{i+1} - \mathbf{x}_i) + R^\top(\mathbf{x}_{i-1} - \mathbf{x}_i) + f_c(\mathbf{x}_i - \mathbf{x}_1) \quad (4.97)$$

$i = \{2, \dots, n\}$, and some general functions f_c, f_p with $f_c(0) = 0$. Denote $\mathbf{x}^\top = [\mathbf{x}_2^\top, \mathbf{x}_3^\top, \dots, \mathbf{x}_n^\top]^\top$.

The overall dynamics can then be written as:

$$\begin{bmatrix} \dot{\mathbf{x}}_1 \\ \mathbf{x} \end{bmatrix} = \begin{bmatrix} f_p(\mathbf{x}_1, \mathbf{x}) \\ \mathcal{L}\mathbf{x} + f_c(\mathbf{x}, \mathbf{x}_1) \end{bmatrix} \doteq F(\xi) \quad (4.98)$$

The interest here is to determine convergence to the subspace defined by $V\bar{\xi} = 0$, where:

$$V = \begin{bmatrix} 0 & V_{rn} \\ nI & -\mathbf{1}_n^T \otimes I \end{bmatrix} \quad (4.99)$$

where $\mathbf{1}_n \in \mathbb{R}^n$ is a vector of ones, $[nI_2 \quad -\mathbf{1}_n^T \otimes I]$ is a projection matrix into a subspace where the target is in the center of the formation and V_{rn} is the projection to the subspace of regular polygons in eq. 4.19. Considering the following results:

$$\mathcal{L}(\mathbf{1}_n \otimes I) = 0, \quad (4.100)$$

$$V_{rn} \frac{df_c}{d\mathbf{x}}[\mathbf{1}_n \otimes I] = 0 \quad (4.101)$$

It is then found that:

$$V \frac{dF}{d\xi} V^\top = \begin{bmatrix} V_{rn} \mathcal{L} V_{rn}^\top + V_{rn} \frac{df_c}{d\mathbf{x}} V_{rn}^\top & 0 \\ n \frac{df_p}{d\mathbf{x}} V_{rn}^\top & n \sum_i \left(\frac{df_c}{d\mathbf{x}_i} - \frac{df_p}{d\mathbf{x}_i} \right) + n^2 \left(\frac{df_p}{d\mathbf{x}_1} - \frac{df_c}{d\mathbf{x}_1} \right) \end{bmatrix} \quad (4.102)$$

Then, if $\frac{df_c}{d\mathbf{x}} < 0$, a sufficient condition to surround the target is:

$$\sum_i \left(\frac{df_c}{d\mathbf{x}_i} - \frac{df_p}{d\mathbf{x}_i} \right) + n \left(\frac{df_p}{d\mathbf{x}_1} - \frac{df_c}{d\mathbf{x}_1} \right) < 0 \quad (4.103)$$

Note that f_c, f_p are arbitrary functions and the result gives a sufficient condition to achieve the mission objective in terms only of the gradients of f_p and f_c .

In the next example we consider a fragmented aperture application, where individual telescopes are deployed in an arbitrary configuration and the objective consists on achieving convergence to a formation where in its final configuration the vehicles are as close as possible to each while maintaining a minimum separation between them to achieve the recreation of a full aperture composed by many small segments. The problem is related to the two-dimensional sphere packing problem and a solution can be described by a series of concentric hexagonal formations. In this example, a distributed control law based on theorem 4.3.1 is proposed and sufficient conditions for global converge to such configuration with any number of spacecraft are derived.

Example 4.4.3 Convergence to a packed formation. Consider a set of agents with first order dynamics $\dot{\mathbf{x}}_i = u_i$, grouped in M sets \mathcal{S}_l of 6 vehicles, and consider the input:

$$u_i = R_{\pi/6}(\mathbf{x}_{i+1} - \mathbf{x}_i) + R_{\pi/6}^\top(\mathbf{x}_{i-1} - \mathbf{x}_i)\mathbf{f}_m \quad \text{for } i \in \mathcal{S}_m \quad (4.104)$$

\mathcal{S}_m being a group of size 6, $m \in \{1, \dots, M\}$. This input was shown to make the system of agents \mathbf{x}_i , $i \in \mathcal{S}_l$ converge to manifold $\mathcal{M}_6 : \{V_6 \mathbf{x} = 0\}$ of regular hexagonal formations.

Now, consider interconnection control laws between the different sets \mathcal{S}_l :

$$u_k = R_{\pi/3}(\mathbf{x}_{k+1} - \mathbf{x}_k) + R_{\pi/3}^\top(\mathbf{x}_{k-1} - \mathbf{x}_k) = \mathbf{f}_{ml} \quad \text{for } k \in \mathcal{S}_{ml}; \quad (4.105)$$

\mathcal{S}_{ml} being a group with 3 agents, some agents in \mathcal{S}_m and some in \mathcal{S}_l , which has been shown to converge to triangular formations such that $\mathcal{M}_3 : \{V_{r3}\mathbf{x} = 0\}$.

The constraints of the desired convergence subspace are $V_m = [V_{r6} \ 0_{4 \times 6}]$, $V_l = [0_{4 \times 6} \ V_{r6}]$, and the corresponding link constraints $V_{ml} = [v_1, \dots, v_N]$, $v_n \in \mathbb{R}^{3 \times 3}$, $v_{m1} = -I$, $v_{m2} = I + R_{2\pi/3}$, $v_{l1} = -R_{2\pi/3}$ for some $m1, m2 \in \mathcal{S}_m$, $l1 \in \mathcal{S}_l$.

The Jacobians will be denoted as $\frac{d\mathbf{f}_\theta}{d\mathbf{x}} = A_\theta$.

Then, from theorem 4.3.1 and corollary 4.3.2 showing global convergence to a grid defined by a pair of concentric, aligned hexagonal patterns \mathcal{S}_m and \mathcal{S}_l with three-agent link interconnections between them \mathcal{S}_{ml} , requires showing that:

$$\begin{aligned} \begin{bmatrix} V_m A_m V_m^\top & V_m (A_{ml} + A_m^\top) V_{ml}^\top \\ V_{ml} (A_m + A_{ml}^\top) V_m^\top & V_{ml} A_{ml} V_{ml}^\top \end{bmatrix} &= \begin{bmatrix} V_{r6} \mathcal{L}^{(6)} V_{r6}^\top & V_m (A_{ml} + A_m^\top) V_{ml}^\top \\ V_{ml} (A_m + A_{ml}^\top) V_m^\top & V_3 \mathcal{L}^{(3)} V_3^\top \end{bmatrix} > 0 \\ &\text{and,} \\ \begin{bmatrix} V_{ml} A_{ml} V_{ml}^\top & V_{ml} (A_l + A_{ml}^\top) V_l^\top \\ V_l (A_{ml} + A_l^\top) V_{ml}^\top & V_l A_l V_l^\top \end{bmatrix} &= \begin{bmatrix} V_{r3} \mathcal{L}^{(3)} V_{r3}^\top & V_{ml} (A_l + A_{ml}^\top) V_l^\top \\ V_l (A_{ml} + A_l^\top) V_{ml}^\top & V_6 \mathcal{L}^{(6)} V_6^\top \end{bmatrix} > 0 \end{aligned} \quad (4.106)$$

where $\mathcal{L}^{(n)} = L \otimes R + L^\top \otimes R^\top$, with $L \in \mathbb{R}^{n \times n}$.

The remarkable value of this result is that it directly verifies global convergence for any number of rings with corresponding interconnecting links and the overall global convergence of the system is verified by the result in eq. 4.106.

Figure 4-4 shows an example of the convergence for such a controller in a scheme with three hexagonal rings. Agents in $\mathcal{S}_1 = \{1, \dots, 6\}$, $\mathcal{S}_2 = \{7, \dots, 12\}$, $\mathcal{S}_3 = \{13, \dots, 18\}$ converge to hexagonal formations. Formations $\mathcal{S}_{12} = \{1, 7, 2\}$, $\mathcal{S}_{12} = \{5, 4, 10\}$, $\mathcal{S}_{13} = \{6, 17, 12\}$, $\mathcal{S}_{13} =$

$\{3, 4, 9\}$, establish links that define a manifold $\mathcal{M} = \bigcap \mathcal{M}_i$ corresponding to a regular sphere packing grid.

To close this section, an example is presented where the result guarantees global convergence to a desired size of formation when the size is commanded by one of the spacecraft using only relative information to its neighbor(s).

Example 4.4.4 Leader based convergence to desired size. Consider a system of n agents with a control law 4.35 and a leader that controls its separation to other agents by a control law $f(d)$ such that:

$$u_i = R(\pi/N)(\mathbf{x}_{i+1} - \mathbf{x}_i) + R(\pi/N)^\top(\mathbf{x}_{i-1} - \mathbf{x}_i) \quad i = 2, 3..N \quad (4.107)$$

$$u_1 = R(\alpha)(\mathbf{x}_2 - \mathbf{x}_1) + R(\alpha)^\top(\mathbf{x}_N - \mathbf{x}_1) + f_r(\|\mathbf{x}_2 - \mathbf{x}_1\|^2 - \bar{\rho})(\mathbf{x}_2 - \mathbf{x}_1) \quad (4.108)$$

where $f_r(p)$ is a positive function of p with equilibrium point 0 such that $f_r(0) = 0$. Then, the system exponentially converges to a symmetric formation with interagent separation $\bar{\rho}$.

Proof: The principle of the proof is to show that the dynamics of an auxiliary system $y = V(x)$ are contracting, and $y = 0$ is a particular solution of the system.

Consider, the overall dynamics of the system of single integrators with control law 4.107:

$$\dot{\mathbf{x}} = -\mathcal{L}_s \mathbf{x} + f_r(\mathbf{x}) A_1 \mathbf{x} \quad (4.109)$$

where \mathcal{L}_s is the Laplacian defined in previous section which converges to regular formations

and $A_1 = \begin{bmatrix} -I & I & 0 & \dots \\ 0 & 0 & 0 & \dots \\ \vdots & \vdots & \vdots & \vdots \end{bmatrix}$. Consider the auxiliary variables

$$\begin{bmatrix} y_1 \\ y_2 \end{bmatrix} = \begin{bmatrix} V \mathbf{x} \\ f_r(\mathbf{x}) \end{bmatrix} \quad (4.110)$$

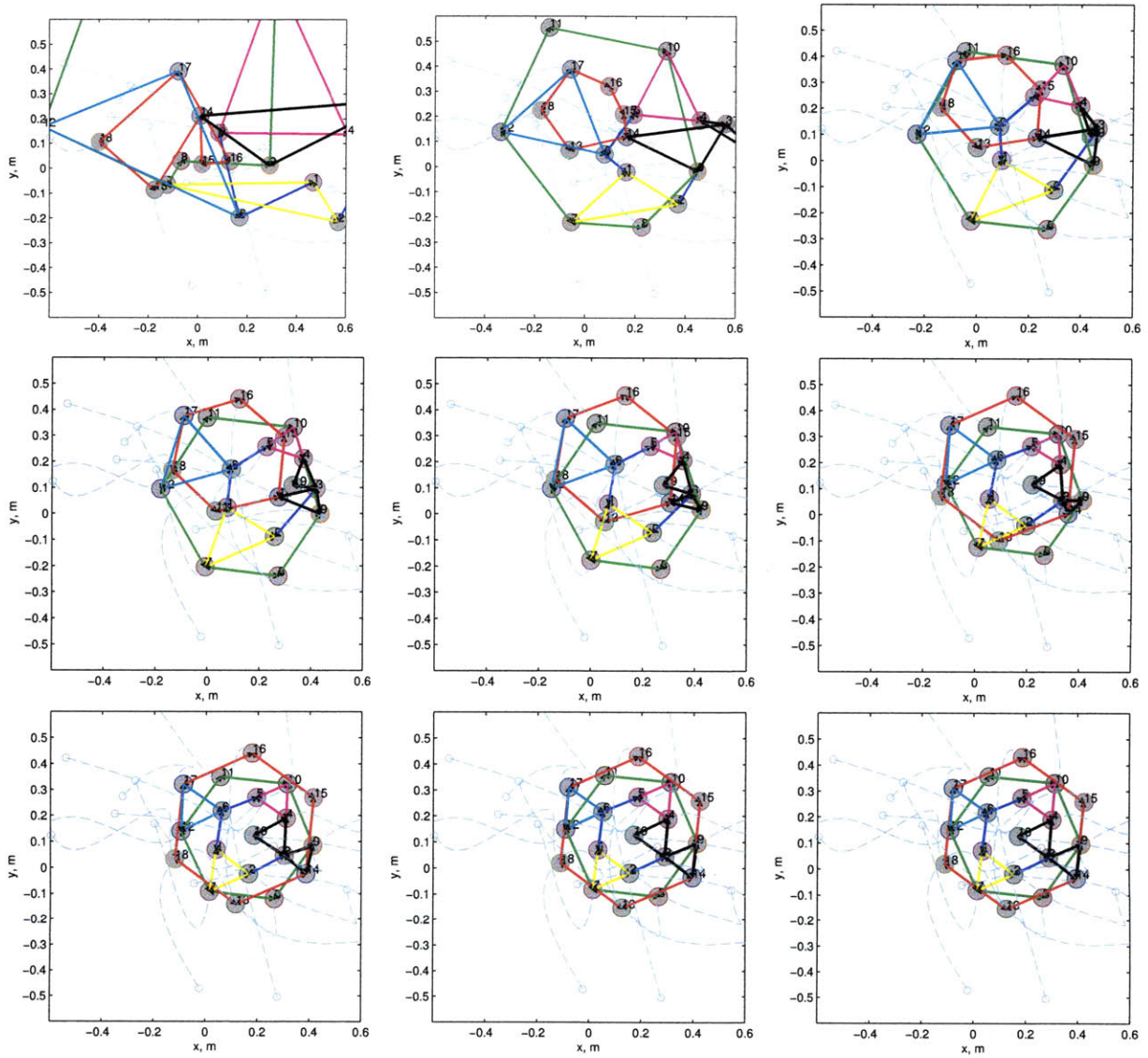


Figure 4-4: Agents converge to a packed grid by imposing some convergence constrains shown by the arrows, two different cases can be designed following the same argument.

where $V^\top V + U^\top U = I$, $\mathcal{L}_s U^\top U \mathbf{x} = 0$, which define an nonlinear invariant manifold $\mathcal{M}_{n\rho}$: $\{\mathbf{x} \mid V\mathbf{x} = 0, f_r(\mathbf{x}) = 0\}$, since $\dot{\mathbf{x}} = 0$ for $\mathbf{x} \in \mathcal{M}_r$. Their dynamics are given by:

$$\begin{aligned} \begin{bmatrix} \dot{y}_1 \\ \dot{y}_2 \end{bmatrix} &= \begin{bmatrix} V\dot{\mathbf{x}} \\ (\nabla_{\mathbf{x}} f_r)\dot{\mathbf{x}} \end{bmatrix} = \begin{bmatrix} V(-\mathcal{L}_s \mathbf{x} + y_2 A_1 \mathbf{x}) \\ (\nabla_{\mathbf{x}} f_r)(-\mathcal{L}_s \mathbf{x} + y_2 A_1 \mathbf{x}) \end{bmatrix} \\ \begin{bmatrix} \dot{y}_1 \\ \dot{y}_2 \end{bmatrix} &= \begin{bmatrix} -V\mathcal{L}_s V^\top & V A_1 \mathbf{x} \\ -(\nabla_{\mathbf{x}} f_r)\mathcal{L}_s V^\top & (\nabla_{\mathbf{x}} f_r) A_1 \mathbf{x} \end{bmatrix} \begin{bmatrix} y_1 \\ y_2 \end{bmatrix} = \mathbf{f}(\mathbf{x}, \mathbf{y}) \end{aligned} \quad (4.111)$$

The auxiliary system (4.111) is contracting and all trajectories will converge to the same trajectory if:

$$\mathbf{F} = \Theta \frac{\partial \mathbf{f}}{\partial \mathbf{y}} \Theta^{-1} < 0 \quad (4.112)$$

Specifically $\mathbf{y} = 0$ is a solution, then, any trajectory of system (4.111) converges to $\mathbf{y} = 0$, which means that any solution of (4.109) converges to $\mathbf{x} \in \mathcal{M}_{n\rho}$.

V and V_{rn} are related through an invertible transformation $V = TV_{rn}$, and consider an invertible transformation that commutes with T , i.e $\Theta = \begin{bmatrix} I & 0 \\ 0 & \theta \end{bmatrix}$, where $\theta > 0 \in R$.

$$\text{Then, } T\Theta \frac{d\mathbf{f}}{d\mathbf{y}} \Theta^{-1} T^\top = \Theta T \frac{d\mathbf{f}}{d\mathbf{y}} T^\top \Theta^{-1} < 0 \Leftrightarrow \mathbf{F} < 0.$$

Then, a sufficient condition for convergence of system (4.109) to a regular formation with characteristic size $\bar{\rho}$ is:

$$J_y = \begin{bmatrix} -V_{rn}\mathcal{L}_s V_{rn}^\top & \theta^{-1} V_{rn} A_1 \mathbf{x} \\ -\theta(\nabla_{\mathbf{x}} f_r)\mathcal{L}_s V_{rn}^\top & (\nabla_{\mathbf{x}} f_r) A_1 \mathbf{x} \end{bmatrix} < 0 \quad (4.113)$$

It has been shown that $V_{rn}\mathcal{L}_sV_{rn}^\top < 0$, and we also have that:

$$V_{rn}A_1\mathbf{x} = \begin{bmatrix} -I \\ 0 \\ \vdots \\ 0 \end{bmatrix} (\mathbf{x}_2 - \mathbf{x}_1) = D_1(\mathbf{x}_2 - \mathbf{x}_1) \quad (4.114)$$

$$\nabla_{\mathbf{x}}f_r = 2(\mathbf{x}_2 - \mathbf{x}_1)^\top \frac{df_r(\rho)}{d\rho} [I \ I \ 0 \ \dots \ 0] = 2\frac{df_r(\rho)}{d\rho}(\mathbf{x}_2 - \mathbf{x}_1)^\top D_2 \quad (4.115)$$

Then, the projected Jacobian J_y is negative definite iff:

$$\begin{aligned} (\nabla_{\mathbf{x}}f_r)A_1\mathbf{x} &= -2(\mathbf{x}_2 - \mathbf{x}_1)^2 \frac{df_r(\rho)}{d\rho} < 0 \\ &\Rightarrow \frac{df_r(\rho)}{d\rho} > 0 \end{aligned} \quad (4.116)$$

and (from a Schur factorization):

$$\begin{aligned} (\nabla_{\mathbf{x}}f_r)A_1\mathbf{x} + \frac{1}{2}(\theta^{-1}V_{rn}A_1\mathbf{x} - \theta((\nabla_{\mathbf{x}}f_r)\mathcal{L}_sV_{rn}^\top))(V_{rn}\mathcal{L}_sV_{rn}^\top)^{-1}\frac{1}{2}(\theta^{-1}V_{rn}A_1\mathbf{x} - \theta((\nabla_{\mathbf{x}}f_r)\mathcal{L}_sV_{rn}^\top))^\top < 0 \\ \Rightarrow \frac{1}{4} \left[(\mathbf{x}_2 - \mathbf{x}_1)^\top \left(D_1 - 2\theta^2 \frac{df_r}{d\rho} D \right) (V_{rn}\mathcal{L}_sV_{rn}^\top)^{-1} \left(D_1 - 2\theta^2 \frac{df_r}{d\rho} D \right)^\top (\mathbf{x}_2 - \mathbf{x}_1) \right] \\ < -2\theta^2 \frac{df_r}{d\rho} (\mathbf{x}_2 - \mathbf{x}_1)^2 \\ \Rightarrow \frac{1}{4} \left[\left(D_1 - 2\theta^2 \frac{df_r}{d\rho} D \right) (V_{rn}\mathcal{L}_sV_{rn}^\top)^{-1} \left(D_1 - 2\theta^2 \frac{df_r}{d\rho} D \right)^\top \right] < -2\theta^2 \frac{df_r}{d\rho} I \end{aligned} \quad (4.117)$$

$$D = D_2\mathcal{L}_sV_{rn}^\top.$$

which verifies that the negative definiteness of J_y does not depend on the value of \mathbf{x} . If for a particular value of \mathbf{x} , a constant transformation Θ is found which verifies the negative definiteness it holds uniformly.

Then, the satisfaction of the two above conditions is sufficient to guarantee convergence

in terms of $\frac{df}{d\rho}$. For example, for $\frac{df}{dx} = 1$, $N = 5$, $\Theta = \begin{bmatrix} I & 0 \\ 0 & 0.5 \end{bmatrix}$, verifies global convergence to any desired size of formation. ■

4.5 Summary and Conclusions of the Chapter

This section presented an approach to the cyclic pursuit laws in the context of contraction theory. By doing so, a wider perspective to analyzing the convergence properties of decentralized control approaches that lead the formation to subspaces or submanifolds of the state space instead of converging to fixed points was devised.

Some of the results are in the form of sufficient conditions that are to be verified numerically, but several important results are obtained as a direct derivation of the approach, namely, nonlinear control laws that verify *global* convergence to a regular formation of specific size as a function of upper bounds of a scalar function, convergence results to time varying formations as a function of the variation rate, laws that can extend the convergence properties to an infinite number of interconnected basic blocks by showing convergence to a basis formation block, or by allowing a straightforward derivation of non-intuitive necessary conditions to achieve a specific mission that can be defined as convergence to a manifold as in the case of deriving conditions to surround a non-cooperative vehicle as illustrated in an example.

The approach to analyzing dynamical systems via contraction theory departs from the most common Lyapunov analysis and appears to be more fit for the case of nonlinear distributed systems, and more specifically systems with circulant interconnections.

Chapter 5

Comparison of the Generalized Cyclic Approach to Relevant Architectures

5.1 Introduction

As mentioned in the introductory chapter, the synthesis of a controller with arbitrary information structure has been widely studied and remains still an open problem. Solving for an optimal controller is a convex problem only for very specific information structures. An important part of the work on this thesis presented in previous chapters aims to define controllers that achieve better performance with reduced complexity in some specific mission scenarios.

The basis of the approach proposed in this thesis considers controllers that maintain a formation by converging to a manifold instead of tracking relative trajectories to other vehicles. One expects that by allowing some extra degrees of freedom the control effort will be reduced as compared to approaches that track relative trajectories and constraint more degrees of the system. Evidence of this effect has been noticed in the experimental results in Chapter 6, showing an improvement as compared to other architectures.

The objective of this section, therefore, is to justify and highlight the importance of

the control approach based on cyclic approach in a more theoretical manner. This is done by considering a benchmark formation control problem and comparing the advantages and disadvantages of different control architectures in a more analytical trade space framework.

As metric of performance, a common quadratic norm that weights the performance error and the control effort is traded with the cost of implementing the control architecture in terms of complexity in as well as the cost of being robust enough to a failure.

5.2 Benchmark Problem

A simple benchmark problem is considered. This problem encompasses the concept of formation maintenance focusing on simple integrator dynamics, but the approach could be extended to more general cases under some specific assumptions. The problem is simplified for the purpose of the analysis, by considering the agents with individual homogeneous dynamics:

$$\dot{\mathbf{x}}_i = A\mathbf{x}_i + B_u\mathbf{u}_i + B_w\mathbf{w}_i \quad (5.1)$$

and for simplicity for our purpose we assume $B_u = I$, $B_w = I$, $C_y = I$ and $A = -\epsilon I$. For the objective of comparing the performance of controllers maintaining a certain shape of the formation, we assume a regular polygon. In that case, the performance can be described by:

$$\mathbf{z} = \begin{bmatrix} -I & I + R_{2\pi/n} & -R_{2\pi/n} & 0 & \dots \\ 0 & -I & I + R_{2\pi/n} & -R_{2\pi/n} & \dots \\ \dots & \dots & \dots & \dots & \dots \end{bmatrix} \doteq Cx \quad (5.2)$$

Depending on the control architecture, the different vehicles in the formation will be required to perform calculations to issue their control commands. In the first place each vehicle has to obtain the state information from itself and from other vehicles which it requires

to calculate the control commands. The trade analysis model in this chapter considers a unit operation per state to be received and a single unit operation per state to be transmitted. Whether the state information from other vehicles is obtained through communications or through measurements is irrelevant to the model, but further research could analyze different situations including differences between such scenarios.

Using the input information each vehicle calculates the control commands. Such calculation is assumed in our model as a matrix multiplication operation and is modeled as the size of the gain matrix for each respective vehicle. Then, if the commands need to be communicated to others vehicles the same scheme is considered, assuming a unit per each command to be transmitted.

5.3 Synthesis of Decentralized Controllers

In general, the control synthesis problem can be described as, given a plant G , find a controller K while minimizing a desired metric of the system $J = ||f(P, K)||$. This metric defines the control objective. As mentioned in the introduction, for our case we are going to analyze the performance of the system in terms of a quadratic metric that considers the control effort and the error in the desired configuration. The results in this section consider a continuous system with state feedback.

The trade is based on studying the controllers that minimize a quadratic cost function of the error and the control effort:

$$J = \int_0^{\infty} \mathbf{z}^T Q \mathbf{z} + \mathbf{u}^T R \mathbf{u} dt \quad (5.3)$$

for a system with dynamics:

$$\dot{\mathbf{x}} = A\mathbf{x} + B_u\mathbf{u} + B_w\mathbf{w} \quad (5.4)$$

and error defined as $\mathbf{z} = C_1\mathbf{x}$.

Consider the dynamics of the closed loop system:

$$\dot{\mathbf{x}}(t) = (A + B_u K)\mathbf{x} + B_1 \mathbf{w} \quad (5.5)$$

with output:

$$\mathbf{z}(t) = (C + DK)\mathbf{x}$$

with $C = C_1 Q^{1/2}$, $R = D^T D$, then the metric of interest is $(\mathcal{H}_2^2)^{\mathbf{w} \rightarrow \mathbf{z}}$, the square of the 2-norm from input \mathbf{w} to output \mathbf{z} .

Given a system G with state space description $A, B, C, 0$, the 2-norm from input to output is given by:

$$\|G\|^2 = \frac{1}{2\pi} \int_{-\infty}^{\infty} \text{Tr} \{P^*(j\omega)P(j\omega)\} d\omega \quad (5.6)$$

which by Plancherel's Theorem is:

$$\|G\|^2 = \int_0^{\infty} \text{Tr} \{B^* e^{A^* t} C^* C e^{A t} B\} dt \quad (5.7)$$

$$= \text{Tr} \{B^* Y_o B\} \quad (5.8)$$

where $Y_o = \int_0^{\infty} e^{A^* t} C^* C e^{A t} dt$ is the observability gramian, which can be shown to be the solution to the lyapunov equation:

$$A^* Y_o + Y_o A + C^* C = 0 \quad (5.9)$$

hence, the optimal solution to an unstructured controller, can be obtained by solving the above equation.

For some very specific cases, the structure of the controller can be derived directly from properties of the system. In a centralized scheme, there are no restrictions on the structure

of K , and a solution of the above equation is calculable though a variety of methods. On other cases, if A, B, C, Q and R belong to a matrix algebra, it is straightforward to show that Y_o and the optimal controller $K = -BR^{-1}Y_o$, belong to the same algebra [56]. Thus, for example, if A and C are rotational circulant matrices (see sec. 2.1) and Q, R, B are a constant time the identity, all of them belong to the algebra \mathcal{CR} and thus the controller is rotational circulant.

However, for a general structure of K accounting for the underlying information transfer structure, the problem is not convex, and even solving for a feasible solution can be a challenging problem. Some structures, like cyclic or leader follower structures can be implemented as convex constraints, however, for many cases the degree of freedoms in the structure of the controller, the best we can do is solve for a constant that multiplies a unitary Laplacian such that $K = kL$.

Since the purpose of this chapter is to compare optimal performances for different approaches, we only consider topologies for which we can solve for an optimal solution under the same Q, R weights. Thus we restrict to solving for the optimal control problem under a fix structure times a constant $K = kL$, where L defines the structure of the decentralized controller.

In that case the $\|G^{w \rightarrow z}\| = Tr\{Y_o\}$, Y_o is given by:

$$(A + kL)^*Y_o + Y_o(A + kL) + (C + kDL)^*(C + kDL) = 0 \quad (5.10)$$

which is a convex function of k , and a minimum can be found. Figure 5-1 shows the J as a function of k highlighting the minimum for different architectures.

The structures considered in the analysis are:

1. **Centralized control** In this case the computation of the control commands is performed in one of the vehicles. It requires knowledge of the states of all the other vehicles in the formation which can be either measured or communicated. It also needs to com-

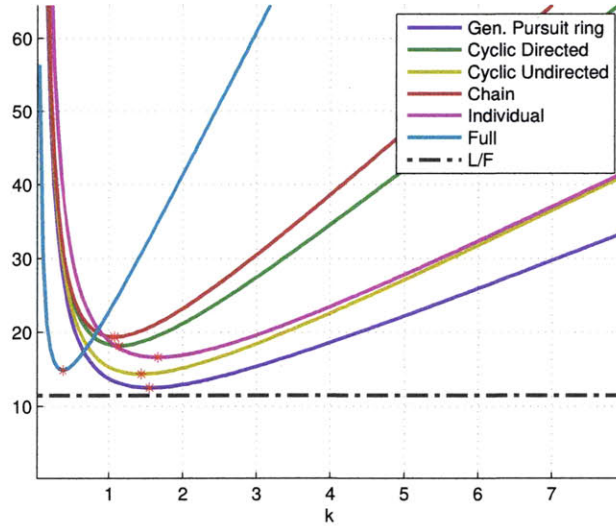


Figure 5-1: Optimal Cost as the number of vehicle increases

municate the commands to each one of them as well. In this case the only essential vehicle is the central controlling unit.

2. **Parallel implementation of the controller** This is a common approach presented in the literature [29, 92], which is decentralized in the sense that it does not require a unique vehicle to issue the control commands, each vehicle, individually calculates its own commands based on knowledge of the overall formation state. It requires measuring the state of all the other vehicles in the formation but no vehicle is essential to the operation of the control architecture. We assume that the state estimate of the formation among all the vehicles is equivalent and the performance can be equivalent to the centralized approach.
3. **Synchronized individual regulation with a global reference frame** In this case, the formation requires an external coordination mechanism, e.g. GPS information, which allows them to track individual points and have accurate synchronized timers to achieve the desired formation. In this case the vehicles do not require any communication between them, but require individual measurement to a global reference frame and a time coordination mechanism.

4. **Relative fixed trajectory regulation** This is the approach described in the introductory chapter, related to the consensus problem which has been widely studied and is very common approach to decentralized formation control. In this case, each vehicle requires information of only its neighbors as dictated by the specific interconnection topology in order to calculate its own control commands. Consider the consensus-like approach where an individual controller is given by:

$$u_i = \sum_{j \in \mathcal{N}} k_{ij}(\mathbf{x}_j - \mathbf{x}_i - \mathbf{h}_{ji}), \quad (5.11)$$

and h_{ij} are the agreement biases as described in section 2.2.3. Then the overall closed loop system is:

$$\dot{\mathbf{x}} = (A - k\mathbf{L})\mathbf{x} + \mathbf{w} \quad (5.12)$$

where \mathbf{x} describes the overall description of the formation and \mathbf{w} is a vector of uncorrelated disturbances. The interconnection between vehicles defined by a matrix \mathcal{L} , then, finding an optimal controller with a given topology reduces to an optimization on the parameter k .

We consider the following interconnection topologies, for which an optimal controller can be derived via solving an LMI:

5. **Generalized pursuit 1-circulant cyclic topology** In a parallel approach, consider the manifold approach described in eq. 4.35. In that case the controller can be written as:

$$\mathbf{u}_i = \sum_{j \in \mathcal{N}} R(\mathbf{x}_j - \mathbf{x}_i), \quad (5.13)$$

where R is a rotation matrix such that $V(A + k\mathcal{L})\bar{\mathbf{x}} = 0$ for $V\bar{\mathbf{x}} = 0$ and the overall

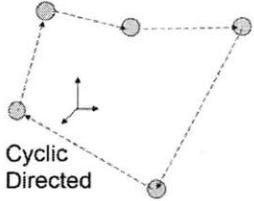
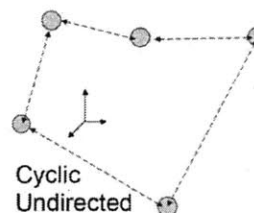
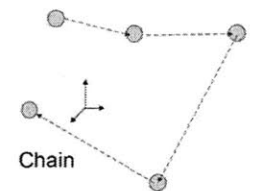
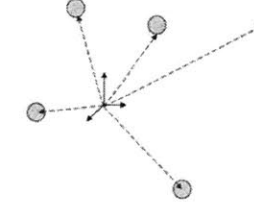
 <p>Cyclic Directed</p>	$L = \begin{bmatrix} I & -I & 0 & 0 & 0 \\ 0 & I & -I & 0 & 0 \\ 0 & 0 & I & -I & 0 \\ 0 & 0 & 0 & I & -I \\ -I & 0 & 0 & 0 & I \end{bmatrix}$
 <p>Cyclic Undirected</p>	$L = \begin{bmatrix} 2I & -I & 0 & 0 & -I \\ -I & 2I & -I & 0 & 0 \\ 0 & -I & 2I & -I & 0 \\ 0 & 0 & -I & 2I & -I \\ -I & 0 & 0 & -I & 2I \end{bmatrix}$
 <p>Chain</p>	$L = \begin{bmatrix} I & -I & 0 & 0 & 0 \\ 0 & I & -I & 0 & 0 \\ 0 & 0 & I & -I & 0 \\ 0 & 0 & 0 & I & -I \\ 0 & 0 & 0 & 0 & I \end{bmatrix}$
 <p>Individual Synchronized</p>	$L = \begin{bmatrix} -I & 0 & 0 & 0 & 0 \\ 0 & -I & 0 & 0 & 0 \\ 0 & 0 & -I & 0 & 0 \\ 0 & 0 & 0 & -I & 0 \\ 0 & 0 & 0 & 0 & -I \end{bmatrix}$

Table 5.1: Different topologies considered for comparison of decentralized controller

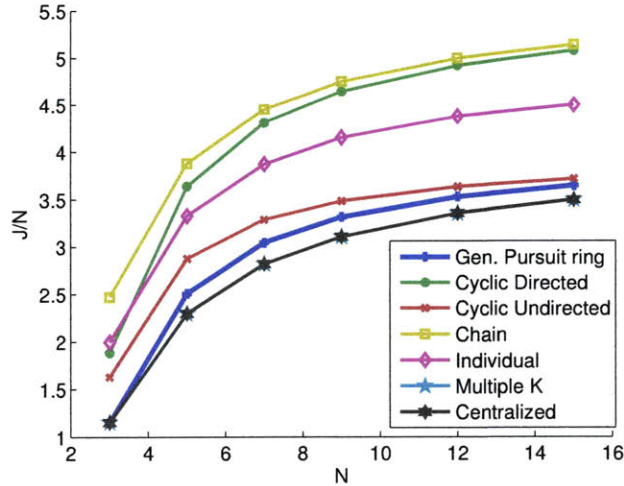


Figure 5-2: Optimal Cost as the number of vehicle increases

structure of the closed loop system is:

$$\dot{\mathbf{x}} = (A - k\mathcal{L}_s)\mathbf{x} + \mathbf{w} \quad (5.14)$$

where \mathbf{x} describes the overall state of the formation, and \mathbf{w} is a vector of uncorrelated disturbances. The interconnection between vehicles defined by a matrix $\mathcal{L}_s = L \otimes R + L^\top \otimes R^\top$.

Figure 5-2 shows the solution to the optimization problem for different considered architectures as the number of vehicles increases. It can be noticed that as the number of vehicles increases the centralized control is always the most favorable in terms of performance optimality.

5.4 Cost Metrics

In the previous section, we consider only a quadratic performance metric, and the obvious result is that a centralized controller is the best approach if we are only concerned about the performance in terms of error and fuel. However, one of the major drivers of the research in

decentralized control is that the effective realization of centralized approaches becomes more difficult or impossible as the number of vehicles increases.

The incurred cost in the realization of a centralized architecture, is mainly due to the cost of communicating all the team information to and from one single unit and processing all that information in the same unit for every control period. This justifies a first cost metric in the trade analysis. This *Cost of implementation* ($Cost_I$) metric considers the maximum number of operations in any single unit at every control period. The metric is defined as:

$$Cost_I = \max_i C_I(i)$$

$$C_I(i) = N_{ops_i} + N_{com_i} + N_{sens_i}$$

where N_{ops_i} , N_{com_i} , N_{sens_i} are the estimated number of algebraic operations, number of communication operations and number of estimation operations on the i th vehicle.

Another disadvantage of the centralized approach, mentioned in the introductory chapter, is the risk of failure of the overall formation if any one of the vehicles fails, specifically, if the central control unit or the communication to or from it fail, the whole control scheme is doomed. A way to circumvent such situation is by allowing more than one of the spacecraft the same capabilities. This is the justification of a second metric considered in this study which accounts for the the expected cost of an extra unit to achieve robustness to a failure. This *Cost of robustness* metric is defined as:

$$C_r = \sum r_i p_{fail}(i) C_I(i)$$

Where p_{fail} is the failure probability of a specific unit i and r_i is a parameters that define how 'critical' role in achieving control i is and for our analysis we set it to be $r_i \in \{0, 1\}$

5.5 Results

Figure 5-4 presents a trade space of the performance of different architecture versus the cost of complexity as the number of vehicles in the formation is increased.

The following conclusions can be drawn:

- A centralized approach is optimal and the optimal performance per vehicle does not depend on the number of vehicles
- For every case, the cyclic controller is a non-dominated solution
- Among all non centralized solutions, the cyclic approach has the best performance, however if the only metric of concern is the cost of implementation, there are topologies cheaper to implement, for example a chain topology, or each vehicle tracking individual coordinated trajectories. This last one however, assumes that the cost of having a common global reference frame is negligible (as might be the case of GPS for LEO formations)
- Under the defined metric, the centralized solution is dominated, particularly, having multiple instantiations of the controller has better robustness (in the sense of surviving a failure).
- If the performance and robustness to failures are metrics of importance, the cyclic approach that converges to a manifold of regular formations is the predominant architecture
- For formations with large number of vehicles, the performance difference between a generalized cyclic controller with convergence to regular formations and a cyclic topology tracking relative trajectories tends to vanish

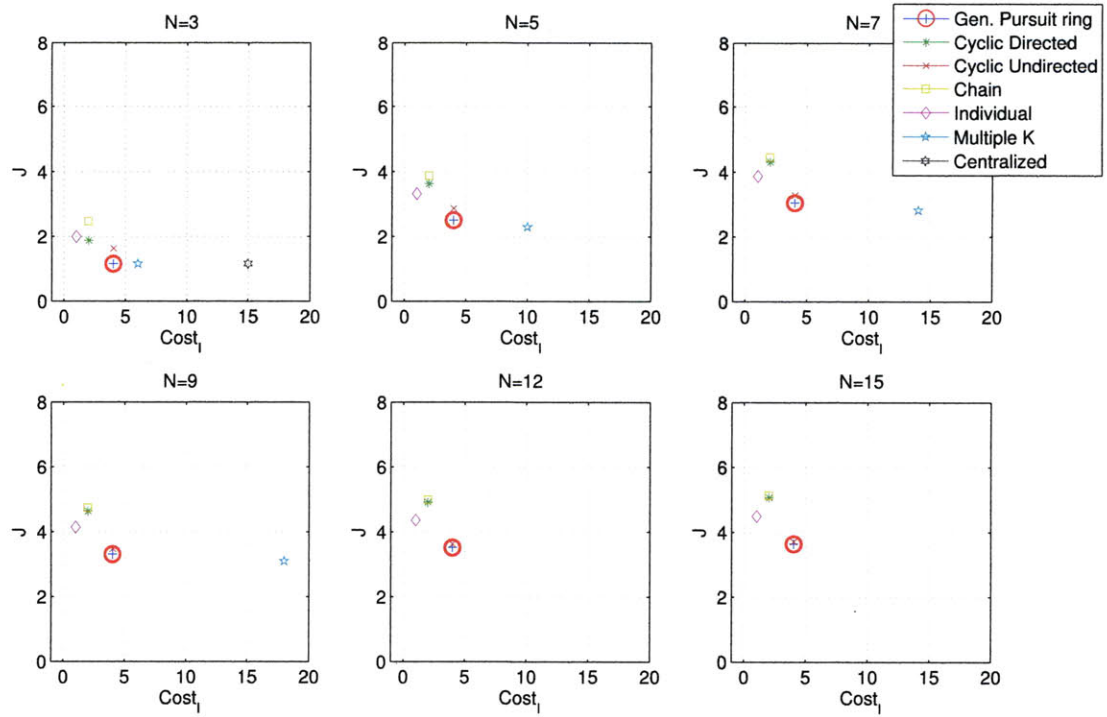


Figure 5-3: Trade space Performance vs Complexity of Implementation as a function of the number of vehicles in the formation

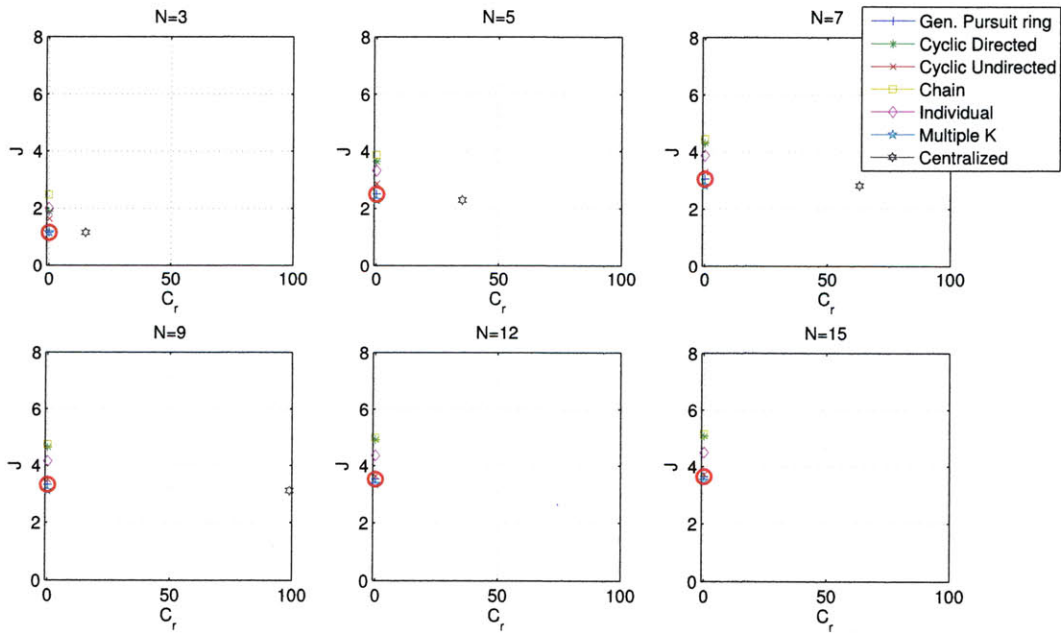


Figure 5-4: Trade space Performance vs Cost of Robustness as a function of the number of vehicles in the formation

Chapter 6

Experimental Results: Decentralized Formation Flight in Microgravity Environment

6.1 Introduction

The SPHERES testbed provided a hardware platform for validating the formation flight algorithms in a relevant space environment. The experimental demonstration of the formation control algorithms and the validation of their expected properties were achieved by implementing cyclic pursuit control laws and testing them in a relevant hardware platform in the microgravity environment aboard the International Space Station. The experiments present the first known implementation of decentralized formation flight in space.

The performance of the algorithms as a formation control strategy was verified while demonstrating their capabilities to accomplish several simulated mission scenarios relevant for a fractionated spacecraft mission. Such scenarios are specifically inspired by DARPA's system F6 mission objectives.

The F6 (Future, Fast, Flexible, Fractionated, Free-Flying Spacecraft United by Informa-

tion Exchange) mission (<http://www.darpa.mil/tto/programs/systemf6/index.html>) mission is currently in development. Its objectives include demonstrating the advantages and feasibility of fractionated spacecraft on a near-Earth environment. Among the milestones to be achieved in order to validate formation flight feasibility are array initialization, satellite addition maneuvers, collision avoidance and rejection maneuvers. The experiments performed on SPHERES addressed some of the issues for such mission scenarios using decentralized cyclic pursuit algorithms, testing the reliability and verifying the important properties of this approach to formation control.

This chapter is structured as follows: the first section describes the SPHERES testbed and the implementation of the algorithms, a second section describes the performed tests and their results, a third section uses experimental data from the different tests to verify and quantify the performance of the implementations of the algorithm and compare their performance to other control approaches.

6.1.1 The SPHERES testbed

SPHERES (Synchronized Position Hold Engage Reorient Experimental Satellites) are an experimental testbed consisting of a set of small vehicles with the basic functions of a satellite. Three of them are aboard the International Space Station and are operated by the astronauts in a test volume that allows 6DOF microgravity maneuvering. The operational volume is approximately a cube of about $1m \times 1m \times 1m$.

There are also three identical vehicles on the ground that can perform 2D maneuvers by means of frictionless sliding air bearings. This vehicles operate on a flat table and are used for a first level validation of the algorithms before sending them to the ISS.

The propulsion system of a SPHERES vehicle consists of 12 microthrusters that use compressed CO₂ gas. The microthrusters are controlled by solenoid valves that can achieve pulses between 10 to 180ms at each control period. Each thrusters delivers 0.11N. The wet mass of each SPHERE on the ISS is approximately 4.3kg.

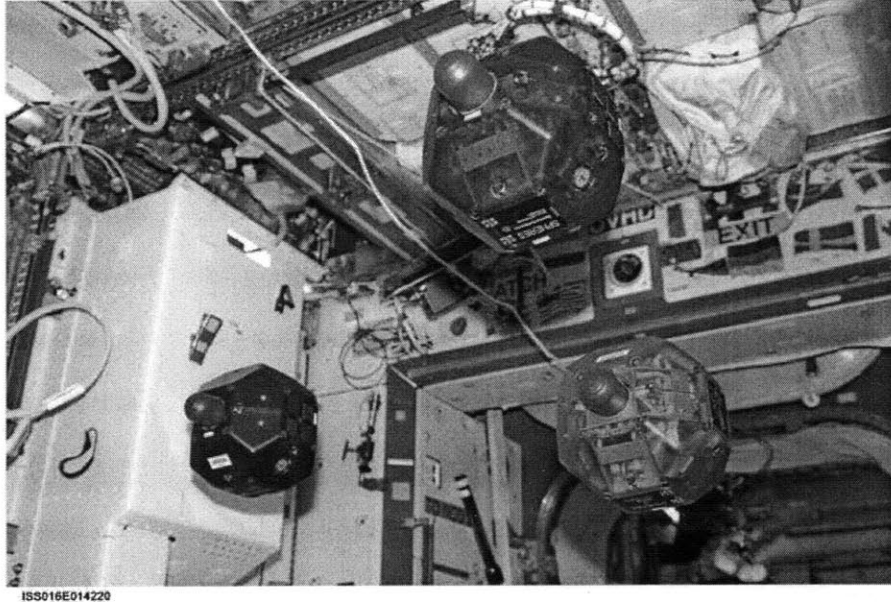


Figure 6-1: Picture of three SPHERES satellites performing a test on board the ISS. (Photo-credit: NASA - SPHERES)

The metrology system of the SPHERES emulates a global positioning system by calculating its position and velocity with respect to a fixed frame by measuring the travel time of synchronized ultrasound signals. Each vehicle has a local estimator that calculates its global position based on ultrasound and IMU measurements with an accuracy of approximately 2mm. This metrology system can also be used to calculate the relative range and bearing, and corresponding rates to a beacon in another vehicle. Such mode of operation is intended to allow experimentation using pure relative information. In the tests presented on this thesis however, relative measurements were *synthesized* from communicated states as the vector difference of each vehicles *global* estimate. This simplification is irrelevant to the verification of the control performance.

A single RF channel is used to communicate the state between/among spacecraft and the ground. The communication is TDMA based, and allows for a small bandwidth for transmission within each control period.

Figure 6-1 shows a picture of three SPHERES spacecraft aboard the ISS.

The dynamics of each spacecraft are well approximated by a double integrator. The

control commands calculated by the control law are the desired forces which are converted into open loop pulse times of a set of thrusters to achieve the desired force by a control allocation (mixing) algorithm.

6.2 Algorithm Implementation

The algorithms were implemented in *C*, the standard programming language of the testbed and packed as a library for the SPHERES science utility module.

Three different versions of the control algorithm were implemented and tested on different experiments performed at different stages of its development.

On a first implementation, a velocity tracking inner loop was used as an approximated implementation of the single integrator dynamics, in this case the control algorithm was setup as:

$$\mathbf{f}_i = -\bar{m}\gamma(k_d R(\alpha)(\hat{\mathbf{x}}_{i+1} - \hat{\mathbf{x}}_i) - \hat{\mathbf{v}}_i) \quad (6.1)$$

where \bar{m} is the mass of the vehicle, $\hat{\mathbf{x}}_i$ and $\hat{\mathbf{v}}_i$ are position and velocity variables from the local estimator, $\hat{\mathbf{x}}_{i+1}$ is a communicated estimated position variable from the estimator in vehicle $i + 1$ and γ and k_d are control gains. k_d is a time scaling which defines the angular speed of the formation rotational motion and γ is a regulation gain that dictates the behavior of the velocity tracking. This controller is basically, the simplistic approach to double integrator dynamics described by Ren [75].

This implementation requires the agreement on an inertial frame to which v is measured with respect to, an agreement on a global orientation and does not consider feedforward terms. It does not require an agreement on an origin of coordinates since it only requires relative position measurements.

An important consideration for implementation is the discrete nature of the actual system

in the selection of the gain γ . In a theoretical sense, for the continuous, unperturbed case, large values of γ , improve the tracking performance of the velocity regulation, however, in a discrete, saturation constrained implementation, large gains can easily turn the system unstable. For the experiments, the gain was selected considering the limitations of the testbed by selecting it such that the settling time of the velocity tracker is about 1 period.

A second implementation considers a more correct approach to second order systems by adding a feedforward term which improves the performance. This is specifically, the approach presented in section 3.32, by setting up the force to:

$$\mathbf{f}_i = -\bar{m}(\gamma k_g R(\alpha)(\hat{\mathbf{x}}_{i+1} - \hat{\mathbf{x}}_i) + k_g R(\hat{\mathbf{v}}_{i+1} - \hat{\mathbf{v}}_i) - \gamma \hat{\mathbf{v}}_i - k_c \hat{\mathbf{x}}_i) \quad (6.2)$$

In this case, the gain γ was tuned by considering the rejection of a 2 cm disturbance over a control period and the value of k_g was setup to achieve the desired angular speed for each specific scenario. Notice that for this implementation too, an agreement on a reference velocity to which \mathbf{v} is measured with respect to and an agreement on a global orientation are required but not an agreement on the origin of coordinates.

The third version used in the experiments considers the approach in Section 3.42, which was implemented as:

$$\mathbf{f}_i = -\bar{m}(k_1 R(\alpha)(d\hat{\mathbf{x}}_1 + d\hat{\mathbf{x}}_2) + k_2 R(2\alpha)d\hat{\mathbf{v}}_1) \quad (6.3)$$

where $d\hat{\mathbf{x}}_1 = \hat{\mathbf{x}}_{i+2} - \hat{\mathbf{x}}_i$, $d\hat{\mathbf{x}}_2 = \hat{\mathbf{x}}_{i+1} - \hat{\mathbf{x}}_i$, $d\hat{\mathbf{v}}_1 = \hat{\mathbf{v}}_{i+1} - \hat{\mathbf{v}}_i$ are synthesized relative measurements where $\hat{\mathbf{x}}_i$ and $\hat{\mathbf{v}}_i$ are from the local estimator, $\hat{\mathbf{x}}_j, \hat{\mathbf{v}}_j$ are communicated estimated state variables from the estimator in vehicle j . k_1 , and k_2 were selected to achieve circular or spiral motion with the desired angular velocity.

As described in the theoretical results, in this implementation, the vehicles do not require any global positioning information, only an agreement on a global orientation. It is to note

that, for real missions, this agreement on the orientation can be achieved through star trackers, and therefore this approach seems useful for deep space missions.

The tests were designed as a sequence of maneuvers using one of the above described implementations and will be described in the next section. Every test starts with standard estimator convergence and initial positioning maneuvers. Each vehicle is programmed with a role defining a unique identifier and in the description below. The vehicle loaded with role i will be referred as spacecraft i or SPHi.

Videos of experimental results can be accessed online¹.

6.3 Description and Results of the Tests

The experiments present the first known implementation of decentralized formation flight in space. The main objective of these experiments was to demonstrate the use of the decentralized algorithms as a formation control tool for several mission scenarios. In a first test, the decentralized properties of the algorithm to achieve a formation and achieve easy addition of modules were verified. The vehicles performed circular maneuvers, elliptical maneuvers, and a joining maneuver. In a second set of test we verified the practical implementation of a controller that uses only relative information to maintain a formation achieving circular and Archimedean spiral formations. In later tests we use the cyclic pursuit algorithm to achieve reconfiguration of the maneuver when a failure is detected. In other tests the algorithm was implemented with a heuristic collision avoidance mechanism that addresses some of the risks associated with collision while converging to a formation from an arbitrary initial position. In a last set of experiments presented in this chapter, a simulation of a deployment scenario is presented where each vehicle joins a circular formation in the order and timing manually selected by the crew member.

¹<http://ssl.mit.edu/spheres/video/CyclicPursuit>

6.3.1 Test 1: Joining maneuver 2-sat to 3-sat formation

The test described in this section was performed during test session 14C, in November 2008. It was designed as a sequence of maneuvers intended to incrementally build on complexity following the general guideline protocol for testing on SPHERES. The main idea was to test the algorithm achieving a circular formation with two vehicles, then add a third one and then achieve elliptical trajectories. For this test the cyclic pursuit algorithm was implemented following control law in eq. 6.1.

After initial estimator convergence and positioning the test was designed to achieve the following maneuver sequence:

1. Two spacecraft perform a rotation maneuver in the x-z plane with a radius $r = 0.3m$;
2. A change in the desired radius is commanded and the spacecraft spiral out to achieve a circular formation with $r = 0.4m$;
3. A third spacecraft joins the formation and the system reconfigures into a three-spacecraft evenly-spaced circular formation with $r = 0.35m$;
4. A similarity transformation T is applied to the rotation matrix in a way that the spacecraft achieve an elliptical formation with eccentricity 0.8.

The initial positioning was $x_1 = [0, -0.1, -0.2]^T$, $x_2 = [0, 0.1, 0.2]^T$, $x_3 = [0, 4, 0]^T$ with zero initial velocity (with respect to the ISS).

6.3.1.1 Test 1 (P237 -T2) results

Data from telemetry shows the formation achieving the defined sequence of maneuvers. In figure 6-2 the global position and velocity time history is shown. The time history of the states is depicted for each spacecraft (with respect to the ISS). In fig. 6-3 the trajectories performed by the spacecraft during the maneuvers 1), 2), 3) and 4) are shown.

After a successful initial positioning of the three satellites at 75 seconds, SPH1 and SPH2 start moving to eventually achieve a circular rotating formation (Fig. 6-3a). In the next maneuver (Fig. 6-3b), after spiraling out to achieve a larger formation size, the vehicles asymptotically converge to a constant radius until the next maneuver (Fig. 6-3c) is initiated. In that next maneuver, satellite 3 joins and a new radius is achieved. A profile plot is also presented which shows the satellites converge from different $x - z$ planes. In this maneuver the topology is reconfigured. SPH2 changes its target from SPH1 to SPH3, SPH3 starts following SPH1 and a natural reconfiguration occurs. In a last maneuver (Fig. 6-3d), a transformation is applied to the control law as described in sec, 3.5.2 and the vehicles achieve a slightly elliptical formation with eccentricity 0.8.

The experimental results (see in particular Fig. 6-3) present the first demonstration of the effectiveness of the proposed cyclic-pursuit controllers. It verified the modularity properties of the algorithm in the sense that each vehicle was running the exact same code, and the coordination was achieved by defining the interconnection topology. It additionally experimentally verified the extension to achieving elliptical formations.

6.3.2 Test 2: Convergence to 3-sat formation from arbitrary initial conditions

This second test, like to the previous one, was performed during test session 14C in November 2008. Again, for this test, the cyclic pursuit algorithm was implemented following control law in eq. 6.1. The sequence of maneuvers, after initial estimator convergence was defined as:

1. Three spacecraft achieving a evenly-spaced rotation maneuver in the $x-z$ plane with radius $r = 0.35m$;
2. After 75 seconds, a similarity transformation T is applied to the rotation matrix for the spacecraft to achieve an elliptical formation with eccentricity equal to 0.8.

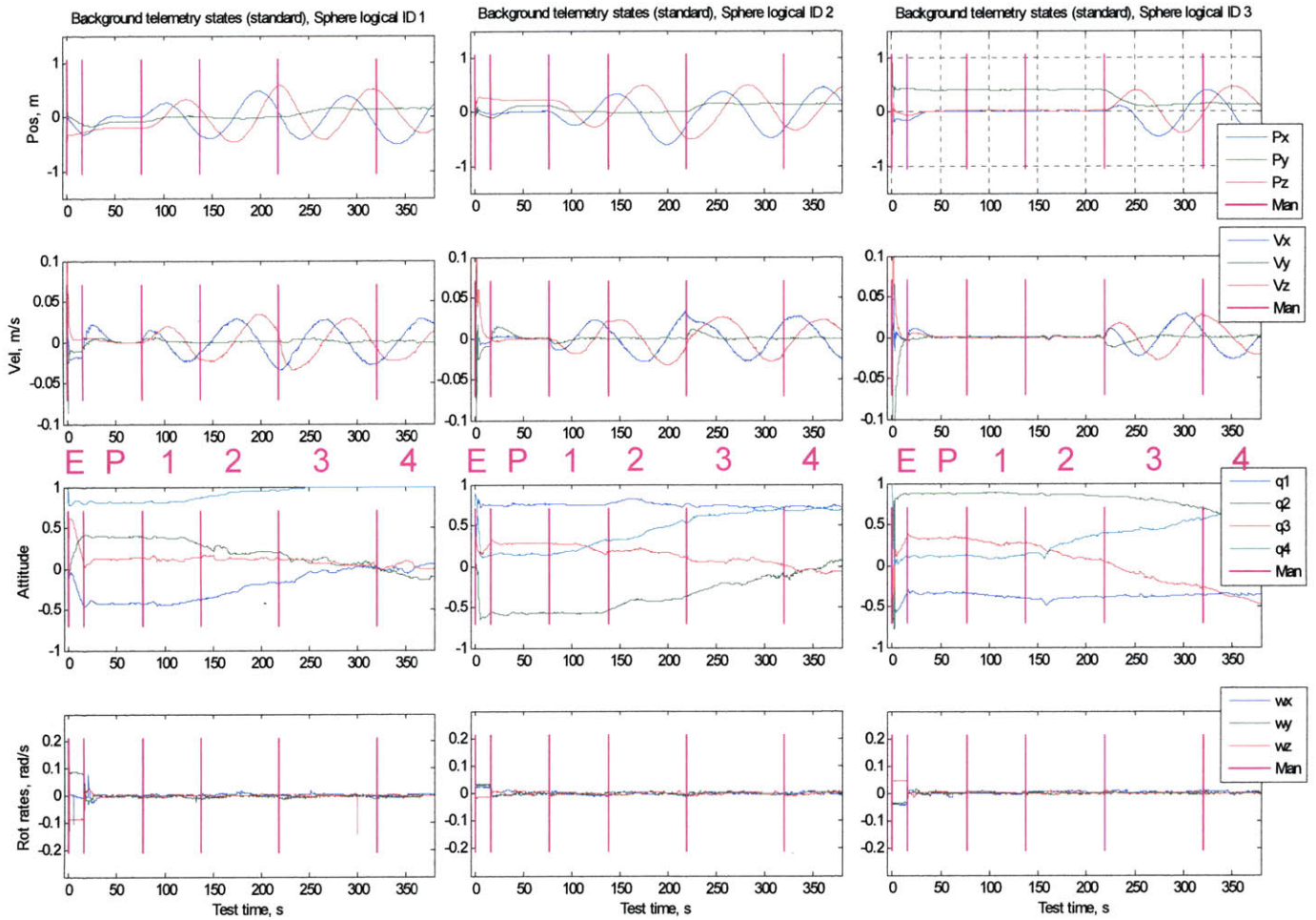


Figure 6-2: Experimental results from Test 1: Position and velocity vs. time. From left to right: satellites 1, 2 and 3. Maneuvers indicated by numbers.

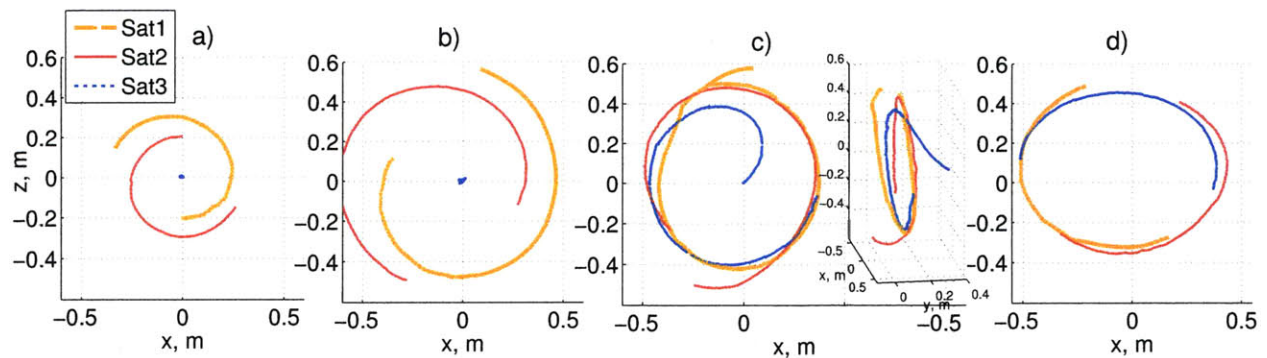


Figure 6-3: Experimental results from Test 1: x-z plane. Sequence of maneuvers a) Maneuver 1, b) Maneuver 2, c) Maneuver 3 and d) Maneuver 4.

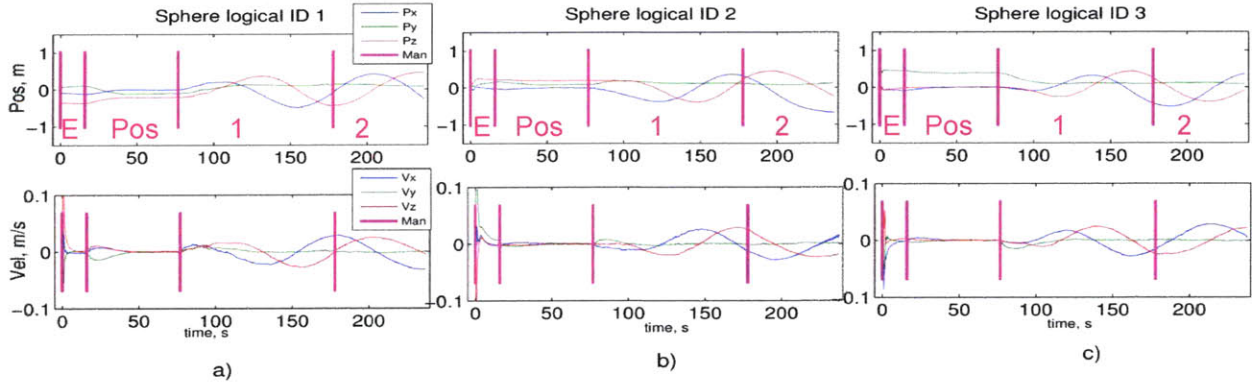


Figure 6-4: Experimental results from Test 2: Position and velocity vs. time. From left to right: satellites 1, 2 and 3.

6.3.2.1 Test 2 (P237 -T6) results

Figure 6-4 shows the time history of the global position and velocity of each spacecraft (with respect to the ISS) from telemetry data; while fig. 6-5 shows the trajectories achieved by the spacecraft during the maneuvers 1) and 2). The results demonstrate the controller achieving its objective of converging from an arbitrary initial position into a 3-sat rotating formation.

It is important to notice that, the formation converged to a larger size than the designed $0.35m$. A similar behavior was observed in test 1. This effect is explained as a consequence of the discretization and delays effects and the lack of a feedforward term. Specifically, the value of α (from Section 3.2.4), at the equilibrium state has to be less than π/N in order to maintain a non expanding formation. This means that the nonlinear term $\|x_{i+1} - x_i\| - \rho$ is greater than zero, and thus $\|x_{i+1} - x_i\| > \rho$ when a stable size is achieved. In the later tests we show how this situation is improved when adding a feedforward term and in the conclusions section we address how other improvements could achieve even more precise results.

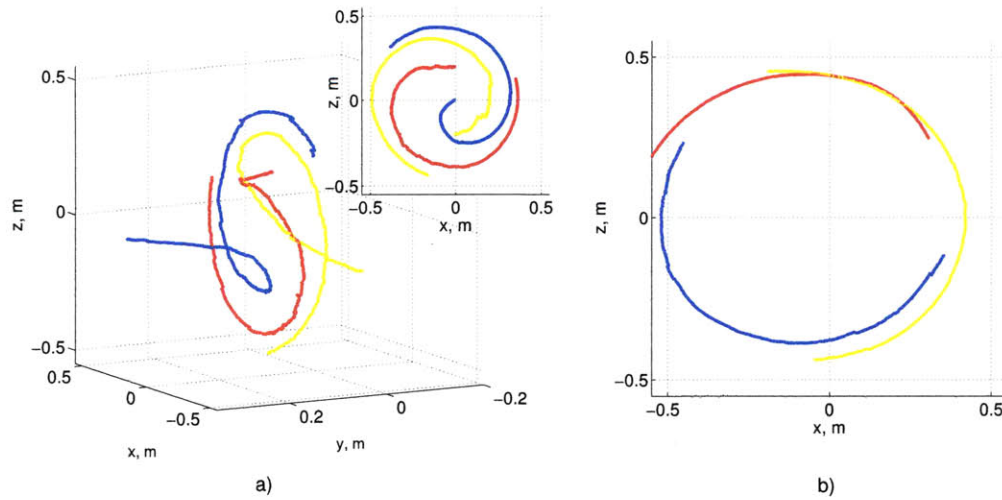


Figure 6-5: Experimental results from Test 2: x-z plane. Sequence of maneuvers a) and b).

6.3.3 Test 3: Pure relative formation maintenance

This test validated the decentralized algorithm based on the cyclic pursuit approach that uses only relative measurements to maintain a formation. This test was performed during test session 20, in December 2009. In this test, the control approach in eq. 6.3 was used. In the previous implementations of cyclic pursuit algorithm, the distributed controller relies on measurements of relative positions but required an agreement on the velocity of the inertial frame. In this version of the controller, the commands are issued based exclusively on relative measurements to the neighbors. This characteristic is of important value for deep space formation flight applications. The algorithm to be used in this test is an implementation of the cyclic pursuit algorithm for double integrator dynamics with only relative information. The constants k_1 , k_2 were defined to achieve an angular speed of $\omega = 2\pi/120rad/sec$. After the first 45 seconds are for estimator convergence and initial positioning, the sequence of maneuvers was defined as following:

1. In the first active maneuver the satellites position themselves 60 centimeters from each other in opposite directions from the center of the test volume and an initial formation acquisition maneuver using the cyclic pursuit algorithm from previous test sessions

achieve a circular formation.

2. After 40 seconds into this maneuver the controller in both satellites switches to the control law described in eq.6.3 with parameters k_1 , k_2 to achieve an spiraling maneuver under free drift mode.
3. When reaching a radius of 50cm, the controller switches to maintain a circular formation including a mode controlling the center of the formation,
4. After 40 seconds the controller mode switches to free drift mode with parameters k_1 , k_2 , α to achieve circular formation (using only relative measurements) and allows the center of the formation to drift free.
5. Lastly, a stopping maneuver finalizes the test.

6.3.3.1 Test 3 (P282-T3) results

The satellites performed the specified maneuvers, achieving the desired relative motion in the x-y plane, i.e. relative circular and spiral trajectories. This test successfully validates a new type of controller inspired by the cyclic pursuit algorithm, which uses only relative position and velocity information of neighbors to converge to a desired relative motion.

The distributed control laws, shows the desired performance and convergence properties to achieve an overall desired formation behavior in the x-y plane. A discernible result from hardware implementation is however, that the relative motion in the z direction showed very slow convergence to the desired state due to a suspected constant disturbance in the +Z direction.

The implemented control law shows a slow convergence because of too low gains assigned for the z-motion control which is the direction perpendicular to the formation maneuvers and is completely decoupled from the cyclic pursuit control. From eq. 3.42 it can be noticed that the dynamics in the z-direction are decoupled of the other coordinates. The relative dynamics

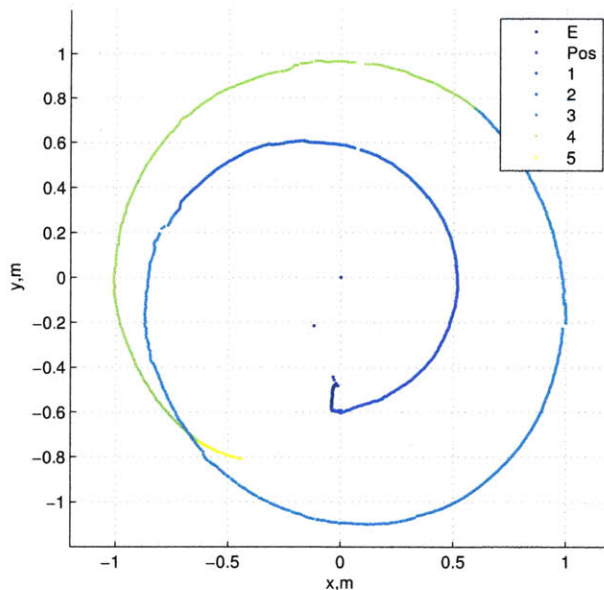


Figure 6-6: Experimental results from Test 3: Sequence of maneuvers indicated by colors.

in such direction reduce to a dynamic consensus which should converge to an agreement in the z-positions, if the gain is large enough [77]. Therefore, the gains for z-motion, could have been independently assigned from the gains for x-y motion.

For the purposes of this thesis, the important result is the validation of the performance in the x-y plane. As mentioned, the x-y motion is decoupled from the z motion, which is described by consensus dynamics under disturbances, which have been studied in other contexts and are out of the scope of this thesis.

In Figure 6-6, the relative motion in the x-y directions is shown performing the different maneuvers. The figure shows the relative state of the satellites as a function of time as well as the control commands on each vehicle. The underperformance of the controller in the z-direction is evident when the free drift mode is active. In the maneuvers 1 and 3 in figure 6-7, the center of mass is free and it is noticeable how both vehicles drift in the positive Z direction.

This experiment was the first experimental validation of the cyclic pursuit approach that relies only on relative information to control a circular and spiral formation.

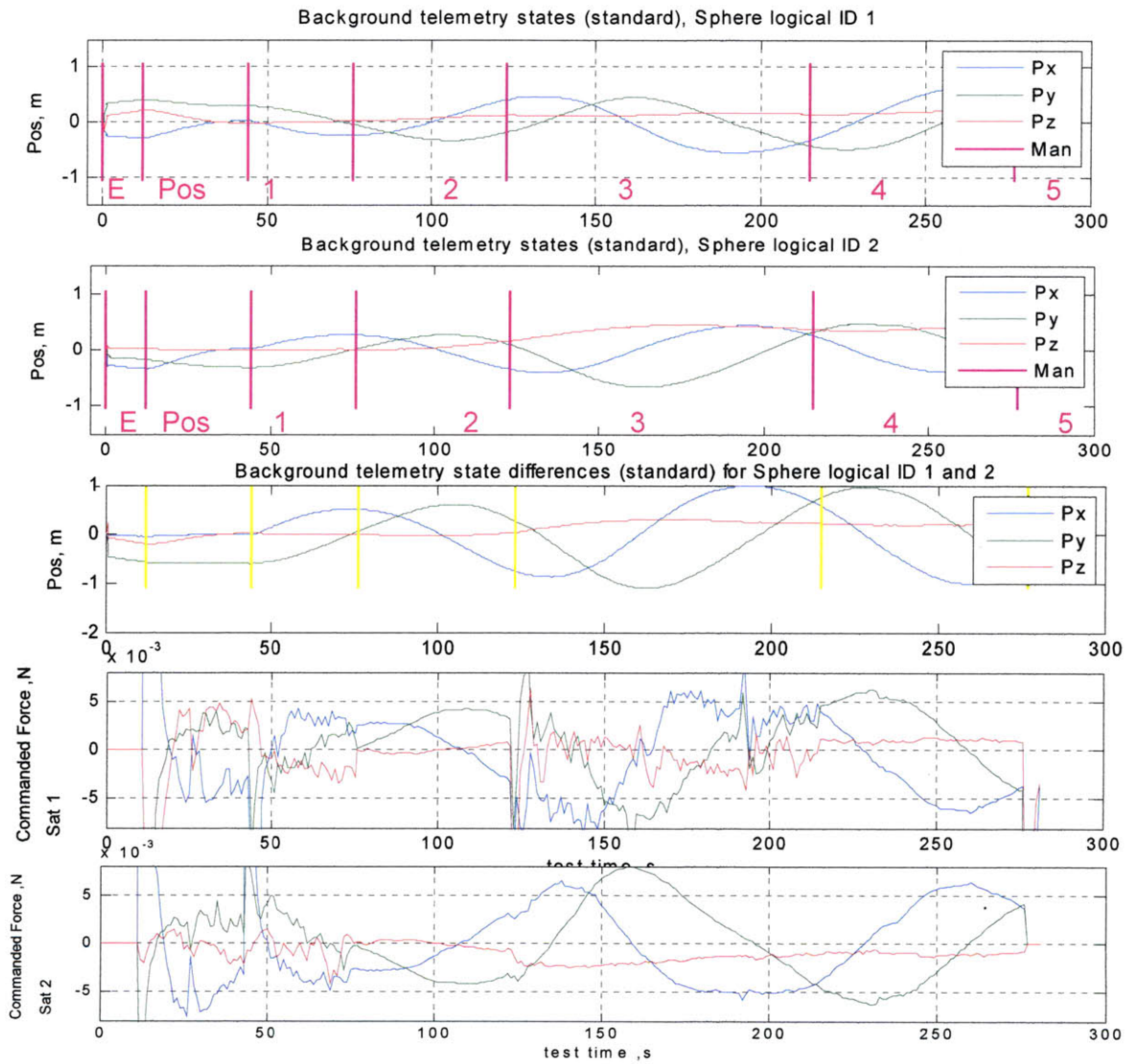


Figure 6-7: Experimental results from Test 3: Position, velocity and control commands vs. time.

6.3.4 Test 4: Implementation with a fault detection and recovery algorithm

The purpose of this test was to verify a cyclic pursuit algorithm as a responsive control method to achieve reconfiguration maneuvers in a satellite formation in the event of a failure. This test used a communication failure detection, isolation and recovery (FDIR) algorithm demonstrated in tests run in previous test sessions developed as part of parallel research on formation flight at MIT space systems lab.

A feature of the implemented algorithm, is the setup of a logic algorithm that reconfigures the topology of the formation. Based on this logic, each vehicle decides the vehicle that it uses as a partner to control its state. In this case it uses knowledge of a global variable which is updated through communication by the fault detection and identification mechanisms, but current research aims to identify the formation overall state through local knowledge.

When a vehicle is rejected because a failure was detected, a set of the parameter that defines the formation and the formation changes automatically reconfigures into a new configuration. In this test, for the purposes of algorithm demonstration, the reconfiguration consists only on a change to a parallel formation plane. In a more realistic implementation the idea can be applied to a more general set of parameters that define a reconfiguration to a formation that optimizes some specific metric, for example, minimizing collision probabilities with the unresponsive vehicle.

In all the following tests the implemented controller is an improved implementation of the cyclic pursuit algorithm that includes a feedforward term, specifically 6.2.

The sequence of maneuvers after estimator initialization and initial positioning in this test was defined as follows:

1. At 55 seconds, a 3-satellite rotating formation in the x-y plane, with center on the $z = 0.2m$ plane is commanded.
2. At 120 seconds, a failure is simulated in SPH1, by blocking the transmission of data.

In response to this, SPH2 and SPH3 should change the formation plane, specifically to the $z = 0m$ plane.

6.3.4.1 Test 4 (P273-4) results

The results from this test demonstrated a complete fault detection isolation and recovery mechanism for multi-vehicle formations under a simulated failure and even under an actual failure. The awareness of the state of the communication link with the other satellites in each vehicle is monitored by the fault detection module. The plots on the left in Figure 6-8, show the perception of the transmitters for each one of the satellites. 0 means nominal operation, 1 means a failure was detected. The black line describes the number of satellites in the formation for each satellite. The simulated failure in the transmitter of SPH1 (SPH1) is indicated by the thin line at 120 seconds. 5 seconds later, the detection algorithm on each vehicle detects that there is a failure seen in the change of the variable defining the perception of the state of the transmitter (TX1) from 0 to 1.

The detected failure triggers a reconfiguration maneuver in the controller module, which commands a change in the configuration of the interconnection links and moves the center of the formation in a way that avoids the failed vehicle. The number of vehicles in the formation is used by the decentralized algorithm to define the formation parameters. At about 125 seconds satellite 1 reconfigures.

An actual failure was detected and addressed by the algorithm. At about 160 seconds, SPH2 reset. SPH1 and SPH3 detected the failure. SPH3 then reconfigures its formation parameters and changes planes again.

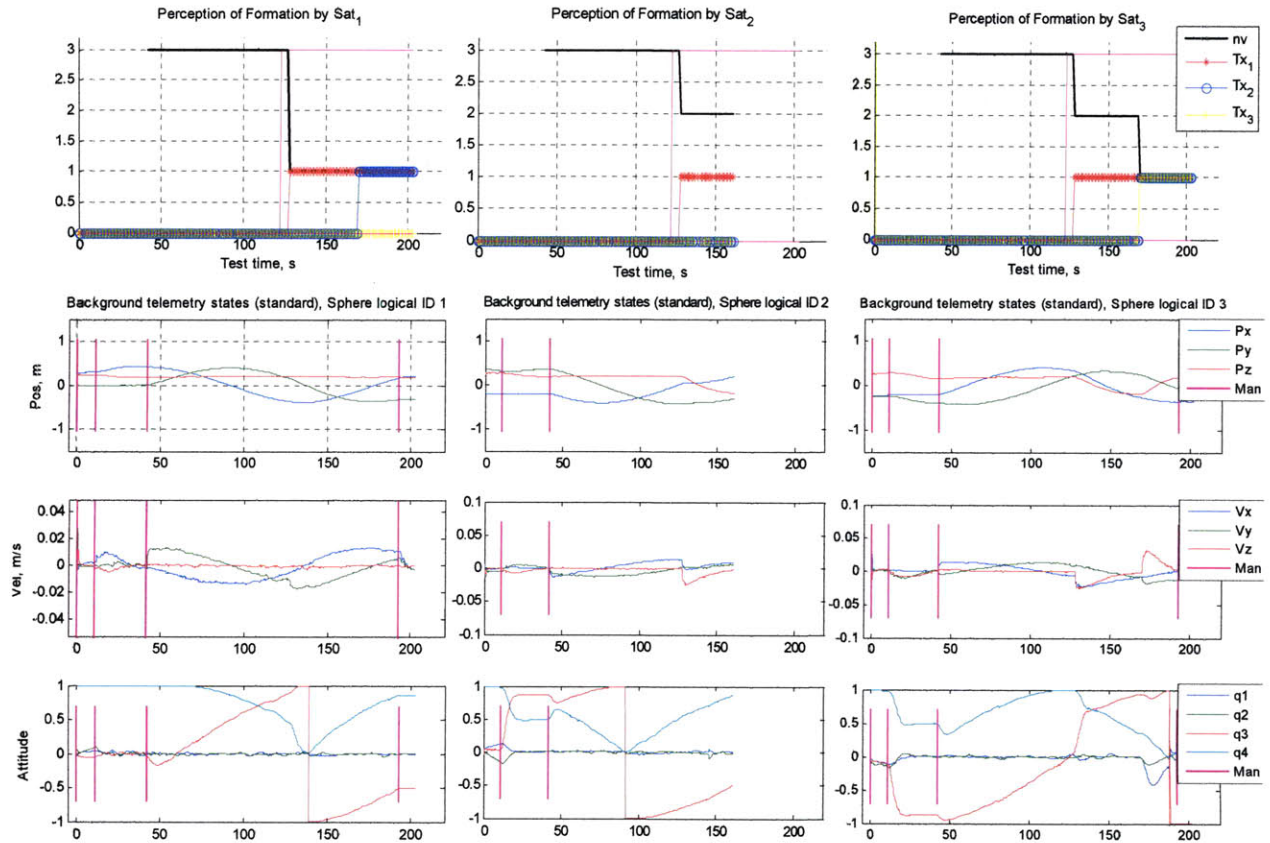


Figure 6-8: Experimental results from Test 4. Top: perception of the formation by each satellite.

6.3.5 Test 5: Implementation with a collision avoidance mechanism

This test was designed to evaluate the performance of a combination of algorithms to achieve formation initialization avoiding any possible collision. A high level algorithm commands the formation acquisition and maintenance using the cyclic pursuit decentralized algorithm. In case of a potential collision, a low level collision avoidance algorithm overrides the high level controller to prevent trajectory overlaps. The algorithm assumes that a vehicle has a detection system capable of detecting position and velocity of nearby objects. For the experimental setup, each vehicle was given the information of the other satellites via communication.

The test sequence was the following after estimator convergence and initial positioning:

1. SPH1 and SPH2 start a circular formation maneuver. SPH3 holds position at a point that interferes with the path of the formation of SPH1 and SPH2.
2. After a few seconds into this maneuver, SPH1 and SPH3 detect a possible collision with each other and the collision avoidance algorithm on each one executes a path correction.
3. Ten seconds after the execution of the collision avoidance maneuver in SPH3 has occurred, the satellite signals the others that it is joining the formation and the vehicles reconfigure in a 3-satellites formation.
4. The cyclic controller continues issuing control commands in each satellite, while the collision avoidance runs in the background executing path corrections in case of any possible collision with another vehicle is detected.

6.3.5.1 Test 5 (P273-3) results

This test was successfully completed and the vehicles performed the expected behavior. An error in the instructions to the crew in the test procedure files cause an initial misplacement in the desired position of satellite 1, however, this misplacement did not affect the overall development of the test.

The plots in Figures 6-9 show the trajectories of the satellites. During the initialization maneuver, satellite 3 had to move from the negative x position to a positive 0.4m position. An initial small correction was actually executed by the collision avoidance mechanism during this positioning stage as noticed in figure. The trajectory initially described by satellite 3 in the x direction is due to the above mentioned misplacement.

Figure 6-10 show the time history of the states for each vehicle. It can be noticed how primary (SPH1) and secondary (SPH2) satellites start a circular formation until SPH1 detects the possible collision with the tertiary and activate the collision avoidance path correction. The trajectory of SPH1 deviates from the circle; SPH3 also tried to move out of the path. Additionally, the SPH2 was also affected by the path correction since its commands are coupled to the motion of the other satellites in the formation. Eventually when no more collision threats are detected the 3-satellite formation continues its path to finally achieve the formation.

6.3.6 Test 6: Implementation as a random initialization algorithm

This test demonstrates the performance of an algorithm for random formation initialization. This test builds up on the results of P273 Test 3, by using the same algorithm with an addition of a module for astronaut input. In this test, the astronaut was able to manually command, when and which satellite joins the formation.

After the initialization maneuver, the satellites reach initial positions in the boundaries of the test volume. After the 30 seconds allowed for this positioning, the astronaut was in charge

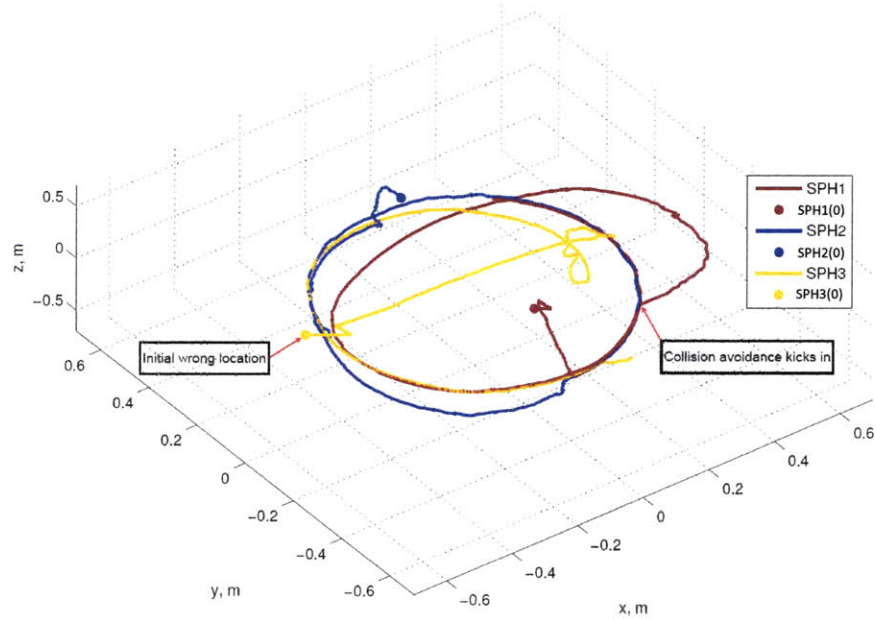


Figure 6-9: Experimental results from Test 5: Trajectories.

of indicating each satellite to join the formation by pressing a key in the laptop. Pressing the "A" key commands the SPH1 to join the formation, pressing the "S" key commands the SPH2 to join the formation, and pressing the "D" key commands the third satellite to join the formation. The astronaut was free to select in which order and when to press the key. After the three satellites had been commanded to join the formation and the formation is achieved, the test ends.

6.3.6.1 Test 6 (P273-6) results

This test was partially successful. In general the tests achieved the objective and the performance of the control was as expected. However, one of the satellites showed poor performance on the initial estimator convergence, due to this, its initial positioning was flawed.

The satellites joined the formation as commanded, and achieved the desired configuration in their estimated states, with the SPH2 having a biased estimation of its state.

Figures 6-12 through 6-15 show the corresponding trajectories and the position and attitude states for each satellite. Each one joined the formation from an arbitrary location when

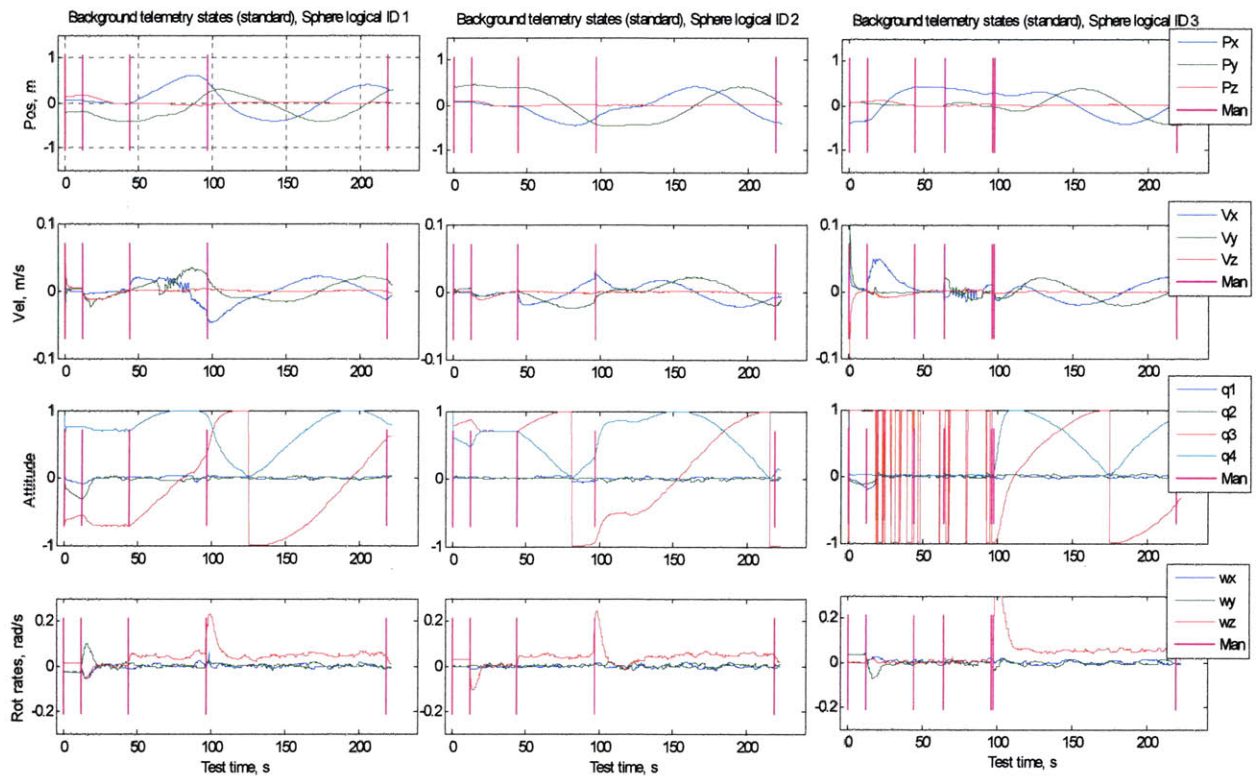


Figure 6-10: Experimental results from Test 5: States vs. time.

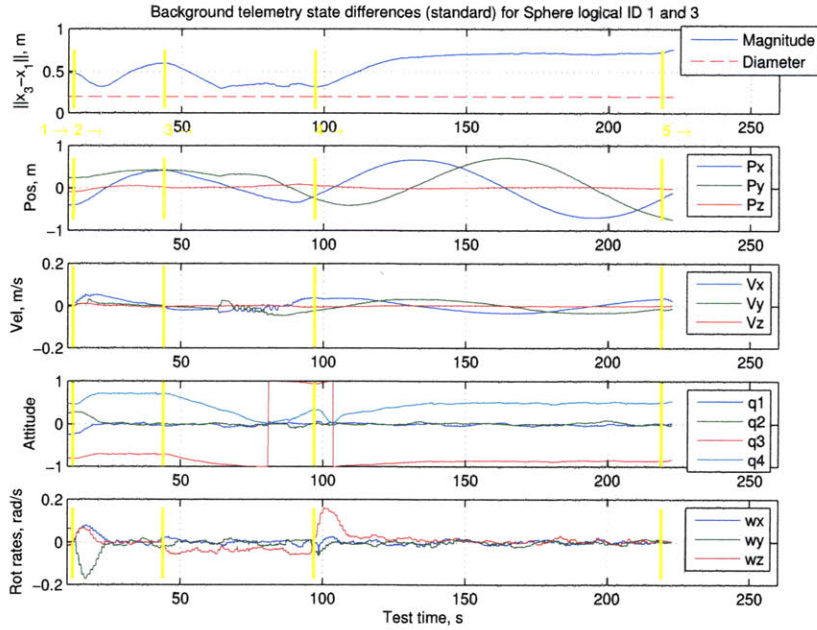


Figure 6-11: Experimental results from Test 5: Relative states SPH1 to SPH3 vs. time.

randomly commanded by the astronaut. The time when each satellite joined is indicated by the black arrow. Even though the test is not considered completely successful due to the divergence of the estimator in the SPH2, the actual performance of the algorithm was as expected.

This test verified the modularity and interchangeability properties of the control approach, while maintaining reduced complexity as the number of vehicles is increased.

6.4 Performance Analysis

In this section we consider an analysis of the 'steady state' performance of the formation control mechanism by considering some metrics that describe the efficiency of the algorithms in achieving a synchronized rotating formation. The analysis is based on steady state data extracted from the tests described above and predated tests, performed in early test sessions.

As metrics to analyze the performance of the system we consider the ratio between the theoretical fuel usage and the actual fuel usage for a given maneuver while also comparing

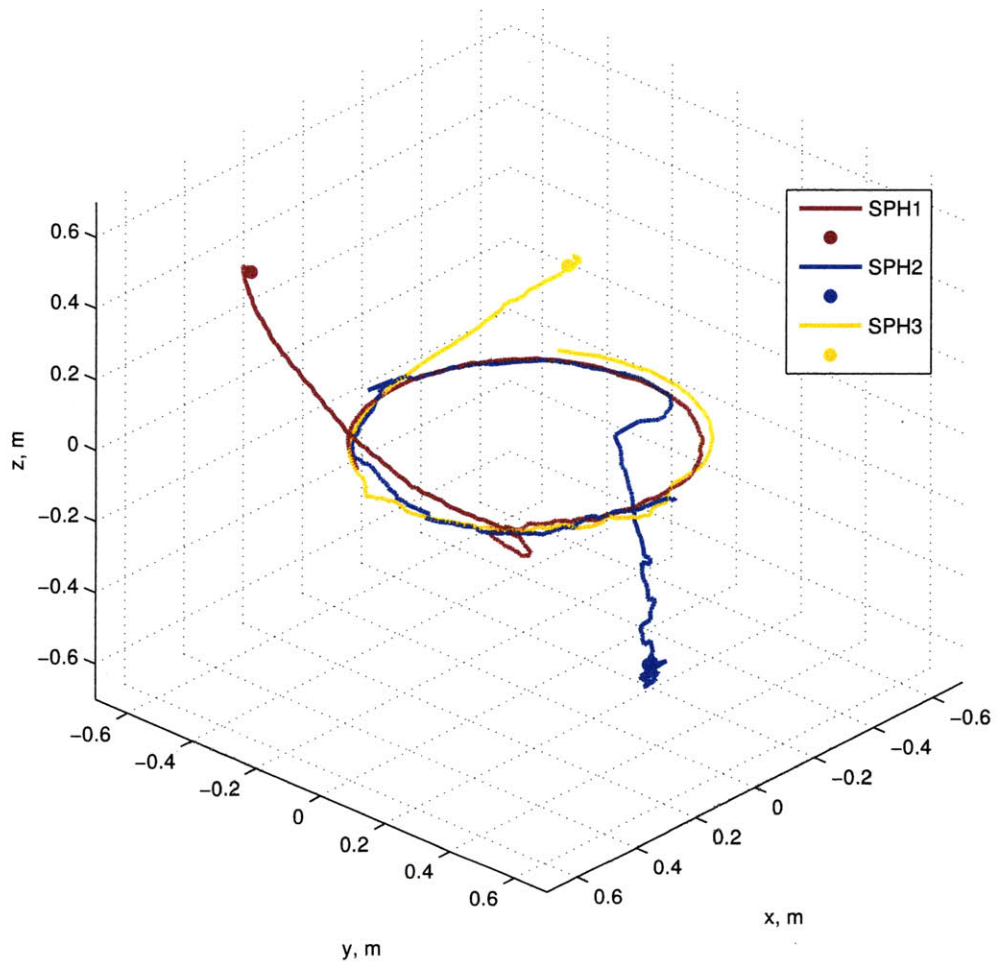


Figure 6-12: Experimental results from Test 6: Trajectories.

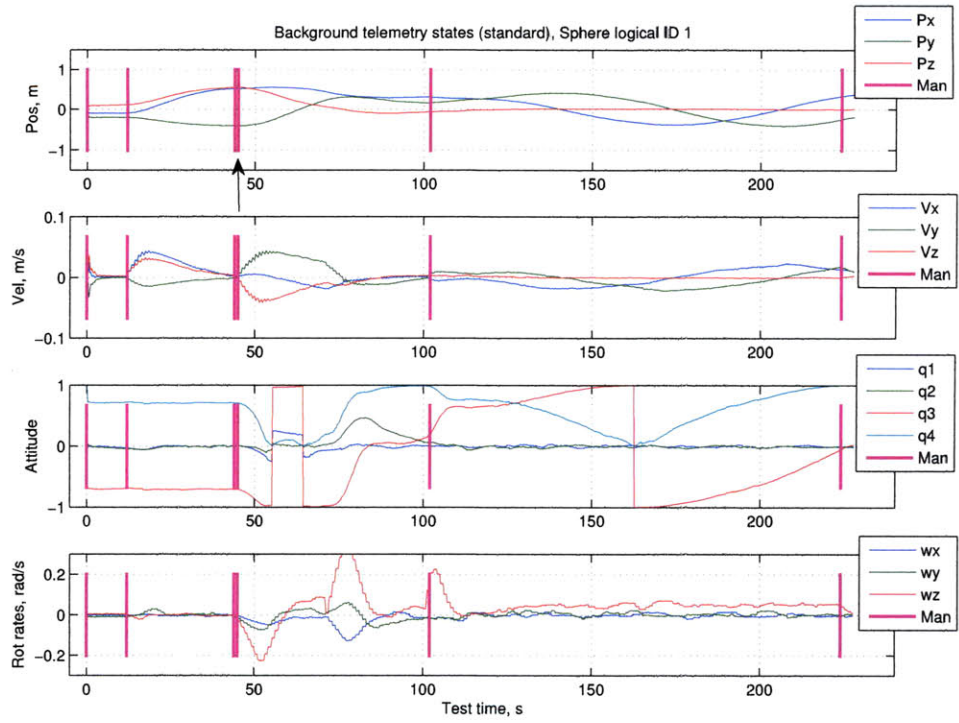


Figure 6-13: Experimental results from Test 6: SPH1 States vs. time.

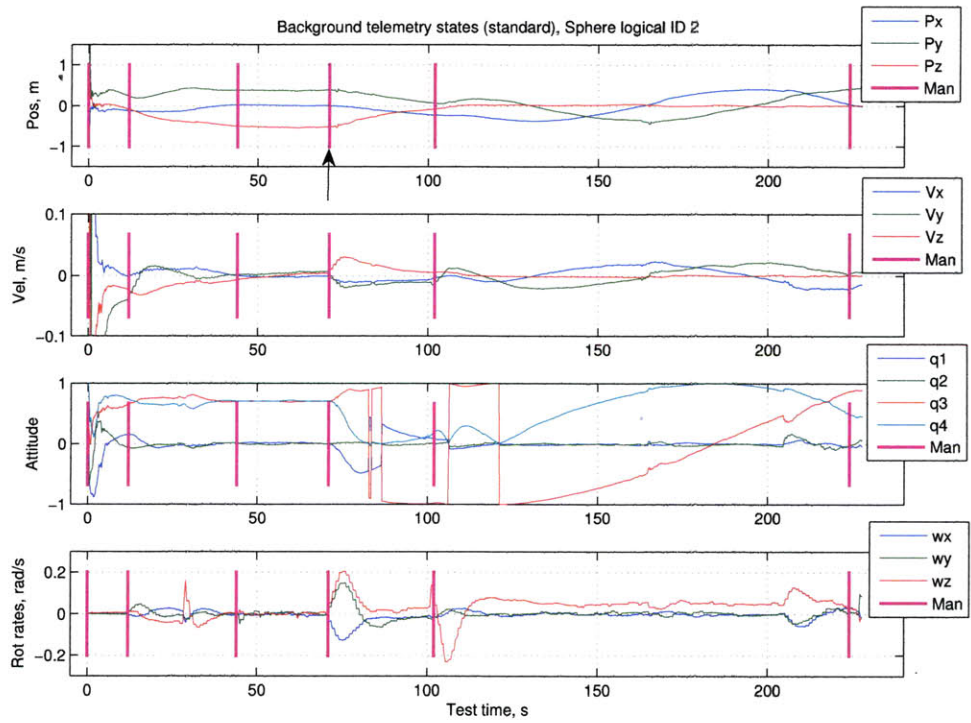


Figure 6-14: Experimental results from Test 6: SPH2 States vs. time.

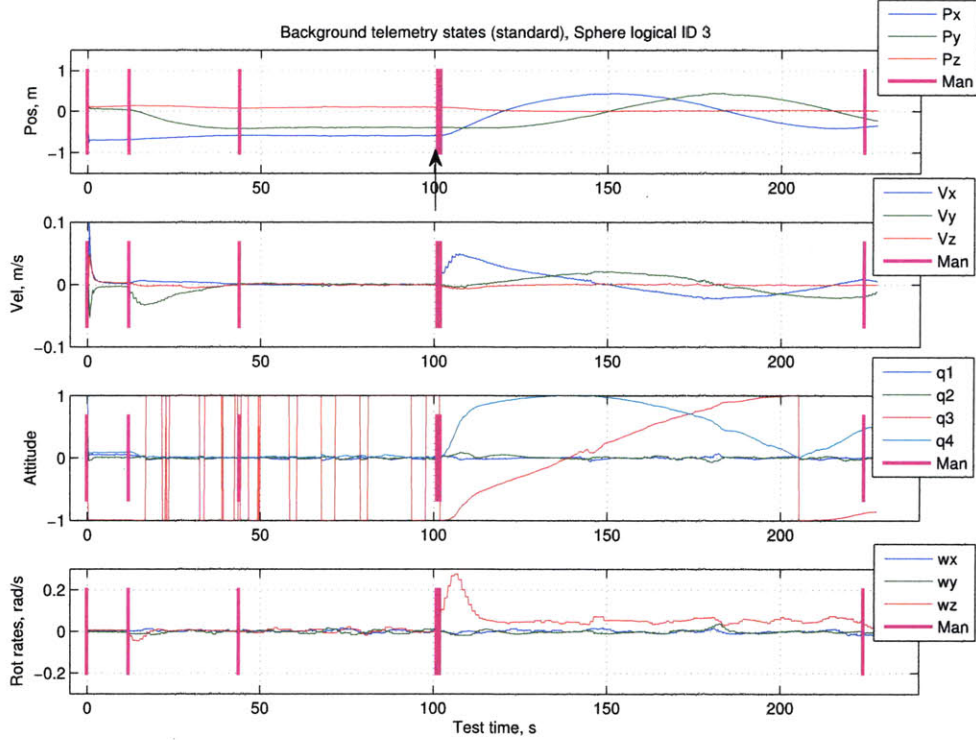


Figure 6-15: Experimental results from Test 6: SPH3 States vs. time.

the error metric to symmetric formation $\mathbf{e} = V_{rn}\mathbf{x}$ where, $V_{rn} = L_1 \otimes R_{\pi/N} + L_1^T \otimes R_{\pi/N}^T$ is a projection into the subspace of regular polygons as presented in Chapter 4. This metric of error however is only valid for 3 or more satellites. Two satellites will always be in a 'perfect formation' under this metric.

The theoretical ΔV is calculated as an integral of the theoretical acceleration magnitude $\Delta V = \int_{t_o}^{t_f} \|a\|_2 dt$.

Table 6.1 compares the fuel performance achieved in different maneuvers in different ISS test sessions and under different architectures. Figure 6-16 shows the maneuver and the error performance.

It is important to note that under the error performance as defined by the 'polygon symmetry' metric mentioned above is valid only for more than two vehicles. Under this metric the cyclic pursuit approach shows for all cases error performance better than the other architectures as shown in fig. 6-16.

Test	Control Architecture	Maneuver Description	$\frac{\Delta V}{\Delta V_{min}}$ ratio
P272.T4	Relative States Central LQR	Circle 2-sat, $\omega = \frac{2\pi}{180}$, $r = 0.4m$	6.0
P162.T2	Individual PID tracker	Circle 3-sat, $\omega = \frac{2\pi}{180}$, $r = 0.4m$	1.49
P265.T2	Individual PID tracker	Spiral 2-sat, $\omega = \frac{2\pi}{180}$, $r = 0.1 - 0.7m$	1.47
P264.T2	Cyclic pursuit w/ ref. vel.	Spiral 2-sat, $\omega = \frac{2\pi}{90}$, $r_i = 0.35 - 0.5m$	1.30
P264.T2	Cyclic pursuit w/ ref. vel.	Circle 3-sat, $\omega = \frac{2\pi}{90}$, $r = 0.4m$	1.40
P273.T6	Cyclic pursuit w/ ref. vel.	Circle 3-sat, $\omega = \frac{2\pi}{120}$, $r = 0.4m$	1.40
P273.T4	Cyclic pursuit w/ ref. vel.	Circle 3-sat, $\omega = \frac{2\pi}{180}$, $r = 0.4$	1.39
P282.T2	Cyclic pursuit Relative Navigation	Circle 2-sat, $\omega = \frac{2\pi}{120}$, $r = 0.5$	1.36

Table 6.1: Comparative fuel use for several control architectures

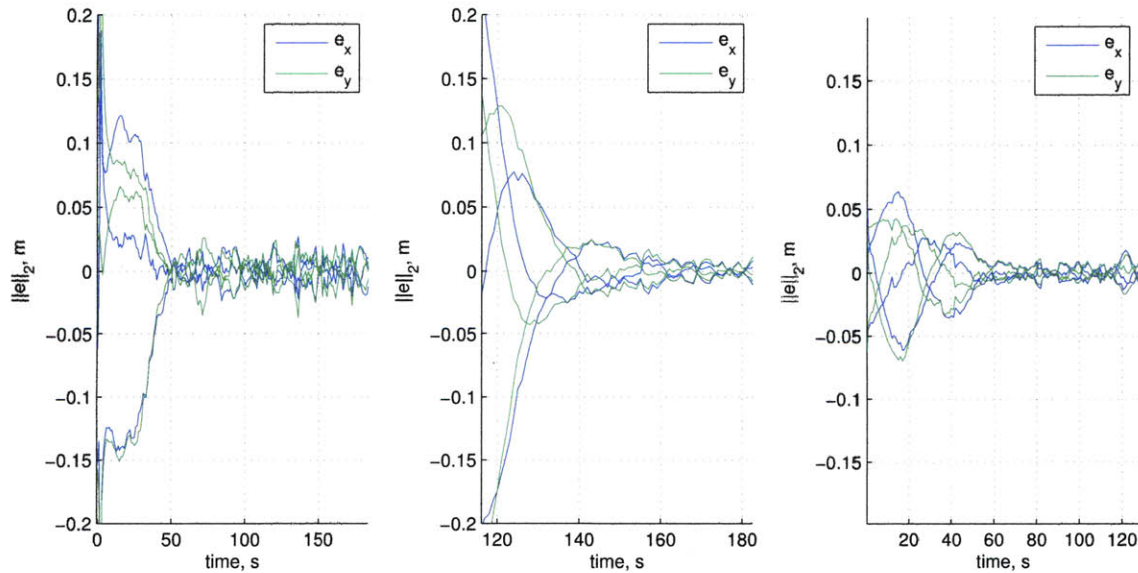


Figure 6-16: Error in symmetry for three cases in table 6.1. from left to right P162.T2, P273.T4, P273.T6. Cyclic Pursuit cases are the two on the right.

The fuel performance presented in table 6.1 shows experimental results agreeing with the expected improvement on reducing the control effort by using the cyclic pursuit architecture while maintaining the symmetry of the formation. These results however, should not be taken as direct verification of this improvement effect since the data used in the comparison was not specifically designed for achieving the same objective and the variability in the experiment conditions have not been considered in the analysis. Nevertheless, the results do show that for the formation flight experiments flown in microgravity environment, the cyclic pursuit approach has lower fuel use while maintaining similar performance in maintaining a symmetric formation.

6.5 Summary and Conclusions of the Chapter

This chapter presented experimental results for the first ever implementation of decentralized formation flight in space. Several experiments were performed on the SPHERES testbed aboard the International Space Station. Such experiments demonstrate the validity of the algorithms in achieving geometric pattern formation control in relevant hardware. The applicability in multiple scenarios demonstrates the versatility and inherent simplicity of the proposed decentralized approach. Additionally, the analysis of the fuel performance and error as compared to previously implemented approaches agreed with the expected reduced control effort in achieving the pattern without specifically tracking trajectory fixed points.

The performance of the algorithms as a formation control strategy was verified while demonstrating their capabilities to accomplish several simulated mission scenarios relevant for a fractionated spacecraft mission.

In the joining maneuver test (Test 2), the center of the formation an uncontrolled state. The invariance of the geometric center of the formation is noticeable in the experimental results: when the third vehicle joins the two-vehicle formation the center of the formation moves to include the effect of the initial position of the third vehicle. This effect is of course

controllable by using $k_g > 0$ as described in remark at the expense of control effort and knowledge of the global positioning.

The importance of a nonlinear extension was evident from initial experimental results. When using only a linear approach, the discretization effects and the time delays caused a divergent behavior. The effect was compensated by adjusting the pursuit angle applying the extension as mentioned in Section 3.2.4.

The addition of a feedforward term by upgrading the control approach to eq. 3.32, improved the performance of the controller by achieving a more precise radial control. In the initial implementation, the equilibrium value of the dynamic angle α was achieved at a radial distance different from the one specified. In later tests when the feedforward term was implemented, the radius of the formation was much more precise as can be appreciate in figs. 6-3 as compared to 6-8, 6-9. The precision can be further improved by implementing an integral control approach by including a term: $\alpha = \pi/N - k(|x_{i+1} - x_i| - \rho) - k \int (|x_{i+1} - x_i| - \rho) dt$, dependent on the accumulated error. The theoretical development of this approach is however, out of the scope of this thesis. Preliminary simulations demonstrate it as a valid approach but it was not implemented on the tests and is left as a possible venue for future work.

In the implementation of the only relative measurements controller, based only on theoretical results the z-motion gains were setup to 1. Simulations without accounting for noise, disturbances and constrained actuation showed good convergence performance. However, under the actual testing conditions on hardware, the underperformance of the control in the z-direction became evident as seen in the data plots shown below, especially, due to a constant disturbance in the +Z direction discernible from the debug data.

Chapter 7

Decentralized Control in Electromagnetic Formation Flight

7.1 Introduction

In this chapter, the idea of decentralized control is extended to the case of Electromagnetic Formation Flight (EMFF) systems. EMFF is a very innovative concept envisioned for propellantless spacecraft formation. However, these systems have very particular coupled dynamics and a straightforward implementation of decentralized control techniques designed for decoupled systems fails to address their strong actuation coupling.

To achieve the benefits of decentralization in this type of system, an analysis of some ideas for decentralization of electromagnetic formations is formally presented in this chapter.

A first section introduces the concept of electromagnetic formation flight technology, with some emphasis on the coupled nature of the actuation commands. Then, the approaches to decentralization are presented. In summary, several techniques that can achieve control of a system of EMFF satellites in a decentralized manner are studied by considering two main different directions. The first one consists on decoupling the dynamics. The second one addresses the problem by distributing the computation and the need for a central computer.

The general approach to the methods presented in this chapter is rather heuristic given the difficulty of the problem but some specific theoretical results are discussed. The different proposed ideas are implemented in simulation to compare their performance to a centralized approach. A more extensive theoretical analysis of each one of them is left out of the scope of the present work and is suggested as a direction in future work.

7.1.1 Electromagnetic Formation Flight

The Electromagnetic Formation Flight (EMFF) technology has been recently studied and is currently being developed by the Space Systems Laboratory at MIT in collaboration with Aurora Flight Science (formerly Payload Systems). Similar approaches have been independently proposed by groups at the University of Tokyo and the Boeing company. The principal advantage of EMFF systems is the independence from expendable propellants. This can be an extremely important factor for long duration missions, missions that require extensive reconfiguration maneuvering or missions where the impingement of propellant particles can affect the system performance.

The principle of operation behind EMFF is the used the coupled electromagnetic forces and torques to control the relative position of a group of vehicles in space. The mechanism used to create the electromagnetic forces between vehicles consists of a set of orthogonal coils that generate magnetic fields when current is run through them.

As opposed to other systems proposed for propellantless formation flight, like flux pinned [58] or coulomb force formation flight [85], electromagnetic formation flight achieves control of 3N translational degrees of freedom, including shear forces which are not achievable through other proposed non propellant methods. In EMFF any force and torque command can be readily achieved by controlling currents running through individual coils on each vehicle.

Different architectures for the coils have been envisioned and studied. In one, the coils are made out of conventional conductive material. Aluminum has been identified as the most competitive non-superconductive material for this purpose [82]. In this case pulsed currents

used as a mechanism to prevent overheating due to the heating effects of the finite resistance in this type of materials. Theoretical analysis and experimental results have validated the principle of operation and the capabilities to achieve net forces which can be large enough to counteract the effects of J_2 differential terms in low Earth multi-satellite systems.

In a second type of architecture, High-Temperature Superconducting (HTS) material can be used to build the coils. In this case, YBCO or BSSCO composites can be cooled down below a critical temperature, achieving superconducting behavior. In this case, constant currents of higher intensity can be run through the coils, generating much larger effective forces between vehicles.

7.1.1.1 Dynamics of EMFF systems

In this section, we discuss the relevant dynamics of an EMFF system, developed in previous literature. [3, 87]

In a vehicle i , a current I_{ix} is generated and controlled though an internal computer to run through the coils. In a circular coil aligned with the body x -axis in vehicle i generates a magnetic field which can be approximated, as the field generated by a magnetic dipole $\mu_{ix} = nI_{ix}A$.

When running independent currents through each one of the orthogonal coils in one satellite, a composed dipole $\mu_i = \mu_{ix}\hat{x} + \mu_{iy}\hat{y} + \mu_{iz}\hat{z}$ corresponding to the vectorial sum of the orthogonal dipoles in satellite i is generated and can be steered in any direction in the i body-frame. This allows each satellite to independently command its dipole in any direction and under an agreement on a global coordinate frame, the overall formation can be seen as a group of interacting dipoles that can be pointed on any direction. Then, the magnetic field generated by agent i is:

$$B_i(r_{ij}) = \frac{-\mu_0}{4\pi} \left(\frac{3\mu_j \cdot r_{ij}}{r_{ij}^5} r_{ij} - \frac{\mu_j}{r_{ij}^3} \right) \quad (7.1)$$

The interaction between the fields of the dipoles generate forces between them. The resultant force of the interaction of two dipoles μ_i, μ_j is given by:

$$\mathbf{F}_i = \sum_{j \neq i}^n F_{ij} \quad (7.2)$$

$$F_{ij} = \frac{-3\mu_o}{4\pi} \left(\frac{\mu_i \cdot \mu_j}{|d_{ij}|^5} d_{ij} + \frac{\mu_i \cdot d_{ij}}{|d_{ij}|^5} \mu_j + \frac{\mu_j \cdot d_{ij}}{|d_{ij}|^5} \mu_i - 5 \frac{(\mu_i \cdot d_{ij})(\mu_j \cdot d_{ij})}{|d_{ij}|^7} \right) d_{ij} \quad (7.3)$$

and, the overall force of a formation of vehicles $i \in \{1, ..N\}$, is given by:

$$\mathbf{F}_i = \sum_{j \neq i}^n F_{ij} \quad (7.4)$$

where F_i is the force on vehicle i , F_{ij} is the force on vehicle i due to vehicle j , μ_0 is the magnetic permeability constant of vacuum and r_{ij} is the vector position between vehicle i and vehicle j .

These set of equation are called the dipole equations. The control commands are the currents run through each one of the coils on each vehicle which directly translate into dipole magnetic fields affecting the forces of the overall formation.

The special coupling in a system of EMFF vehicles is evident from this equation: Individual control command alters the forces on each other vehicle in the formation, therefore a straightforward extrapolation of distributed control mechanisms proposed for other type of propulsion, specifically non-coupled actuation, is not feasible.

Achieving a commanded force requires coordination with at least one other vehicle, since the force directly depends on the vectorial value of another dipole. Additionally, the dipole enters into the force equation as a multiplicative parameter, which means that local constraints in its magnitude do not guarantee global constraints in its disturbance effect on the other vehicles in the formation. These coupling effects pose an important challenge to the decentralization of EMFF.

For the closed loop control approaches in the existing literature, the overall formation state information is gathered in a central computer, the set of dipole equations are solved every control period and the current commands issued to each one of the vehicles in the formation.

In this chapter of the thesis we discuss and compare different approaches to achieve the objective of achieving control of an electromagnetic formation without the need of using a central computer that solves the set of equations every control period.

7.2 Token Based Decoupled Maneuvering

In this section we study a solution to the EMFF decentralization problem by decoupling the actuation through time allocation.

A token based mechanisms is used as the time allocation mechanism. The approach considers the solution to a constrained optimization problem such that only one subset of the vehicles actuate at a time. It is a token based approach, because only vehicles owning a 'token' can actuate at a given time. The token sequence is calculated as part of an overall optimization problem.

In the general trajectory optimization problem, a centralized solution can be obtained, without restricting the number of vehicles that can actuate at a time. Open loop tracking of the input time history should achieve the final configuration. It is however known that any small disturbance, and especially in a nonlinear system like EMFF, will cause divergence from the desired final state. Therefore, the best approach is a close loop tracking of the optimal state time history. If however, the solution of the optimization problem is obtained under the constraint that only a subset of vehicles can actuate at a time, a natural decentralization of the trajectory tracking problem occurs. Tracking the trajectories would not require an agreement of the overall set of vehicles but only a subset of them, reducing the complexity of the tracking problem.

Such trajectory optimization problem is special in the sense that it has specific constraints on the number of vehicles that can be used at a given time and needs to be approached in a special manner. This problem can be solved considering a two-level structured optimization problem.

In a lower level problem a set-wise subproblem is to be solved, considering the optimal dipole selection for achieving an optimal reconfiguration maneuver using only a subset of vehicles. In the higher level problem, the sequence of vehicles participating at each allocated time slot is considered.

The approach to solve the lower level trajectory optimization problem was implemented by using a pseudo-spectral method approach, where the states and controls are mapped into a parameter discretization based on Legendre polynomials. Optimal reconfiguration maneuvers using this approach, have been studied in the past for formations with several vehicles [3] for deep space dynamics. In this thesis, these results are extended by solving for optimal reconfiguration maneuvers considering more complex dynamic situations, in particular, Clohessy-Wiltshire dynamics.

A solution algorithm for the higher level problem was implemented using a Dynamic Programming (DP) approach, solving for the sequence that achieves minimum cost.

The overall reconfiguration problem, considers a set of N vehicles on initial positions $\mathbf{x} = \mathbf{x}(t_0) = [\mathbf{x}_1(t_0), \mathbf{x}_2(t_0), \dots, \mathbf{x}_N(t_0)]$ which we are interested in reconfiguring to final positions $\mathbf{x}_f = \mathbf{x}(t_f)$ while minimizing some cost (time, angular momentum, current intensity or a combination of them). A general case with dynamics $\ddot{\mathbf{x}} = f(\mathbf{x}) + u_i$ is assumed.

In a token based time divided decentralized approach like the one proposed in this section, the vehicles reach the final positions by moving in a sequence $S_{opt} = \{S_1, S_2, \dots, S_{N-a}\}$, where S_1 is the set of active vehicles during time interval $[t_i, t_{i+1})$.

The total time is assumed to be $t_f - t_0 = \sum_{v_i} t_i$, and at each interval only a vehicles can be active, ($\text{card}(S_i) = a$), and at least $a - 1$ vehicles reach $\bar{x}_i(t_{i+1})$, such that $\mathbf{x}_i(t_f) = x_{if}$.

The description of the two subproblems is specified in the sections below.

7.2.1 Lower level problem solution

The lower level problem consist of finding the optimal reconfiguration maneuver for vehicles $i \in S[k]$, where $S[k]$ is the set of vehicles active at interval k .

The approach presented in the solutions in this sections uses the Legendre pseudospectral decomposition approach developed in [3]. In this method the control and the state variables are discretized and an optimization problem tries to find the values at the specific discretization points such that the solution minimizes the desired cost function. Extending this approach we consider a method to achieve solutions for maneuvers under Clohessy-Wiltshire dynamics.

The reconfiguration maneuver, bringing a set of vehicles with initial conditions \mathbf{x}^0 , to a formation with final condition \mathbf{x}^f can be written as the continuous optimization problem [3]:

$$g(\mathbf{x}) = \min_{\boldsymbol{\mu}(t)} J(t, \mathbf{x}, \boldsymbol{\mu}) \quad (7.5)$$

subject to :

$$\dot{\mathbf{x}} = \mathbf{f}(\mathbf{x}, \boldsymbol{\mu}) \quad (\text{Dynamics})$$

$$\mathbf{x}^0 = \mathbf{x}(t_0) \quad (\text{Initial state})$$

$$\mathbf{x}^f = \mathbf{x}(t_f) \quad (\text{Final State})$$

$$|\mu_i| < \boldsymbol{\mu}_{max} \quad (\text{Actuation saturation})$$

$$\inf d_{ij}(t) > D_{min} \quad (\text{Collision avoidance})$$

$$|h_{RW_i}(t)| < H_{max} \quad (\text{angular momentum constraint})$$

where $\mathbf{x} = [\mathbf{p}\mathbf{v}]$, \mathbf{p} being the position and \mathbf{v} being the velocity defining the state of the overall formation, $\boldsymbol{\mu}(t)$ is the control variable and $J(t, \mathbf{x}, \boldsymbol{\mu})$ is a cost function to be minimized.

When using the pseudospectral method, the unknown state and control trajectories are

parametrized by coefficient of Legendre polynomials:

$$\dot{\mathbf{p}} = \sum_{i=0}^{N_d} \mathbf{p}(t_i) \phi_i(t) \quad (7.6)$$

$$\dot{\mathbf{u}} = \sum_{i=0}^{N_d} \mathbf{u}(t_i) \phi_i(t) \quad (7.7)$$

where $\phi_i(t)$ are degree interpolating basis for the Legendre polynomials. The optimization problem is then, mapped into a Nonlinear Programming Problem as a function of the coefficients $\mathbf{P} \in \mathbb{R}^{N \times N_d+1}$, $\mathbf{U} \in \mathbb{R}^{M \times N_d+1}$ and t_f :

$$g = \min_{\mathbf{P}, \mathbf{U}, t_f} J(t, \mathbf{p}, \mathbf{v}, \boldsymbol{\mu}) \quad (7.8)$$

subject to :

$$\mathbf{D}^2 \mathbf{P} - \left(\frac{\tau_f - \tau_0}{2} \right) \mathbf{F} = 0 \quad (\text{Dynamics})$$

$$\psi_0(\mathbf{p}_0, \mathbf{v}_0, \tau_0) = 0 \quad (\text{Initial state})$$

$$\psi_f(\mathbf{p}_{N_d}, \mathbf{v}_{N_d}, \tau_f) = 0 \quad (\text{Final state})$$

$$\mathbf{c}_0(\mathbf{p}_0, \mathbf{v}_0, \mathbf{u}_k, t_k) \leq 0 \quad \forall k \in \{0, 1, \dots, N_d\} \quad (\text{Linear constraints})$$

(e.g. collision avoid., saturation)

$$\left(\frac{\tau_f - \tau_0}{2} \right) \mathbf{W} \mathbf{Q} - \mathbf{Z} \leq 0 \quad (\text{Integral constraints (e.g. angular momentum)})$$

where $\mathbf{D} \in \mathbb{R}^{N_d \times N_d}$ is a differentiation matrix, $\mathbf{P} \in (N_d + 1) \times n$ is a matrix with columns \mathbf{p}_i , that is, each column of \mathbf{P} represents the position coefficients at each discretization point. $\mathbf{F} \in \mathbb{R}^{N_d+1 \times n}$ approximates the dynamic vector field in the space of N_d^{th} order polynomials, $\mathbf{W} \in \mathbb{R}^{N_d \times (N_d+1)}$ is an integration matrix, $\mathbf{Q} \in \mathbb{R}^{(N_d+1) \times 1}$ approximates the constraint integrands, and $\mathbf{Z} \in \mathbb{R}^{N_d \times 1}$ is a given matrix of the constraint value at each discretization point. A more detailed description of this definitions is found in [3].

7.2.1.1 Results of the low level optimization problem

The results presented in here use this approach to solve for the optimal reconfiguration maneuvers for relevant dynamic cases. The solution of the problem was implemented using a Sequential Quadratic Algorithm (SQP) in MATLAB[®] using the SNOPT 6.0 package routines.

Figure 7-1 shows a surface plot of the the optimal cost for a 2-sat reconfiguration maneuver under Clohessy-Wiltshire dynamics and some examples of the solutions obtained.

In this example the initial relative location of the second satellite is $(1,0)km$ and the maneuver time is fixed to half an orbital period. The surface plot is a function of the desired final position. The boundary conditions are such that the initial and final state of both vehicles are closed natural orbits (ellipses with the appropriate angular period).

7.2.2 Higher level problem solution

The higher level subproblem consists on defining an ordered sequence $\{S\}_k = \{S[1], S[2], \dots, S[N]\}$ of agent subsets such that the overall cost function J is minimized.

The overall cost of achieving the reconfiguration maneuver is the addition of the cost for each individual reconfiguration maneuver. Then, the overall problem can be written as finding J_{S^*} such that:

$$J_{S^*} = \min_{S \in \bar{S}} J_S(x[0])$$

$$J_S(x[0]) = E \left\{ g_n(\mathbf{x}_n) + \sum_{k=0}^{n-1} g_k(\mathbf{x}[k], S[k], w[k]) \right\}$$

where $n = N - p$ is the number of reconfiguration maneuver to achieve the final desired state, $S[k] = \{s, \bar{s}\}$ is the set used at interval $[k]$, s is one of the agents and \bar{s} is the rest of the agents in a subset S , and g_k is cost of achieving a subset-wise reconfiguration maneuver, with initial state \mathbf{x} such that agent s , achieves its desired final state at the final time.

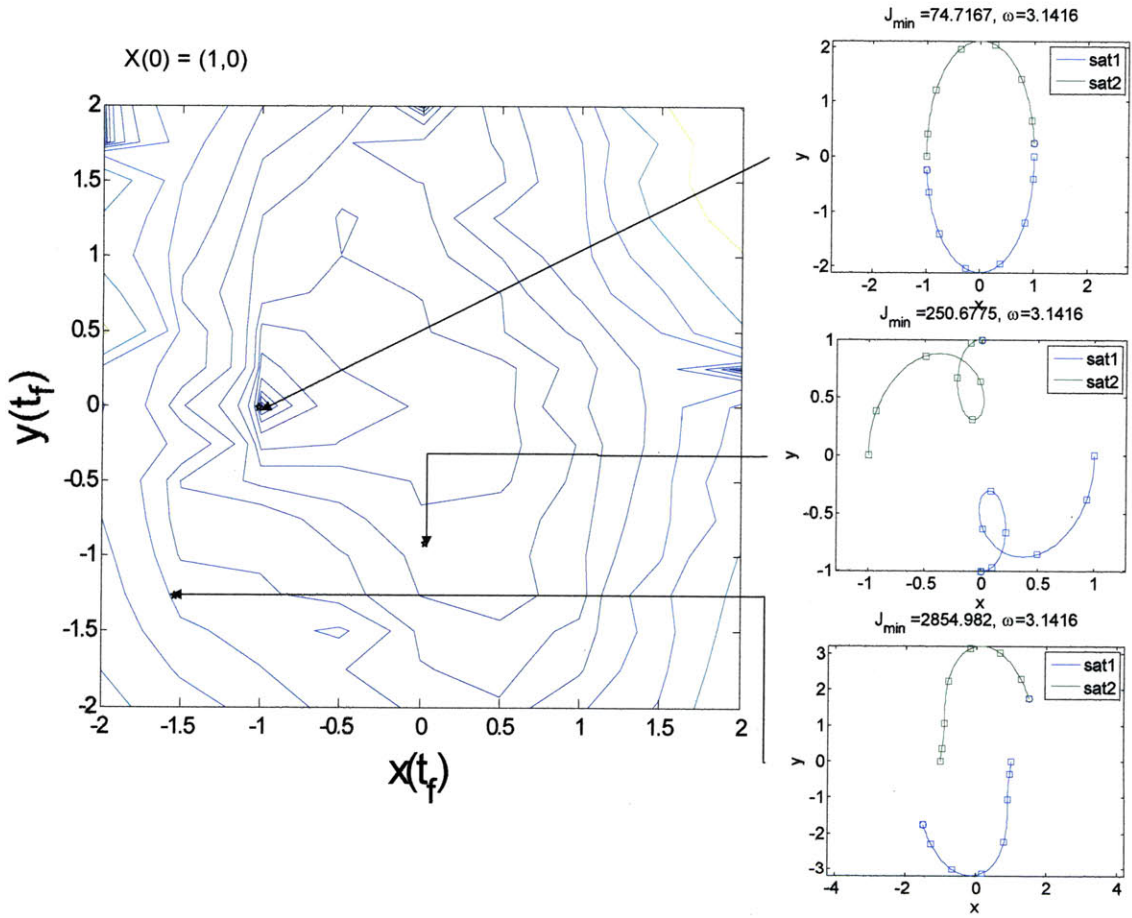


Figure 7-1: Optimal minimum current two-vehicle maneuvers in Clohessy-Wiltshire dynamics

A Dynamic Programming (DP) approach to the problem can be used by defining the optimization problem with the variables as described in table 7.1:

State variable	$\mathbf{x}[k] = [\mathbf{x}_1[k], \mathbf{x}_2[k], \dots, \mathbf{x}_N[k]]$	$\mathbf{x}[k]$ is the state of the vehicles at time interval $[k]$
Control variable	$\mathbf{u}[k] = S_k \in U_k, U_k(x_k) = \{s, \bar{s}\},$	S_k is the ordered pair active, allowed to maneuver during interval $[k], s \in \{1, 2, \dots, N\}$
Dynamics	$\mathbf{x}[k+1] = f(\mathbf{x}[k], \mathbf{u}[k], \mathbf{w}[k])$	\mathbf{x} evolves given $\mathbf{u}[k]$ and a random disturbance $\mathbf{w}[k]$
Cost function	$J[k] = g(S_k, \mathbf{x}[k])$, s.t. $\mathbf{x}_s[T] = x_s^f$	

Table 7.1: Variable descriptions for the higher level DP optimization problem

Then, the DP approach consists on solving the problem:

$$J[k] = \min_{\mathbf{u}[k] \in U_k} E \{g_k(\mathbf{x}[k], \mathbf{u}[k], w[k]) + J_{k+1}(f(\mathbf{x}[k], \mathbf{u}[k], w[k]))\} \quad (7.9)$$

$$J_N(x_N) = g_N(x_N) \quad (7.10)$$

Fig.7-2 shows the a reconfiguration maneuver where only 2 vehicles are allowed to move at a given time. The reconfiguration sequence can be compared to a centralized approach where all vehicles can actuate at the same time in Fig. 7-3. The dashed lines show the interconnection at a given time.

N_{spc}	$\text{card}(S)$	Optimal Sequence	$CostAmps/\gamma$	Cost Increase
5	2	$\{(4, 5) (2, 3) (3, 5) (5, 1)\}$	2.984×10^7	18%
5	3	$\{(4, 5, 1) (2, 3, 1)\}$	2.958×10^7	17%
5	4	$\{(2, 4, 5, 1) (1, 3, 0, 0)\}$	2.658×10^7	5%
5	5	$\{(1, 2, 3, 4, 5) (2, 3, 1)\}$	2.524×10^7	-

Table 7.2: Increase in RMS current in coils as the number of vehicles that can be moved at a time changes

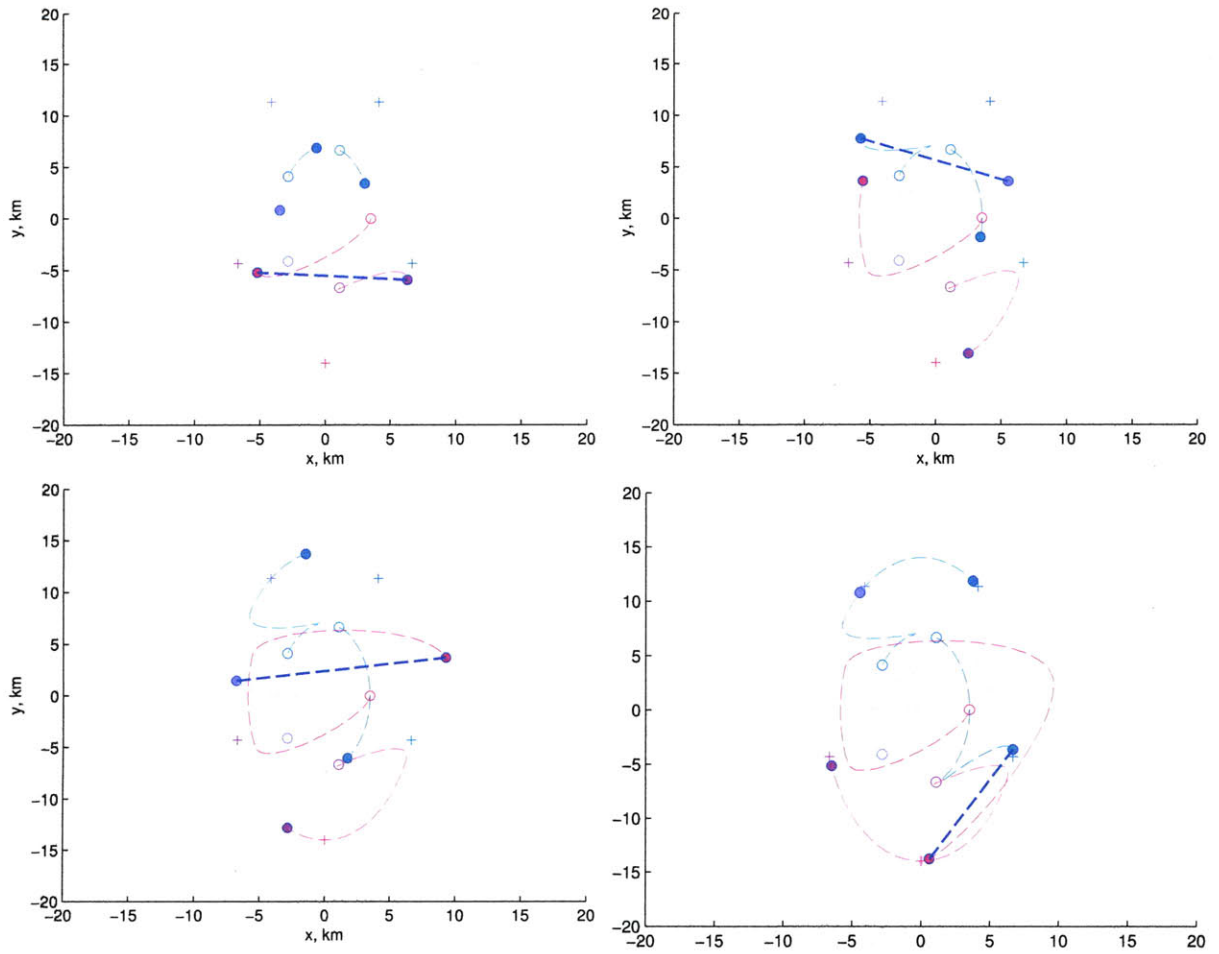


Figure 7-2: Optimal reconfiguration maneuver - Clohessy-Wiltshire dynamics only two vehicles actuate at the same time.

N_{spc}	$\text{card}(S)$	Optimal Sequence	Maneuver times	Total Time
5	3	$\{ (1, 3, 2) (4, 5, 2) \}$	41.8, 61.8	103.6
5	4	$\{ (2, 3, 5, 1) (1, 4, 0, 0) \}$	34.1, 41.2	75.3
5	5	$\{ (1, 2, 3, 4, 5) \}$	37	37

Table 7.3: Minimum maneuver time as the number of vehicles that can be moved at a time changes

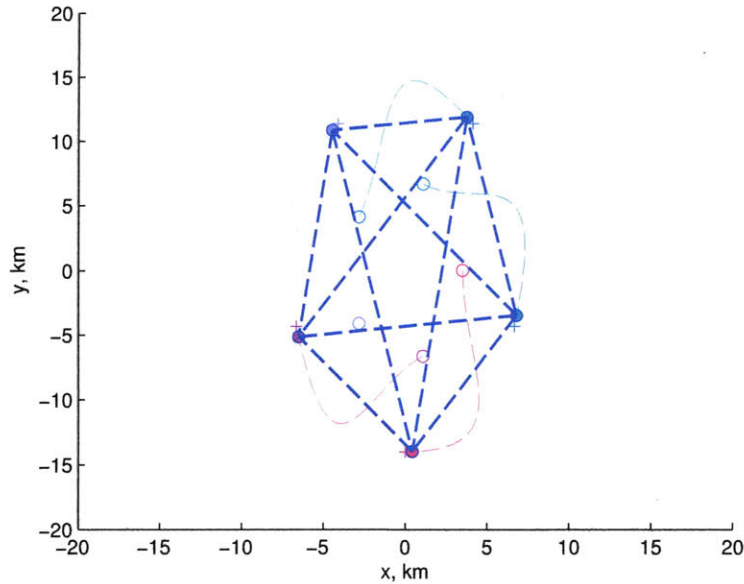


Figure 7-3: Optimal reconfiguration maneuver - Clohessy-Wiltshire dynamics only two vehicles actuate at the same time.

7.3 Decoupled Regulation by Resource Allocation

In this section we consider a method for decentralizing EMFF, based on the 'allocation' of the magnetic interaction. This allocation is performed in an analogous manner to a communication channel allocation. By allocating the interaction, the approach guarantees that the dynamics are coupled only among the set of vehicles that can coordinate their dipoles through local information sharing. Two possibilities are considered, a time based division and a frequency based division.

7.3.1 Schedule based regulator

A method to achieve time division consists in using a synchronization mechanism, based on synchronized clocks on each vehicle or by an external signal. Additionally, the spacecraft will require an external agreement or an intervehicle consensus mechanism to define the time schedule for each set of vehicles. The definition of this higher level time agreement mechanisms is not in the scope of this work. If the vehicles have access to a global signal

like the GPS signal, they will have a synchronization resource available.

The scheduling mechanism has to take into account the interconnection topology. A set of neighbors that are active have to be able to communicate during the actuation period. Once each vehicle has knowledge of the time schedule when it can actuate and the neighbors it is actuating with, the solution of the dipole equation needs to be found for those active vehicles. A reduced order set of dipole equations is to be solved for the members of the subset, in a distributed manner as discussed in a later section or by one of them and communicated to the rest of group.

Several results in the literature have addressed the effects of time varying topologies and can be used to address the stability of the mechanisms presented in this section [72, 79] for simple dynamic cases which could be extended to more complex dynamics. Specifically, the result for theory of consensus regarding convergence under switching information exchange topologies. Necessary conditions for convergence for consensus based control laws are presented in [79]. A main result is that the interconnection topology has to be connected over some time interval. Its extrapolation to more general dynamics is still a topic of research and some results for connected topologies have been described in more recent work [72].

In general, for fast enough switching rates, the results can be shown to approximate the constant interconnection case with a disturbance that depends on the length of the time intervals. It is important however, to consider in the design of the control protocol the fact that EMFF forces only produce internal forces, and thus, when applying the desired forces to only a subset of the full formation it is not guaranteed that the sum of the desired forces of the subset is zero. This situation is addressed in the protocol presented in the next section and a further theoretical analysis of the effects of the switching period is discussed in a section below.

7.3.1.1 Results

In this section we introduce a switching protocol to decouple the dynamics of the electromagnetic formation through time division. Simulations show the protocol implementability and performance. As mentioned in the introduction to the approach, the idea is based on periodic switching topologies, in a way that over a full cycle, every vehicle has been active at least for one period. Without loss of generality, in examples below, we explore the performance of an approach based on cyclic sequencing.

The cyclic sequencing can be described as follows: For a formation with vehicles $i \in N = \{1, 2, \dots, N\}$, the active set of vehicles at time interval t_k , $S(t_k) = \{s_1, s_2, \dots, s_{N_s}\}$, $s_n \in N, s_n = \text{mod}(s_n, N)$ is such that $S(t_{k+1}) = S(t_k) + n_o$, where $n_o < \text{card}(S) = N_s$ is an offset such that at each switching time $S(t_k) \cap S(t_k + 1) \neq \emptyset$.

A control period is the time interval t_c for which the force command is constant. A switching period $t_k = n_d t_c$ is the time interval between subset switching. A switching cycle, is a time interval over which the topology switching repeats itself, specifically, if the switching cycle is a uniform cyclic protocol $T_s = N t_k$.

Since at each switching period, the sum of the commanded forces for the subset of vehicles is not necessarily zero, at least one of the vehicles in the set will not be able to actuate the commanded force. The key development on the protocol presented in this section consists of considering one of the vehicles in the subset as a leader. The dipole configuration of the subset will be setup such that each vehicle in the group other than the leader will set up its commanded forces as per control law and the leader will have a known residual force which will be taken into account as the subset changes and the leader changes. If sum of forces over the whole formation maintains the constraint that the sum of all forces is zero, the residual force over a cycle through the graph should approximately cancel out.

The following synchronous control protocol with homogeneous switching intervals is proposed and implemented in simulation for different control laws:

Sequential Subsetwise Control Algorithm

1. Vehicles in set $S(t_k) = \{s_1, s_2, \dots, s_{N_s}\}$ share measurement information and calculate best estimate of current relative states.
2. Desired force for each vehicle in the set is calculated as per control law adding any residual force F_s from previous control periods.
3. The set solves for the dipole configuration, either in a locally centralized way or in a distributed way as described in Section 7.4. Leader of the set, vehicle s_1 , sets its force to:

$$F_r = - \sum_{i \in S(t_k)/s_1} F_i$$

such that

$$\sum_{i \in S(t_k)} F_i = 0$$

and stores F_r as its residual force. All other vehicles in the set have zero residual force.

4. If $t \geq t_{k+1}$ a new set of vehicles $S(t_{k+1})$ is activated.
 5. goto 1.
-

7.3.2 Frequency division

In a frequency divided resource allocation strategy, subsets of vehicles can act simultaneously applying currents shaped by orthogonal functions on each different subset. The forces due to magnetic fields from different subsets average to zero over a control period, thus effectively decoupling the actuation between different subsets. This approach is inspired by the approach presented by the work of Kaneda et al. [34], where the electromagnetic formation was decoupled from constant perturbations.

Consider for example the case of sinusoidal functions. The imparted Δv on each vehicle over a period of time is:

$$\Delta v_{2\pi} = (1/m) \int_0^{2\pi} |\mu_i| |\mu_j| \vec{q}(t) dt$$

where $\vec{q}(t)$ is a vector that depends on the position of the vehicles and the direction of the

dipoles.

If the dipole magnitudes on the vehicles are setup to be sinusoidal functions $\mu_i = \mu_{io} \sin(\omega_i t)$, with high enough frequency ω_i so that \vec{q} can be considered constant, consider vehicle i , interacting at the same time with vehicles j and k , $\omega_j = \omega_i$, $\omega_k = n\omega_i$, $n > 1$, $n \in \mathcal{Z}$:

$$\begin{aligned} \Delta v_{2\pi} &= (1/m) |\mu_{io}| |\mu_{jo}| |\vec{q}_{ij}| \int_0^{2\pi} \sin(\omega_i t) \sin(\omega_j t) dt + |\mu_{io}| |\mu_{ko}| |\vec{q}_{ik}| \int_0^{2\pi} \sin(\omega_i t) \sin(\omega_k t) dt \\ &= |\mu_{io}| |\mu_{jo}| |\vec{q}_{ij}| / 2m + 0, \text{ for } n \neq 1 \end{aligned}$$

Then, vehicle i and j actuate independently of the actuation of vehicle k with any other vehicles in the formation.

In general, consider the formation of vehicles $i \in N = \{1, 2, \dots, N\}$, consisting of subsets of vehicles S_i , shaping their control inputs over a period t_k by multiplication by a function $\phi_i(t)$ such that $\mu_i(t) = \mu_{io} \phi_i(t - t_k - T)$, for $t \in [t_k, t_k + 2T)$.

Make each ϕ_i , a function of a set of shaping functions $\{\phi_i(t), \phi_j(t), \dots, \phi_{N_f}(t)\}$ orthogonal over the interval $[-T, T]$, such that:

$$\int_{-T}^T \phi_i \phi_j dt = \delta_{ij} \quad (7.11)$$

Then, the impulse during a control period between a pair of vehicles with dipole $\mu_i = \mu_{io} \phi_i$, and $\mu_j = \mu_{jo} \phi_j$, under the assumption that the control period is small enough such that \vec{q} can be considered constant, will be given by:

$$\begin{aligned} \Delta v_{t_k} &= (1/m) \int_{t_k}^{t_k+2T} |\mu_{io}| |\mu_{jo}| |\vec{q}_{ij}| \phi_i \phi_j dt \\ &= (1/m) |\mu_{io}| |\mu_{jo}| |\vec{q}_{ij}| \delta_{ij} \end{aligned}$$

Then, vehicles sharing the same shaping frequency ϕ_i will interact between them, but not vehicles with shaping functions ϕ_j . Then, the size of the dipole equation reduces to the size of the subset S_i with dipole shaping ϕ_i , and the interactions with other vehicles can be

disregarded.

Interconnections between different subsets is achieved by 'shared' members, which coordinate their dipole configuration with different subsets and apply a superposition of dipoles, i.e the vectorial sum of its dipole corresponding for each subset. Corresponding orthogonal sets will cancel out and the 'shared' vehicle will create forces between different subsets.

As mentioned before, any set of orthogonal functions over a bounded set can be used as shaping functions. For example, Legendre polynomials are orthogonal over the set $[-1, 1]$ and any set of polynomials can be used to shape the currents over a period. An advantage of using a polynomial function is the lower frequency content of the first n^{th} base functions, however, the lack of periodicity implies that the final value of the current at one period does not match the initial value of the current (and slope) at the end of that period. There are however, orthogonal sets of functions that could be more fitted for an specific situation.

If the limitation of the system is given by the maximum current that can be achieved on a coil (equivalently a maximum dipole magnitude), other type of orthogonal functions can improve the performance. Consider the Walsh functions:

$$\begin{aligned}
 \mu_i(t) &= |\mu_i(t)|\hat{n}_i \operatorname{sgn}(\sin(\omega_i t)) \\
 \mu_j(t) &= |\mu_j(t)|\hat{n}_j \operatorname{sgn}(\sin(\omega_j t)) \\
 \Delta v &= (1/m)|\mu_{io}||\mu_{jo}|\vec{q}_{ij} \int_0^{2\pi} \operatorname{sgn}(\sin(\omega_i t))\operatorname{sgn}(\sin(\omega_j t))dt \\
 &= \begin{cases} (1/m)|\mu_{io}||\mu_{jo}|\vec{q}_{ij} & \text{if } \omega_j = \omega_i \\ 0 & \text{if } \omega_j = 2^n \omega_i, n \in \mathcal{Z} \end{cases}
 \end{aligned}$$

The plots in 7-4 show the basic principle behind the proposed approach.

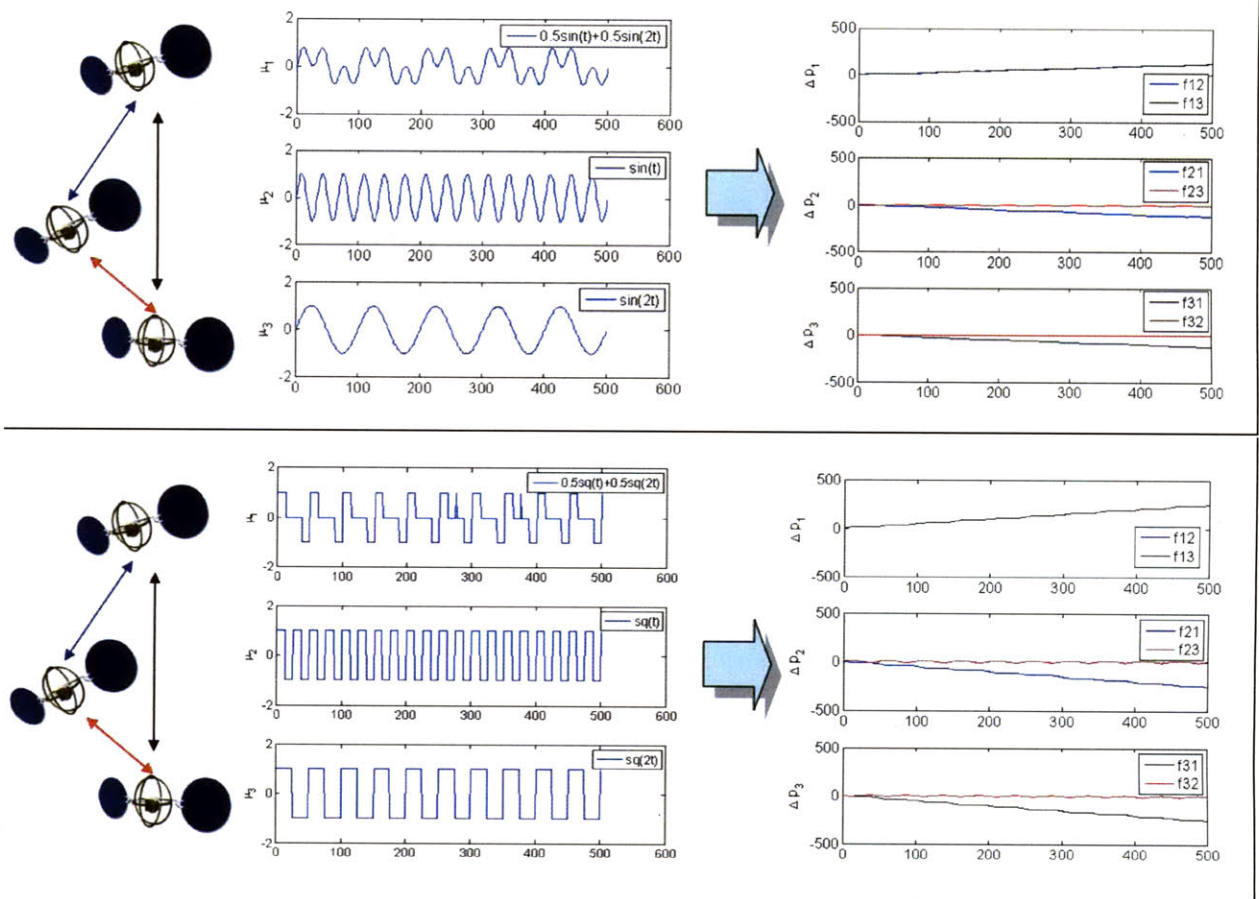


Figure 7-4: . Basic results showing the principle of operation of the implementation of decentralization by resource division

7.3.3 Resource allocation: Simulation results

Two benchmark case scenarios are considered to illustrate the performance using this approach. In one, a formation of vehicles achieving a rotating circular formation, where we study the performance as the a steady state response for a nonzero required output force, and two, a transient scenario where we study the convergence to formation from the same arbitrary initial perturbed state.

The simulations in a preliminary way the viability of this methods. In the case in fig. 7-5, the formation achieves a regular polygon from a random disturbed position and the control currents are shown for each case. The input magnitudes are shown as d^2/r^2I , which indicate the required currents to achieve the equivalent (far-field) forces normalized for a 1 meter formation with coils 1 meter in radius. Therefore, the currents in the results scale with the term r^2/d^2 where d is the radius of the coil and r is the distance between vehicles.

As it is to expect, as the number of active vehicles decreases the coil currents required to achieve the forces are larger. The coils are thus, saturated for a longer time. An appropriate selection of the control gains can assure in any case preventing saturation while making the most of the maximum currents of the system. The simulations are meant to show how the approach is valid despite the reduction in control authority.

In a second case we compare the currents, required to maintain a rotating formation under double integrator dynamics using the cyclic pursuit approach, as a way to integrate the results in previous chapter to the current approach. The results are shown in fig 7-6

On the other hand we illustrate the approach using the frequency division based approach in the results presented in figures 7-7, 7-8. The results illustrate how, the control objective can be achieved, at the expense of larger required currents. Since larger currents are required to achieve the same forces, the control authority of the actuation system is reduced.

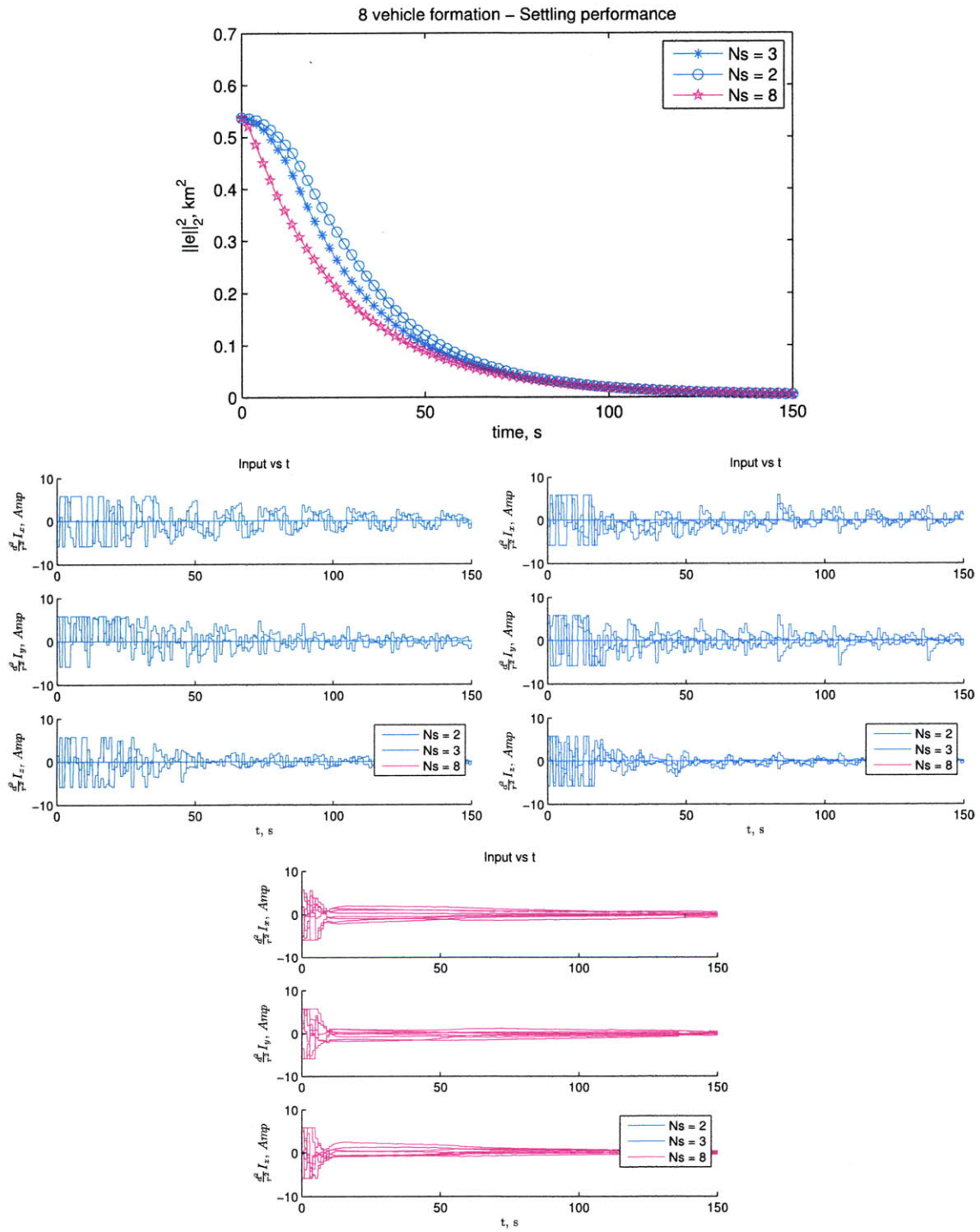


Figure 7-5: Time Division allocation - Disturbance rejection transient

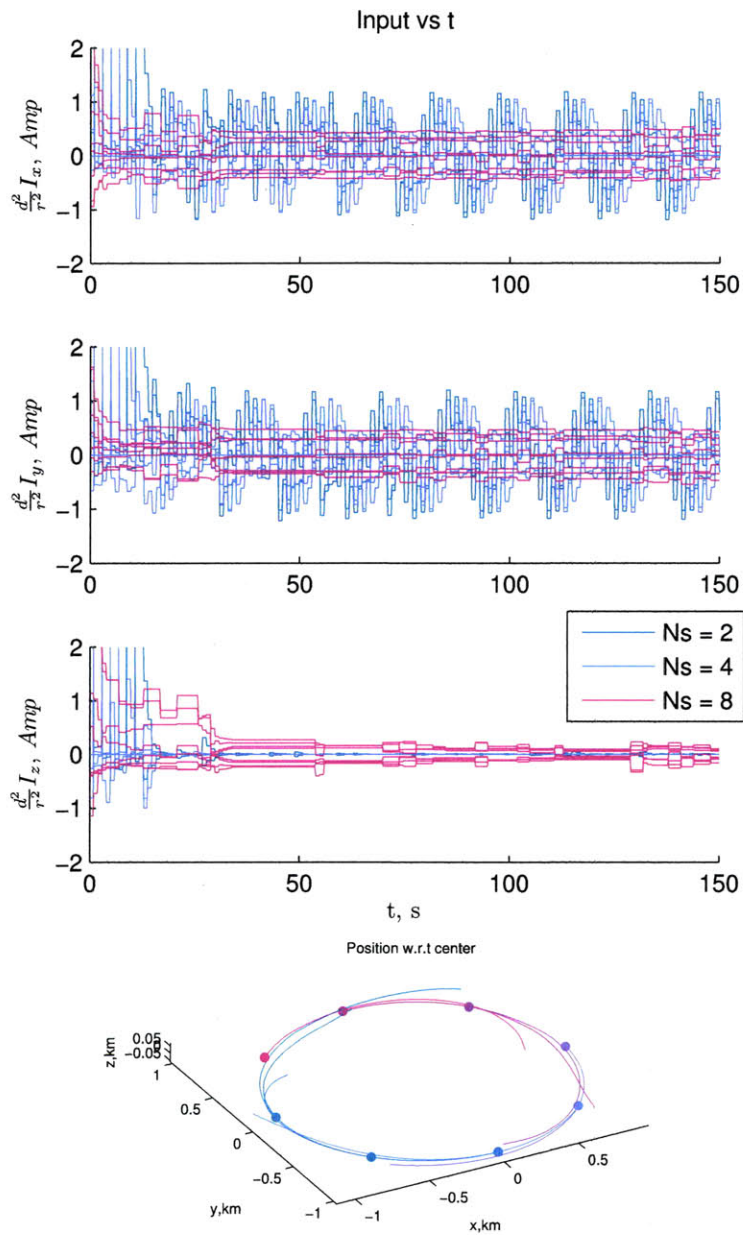


Figure 7-6: Currents in coils Time Division for different number of vehicles actuating at a time - Bottom: Steady State Cyclic Pursuit (2 active vehicles)

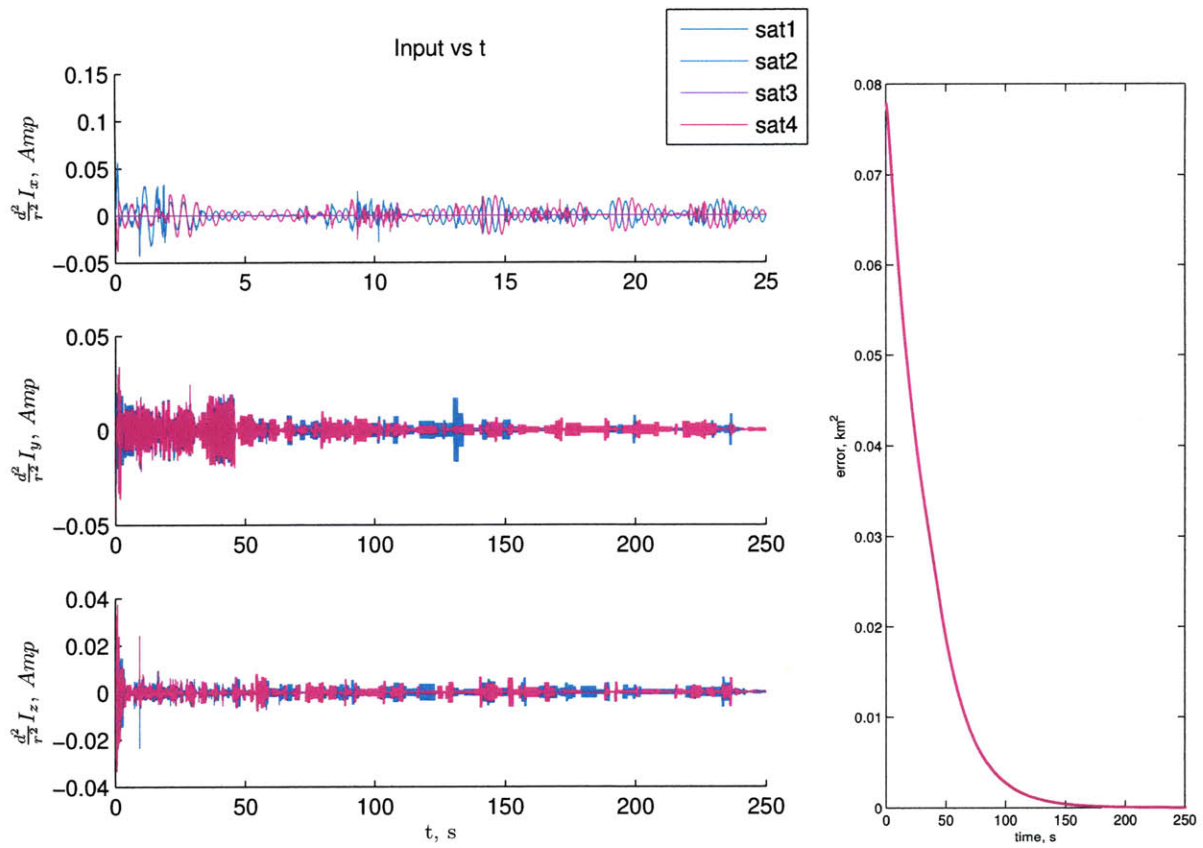


Figure 7-7: Frequency Division allocation - Disturbance rejection transient. The x -input is zoomed into the first 25 seconds

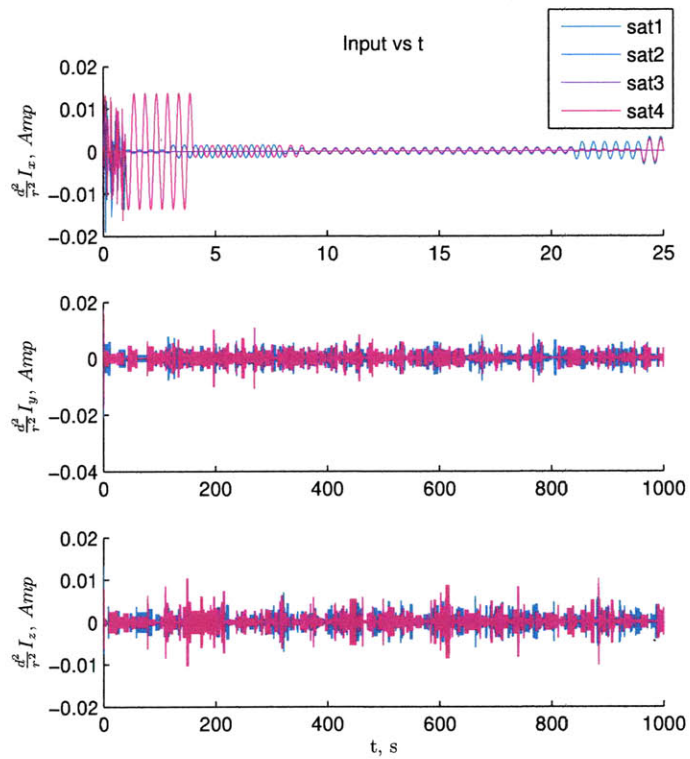


Figure 7-8: Frequency Division allocation - Steady State Cyclic Pursuit. The x -input is zoomed into the first 25 seconds

7.4 Distributed Computation of the Solution to the Dipole Equation

In this section we explore a different method to achieve decentralization of EMFF systems which addresses the objective by solving the dipole equation (eq. 7.2) in a distributed manner. In this sense, the method achieves the objective of defining the control commands μ , i.e. the dipoles on each vehicle, without recurring to a centralized computing unit and subsequent communication load to issue the commands to each vehicle in the formation as proposed in previous approaches [3].

In the proposed technique, the solution is obtained by sharing relative position knowledge and the solution of a local optimization problem. A first approach to applying this technique does not necessarily imply the desired characteristics of decentralization at its best, since it would still require an interconnected network to share states and local optimization solution results. However, other important characteristics of a decentralized system are achieved like deployment independence, robustness to individual failures, homogeneity and repeatability, and more importantly it does not require a powerful central unit solving the nonlinear dipole equation at each control step.

7.4.1 Theoretical description

The approach to a distributed solution, considers a distributed protocol for solving a global optimization objective that minimizes the overall formation error while locally solving an optimization problem. Consider the dipole equation 7.2 that defines the control commands to achieve the commanded forces:

$$\mathbf{F}_i = \sum_{j \neq i}^n F_{ij}$$

$$F_{ij} = \frac{-3\mu_o}{4\pi} \left(\frac{\mu_i \cdot \mu_j}{|d_{ij}|^5} d_{ij} + \frac{\mu_i \cdot d_{ij}}{|d_{ij}|^5} \mu_j + \frac{\mu_j \cdot d_{ij}}{|d_{ij}|^5} \mu_i - 5 \frac{(\mu_i \cdot d_{ij})(\mu_j \cdot d_{ij})}{|d_{ij}|^7} \right) d_{ij}$$

The electromagnetic force for a pair of vehicles i, j is a bilinear equation on the inputs μ_i, μ_j which can be written as:

$$F_{ij} = -\frac{1}{|d_{ij}|^5} \left[d_{ij} \cdot \mu_j^T + \mu_j \cdot d_{ij}^T + \left(I - 5 \frac{d_{ij} \cdot d_{ij}^T}{d_{ij}^T \cdot d_{ij}} \right) \mu_i \right] \quad (7.12)$$

and then, the overall system of equations can be written as:

$$\begin{bmatrix} F_1 \\ F_2 \\ \vdots \\ F_n \end{bmatrix} = \begin{bmatrix} M_1(\bar{\mu}_i) \\ M_2(\bar{\mu}_i) \\ \vdots \\ M_n(\bar{\mu}_i) \end{bmatrix} \mu_i + \begin{bmatrix} V_1(\bar{\mu}_i) \\ V_2(\bar{\mu}_i) \\ \vdots \\ V_n(\bar{\mu}_i) \end{bmatrix}$$

where:

$$M_i = \sum_{j \neq i} \frac{1}{|d_{ij}|^5} \left[d_{ij} \cdot \mu_j^T + \mu_j \cdot d_{ij}^T + \left(I + 5 \frac{d_{ij} \cdot d_{ij}^T}{d_{ij}^T \cdot d_{ij}} \right) \right]$$

$$M_{\bar{i}} = \frac{1}{|d_{ij}|^5} \left[d_{ij} \cdot \mu_j^T + \mu_j \cdot d_{ij}^T + \left(I + 5 \frac{d_{ij} \cdot d_{ij}^T}{d_{ij}^T \cdot d_{ij}} \right) \right]$$

$$V_i = \sum_{k \neq i, j} \frac{1}{|d_{ij}|^5} \left[d_{ij} \cdot \mu_j^T + d_{ij} \cdot \mu_j^T + \left(I + 5 \frac{d_{ij} \cdot d_{ij}^T}{d_{ij}^T \cdot d_{ij}} \right) \right] \cdot \mu_k$$

$$V_i = 0$$

where $\bar{i} = \{1, \dots, N\}/i$ is the set of vehicles in the formation except i , and $\mu_{\bar{i}}$, the set of corresponding dipoles.

For a given set $\mu_{\bar{i}}$, the dipole equation can be written as:

$$\mathbf{F} = \mathbf{M}(\mu_{\bar{i}}, \mathbf{x})\mu_i + \mathbf{V}(\mu_{\bar{i}}, \mathbf{x}) \quad (7.13)$$

where the term $\mathbf{M}(\mu_{\bar{i}}, \mathbf{x})\mu_i$ describe the forces caused on each vehicle by dipole i , and $\mathbf{V}(\mu_{\bar{i}}, \mathbf{x})$ the forces caused on each vehicle by vehicles other than i .

The proposed protocol makes use of this structure and considers solving the problem through a sequence of steps in which each vehicle minimizes a cost function by sharing the result of solving the local problem:

$$\mu_i^* = \arg \min_{\mu_i} \|\mathbf{F}_d(\mathbf{x}) - \mathbf{F}\|_2^2 \quad (7.14)$$

$$s.t. \quad \mathbf{M}(\mu_{\bar{i}}, \mathbf{x})\mu_i = (\mathbf{F} - \mathbf{V}(\mu_{\bar{i}}, \mathbf{x})) \quad (7.15)$$

$$h(\mu_i) < 0 \quad (7.16)$$

where $\mathbf{F}(\mathbf{x})$ is the control command known by each vehicle. Notice that to solve this problem, agent i requires \mathbf{x} , the state information of the formation (more specifically, only the *relative* states) and $\mu_{\bar{i}}$, the value of the dipole solution for the other vehicles in the formation. By an iterative process, where μ_i^* is shared through a connected network, the convergence to a stationary solution is guaranteed if $h(\mu_i)$ define a convex subspace. The analysis is presented in the next section.

7.4.2 Convergence analysis

Consider the following synchronous protocol following a periodic sequence $\{1, 2, \dots, N, 1, 2, \dots\}$:

The analysis of the convergence properties of this protocol are based on the fact that the overall algorithm can be casted as a gradient method with gradient related descent direction. Notice that the agent do not update their dipole values until the error in the actuated force

Distributed Control of EMFF via distributed solution of dipoles

-
0. Vehicle i receives information from the network: current state estimate \mathbf{x} and dipole values μ .
 1. Solves optimization problem 7.14,
 2. If $\|\mathbf{F}_d(\mathbf{x}) - F\| < \epsilon_{min}\|F_d\|$ or $dt > T_{max}$ set own dipole to $\mu = \mu_i^*$.
 3. Communicate state knowledge and updated dipole value to the network.
 4. Wait until next cycle.
-

Table 7.4: Sequential Distributed Dipole Solution

is less than a minimum value $\epsilon_{min}\|F_d\|$, or the maximum allocated time T_{max} to converge to a solution has been reached.

Consider a following general optimization problem:

$$\begin{aligned} \min_x f(x) \\ s.t. x \in X \end{aligned}$$

A descent method is defined such that $x^{k+1} = x^k + \alpha^k d^k$, where d^k and α are selected to eventually reach a minimum of the function $f(x)$

Consider the following definition in [11]

Definition 7.4.1 *A direction sequence $\{d^k\}$ is gradient related if for any subsequence $\{x^k\}_{k \in \mathcal{K}}$ that converges to a non-stationary point, the corresponding subsequence $\{d^k\}_{k \in \mathcal{K}}$ is bounded and satisfies:*

$$\limsup_{k \rightarrow \infty} \sup_{k \in \mathcal{K}} \nabla_x f(\mathbf{x})' d^k < 0$$

and

Definition 7.4.2 *A gradient method with minimization rule updates α^k is such that $x^k + \alpha^k d^k \leq x^k + \beta d^k$, $\beta \in \mathbb{R}$.*

Proposition 7.4.3 *Consider the global optimization problem:*

$$\min_{\mu} \|F_d - F(\mu)\| \quad (7.17)$$

For F_d constant, in the overall algorithm in protocol 7.4, μ is updated as a gradient method with minimization rule updates and with gradient related descent. When including constraints $h(\mathbf{x}) < 0$, the algorithm is a gradient feasible direction method with minimization rule and gradient related direction sequence.

Proof: The algorithm in protocol 7.4 can be shown to be an implementation of a gradient method with gradient related direction and α^k selected by minimization rule. The proof that a gradient descent method with feasible gradient related direction converges to a stationary point is presented in proposition 2.2.1 in [11].

The gradient of $f(\mathbf{x})$ is given by:

$$\nabla_x f(\mathbf{x}) = 2 \left((\mathbf{M}(\mu_{\bar{1}})\mu_1 + \mathbf{V}(\mu_{\bar{1}}) - \mathbf{F})'\mathbf{M}(\mu_{\bar{1}}) \quad (\mathbf{M}(\mu_{\bar{2}})\mu_2 + \mathbf{V}(\mu_{\bar{2}}) - \mathbf{F})'\mathbf{M}(\mu_{\bar{2}}) \quad \dots \right) \quad (7.18)$$

$d_i^k \in \mathbb{R}^{3N}$ is zero for $\{\bar{i}\}$, then:

$$\nabla_x f(\mathbf{x})'d_i^k = (\mathbf{M}(\mu_{\bar{1}})\mu_1 + \mathbf{V}(\mu_{\bar{1}}) - \mathbf{F})'\mathbf{M}(\mu_{\bar{1}})\mu_i^* \quad (7.19)$$

At every iteration step, if a minimum to the local problem is found, such that $\mu_i^* < \mu_i$, the global variable μ is updated such that $\mu^{k+1} = \mu + \alpha^k d^k$, with d^k is a vector with zeros in the components not corresponding to agent i . Otherwise, if a minimum $\mu_i^* < \mu_i$ is not found, μ is not updated and the iteration corresponds to another vehicle in S . Thus, not necessarily at each iteration of the protocol, there is an update.

If a minimum to the local problem the control variable μ is found, μ is updated as $\mu_i = \mu_i^*$ otherwise it is not updated. Then, the update sequence is updated at least once every cycle. As the protocol progresses over S , μ is updated as $\mu = \mu$. ■

Proposition 7.4.4 *If a stationary value has not been reached, at least 1 update occurs over a cycle over S .*

Proof: Assume that a stationary value has not been reached, and no update occurred over a cycle, in the next cycle, all the values of μ_i are the same, which means there will not be further updates, and a stationary point has been reached. ■

A straightforward observation from the above proposition is a lower bound in the convergence of the algorithm.

Corollary 7.4.5 *The convergence rate over iterations for the distributed protocol 7.4 is lower bounded by $\frac{1}{N}r$, where r is the convergence rate of a gradient based with minimization rule and gradient related direction sequence for the global problem.*

Consider for example, that the set $h(\mu_i)$ is given by the constraints in the maximum current that can be run through the coils, then the set C is a convex set.

7.4.3 Closed loop convergence

The relationship between state update, dipole update and distributed optimization step rate in protocol 7.4, are parameters that affect the behavior of the system.

When the information sharing rate is fast enough compared to the dynamics of the overall system, the convergence problem can be approximated to the static case where the desired force $F_d(\mathbf{x})$ is basically constant while the algorithm converges. However, as the data sharing rate is reduced to the point that it is comparable to the dynamics time constant, a more complex dynamic situation has to be addressed. In this case the overall objective to be addressed is the stability of the formation error under the dynamics:

$$\begin{aligned} \mathbf{x}^+ &= f(\mathbf{x}, F_d + d) \\ d &= \min_{\mu_i} (F(\boldsymbol{\mu}, \mathbf{x}) - F_d(\tilde{\mathbf{x}})) \\ s.t. & h(\boldsymbol{\mu}) < 0 \end{aligned}$$

Initial simulations show that including this algorithm in a control loop can work to achieve stable control to a fixed point or to follow trajectories, but the theory has to be further researched to understand under which conditions this approach would work and its usefulness compared to a centralized approach. Figure 7-9 shows the results of a simulation where the forces are calculated to follow circular trajectories using a PD controller and the forces are setup by the distributed calculation of the dipoles as suggested in this section. The vehicles follow a circular trajectory setting up the dipoles in a distributed manner. The bottom plot shows the dipole for one of the vehicles

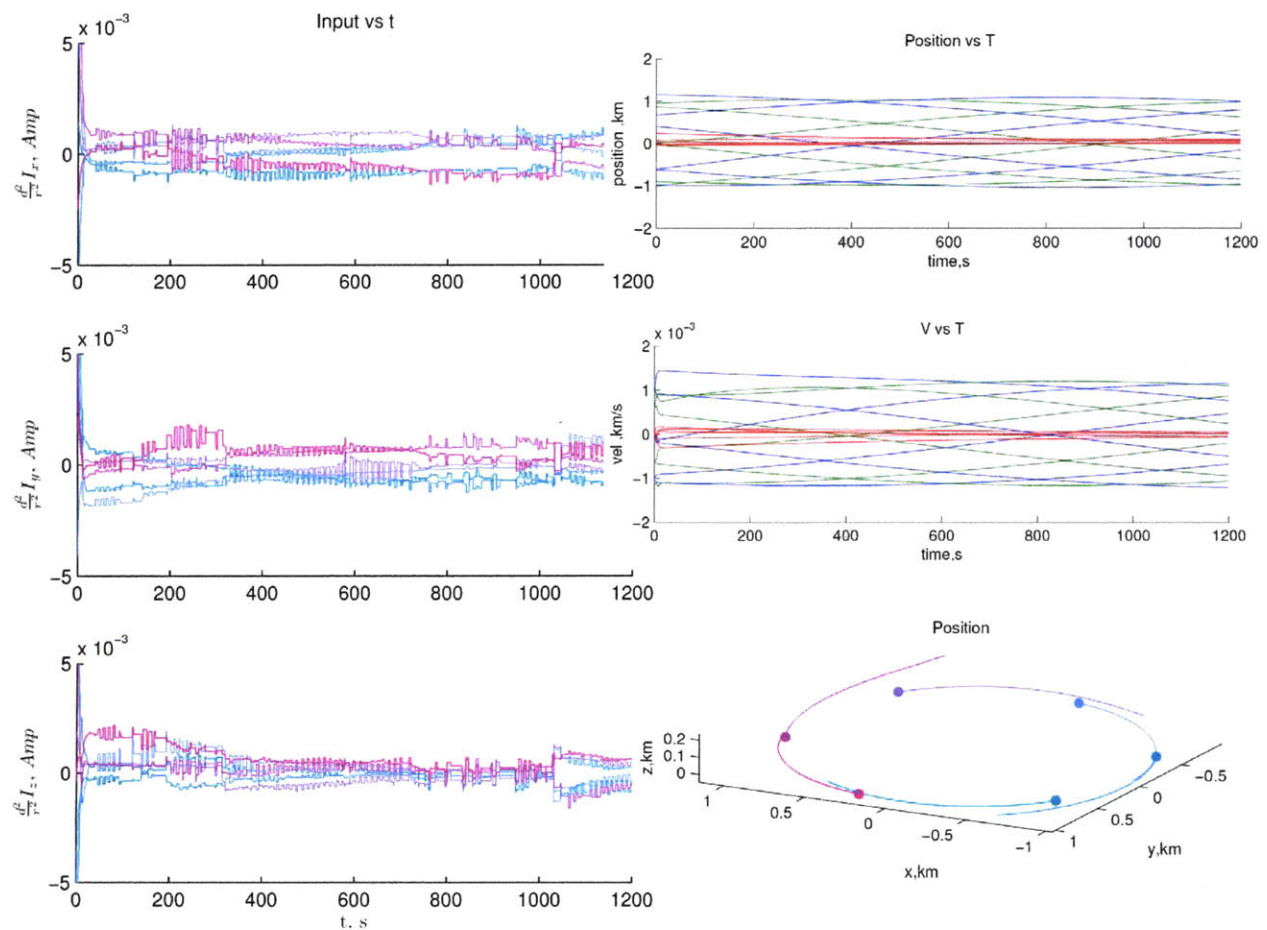


Figure 7-9: Figure showing a group of vehicles following a circular trajectory setting up the dipoles in a distributed manner.

7.5 Summary and Conclusion of the Chapter

Control algorithms that require a centralized solution of the dipole equation could be unfeasible due to limitations in the computation power or communication capabilities. The methods discussed in this section present an alternative, which can be of major importance in the implementation of formations with large number of electromagnetic propelled vehicles by allowing the implementation of control algorithms that do not require a central coordinating unit calculating, allocating and communicating the formation control commands.

It is important however, to consider the limitations and practical considerations when implementing the proposed mechanisms. In the case of time divided control, one of the assumptions is that the control cycles have to be fast enough to reduce the effects of the time divided actuation. This could imply requirements for the control frequency to be higher than what it would be for a centralized calculation and thus increasing the number of computations per second and reducing one of the advantages of decentralization. However, it is to be noticed that the solution of the dipole equation is a nonlinear optimization problem with exponentially increasing complexity as the number of dipoles increases. The increase in the number of cycles per second to achieve the time divided control approach increase required to achieve similar performance is sublinear. Additionally, there is a limit in the number of operations per cycle that can be achieved by a computing unit, and the power requirements and cost of computation translated also escalates exponentially.

The advantage of the token time divided maneuvering as presented in this chapter is that it derives feasible optimal reconfiguration maneuvers for a problem with a constraint in the number of active vehicles, however the implementation may require another propulsion system that maintains control of the unactuated vehicles, a sequential maneuvering that achieves the final objective in stages and reduce the inactivity period for the vehicles

For the frequency division, the maximum number of different orthogonal sets is driven by the properties of the mechanism to generate the shaping functions, specifically, the frequency

content of the shaping function and the accuracy within which the clocks on each vehicle can be synchronized.

The frequency division control approach could be combined with the time division approach in a hybrid mechanism mentioned in the previous section to achieve even better performance. In such a case, up to N_f sets of vehicles could be active at the same time without interfering with each other, where N_f is the number of available shaping orthogonal functions.

The distributed solution to the dipole equation presents also a valid alternative that can reduce the computational burden and scale down the computational requirements of EMFF formations with a large number of vehicles. This solution however requires continuous communication to distribute the information regarding the dipole configuration of all the vehicles in the formation.

Chapter 8

Conclusions and Final Remarks

8.1 Thesis Summary and Conclusions

A new approach to formation flight control has been proposed in this thesis. In this approach the formation globally converges to patterns defined by constraints of the desired state and not to (time varying) trajectory fixed points. Additionally, the innovative methods introduced to analyze distributed control laws opened up a new avenue for research to address more efficient and stable controllers.

In a first part, the cyclic pursuit approach that had previously been studied in the literature as an algorithm to achieve circles and log-spiral patterns was extended by deriving a full linear eigendecomposition analysis of the three-dimensional case. The eigendecomposition analysis lead to the derivation of control approaches more relevant to the dynamics of spacecraft formations. Extensions addressing robustness and convergence to other type of trajectories were developed to address controllers useful for near-earth and deep space formation flight missions.

The initially introduced formation acquisition approach was then extended by considering it as a manifold convergence problem and using the tools of contraction theory to perform an analysis of its performance. The analysis in the context of the partial contraction the-

ory leads to a more general understanding of the problem and allows the generalization to achieve results for nonlinear and time varying systems otherwise unachievable by the eigendecomposition method.

The contraction theory approach to the analysis of distributed controllers opened new avenues for research. First, it demonstrates an approach that determines global stability in terms of the negative definiteness of a matrix, which for the case of distributed controllers might seem a more convenient approach than Lyapunov methods where the stability is defined by demonstrating the negativeness of a function. The general notion of convergence is reshaped to the more general notion of manifolds (or subspaces) which defines a new dimension to the widely studied consensus problem.

The experimental results in a relevant testbed under microgravity conditions demonstrated that the implementation is feasible in the context of spacecraft formation control. Specifically, the successful results are partially attributed to the decentralized nature of the approach since the achievement of the desired global behavior emerges from appropriately verifying the local behavior of the vehicles.

8.2 Contributions

The main contributions of this thesis are:

1. Developed a new approach to decentralized spacecraft formation control inspired by the cyclic pursuit algorithm. It can be more efficient in terms of control effort by not tracking trajectories but by converging to a specified manifold. The approach achieves improved properties with respect to the most common approaches, namely:
 - Reduced control effort by not tracking irrelevant degrees of freedom.
 - Reduced need for coordination, i.e does not need to agree on relative trajectories.
 - Leader(s) can control free degrees freedom of the overall formation.

2. Addressed the robustness issues of classic cyclic pursuit by introducing a nonlinear extension to the control law that achieves equilibrium at a splay-state formation of determined radius and a corresponding theoretical stability result.
3. Devised a transformation scheme that allows for the design of distributed controllers that converge to very general types of synchronized trajectories.
4. Developed decentralized control laws based on the cyclic pursuit approach for LEO formation flight that globally converge to near natural relative trajectories. Theoretical results include a full eigendecomposition of the dynamics showing the global convergence as well as simulation results showing its implementation accounting for J_2 effects.
5. Formulated decentralized control laws for second order systems that require only relative information to converge to different geometric patterns and can be of importance for formation flight in deep space missions without an accurate global reference frame. The patterns of convergence include circular formations, ellipse, logarithmic, archimedean spirals and polygons.
6. Introduced an analytic approach based on contraction theory that allows for a wide range of global convergence results for nonlinear controllers and complex configurations based on combinations of cyclic algorithms. The wide extent of the approach is exemplified by obtaining several important results:
 - (a) Proofs of global convergence to regular formations based general on cyclic interconnections.
 - (b) Global convergence results for distributed controllers that converge to regular formations of specified size.
 - (c) Extensions of the contraction theory theorems to allow for proofs of convergence to time varying manifolds.

- (d) Corollaries that allow for proofs of global convergence to formations based on any number of interconnected subformations.
 - (e) Proof of convergence to formations of specified size through a leader.
 - (f) Derivation of sufficient conditions for global convergence to surrounding a target using a cyclic control approach under general tracking functions.
7. Implemented hardware tests and obtained experimental results that validate the characteristics of the approach, namely: no need of central coordination, extensible to any number of vehicles, reduced control effort and simplicity of implementation for several formation flight scenarios.

8.2.1 Secondary contributions

Additionally, the thesis added to the field along with other contributions that include:

1. An investigation that compares different formation control architectures to a decentralized control approach where the control is not based on tracking relative trajectories.
2. A preliminary study of the solution to EMFF reconfiguration maneuvers with a reduced interconnection complexity by solving for the optimal maneuvers that only use a subset of vehicles at a time.
3. The development and a preliminary comparison of several methods to achieve decentralized control of EMFF by decoupling the dynamics.
4. A protocol to decentralizing EMFF by distributing the solution of the dipole equation.

8.3 Future Work

There are several points that can be addressed as a continuation of this work and new avenues for future research that were opened by the developments of this thesis.

As a first direction, having demonstrated that the convergence to geometric patterns is achievable under more general cyclic interconnections, a new direction should consider the design of more robust control approaches that can use informations of neighbors interchangeably, reducing the constraint of a cyclic interconnection. At first glance this seems like a straightforward extension but it may require developing some machinery to achieve formal proofs that verify the convergence properties.

In this work, the attitude control was left out of the scope other than a basic development for the experimental setup. It can be convenient however to define controllers that combine measurements in the local body reference frame of the spacecraft which could achieve a more precise control performance in cases where measurements are dependent on the relative orientation of sensor and target.

In Section 3.4, it was shown how a 'similarity' mapping scheme can be used to achieve convergence to complex trajectories. Converging to elliptical trajectories was shown to be useful for a specific application, namely closed natural relative trajectories for near circular orbits. However, closed natural relative trajectories for orbits with increasing eccentricity are different from ellipses. A parallel approach, using nonlinear similarity transformations can be useful for converging to such relative trajectories. Additionally, applications in other fields can deem useful applications for convergence to formations with very specific geometric patterns.

A whole new avenue of research has been opened by demonstrating the use of the contraction theory approach to the analysis of distributed controllers. Several considerations that could be addressed are including the effects of saturation, the convergence properties when collision avoidance mechanisms are added, the effects of delays and random varying graphs, etc. Further research would consider linear or affine transformation for convergence to not only regular formations, and the use of the convergence primitive tools to define more complex convergence states.

Reshaping the general notion of convergence to the more general sense of manifolds (or

subspaces) defines a new dimension to the widely studied consensus problem. There might exist applications in many other fields where the distributed system objective can be achieved without convergence to the 'common agreement' subspace (namely \mathcal{M} is spanned by $\mathbf{1}$) but by converging to some more general 'coordination subspace' defined as $h(\mathbf{x}) = 0$.

A dual of the control problem is of course, the estimation problem. The application of the cyclic approach for convergence to a subspace, can be defined in the context of distributed sensors that are required to converge to a coordinated estimate, defined by a linear transformation of the overall state.

Chapter 7 presented a preliminary study of options that can be applied to decentralize the control of electromagnetic formation flight systems. Simulations show the feasibility of the approaches. A deeper and more complete approach to theoretical convergence results and control design are possibilities for future work.

In the case of time divided resource allocation, the design of the controller is a next step to be addressed which should take into account the intrinsic disturbance due to the non-complete nature of the approach (i.e. the desired force cannot be applied instantly but only as an 'average' over a cycle) . The effects in performance defines a clear direction for future developments.

Experimentation of the time based and frequency based allocation could be feasible on the HTS EMFF testbed. Resonant frequencies that take advantage of the design of the coils could also be considered as future developments.

Finally, hybrid methods that use time based, frequency based and distributed solution of the dipole equation can have important advantages. A higher level analysis that can identify the most advantageous architectures for decentralized EMFF could also be addressed, as well as identifying missions that would truly benefit from this developments.

Appendix A

Mathematical derivation of proofs

A.1 \mathcal{CR} Matrices

All matrices in the \mathcal{CR} have the same set of linearly independent eigenvectors, and are diagonalizable by the matrix T of eigenvectors $\nu_{L \otimes R, ij}$.

Proof: The eigenvectors of $L \otimes R$ are such that

$$\nu_{L \otimes R, ij} = \nu_{L_i} \otimes \nu_{R_j} \tag{A.1}$$

The eigenvectors of L are the same for all circulant matrices L which following Section 2.1.5 are shown to be independent. Equivalently, the eigenvectors of R are the same for all rotation matrix R that share an axis of rotation and following Section 2.1.4 are shown to be linearly independent. Then, the set of eigenvectors for all matrices \mathcal{CR} which are described as $L \otimes R$ is linearly independent. The Kronecker composition of this two sets of linearly independent vectors:

$$\begin{aligned} \mu_k &\doteq \psi_k \otimes (0, 0, 1)^T = (0, 0, 1, 0, 0, \chi_k, \dots, 0, 0, \chi_k^{n-1})^T, \\ \mu_k^+ &\doteq \psi_k \otimes (1, j, 0)^T = (1, j, 0, \chi_k, j \chi_k, 0, \dots, \chi_k^{n-1}, j \chi_k^{n-1}, 0)^T, \\ \mu_k^- &\doteq \psi_k \otimes (1, -j, 0)^T = (1, -j, 0, \chi_k, -j \chi_k, 0, \dots, \chi_k^{n-1}, -j \chi_k^{n-1}, 0)^T, \end{aligned} \tag{A.2}$$

where $k \in \{1, \dots, n\}$ and $\psi_k = \left(1, \chi_k, \chi_k^2, \dots, \chi_k^{n-1}\right)^T$, where $\chi_k = e^{2\pi jk/n}$, $k \in \{0, \dots, n-1\}$ are the eigenvectors of L (omitting the constant $1/\sqrt{n}$). The composed set of eigenvectors, can then be verified to be a set of linearly independent eigenvectors and since L is diagonalizable, R is diagonalizable, then all \mathcal{CR} matrices are diagonalizable by a matrix T of eigenvectors $\nu_{L \otimes R}$, (See Thm. 13.12 in [41]) namely, the diagonal matrix:

$$(P^{-1}LP) \otimes (Q^{-1}RQ) = (P^{-1} \otimes Q^{-1})(L \otimes R)(P \otimes Q) \quad (\text{A.3})$$

$$= (P \otimes Q)^{-1}(L \otimes R)(P \otimes Q) \quad (\text{A.4})$$

where P is a matrix of eigenvectors of L and Q is a matrix of eigenvectors of R . ■

Therefore, if $A, B \in \mathcal{CR}$

$$\begin{aligned} \text{eig}(A + B) &= \text{eig}(T\Lambda_A T^{-1} + T\Lambda_B T^{-1}) \\ &= \text{eig}(T(\Lambda_A + \Lambda_B)T^{-1}) \end{aligned} \quad (\text{A.5})$$

where Λ_A is a diagonal matrix the eigenvalues of A $\lambda_{A,i}$ in the diagonal (and correspondingly the same holds for B). Therefore $\lambda_{A+B,i} = \lambda_{A,i} + \lambda_{B,i}$.

We also have then that:

$$\begin{aligned} AB &= \text{eig}(T\Lambda_A T^{-1} T\Lambda_B T^{-1}) \\ &= \text{eig}(T(\Lambda_A \Lambda_B)T^{-1}) \\ &= \text{eig}(T(\Lambda_B \Lambda_A)T^{-1}) \\ &= BA \end{aligned} \quad (\text{A.6})$$

A.2 System (3.10) in Polar Coordinates

Assume that $\|\mathbf{p}_i\| = \varrho_i > 0$. Note that $\mathbf{p}_i = \varrho_i R(-\vartheta_i) e_1$, where e_1 is the first vector of the canonical basis, i.e., $e_1 = (1, 0)^T$. Then, we can write \mathbf{p}_{i+1} as

$$\mathbf{p}_{i+1} = \frac{\varrho_{i+1}}{\varrho_i} \varrho_i R(-\vartheta_{i+1}) e_1 = \frac{\varrho_{i+1}}{\varrho_i} \varrho_i R(-\vartheta_{i+1}) R(\vartheta_i) R(-\vartheta_i) e_1 = \frac{\varrho_{i+1}}{\varrho_i} R(\vartheta_i - \vartheta_{i+1}) \mathbf{p}_i. \quad (\text{A.7})$$

Moreover, it also holds

$$\mathbf{p}_i^T R(\gamma) \mathbf{p}_i = \|\mathbf{p}_i\|^2 \cos(\gamma) = \varrho_i^2 \cos(\gamma), \quad \text{for any } \gamma \in \mathbb{R}. \quad (\text{A.8})$$

First, we find the differential evolution for the magnitude of \mathbf{p}_i , i.e., for ϱ_i . We have

$$\dot{\varrho}_i = \frac{d\|\mathbf{p}_i\|}{dt} = \frac{\mathbf{p}_i^T \dot{\mathbf{p}}_i}{\|\mathbf{p}_i\|} = \frac{1}{\varrho_i} \mathbf{p}_i^T (R(\alpha_{i+1}) \mathbf{p}_{i+1} - R(\alpha_i) \mathbf{p}_i). \quad (\text{A.9})$$

By using Eqs. (A.7) and (A.8) we then obtain

$$\dot{\varrho}_i = \frac{1}{\varrho_i} \mathbf{p}_i^T \left(R(\alpha_{i+1}) \frac{\varrho_{i+1}}{\varrho_i} R(\vartheta_i - \vartheta_{i+1}) \mathbf{p}_i - R(\alpha_i) \mathbf{p}_i \right) = \varrho_i \cos((\vartheta_{i+1} - \vartheta_i) - \alpha_{i+1}) - \varrho_i \cos(\alpha_i) \quad (\text{A.10})$$

We now find the differential evolution for the phase of \mathbf{p}_i , i.e., for ϑ_i . Taking time derivative in both hands of the identity $p_{i,1} \sin \vartheta_i - p_{i,2} \cos \vartheta_i = 0$, we easily obtain

$$\dot{\vartheta}_i = \frac{p_{i,1} \dot{p}_{i,2} - p_{i,2} \dot{p}_{i,1}}{\varrho_i^2} = \frac{1}{\varrho_i^2} \mathbf{p}_i^T R\left(\frac{\pi}{2}\right) \dot{\mathbf{p}}_i = \frac{1}{\varrho_i^2} \mathbf{p}_i^T R\left(\frac{\pi}{2}\right) \left(R(\alpha_{i+1}) \mathbf{p}_{i+1} - R(\alpha_i) \mathbf{p}_i \right). \quad (\text{A.11})$$

Then, by using Eqs. (A.7) and (A.8) we obtain

$$\dot{\vartheta}_i = \frac{1}{\varrho_i^2} \mathbf{p}_i^T R\left(\frac{\pi}{2}\right) \left(R(\alpha_{i+1}) \frac{\varrho_{i+1}}{\varrho_i} R(\vartheta_i - \vartheta_{i+1}) \mathbf{p}_i - R(\alpha_i) \mathbf{p}_i \right) = \frac{\varrho_{i+1}}{\varrho_i} \sin((\vartheta_{i+1} - \vartheta_i) - \alpha_{i+1}) + \sin(\alpha_i). \quad (\text{A.12})$$

A.3 Proof of Lemma 3.2.8

Proof: The eigenvalues of P are solutions to the characteristic equation

$$0 = \det \left(\begin{bmatrix} \lambda I_n - a_n L_1 + 2k_\alpha s_n I_n & s_n I_n \\ -b_n L_1^2 & \lambda I_n - c_n L_1 \end{bmatrix} \right). \quad (\text{A.13})$$

Note that both matrix $(\lambda I_n - a_n L + 2k_\alpha s_n I_n)$ and matrix $-b_n L^2$ are circulant; then, since circulant matrices form a commutative algebra (see Section 2.1), we can apply the result in equation (2.1) and obtain

$$0 = \det \left((\lambda I_n - a_n L + 2k_\alpha s_n I_n)(\lambda I_n - c_n L) + s_n b_n L^2 \right) \quad (\text{A.14})$$

$$= \det \left(\lambda^2 I_n + \lambda \underbrace{(2k_\alpha s_n I_n - (a_n + c_n)L)}_{\doteq B} \underbrace{(-2k_\alpha s_n c_n L + (a_n c_n + s_n b_n)L^2)}_{\doteq C} \right) \quad (\text{A.15})$$

$$= \det \left(\lambda^2 I_n + \lambda B + C \right) \quad (\text{A.16})$$

$$= \det \left(\lambda^2 I_n + \lambda B + B^2/4 - S \right), \quad (\text{A.17})$$

where $S \doteq B^2/4 - C$. Note that B and C are circulant, therefore S is also circulant. Since S is circulant, it can be diagonalized according to $S = U D_S U^*$, where D_S is a diagonal matrix with the eigenvalues of S on the diagonal; accordingly, we have $S^{1/2} = U D_S^{1/2} U^*$. Note that B and $S^{1/2}$ commute. In fact, since B is circulant, it can be diagonalized via the same orthogonal matrix U : $B = U D_B U^*$, where D_B is a diagonal matrix with the eigenvalues of B on the diagonal; hence

$$S^{1/2} B = U D_S^{1/2} U^* U D_B U^* = U D_S^{1/2} D_B U^* = U D_B D_S^{1/2} U^* = U D_B U^* U D_S^{1/2} U^* = B S^{1/2}.$$

Therefore, we have

$$0 = \det \left(\lambda^2 I_{n \times n} + \lambda B + B^2/4 - S \right) = \det \left(\lambda I_n - (-B/2 + \sqrt{S}) \right) \det \left(\lambda I_{n \times n} - (-B/2 - \sqrt{S}) \right).$$

Hence, the eigenvalues of P are the union of the eigenvalues of $(-B/2 + \sqrt{S})$ and $(-B/2 - \sqrt{S})$. Since B and $S^{1/2}$ are diagonalized by the same similarity transformation U , we have

$$-\frac{B}{2} \pm S^{1/2} = U \frac{D_B}{2} U^* \pm U D_S^{1/2} U^* = U \left(\frac{D_B}{2} \pm D_S^{1/2} \right) U^*. \quad (\text{A.18})$$

Let $\lambda_{B,k}$ be the k th eigenvalue of B , and $\lambda_{S,k}$ be the k th eigenvalue of S , $k \in \{1, \dots, n\}$. Then, from equation (A.18), we have that

$$\text{eig}(P) = \left\{ \lambda_{B,k}/2 \pm \lambda_{S,k}^{1/2} \right\}_{k=1}^n. \quad (\text{A.19})$$

Hence, we are left with the task of computing the eigenvalues of B and S . Such eigenvalues can be easily found by using equation (2.4):

$$\text{eig}(B) = \left\{ 2k_\alpha s_n + (a_n + c_n)(1 - e^{2\pi jk/n}) \right\}_{k=1}^n, \quad (\text{A.20})$$

$$\begin{aligned} \text{eig}(S) &= \left\{ (\lambda_{B,k}^2/4 - \lambda_{C,k}) \right\}_{k=1}^n = \left\{ (2k_\alpha s_n + (a_n + c_n)(1 - e^{2\pi jk/n})^2/4 \right. \\ &\quad - \left. \left((2k_\alpha s_n c_n + a_n c_n + s_n b_n) - (2k_\alpha s_n c_n + 2a_n c_n + 2s_n b_n) e^{2\pi jk/n} \right. \right. \\ &\quad \left. \left. + (a_n c_n + b_n s_n) e^{4\pi jk/n} \right) \right\}_{k=1}^n. \end{aligned} \quad (\text{A.21})$$

We first consider the eigenvalues of B . By using the following identities

$$(1 - e^{\alpha_k j}) = 2 \sin(\alpha_k/2) e^{j \frac{\alpha_k - \pi}{2}}, \quad (1 - \frac{1}{2}(1 - e^{j\alpha_k})) = \cos(\alpha_k/2) e^{j\alpha_k/2}, \quad (\text{A.22})$$

and after some algebraic manipulations omitted for brevity, the eigenvalues of B can be written as

$$\lambda_{B,k} = (2k_\alpha s_n) + 2(2c_n - k_\alpha s_n) \sin(k\pi/n) e^{j(k\pi/n - \frac{\pi}{2})}, \quad k \in \{1, \dots, n\}. \quad (\text{A.23})$$

Hence, we have, for $k \in \{1, \dots, n\}$,

$$\operatorname{Re}(\lambda_{B,k}) = 2k_\alpha s_n + 2(2c_n - k_\alpha s_n) \sin^2(k\pi/n), \quad (\text{A.24})$$

$$\operatorname{Im}(\lambda_{B,k}) = -2(2c_n - k_\alpha s_n) \sin(k\pi/n) \cos(k\pi/n). \quad (\text{A.25})$$

Next, we consider the eigenvalues of S . By using, again, the identities in equation (A.22), and with simple algebraic manipulations, we can write, for $k \in \{1, \dots, n\}$,

$$\begin{aligned} \lambda_{S,k} &= k_\alpha^2 s_n^2 (\cos(k\pi/n) e^{jk\pi/n})^2 + (k_\alpha s_n c_n + s_n^2) (2 \sin(k\pi/n) e^{j(k\pi/n - \frac{\pi}{2})})^2 \\ &= [k_\alpha^2 s_n^2 + 4 \sin^2(k\pi/n) + (4k_\alpha s_n c_n - k_\alpha^2 s_n^2 - 4c_n^2) \sin^2(k\pi/n)] e^{i2k\pi/n}. \end{aligned}$$

Notice that k_α , c_n and s_n are positive real numbers; then the term inside the square brackets is a positive real number. Therefore we have, for $k \in \{1, \dots, n\}$,

$$\operatorname{Re}(\sqrt{\lambda_{S,k}}) = (k_\alpha^2 s_n^2 + 4 \sin^2(k\pi/n) + (4k_\alpha s_n c_n - k_\alpha^2 s_n^2 - 4c_n^2) \sin^2(k\pi/n))^{1/2} \cos(k\pi/n),$$

which can be rearranged as

$$\begin{aligned} \operatorname{Re}(\sqrt{\lambda_{S,k}}) &= ((k_\alpha s_n + (2c_n - k_\alpha s_n) \sin^2(k\pi/n))^2 + 4 \sin^2(k\pi/n) (s_n^2 - \sin^2(k\pi/n)))^{1/2} \\ &= ((\lambda_{B,1}/2)^2 + 4 \sin^2(k\pi/n) (s_n^2 - \sin^2(k\pi/n)))^{1/2}. \end{aligned} \quad (\text{A.26})$$

From equations (A.24) and (A.26) it is straightforward to show that

- For $k = n$: we have

$$\lambda_{P,n} = -\lambda_{B,n}/2 + \sqrt{\lambda_{S,n}} = k_\alpha s_n - k_\alpha s_n = 0.$$

- For $k = 1, k = n - 1$:

$$\begin{aligned} \operatorname{Re}(\sqrt{\lambda_{S,1}}) &= \operatorname{Re}(\lambda_{B,1}/2) = (k_\alpha s_n c_n^2 + 2s_n^2 c_n), & \operatorname{Im}(\sqrt{\lambda_{S,1}}) &= k_\alpha s_n^2 c_n + 2s_n^3, \\ \operatorname{Re}(\sqrt{\lambda_{S,n-1}}) &= \operatorname{Re}(\lambda_{B,n-1}/2) = (k_\alpha s_n c_n^2 + 2s_n^2 c_n), & \operatorname{Im}(\sqrt{\lambda_{S,n-1}}) &= -k_\alpha s_n^2 c_n - 2s_n^3. \end{aligned}$$

Therefore, we obtain

$$\begin{aligned} \operatorname{Re}(\lambda_{P,1}) &= -\operatorname{Re}(\lambda_{B,1}/2) + \operatorname{Re}(\lambda_{B,1}/2) = 0, \\ \operatorname{Im}(\lambda_{P,1}) &= (2c_n - k_\alpha s_n) s_n c_n + k_\alpha s_n^2 c_n + 2s_n^3 = 2s_n, \\ \operatorname{Re}(\lambda_{P,n-1}) &= -\operatorname{Re}(\lambda_{B,n-1}/2) + \operatorname{Re}(\lambda_{B,n-1}/2) = 0, \\ \operatorname{Im}(\lambda_{P,n-1}) &= -(2c_n - k_\alpha s_n) s_n c_n - k_\alpha s_n^2 c_n + 2s_n^3 = -2s_n. \end{aligned}$$

- For $1 < k < n - 1$, since $\sin(k\pi/n)^2 > \sin(\pi/n)^2$, we have:

$$\operatorname{Re}(\sqrt{\lambda_{S,k}}) \leq \operatorname{Re}(\lambda_{B,k}/2),$$

and thus $\operatorname{Re}(\lambda_{P,k}) < 0$ for $k \notin \{0, 1, n - 1\}$.

Now, we proceed to show that v_1, v_2, v_3 in lemma 3.2.8 are the eigenvectors corresponding to the eigenvalues $0, 2s_n j$ and $-2s_n j$ respectively. First, consider the zero eigenvalue. Since $L \cdot \mathbf{1}_n = \mathbf{0}_n$ (where $\mathbf{0}_n = (0, 0, \dots, 0)^T \in \mathbb{R}^n$), it is easy to verify that:

$$P v_1 = \begin{bmatrix} a_n L - 2k_\alpha s_n I_n & -s_n I_n \\ b_n L^2 & c_n L \end{bmatrix} \begin{bmatrix} \mathbf{1}_n \\ -2k_\alpha \mathbf{1}_n \end{bmatrix} = \mathbf{0}_{2n}. \quad (\text{A.27})$$

Now, consider the imaginary eigenvalue $\lambda_2 = 2s_n j$. By replacing v_2 into the eigenvalue

equation we obtain

$$\begin{bmatrix} a_n L - 2k_\alpha s_n I_n & -s_n I_n \\ b_n L^2 & c_n L \end{bmatrix} \begin{bmatrix} \psi_1 \\ f_{n,2}(k_\alpha)\psi_1 \end{bmatrix} = 2s_n j \begin{bmatrix} \psi_1 \\ f_{n,2}(k_\alpha)\psi_1 \end{bmatrix}, \quad (\text{A.28})$$

Note that L and L^2 (which are both circulant matrices) satisfy, respectively, $L\psi_1 = (e^{2\pi j/n} - 1)\psi_1 = (-2s_n j(c_n + js_n))\psi_1$, and $L^2\psi_1 = (e^{2\pi j/n} - 1)^2\psi_1 = -4s_n^2 e^{2\pi j/n}\psi_1$; hence, v_2 is an eigenvector for P if and only if:

$$(a_n(e^{2\pi j/n} - 1) - 2k_\alpha s_n)\psi_1 + 2b_n e^{j\pi/n} s_n \psi_1 = 2s_n j \psi_1 \quad (\text{A.29})$$

$$-4b_n s_n^2 (c_n + js_n)^2 \psi_1 - c_n (-2s_n j(c_n + js_n)) 2b_n e^{j\pi/n} \psi_1 = -4b_n e^{j\pi/n} s_n j \psi_1 \quad (\text{A.30})$$

By using the identities in equation (A.22), the first condition can be verified according to

$$\begin{aligned} 2s_n(-c_n + k_\alpha s_n)j e^{j\pi/n} - 2s_n k_\alpha + 2s_n b_n e^{j\pi/n} &= 2s_n j, \\ 2((c_n - k_\alpha s_n)j - (k_\alpha + j)(c_n - js_n))e^{j\pi/n} &= -2b_n e^{j\pi/n}, \\ -2(s_n + k_\alpha c_n)e^{j\pi/n} &= -2b_n e^{j\pi/n}. \end{aligned}$$

Similarly, the condition in equation (A.30) can be verified according to

$$\begin{aligned} -2b_n s_n^2 (c_n + js_n)^2 + 2c_n (js_n (c_n + js_n)) b_n e^{j\pi/n} &= -2b_n e^{j\pi/n} s_n j, \\ -s_n (c_n + js_n) + c_n (j(c_n + js_n)) &= j, \\ j(s_n^2 + c_n^2) &= j. \end{aligned}$$

Similar arguments hold for λ_3 and v_3 (which are complex conjugates of λ_2 and v_2). This concludes the proof. ■

A.4 Proof that $v_i \notin T_{(\varrho^*, \varphi^*)} \tilde{\mathcal{M}}$

Proof: It is enough to prove that at least one of the components of $G \cdot v_i$ is nonzero. The proof that $G \cdot v_1 \neq 0$ is trivial. We proceed to show that $\nabla g_1 \cdot v_2 \neq 0$, i.e.:

$$\begin{aligned} & \left[1 \cos\left(\frac{2\pi}{n}\right) \dots \cos\left(\frac{2\pi(n-1)}{n}\right) - \sum_{i=2}^n r \sin\left(\frac{2\pi(i-1)}{n}\right) \dots - r \sin\left(\frac{2\pi(n-1)}{n}\right) 0 \right] \begin{bmatrix} \psi_1 \\ -2b_n e^{j\pi/n} \psi_1 \end{bmatrix} \\ &= (\nabla_{\varrho} g_1) \cdot \psi_1 + (\nabla_{\varphi} g_1) \cdot (-2b_n e^{j\pi/n} \psi_1) \neq 0. \end{aligned}$$

Both terms in the above sum can be shown to be real and positive. For the first term we have that:

$$\begin{aligned} (\nabla_{\varrho} g_1) \cdot \psi_1 &= \sum_{k=0}^{n-1} \cos(2\pi k/n) (\cos(2\pi k/n) + j \sin(2\pi k/n)) \\ &= \sum_{k=0}^{n-1} \cos^2(2k\pi/n) + j \sum_{k=0}^{n-1} 2 \sin(k\pi/n) = \sum_{k=0}^{n-1} \cos^2(2k\pi/n) \in \mathbb{R}_{>0}. \end{aligned}$$

For the second term we have:

$$\begin{aligned} (\nabla_{\varphi} g_1) \cdot (-2b_n e^{j\pi/n} \psi_1) &= \sum_{k=0}^{n-1} \sum_{i=k+1}^n \sin(2\pi k/n) 2b_n e^{j\pi/n} e^{2\pi k/n} \\ &= 2b_n \sum_{k=0}^{n-1} a_k e^{(2k+1)\pi j/n}, \end{aligned}$$

where $a_k = \sum_{i=k+1}^n \sin(2\pi i/n) = -\sum_{i=1}^k \sin(2\pi i/n)$. Now we show that $\sum_{k=0}^n a_k e^{(2k+1)\pi j/n} > 0$. First, consider the following facts:

$$\begin{aligned} a_k &\leq 0 \quad \forall k, \\ a_{k+1} &= a_k - \sin(2\pi(k+1)/n) < a_k \quad \text{for } 0 \leq k < n/2 - 1, \\ a_{\lfloor (n-1)/2 \rfloor} &< a_k \quad \forall k \neq \lfloor (n-1)/2 \rfloor, \\ a_{n-k} &= -\sum_{i=1}^{n-k} \sin(2\pi i/n) = \sum_{m=k+1}^n \sin(2\pi m/n) = a_k, \end{aligned}$$

$$\begin{aligned}
\sum_{k=0}^{n-1} a_k e^{(2k+1)\pi j/n} &= \sum_{k=0}^{\lfloor (n-1)/2 \rfloor} (a_k e^{k\pi j/n} + a_{n-k} e^{-k\pi j/n}) + q a_{(n-1)/2} \\
&= \sum_{k=0}^{\lfloor (n-1)/2 \rfloor} a_k (e^{\pi k j/n} + e^{-\pi k j/n}) + q a_{(n-1)/2}
\end{aligned}$$

$$\sum_{k=0}^{n-1} e^{(2k+1)\pi j/n} = \sum_{k=0}^{\lfloor (n-1)/2 \rfloor} (e^{\pi k j/n} + e^{\pi - k j/n}) + q = 0$$

where $q = 0$ if n is even. Then,

$$\sum_{k=0}^{n-1} a_k e^{(2k-1)\pi j/n} > \sum_{k=0}^{n-1} a_{\lfloor (n-1)/2 \rfloor} e^{(2k-1)\pi j/n} = 0.$$

Since $b_n = (s_n + k_\alpha c_n) > 0$, we have that $\nabla_\varphi g_1 \cdot (-2b_n e^{j\pi/n}) \in \mathbb{R}_{>0}$.

The proof for $G \cdot v_3 \neq 0$ is analogous; in particular, it requires to show that $j \nabla_\varphi g_2 \cdot \psi_1 \in \mathbb{R}_{>0}$ and $j \nabla_\varphi g_2 \cdot (-2b_n e^{j\pi/n} \psi_1) \in \mathbb{R}_{>0}$.

■

A.5 Eigenvalues of the projected Laplacian

The derivation of the eigenvalues of $\mathcal{R} \mathcal{L}^{(N)} \mathcal{L}_m(\alpha) (\mathcal{L}^{(N)})^\top \mathcal{R}^\top$ uses the properties of block-circulant matrices, specifically, the fact that they all belong to a commutative algebra. We have that:

$$\begin{aligned}
\text{eig}[\mathcal{R}_\eta \mathcal{L}^{(N)} \mathcal{L}_{sm}(\alpha) (\mathcal{L}^{(N)})^\top \mathcal{R}_\eta^\top] &= \text{eig}[\mathcal{R} \mathcal{R}^\top] \text{eig}[\mathcal{L}^{(N)}] \text{eig}[(\mathcal{L}^{(N)})^\top] \text{eig}[\mathcal{L}(\alpha) + \mathcal{L}^\top(\alpha)] \\
&= \text{eig}[(I_n \otimes R(\pi/N))(I_n \otimes R^\top(\pi/N))] \\
&\quad \times \text{eig}[(L_1 \otimes I_3)(L_1^\top \otimes I_3)] \text{eig}[\mathcal{L}(\alpha) + \mathcal{L}(\alpha)^\top] \\
&= \text{eig}[(L_1 \otimes I_3)(L_1^\top \otimes I_3)] \text{eig}[\mathcal{L}(\alpha) + \mathcal{L}(\alpha)^\top]
\end{aligned}$$

Then,

$$\begin{aligned}
\text{eig}[\mathcal{R}\mathcal{L}\mathcal{L}_{sm}\mathcal{L}^\top\mathcal{R}^\top] &= \lambda_{ik} \quad i \in \{1, \dots, N\}, k \in \{-1, 0, 1\} \\
\lambda_{ik} &= (1 - e^{-j2im\pi/N})(1 - e^{j2im\pi/N})((e^{jk\alpha} - e^{jk\alpha - j2im\pi/N}) + (e^{jk\alpha} - e^{-jk\alpha + j2i\pi/N})) \\
&= (2 - e^{-j2i\pi/N} - e^{j2i\pi/N})2(\cos(k\alpha) - \cos(k\alpha - 2im\pi/N)) \\
&= 4(1 - \cos(2i\pi/N))(\cos(k\alpha) - \cos(k\alpha - 2im\pi/N)) \tag{A.31}
\end{aligned}$$

Then, for $i = 1$:

$$\begin{aligned}
(1 - \cos(2i\pi/N)) &= 0 \\
\Rightarrow \lambda_{1k} &= 0
\end{aligned}$$

for $i = N$:

$$(\cos(k\alpha) - \cos(k\alpha - 2mi\pi/N)) = 0 \Rightarrow \lambda_{Nk} = 0$$

otherwise for $1 < i < N$, $|\alpha| \leq 2\pi/N$:

$$\begin{aligned}
(\cos(k\alpha) - \cos(k\alpha - 2im\pi/N)) &> 0 \\
(1 - \cos(2i\pi/N)) &> 0
\end{aligned}$$

Proposition A.5.1

$$V_{rn}\mathcal{L}_{sm}V_{rn}^\top = K_n\mathcal{R}_\eta\mathcal{L}(\alpha)\mathcal{L}_{sm}\mathcal{L}(\alpha)^\top\mathcal{R}_\eta^\top K_n^\top > 0 \quad , \tag{A.32}$$

Proof: $\mathcal{R}_\eta\mathcal{L}(\alpha)\mathcal{L}_{sm}\mathcal{L}(\alpha)^\top\mathcal{R}_\eta^\top$ is a symmetric matrix, then, its nullity is the algebraic multiplicity of the 0 eigenvalue. Thus, $\dim\{\mathcal{N}(\mathcal{R}_\eta\mathcal{L}(\alpha)\mathcal{L}_{sm}\mathcal{L}(\alpha)^\top\mathcal{R}_\eta^\top)\} = 6$. On the other

hand, the dimension of $K_n(\mathcal{R}_\eta \mathcal{L}(\alpha) \mathcal{L}_{sm} \mathcal{L}(\alpha)^\top \mathcal{R}_\eta^\top) K_n^\top = 3N - 6$, and thus it is full rank. Since $(\mathcal{R}_\eta \mathcal{L}(\alpha) \mathcal{L}_{sm} \mathcal{L}(\alpha)^\top \mathcal{R}_\eta^\top)$ is positive semidefinite, then $V_{rn} \mathcal{L}_{sm} V_{rn}^\top$ is at least positive semidefinite, but since it is full rank, the proposition is proven. ■

Bibliography

- [1] Becet Acikmese, Fred Y. Hadaegh, Daniel P Scharf, and Scott R Ploen. Formulation and analysis of stability for spacecraft formations. *IET Control Theory & Applications*, 1(2):461, 2007.
- [2] Umair Ahsun and David W. Miller. Dynamics and Control of Electromagnetic Satellite Formations. In *Proc. 2006 American Control Conference*, pages 1730–1735, Minneapolis, MN, 2006.
- [3] Umair Ahsun and David W. Miller. Dynamics and Control of Electromagnetic Satellite Formations, Massachusetts Institute of Technology, PhD Thesis, 2007.
- [4] David Angeli and Pierre-Alexandre Bliman. Stability of leaderless multi-agent systems. Extension of a result by Moreau. *ReCALL*, pages 1–18, 2008.
- [5] M. Aoki. On Feedback Stabilizability of Decentralized Dynamic Systems. *Automatica*, 8:163–173, 1972.
- [6] Randal W. Beard and Jonathan Lawton. A Feedback Architecture. In *Proc. 2000 American Control Conference*, number June, pages 4087–4091, Chicago, IL, 2000.
- [7] Randal W. Beard, Jonathan Lawton, and Fred Y. Hadaegh. A Coordination Architecture for Spacecraft Formation Control. *IEEE Transactions on Control Systems Technology*, 9(6):777–790, 2001.
- [8] Randal W. Beard, T. W. McLain, D.B. Nelson, Derek B. Kingston, and D. Johnson. Decentralized Cooperative Aerial Surveillance Using Fixed-Wing Miniature UAVs. *Proceedings of the IEEE*, 94(7):1306–1324, July 2006.
- [9] C. A. Beichman, N. J. Woolf, and C. A. Lindensmith. The Terrestrial Planet Finder (TPF): a NASA Origins Program to search for habitable planets, 1999.
- [10] Gene M Belanger, Slava Ananyev, Jason L Speyer, David F. Chichka, and J. Russell Carpenter. Decentralized Control of Satellite Clusters Under Limited Communication. In *Proc. AIAA Guidance, Navigation and Control Conference*, number August, pages 1–22, Providence, RI, 2004.
- [11] Dimitri Bertsekas. *Nonlinear Programming*. Athena Scientific, Belmont, MA, 2 edition, 2003.

- [12] Owen Brown and Paul Eremenko. Fractionated Space Architectures: A Vision for Responsive Space. In *Proc. 4th Responsive Space Conference*, Los Angeles, CA, 2006.
- [13] R. Burns, C.A. McLaughlin, J. Leitner, and M. Martin. TechSat 21: formation design, control, and simulation. *Proc. IEEE Aerospace Conference*, 7: 19–25, 2000.
- [14] J. Russell Carpenter. A Preliminary Investigation of Decentralized Control for Satellite Formations. In *Proc. 2000 IEEE Aerospace Conference*, pages 63–74, 2000.
- [15] J. Russell Carpenter. Partially decentralized control architectures for satellite formations. In *Proc. AIAA Guidance, Navigation and Control Conference*, number August, pages 1–11, Monterrey, CA, 2002.
- [16] Suman Chakravorty and Jaime Ramirez. Fuel Optimal Maneuvers for Multispacecraft Interferometric Imaging Systems. *Journal of Guidance, Control, and Dynamics*, 30(1):227–236, January 2007.
- [17] Soon-Jo Chung, Umair Ahsun, and Jean-Jacques E. Slotine. Application of Synchronization to Formation Flying Spacecraft: Lagrangian Approach. *Journal of Guidance, Control, and Dynamics*, 32(2):512–526, March 2009.
- [18] Soon-Jo Chung and David W Miller. Propellant-Free Control of Tethered Formation Flight, Part 1: Linear Control and Experimentation. *Journal of Guidance, Control, and Dynamics*, 31(3):571–584, May 2008.
- [19] Soon-Jo Chung and Jean-Jacques E. Slotine. Cooperative Robot Control and Synchronization of Lagrangian Systems. In *Proc. 2007 American Control Conference*, pages 2504–2509, New Orleans, LA, 2007.
- [20] J. Corfmat and S. Morse. Stabilization with decentralized Feedback Control. *IEEE Transactions On Automatic Control*, pages 679–682, 1973.
- [21] Dimos V. Dimarogonas and Kostas J Kyriakopoulos. Decentralized Navigation Functions for Multiple Robotic Agents with Limited Sensing Capabilities. *Journal of Intelligent and Robotic Systems*, 48(3):411–433, 2007.
- [22] Dimos V. Dimarogonas, Savvas G. Loizou, Kyriakopoulos Kostas J., and Michael M Zavlanos. Decentralized Feedback Stabilization and Collision Avoidance of Multiple Agents, 2004.
- [23] Dimos V. Dimarogonas, Savvas G. Loizou, Kostas J Kyriakopoulos, and Michael M Zavlanos. A feedback stabilization and collision avoidance scheme for multiple independent non-point agents. *Automatica*, 42(2):229–243, February 2006.
- [24] J. Alexander Fax. *Optimal and Cooperative Control of Vehicle Formations*. PhD dissertation, California Institute of Technology, 2002.
- [25] J. Alexander Fax and Richard M. Murray. Graph Laplacians and Stabilization of Vehicle Formations, *Proc. 15th IFAC Congress*, Barcelona, Spain, 2002.

- [26] David Folta and David Quinn. A universal 3-D method for controlling the relative motion of multiple spacecraft in any orbit. *Proc. AIAA/AAS Astrodynamics Specialist Conference*, Paper No. 98-4193, Boston, MA, Aug. 1998.
- [27] C Fridlund. The Darwin mission. *Advances in Space Research*, 34(3):613–617, 2004.
- [28] R.M. Gray. Toeplitz and Circulant Matrices: A review. *Foundations and Trends in Communications and Information Theory*, 2(3):155–239, 2005.
- [29] F. Y. Hadaegh, G Singh, B Acikmese, and D P Scharf. Guidance and Control of Formation Flying Spacecraft. *The Path to Autonomous Robots*, Springer, pages 25–43, 2009
- [30] Dario Izzo and Lorenzo Pettazzi. Autonomous and Distributed Motion Planning for Satellite Swarm. *Journal of Guidance, Control, and Dynamics*, 30(2):449–459, March 2007.
- [31] Ali Jadbabaie, Jie Lin, and A Stephen Morse. Coordination of Groups of Mobile Autonomous Agents Using Nearest Neighbor Rules. *IEEE Transactions On Automatic Control*, 48(6):988–1001, 2003.
- [32] Meng Ji, Abubakr Muhammad, and Magnus Egerstedt. Leader-Based Multi-Agent Coordination: Controllability and Optimal Control. In *Proc. 2006 American Control Conference*, pages 1358–1363, Minneapolis, MN, 2006.
- [33] E.W. Justh and P.S. Krishnaprasad. Steering laws and continuum models for planar formations. In *Proc. 2003 IEEE Conference on Decision and Control*, pages 3609–3614, Maui, HI, 2003. IEEE.
- [34] Ryosuke Kaneda, Fumito Yazaki, Shin-ichiro Sakai, Tatsuaki Hashimoto, and Hirobumi Saito. The relative position control in formation flying satellites using superconducting magnets. *Papers of Technical Meeting on Industrial Instrumentation and Control, IEE Japan*, IIC-04(1):91–96, 2004.
- [35] Wei Kang and Ning Xi. Formation Control of Multiple Autonomous Vehicles. In *Proc. International Conference on Control Applications*, pages 1027–1032, Barcelona, Spain, 1999.
- [36] Vikram Kapila, Andrew G Sparks, and Qiguo Yan. Spacecraft Formation Flying: Dynamics and Control. *Journal of Guidance*, 23(3):561–564, 1999.
- [37] Daniel Koditschek and Elon Rimon. Robot Navigation Functions on Manifolds with Boundary. *Advances in Applied Mathematics*, 442(11):412–442, 1990.
- [38] Edmund M C Kong, Daniel W Kwon, Samuel A Schweighart, Laila M Elias, Raymond J Sedwick, and David W Miller. Electromagnetic Formation Flight for Multi-satellite Arrays. *Journal of Guidance, Control, and Dynamics*, 41(4):659–666, 2004.

- [39] Daniel Kwon and David W Miller. *Electromagnetic Formation Flight of Satellite Arrays* Massachusetts Institute of Technology, M.S. Thesis, 2005.
- [40] G. Lafferriere, A. Williams, J Caughman, and J Veerman. Decentralized control of vehicle formations. *Systems & Control Letters*, 54(9):899–910, September 2005.
- [41] Alan J. Laub *Matrix Analysis for Scientists and Engineers* SIAM Publications, Philadelphia, PA, 2005, p. 141
- [42] Jonathan Lawton. *A behavioral approach to multispacecraft formation flying*, Brigham Young University, PhD Thesis, 2000.
- [43] Jonathan Lawton, Randal W. Beard, and Fred Y. Hadaegh. Elementary attitude formation maneuvers via leader-following and behavior-based control. In *Proc. AIAA Guidance, Navigation and Control Conference*, August, 2000.
- [44] Sang-il Lee. *Design and Implementation of the State Estimator for Trajectory Following of an Electromagnetic Formation Flight Testbed*, Massachusetts Institute of Technology, M.S. Thesis, 2008.
- [45] Z. Lin, M. Broucke, and B. Francis. Local Control Strategies for Groups of Mobile Autonomous Agents. *IEEE Transactions on Automatic Control*, 49(4):622–629, April 2004.
- [46] David M Lobosco, Glen E Cameron, Richard A Golding, and Theodore M Wong. The Pleiades fractionated space system architecture and the future of national security space. In *Proceeding Space 2009 Conference*, pages 1–10, 2009.
- [47] Winfried Lohmiller and Jean-Jacques E. Slotine. On Contraction Analysis for Non-linear Systems. *Automatica*, 34(6):683–696, June 1998.
- [48] Savvas G. Loizou, Herbert G Tanner, Vijay Kumar, and Kostas J Kyriakopoulos. Closed Loop Navigation for Mobile Agents in Dynamic Environments. In *Mechanical Engineering*, 2007.
- [49] Matt Long, Aaron Gage, Robin Murphy, and Kimon Valavanis. Application of the Distributed Field Robot Architecture to a Simulated Demining Task. In *Proc. International Conference on Robotics and Automation*, pages 3193–3200, Barcelona, Spain, 2005.
- [50] Gregory J W Mallory. *Development and Experimental Validation of Direct Controller Tuning for Spaceborne Telescopes*. PhD Thesis, Massachusetts Institute of Technology, 2000.
- [51] Joshua A Marshall, Mireille E Broucke, and Bruce A Francis. Formations of Vehicles in Cyclic Pursuit. *IEEE Transactions On Automatic Control*, 49(11):1963–1974, 2004.
- [52] Joshua A Marshall, Mireille E Broucke, and Bruce A Francis. Pursuit formations of unicycles. *Automatica*, 42(1):3–12, January 2006.

- [53] Colin McInnes. Autonomous Ring Formation for a Planar Constellation of Satellites. *Journal of Guidance*, 18(5):1215–1217, 1993.
- [54] Mehran Mesbahi and Fred Y. Hadaegh. Formation Flying Control of Multiple Spacecraft via Graphs, Matrix Inequalities, and Switching. *Journal of Guidance, Control, and Dynamics*, 24(2), 2001.
- [55] Luc Moreau. Stability of Multiagent Systems With Time-Dependent Communication Links. *IEEE Transactions On Automatic Control*, 50(2):169–182, 2005.
- [56] Nader Motee, Ali Jadbabaie, and Bassam Bamieh. On Decentralized Optimal Control and Information Structures . In *Proc. 2008 American Control Conference*, pages 4985–4990, Seattle, WA, 2008.
- [57] S. Sharma, S. Curtis. *Magnetospheric Multiscale Mission*, Springer, Heidelberg, 2005.
- [58] Michael Norman and Mason A. Peck Modeling and Properties of a Flux-Pinned Network of Satellites. *Advances on Aeronautical Sciences*, In American Astronautical Society, Paper AAS 07-270 2007.
- [59] P. Ogren, E. Fiorelli, and N.E. Leonard. Cooperative Control of Mobile Sensor Networks: Adaptive Gradient Climbing in a Distributed Environment. *IEEE Transactions on Automatic Control*, 49(8):1292–1302, August 2004.
- [60] Reza Olfati-Saber. Distributed Kalman Filter with Embedded Consensus Filters. In *Simulation*, pages 8179–8184, Seville, Spain, 2005.
- [61] Reza Olfati-Saber. Flocking for Multi-Agent Dynamic Systems: Algorithms and Theory. *IEEE Transactions On Automatic Control*, 51(3):401–420, 2006.
- [62] Reza Olfati-Saber, J. Alexander Fax, and Richard M Murray. Consensus and Cooperation in Networked Multi-Agent Systems. *Proceedings of the IEEE*, 95(1):215–233, 2007.
- [63] Reza Olfati-Saber, J. Alexander Fax, and Richard M Murray. Consensus and Cooperation in Networked Multi-Agent Systems. *Proceedings of the IEEE*, 95(1):215–233, January 2007.
- [64] Reza Olfati-Saber and Richard M Murray. Distribute cooperative control fo multiple vehicle formation using structural potential functions. In *IFAC 15th Triennial World Congress*, Barcelona, Spain, 2002.
- [65] Reza Olfati-Saber and Richard M Murray. Consensus Problems in Networks of Agents with Switching Topology and Time-Delays. *IEEE Transactions On Automatic Control*, 49(9):1520–1533, 2004.
- [66] D Paley. Stabilization of collective motion on a sphere. *Automatica*, 45(1):212–216, January 2009.

- [67] Marco Pavone and Emilio Frazzoli. Decentralized Policies for Geometric Pattern Formation and Path Coverage. *Journal of Dynamic Systems, Measurement, and Control*, 129(5):633, 2007.
- [68] Quang-Cuong Pham and Jean-Jacques E. Slotine. Stable concurrent synchronization in dynamic system networks. *Neural networks : the official journal of the International Neural Network Society*, 20(1):62–77, January 2007.
- [69] Marcio S De Queiroz, Vikram Kapila, and Qiguo Yan. Adaptive Nonlinear Control of Multiple Spacecraft Formation Flying. *Journal of Guidance, Control, and Dynamics*, 23(3):385–390, 2000.
- [70] Jaime Ramirez, Marco Pavone, Emilio Frazzoli, and David W Miller. Distributed Control of Spacecraft Formation via Cyclic Pursuit: Theory and Experiments. In *Proc. 2009 American Control Conference*, St. Louis, MO, 2009.
- [71] Wei Ren. *Consensus Keeping, Formation Keeping and Trajectory Tracking in Multiple Vehicle Cooperative Control*. PhD thesis, Brigham Young University, 2004.
- [72] Wei Ren. Cooperative Control Design Strategies with Local Interactions. In *Proceeding IEEE Conference on Decision and Control*, 2006.
- [73] Wei Ren. Collective Motion from Consensus with Cartesian Coordinate Coupling - Part I: Single-integrator Kinematics. In *Proc. 2008 IEEE Conference on Decision and Control*, pages 1006–1011, Cancun, Mexico, 2008.
- [74] Wei Ren. Collective Motion from Consensus with Cartesian Coordinate Coupling - Part II: Double-integrator Dynamics. In *Proc. 2008 IEEE Conference on Decision and Control*, pages 1012–1017, Cancun, Mexico, 2008.
- [75] Wei Ren. On Consensus Algorithms for Double-integrator Dynamics. In *Proc. 2008 IEEE Conference on Decision and Control*, number 2, pages 2295–2300, New Orleans, LA, 2008.
- [76] Wei Ren. Collective Motion From Consensus With Cartesian Coordinate Coupling. *IEEE Transactions on Automatic Control*, 54(6):1330–1335, June 2009.
- [77] Wei Ren and Ella M Atkins. Distributed multi-vehicle coordinated control via local information exchange. *International Journal of Robust and Nonlinear Control*, (November 2006):1002–1033, 2007.
- [78] Wei Ren and Randal W. Beard. Decentralized Scheme for Spacecraft Formation Flying via the Virtual Structure Approach. *Journal of Guidance, Control, and Dynamics*, 27(1):73–82, 2004.
- [79] Wei Ren and Randal W. Beard. Consensus Seeking in Multiagent Systems Under Dynamically Changing Interaction Topologies. *IEEE Transactions On Automatic Control*, 50(5):655–661, 2005.

- [80] Michael Rotkowitz and Sanjay Lall. A characterization of convex problems in decentralized control. *IEEE Transactions On Automatic Control*, 51(2), 2006.
- [81] Gerard Rousset, Laurent Mugner, Cassaing Frederic, and Beatrice Sorrente. Imaging with multi-aperture optical telescopes and an application. *Astronomical techniques*, 2147(01):17–25, 2001.
- [82] Aya Sakaguchi. *Micro-Electromagnetic Formation Flight of Satellite Systems*. Massachusetts Institute of Technology, M.S. Thesis, 2007.
- [83] Daniel P Scharf, Fred Y. Hadaegh, and Scott R Ploen. A Survey of Spacecraft Formation Flying Guidance and Control (Part II): Control. In *Proc. 2004 American Control Conference*, number Part 11, pages 2976–2985, Boston, MA, 2004.
- [84] Hanspeter Schaub and Kyle T Alfriend. Impulsive Feedback Control to Establish Specific Mean Orbit Elements of Spacecraft Formations. *Journal of Guidance, Control, and Dynamics*, 24(4):739–745, 2001.
- [85] H. Schaub, G. Parker, G. and L.B. King Challenges and Prospect of Coulomb Formations. *Advances in Astronautical Sciences*, American Astronautical Society, Paper AAS-03-278, 2003
- [86] Samuel A Schweighart and Raymond J Sedwick. High-Fidelity Linearized J_2 Model for Satellite Formation Flight. 25(6), 2002.
- [87] Samuel A Schweighart and Raymond J Sedwick. Propellantless Formation Flight Operations using Electromagnetic Formation Flight. In *SpaceOps Conference*, 2006.
- [88] Rodolphe Sepulchre, Derek a. Paley, and Naomi Ehrich Leonard. Stabilization of Planar Collective Motion With Limited Communication. *IEEE Transactions on Automatic Control*, 53(3):706–719, April 2008.
- [89] Xuan-Min Shao, William Junor, Aaron Rogers, Raymond Zenick, and Kalpak Dighe. Passive interferometric millimeter-wave imaging: achieving big results with a constellation of small satellites. *Proceedings of SPIE*, 5410:270–277, 2004.
- [90] J-J. E. Slotine and Weiping Li. *Applied Nonlinear Control*. Number 1. Prentice Hall, Upper Saddle River, NJ, 1991.
- [91] Roy S Smith and Fred Y. Hadaegh. Control Topologies for Deep Space Formation Flying Spacecraft. In *Proc. American Control Conference*, pages 2836–2841, Anchorage, AK, 2002.
- [92] Roy S Smith and Fred Y. Hadaegh. Reconfigurable topologies for decentralized control of spacecraft formations in deep space. In *Proc. American Astronomical Society Guidance and Control Conference*, volume 1, Breckenridge, CO, 2004.

- [93] Roy S Smith and Fred Y. Hadaegh. A Distributed Parallel Estimation Architecture for Cooperative Vehicle Formation Control. In *Proc. 2006 American Control Conference*, pages 4219–4224, Minneapolis, MN, 2006.
- [94] Roy S Smith and Fred Y. Hadaegh. Closed-Loop Dynamics of Cooperative Vehicle Formations With Parallel Estimators and Communication. *IEEE Transactions On Automatic Control*, 52(8):1404–1414, 2007.
- [95] Roy S Smith and Fred Y. Hadaegh. Distributed estimation, communication and control for deep space formations. *IET Control Theory and Applications*, 1(2):445–451, 2007.
- [96] Eduardo D. Sontag and Yuan Wang. Notions of Input to Output Stability. In *Proc. European Control Conference*, pages 1–20, Brussels, 1997.
- [97] Jason L Speyer. Computation and Transmission Requirements for a Decentralized Linear-Quadratic-Gaussian Control Problem. *IEEE Transactions On Automatic Control*, (2):266–269, 1979.
- [98] Daniel J Stilwell and Bradley E Bishop. Communication, Feedback, and Decentralized Control. *IEEE Control Systems Magazine*, (December):45–52, 2000.
- [99] Herbert G Tanner, Ali Jadbabaie, and George J Pappas. Stability of Flocking Motion, University of Pennsylvania, Technical Report, 2003.
- [100] Herbert G Tanner, George J Pappas, and Vijay Kumar. Input-to-state Stability on Formation Graphs. In *Proc. 2002 IEEE Conference on Decision and Control*, number December, pages 2439–2444, Las Vegas, NV, 2002.
- [101] Herbert G Tanner, George J Pappas, and Vijay Kumar. Leader-to-Formation Stability. *IEEE Transactions on Robotics and Automation*, 20(3):443–455, 2004.
- [102] Michael Tillerson Coordination and Control of Multiple Spacecraft using Convex Optimization Techniques, Massachusetts Institute of Technology, M.S. Thesis. 2002.
- [103] Michael Tillerson, Louis Breger, and Jonathan P How. Distributed Coordination and Control of Formation Flying Spacecraft. In *Proc. 2003 American Control Conference*, Denver, CO, 2003.
- [104] Yuri Ulybyshev. Long-Term Formation Keeping of Stellite Constellation Using Linear-Quadratic Controller. *Journal of Guidance, Control, and Dynamics*, 21(1):109–115, 1998.
- [105] Stephen G Ungar, Jay S Pearlman, Jeffrey A Mendenhall, and Dennis Reuter. Overview of the Earth Observing One (EO-1) Mission. *IEEE Transactions on Geoscience and Remote Sensing*, 41(6):1149–1159, 2003.
- [106] Tamas Vicsek, Andras Czirok, Eshel Ben-Jacob, Inon Cohen, and Ofer Shochet. Novel Type of phase transition in a system of self-driven particles. *Physics Review Letter*, 75:1226–1229, 1995.

- [107] P. Wang. Navigation Strategies for Multiple Autonomous Mobile Robots moving in Formation. In *Proc. IEEE International Conference on Intelligent Robots and Systems*, pages 486–493, Tsukuba, Japan, 1989.
- [108] P. Wang and Fred Y. Hadaegh. Optimal Formation-reconfiguration for multiple spacecraft. In *Proc. AIAA Guidance Navigation and Control Conference*, pages 686–696, Reston, VA, 1998.
- [109] Shih-ho Wang and Edward Davidson. On the Stabilization of Decentralized Control Systems. *IEEE Transactions On Automatic Control*, 18(5):473–478, 1973.
- [110] Wei Wang and Jean-Jacques E. Slotine. On partial contraction analysis for coupled nonlinear oscillators. *Biological cybernetics*, 92(1):38–53, January 2005.
- [111] Jingyi Yao, Raul Ordonez, and Veysel Gazi. Swarm Tracking Using Artificial Potentials and Sliding Mode Control. *Journal of Dynamic Systems, Measurement, and Control*, 129(5):749, 2007.